STRUCTURAL AND BIOCHEMICAL CHARACTERIZATION

OF THE HEMOPHORE (HasAp) FROM

PSEUDOMONAS AERUGINOSA

By

C2008
AILEEN YUNG ALONTAGA

B. S., Silliman University, 1996
Dumaguete City, Philippines

Submitted to the Department of Chemistry and the
Faculty of the Graduate School of the University of Kansas
In Partial fulfillment of the requirements for the degree of
Doctor of Philosophy

Committee members:

_____
Mario Rivera, Ph. D. (Chair)

_____
Heather Desaire, Ph. D.

_____
Robert C. Dunn, Ph. D.

_____
Julian Limburg, Ph. D.

_____
William D. Picking, Ph. D.

Date Defended: May 29, 2008

The Dissertation Committee for **Aileen Yung Alontaga** certifies that

this is the approved version of the following dissertation:

STRUCTURAL AND BIOCHEMICAL CHARACTERIZATION

OF THE HEMOPHORE (HasAp) FROM

PSEUDOMONAS AERUGINOSA

Committee:

_____
Mario Rivera, Ph. D. (Chair)

_____
Heather Desaire, Ph. D.

_____
Robert C. Dunn, Ph. D.

_____
Julian Limburg, Ph. D.

_____
William D. Picking, Ph. D.

Date Approved: _____

ABSTRACT

HasAp is a hemophore which is believed to "steal" heme from hemoglobin in the extracellular medium and deliver the heme to the cognate receptor, HasR for internalization. The mechanism of heme uptake and release mechanism of HasAp has not been understood. To gain insight on this mechanism, we have elucidated the electronic and coordination state of the heme active site, using a combination of bioanalytical techniques. The ^{13}C-meso chemical shifts were primarily used as a straightforward probe for the coordination and electronic state of HasAp. The results showed that heme-iron is hexacoordinate and in equilibrium between high-spin (S = 5/2) and low-spin (S = ½). The proposed explanation this unique coordination and spin state is the breaking and forming of hydrogen-bond between the axial ligand Tyr75 and His83 which could modulate the heme uptake and release in HasAp.

The heme transfer experiments reveal that HasAp can take heme only from hemoglobin if the heme-iron is in the ferric state. It can not take heme from met-myoglobin, oxyhemoglobin and HbCN. The weak aqua ligand that coordinates the ferric iron in met-Hb is essential to the heme transfer process since its substitution with a stronger ligand inhibits the heme transfer to HasAp. Moreover, the rate of heme transfer is relatively fast and it occurs in two steps. These observations imply that there appear to be a protein-protein interaction between HasAp and hemoglobin before HasAp take the heme from hemoglobin. Hence, the heme transfer event from met-Hb to apo-HasAp is a multi-step process.

The secondary structure of holo-HasAp was determined using X-ray crystallography and NMR spectroscopy. The results showed that the last 21 amino acid residues which composed the tail of the full-length form are highly unstructured and disordered. There is no structural difference in both the holo full-length and truncated form of HasAp except for the tail. However, there is a conformational difference between the apo and holo forms of HasAp. The regions close to the heme active site are in different conformations in both forms which could suggests that the protein uses different bonding interaction to stabilize the heme.

From the protein-protein interaction experiments the data shows that the same regions of the secondary structure in both holo full-length and truncated HasAp were perturbed upon hemoglobin binding. However, the residues in the truncated form are more perturbed which suggests that the truncated form is likely to be the biologically active form of HasAp.

ACKNOWLEDGMENTS

First of all, I would like to thank ALMIGHTY GOD who brought me here for a purpose and for the wonderful blessing of exploring science. I will be forever thankful to several people for without them I would not be here at the end of this journey.

I especially thank my advisor, Dr. Mario Rivera for his encouragement, guidance, and continuous support. I am so privileged and blessed to work with you to become an independent thinker and problem-solver. It has been an honor and a pleasure to be your student and to do research in your laboratory.

I would like to thank my committee members: Dr. Heather Desaire, Dr. Robert Dunn, Dr. Julian Limburg, and Dr. Bill Picking, for all their help and advice.

I want to thank a wonderful group of people who helped me throughout this journey: Dr. Juan Carlos Rodriguez, Dr. Yuhong Zeng, Dr. Christopher O. Damaso, Dr. Gregori A. Caignan, Dr. Adrianna Altuve, Veronica Rodriguez, Andy Wang, Grace Jepkorir, Bailey Morgan, Jordan Stobaugh, Maggie Murphy, Dr. Huili Yao and Saroja Weeratunga. I have been fortunate to work with all of you. You made me appreciate science and thank you all for all the fun and for the gift of friendship.

I want to thank our collaborators, Dr. Pierre Moënne- Loccoz for the EPR, heme transfer results; Dr. Ernst Schönbrunn for solving the crystal structure of our protein; Todd Funke and Huijong Han for their helpful advice on growing protein

TABLE OF CONTENTS

CHAPTER 4   190

Chemical Shift Perturbation Mapping of the Protein-Protein Interaction of HasAp with Hemoglobin

LIST OF TABLES

LIST OF FIGURES

CHAPTER 1

CHAPTER 3

CHAPTER 4

LIST OF SCHEMES

LIST OF APPENDICES

ABBREVIATIONS

ALA	δ-Aminolevulinic Acid
CSI	Chemical Shift Index
DFT	Density Functional Theory
DMSO	Dimethyl Sulfoxide
EDTA	Ethylenediaminetetraacetic Acid
EPR	Electron Paramagnetic Resonance
Has	<u>H</u>eme <u>A</u>cquisition <u>S</u>ystem
HasAp	<u>H</u>eme <u>A</u>cquisition <u>S</u>ystem *<u>P</u>seudomonas aeruginosa*
HasR	<u>H</u>eme <u>A</u>cquisition <u>S</u>ystem <u>R</u>eceptor
HasA$_{SM}$	<u>H</u>eme <u>A</u>cquisition <u>S</u>ystem *<u>S</u>erratia <u>m</u>arcescens*
Hb	Hemoglobin
H/D	Hydrogen/Deuterium
HSQC	Heteronuclear Single Quantum Coherence
IPTG	Isopropyl-β-D-thiogalactopyranoside
Mb	Myoglobin
NMR	Nuclear Magnetic Resonance
NOESY	Nuclear Overhausser Effect Spectroscopy
OD	Optical Density
OM cyt b_5	Outer Mitochondrial membrane Cytochrome b_5
PCR	Polymerase Chain Reaction
PDB	Protein Data Bank
PMSF	Phenylmethylsulfonyl Flouride
SDS PAGE	Sodium dodecyl Sulfate Polyacrylamide Gel Electrophoresis
ShuT	*<u>Shigella</u>* <u>h</u>eme <u>u</u>ptake <u>t</u>ransporter
SW	Sperm Whale
UV-Vis	Ultraviolet-Visible

CHAPTER 1

Introduction

The opportunistic human pathogen *Pseudomonas aeruginosa* is one of the organisms responsible for drug-resistant hospital infections and can seriously infect injured and immunocompromised patients as well as individuals with cystic fibrosis [1-6]. 10% of the two million hospital-related infections each year are caused by this pathogen [7]. Since, *P. aeruginosa* needs to propagate to be pathogenic, it needs all the nutrients required for its growth. One of the essential nutrients needed is iron because it prefers an aerobic metabolism which requires respiratory enzymes that need iron for their function [4]. Bacteria, however, face a shortage of iron supply from the host organism because at aerobic and physiological conditions, insoluble ferric hydroxide complexes are present in solution [8, 9]. Hence, there is practically no free soluble iron available [10-12]. Moreover, another problem encountered by the bacteria is the fact that the majority of the iron in a mammalian host is intracellular and sequestered within heme compounds and iron-sulfur clusters in different proteins and storage molecules. Thus, for pathogenic bacteria to successfully propagate within the host animal, it must be able to utilize or steal iron from these sources [8, 13].

To fulfill their iron requirements, *P. aeruginosa* and several other bacterial pathogens have developed various iron uptake and utilization mechanisms regulated by Fur (**F**e **u**ptake **r**egulator) [3, 4, 14] to scavenge iron from host animals. Poorly soluble ferric iron can be chelated by low molecular weight inorganic iron chelators,

called siderophores, secreted by the bacteria. The iron-containing siderophores then deliver the iron to the specific outer-membrane receptors in an energy-dependent process which allows the delivery of the iron to the bacteria via a TonB-dependent pathway [10, 15]. *P. aeruginosa* can also sequester iron from heme containing proteins by employing two heme-uptake systems, namely *phu* (**P**seudomonas **h**eme **u**ptake) and *has* (**h**eme **a**cquisition **s**ystem).

The *phu* system is composed of a receptor gene, phuR, and the *phuSTUVW* operon encoding an ATP-binding cassette (ABC) transporter [4]. On the other hand, the *has* operon consists of *hasRADEBF* genes (Figure 1) [16]. HasR is the hemophore-specific outer membrane receptor, HasA is a hemophore, HasD an ATP-
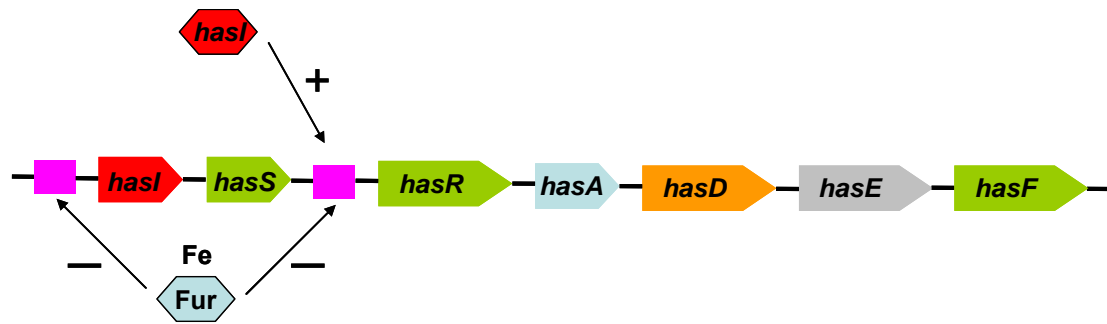
Figure 1. Organization of the *has* (heme acquisition system) operon. HasI and HasS are the sigma and anti-sigma ECF factors, respectively. The pink square boxes are the consensus Fur boxes.

binding inner membrane protein, HasE a membrane fusion protein, HasB a TonB analogue, and HasF an outer membrane protein [17, 18]. In a proteomics study [19], the hemophore, HasAp, of *Pseudomonas aeruginosa*, was identified to be a quorum-sensing regulated protein which suggests that HasAp plays a role in the virulence factor of this human pathogen. The hemophore of *Serratia marcescens* (HasA$_{SM}$) has been structurally and biochemically characterized. This introduction will give an overview on hemophores, and on the progress that has been done toward understanding their heme uptake and release mechanisms.

HasAp and Virulence

Twenty novel quorum-sensing (QS) regulated proteins were identified in the proteomics study of Arevalo-Ferro and coworker [19]. Two of the quorum-sensing regulated genes they identified are phuR and HasAp. As mentioned earlier, these two proteins are components of the two distinct heme uptake systems of *Pseudomonas aeruginosa*. This study suggests that there is a link between quorum-sensing and the iron regulatory system. QS enables individual bacteria to communicate and coordinate its behavior in a cell-density dependent manner or by cell-to-cell communication [20-22]. *P. aeruginosa* has two extensively studied quorum-sensing systems (*lasI-lasR* and *rhlI-rhlR*) that regulate expression of hundreds of genes that encode extracellular virulence factors, antibiotic resistance and biofilm development [3, 23-25]. It has been shown under standard laboratory conditions that the *las* and *rhl* systems are arranged in a hierarchic structure. The *las* system is on the upper level

of the regulation circuit. The QS systems are encoded by the synthase and the receptor or transcriptional regulator gene. The transcriptional regulator of the *las* and *rhl* systems are LasR and RhlR, respectively. While the synthase genes, LasI and the RhlI are specifically involved in the synthesis of the major *N*-acyl homoserine lactones (AHL) autoinducers, 3-oxo-C12-HSL and C4-HSL, respectively [23]. Bacteria produce these diffusible small signals molecules called autoinducers which diffuse in and out of bacterial cells. As the bacterial population increases to reach a "quorum", so does the synthesis of the autoinducers (AHL), and as a result their concentration in the external medium rises [23]. When a threshold level of AHL is reached, it binds with the cognate transcriptional regulator (LasR or RhlR) to activate expression of the QS-regulated genes [24, 26-29].

In this proteomic study [51], they employed both the wild type *P. aeruginosa* PAO1 parent strain and the isogenic *lasI rhlI* double mutant to determine their protein expression patterns in the presence and absence of AHL by two-dimensional gel electrophoresis (2-DE). The intracellular, extracellular, and surface fractions protein spots that were considered to be quorum-sensing regulated were characterized by MALDI-TOF peptide mapping. Moreover, the results also demonstrate that quorum-sensing control also functions by post-transcriptional mechanisms. In fact there were more AHL regulated proteins than the number of up-regulated genes. This was supported by the fact that they observed five spots (spots SN 110, SN 168, SN 190, SN 191, and SN 192) due to HasAp with different intensities. On the other hand, it was also observed that the amount of HasAp in the surface protein fractions and in

the supernatant were different in the PAO1 wild type and *lasl rhll* double mutant. In the wild type strain, the most abundant HasAp spot has a molecular weight of 18 kDa as determined by mass spectrometry. This processed form of HasAp lacks several amino acid residues at the C-terminus. This form is thought to be the active form or the physiologically important form. Whereas, in the *lasI rhlI* double mutant, the most abundant spot has a molecular weight of 20.5 kDa which corresponds to the unprocessed or the full length form of the protein. In addition, spots with molecular weight of 18 and 19 kDa with weaker intensities were also observed. Conversely, growing the *lasI rhlI* double mutant in medium supplemented with AHLs restored the wild type protein pattern. The proteomics study revealed that producing the cleaved HasAp form is indeed quorum sensing regulated and that protease(s) are responsible for the cleavage. However, the protease(s) has not been identified but it has been assumed that three quorum sensing regulated proteases namely, LasA, LasB and AprA, might be responsible for the cleavage at different sites [30]. Besides, HasAp has potential cleavage sites for both LasA and LasB [31, 32].

To further prove that both phuR and HasAp are indeed quorum-sensing regulated, they have shown that the isogenic *lasI rhlI* double mutant did not grow in the medium as well as the wild type with hemoglobin as the only iron source. However, supplementation of AHL in the *lasI rhlI* double mutant growth medium showed increased growth. Hence, the results suggest that one of the phenotypes controlled by quorum sensing in *P. aeruginosa* is hemoglobin-heme utilization. The

heme acquisition systems employed by this pathogen is important to sequester iron from the host animal.

Heme Acquisition System

Under iron starvation conditions, *Pseudomonas aeruginosa*, uses several strategies to sequester iron from the host animal throughout the duration of infection. It is remarkable how this human pathogen controls its iron acquisition and intake using an essential Fur regulator [33]. These Fur-regulated genes in *P. aeruginosa* are responsible for the virulence factors of the bacteria and they encode proteins which are involved in the iron uptake, transport and utilization [8, 33]. When the concentration of iron in the bacterial cell is high, the operon is repressed by the Fur protein. This is accomplished by the formation of a Fur protein-Fe(II) complex which binds DNA at the conserved Fur boxes located in the promoter region [34-36]. As mentioned earlier, *P. aeruginosa* employs two distinct Fur-regulated heme uptake systems to sequester iron from various heme containing proteins. One of these systems, the *has* system depends on the hemophore, HasAp, to sequester heme in the extracellular medium.

The *has* operon (hasRADEBF) is under negative regulation by a Fur box located upstream of the operon (Figure 1). Besides the negative regulation of the *has* operon by the Fur, the *has* operon is also under specific autoregulation of the extra cytoplasmic function (ECF) sigmas or iron-starvation sigma of the *has* system [36]. This process depends on the receptor, HasR and on its two upstream genes, HasI and

HasS. HasI is the ECF sigma factor, while HasS is the anti-sigma factor [37]. It has been shown that HasI and HasS genes are important elements that enable bacteria, in addition to the Fur-dependent mechanism, to tune the expression of the *has* system under iron limited conditions [36].

The *has* signaling cascade is induced by the heme containing HasA. Moreover, both the apo hemophore and heme do not induce the signaling cascade, which suggests that the substrate being transported (heme) and the inducer are different molecules [37]. When the heme containing hemophore, holo-HasA, binds to the cognate outer membrane receptor HasR, the sigma gene, HasI is activated and the anti-sigma gene, HasS is inactivated. Thus, facilitating the transcription of the *has* signaling cascade. When there are optimum iron concentrations, HasI induces transcription of HasS and turns off the anti-sigma of HasS which subsequently leads to an accumulation of inactivated HasS. This is turned on again when the heme concentration is low or when HasR is not bound to holo hemophore, HasA [36-39].

Proposed Working Mechanism of the Has

Heme Uptake System

The proposed working mechanism of the heme acquisition system is shown in Figure 2. Hemophores are secreted into the extracellular medium using the type I or the ATP-Binding Cassette (ABC) secretion pathway. In this pathway, the hemophores are secreted in a Sec-independent process by the ABC transporters. Typically proteins

Figure 2. Proposed working mechanism of the *has* system. SecB and HasDEF secrete the apoHasAp to the extracellular medium where it captures heme and delivers it to HasR. The internalization of heme is HasB-ExbB-ExbD dependent. Extracellular medium (E); Outer Membrane (OM); Periplasm (P); Cytoplasmic Membrane (CM); Cytosol (C); and (•) heme.

secreted by the type I secretion pathway have an α-helical C-terminal secretion signal that remains accessible because of the cytoplasmic chaperone, SecB, that is required for the hemophore secretion. The C-terminal secretion signal interacts with the ABC transport protein, regulates its ATPase activity and induces a multiprotein complex formation comprising the secreted protein (HasA) and the three secretion proteins (HasD, HasE and HasF). It has been reported by Wolff *et. al.* [40] that under various conditions the C-terminal region displays high flexibility and is a relatively unstructured part of the polypeptide chain.

Without the secretion apparatus, SecB, the hemophore cannot be secreted from the cytoplasm. At the same time, SecB also prevents the folding of the hemophore and keeps it in a secretion-competent form prior to transport. [41]. Properly folded hemophore in the cytoplasm can pose a problem to the bacterium because not only it can prevent the secretion of newly synthesized hemophores, but it will also be able to take heme from other cytoplasmic heme proteins [39, 40, 42, 43]. Thus, the tight coregulation of genes encoding the hemophore and its secretion components is crucial [13].

Once the hemophore is transported to the extracellular milleu, apo-HasA captures free heme and "steals" the heme from heme containing proteins such as hemoglobin, myoglobin and hemopexin to deliver it to the specific surface receptor HasR by protein-protein interaction. According to Létoffé *et. al.*, [44], it sequesters heme with its iron in redox states (Fe^{II} and Fe^{III}). These authors proposed that the hemophore does not capture the heme from other heme containing protein by protein-

protein interaction. This conclusion is based on the analytical ultracentrifugation experiments where they did not observed a stable complex between hemoglobin and HasA$_{SM}$. Thus, they concluded that there is passive transfer of heme from the heme containing protein to HasA [30] because of its high affinity for heme. It is probable that they were not able to see the HasA$_{SM}$-hemoglobin complex using analytical ultracentrifugation technique because the binding is weak and transient. Moreover, their results also suggest that the heme transfer is fast and it cannot be determined by the technique they use. In this research work, we attempted to determine the weak HasAp-hemoglobin interaction at the molecular level. We also did experiments to determine whether apo-HasAp can take both ferrous and ferric heme-iron and measured the kinetics of fast heme transfer from hemoglobin to apo-HasAp. These experiments are discussed in detail in Chapters 3 and 4.

The mechanism of heme transfer from the hemophore to its receptor is also not well understood because the affinity of HasA for heme is higher than that of HasR [45, 46]. The receptor can bind apo- and holo-HasA with the same affinity and at unique and overlapping sites [44]. Furthermore, HasR can also take up free heme or heme from hemoglobin. However, the HasA-HasR heme uptake is much more efficient than HasR alone because it can reduce by 100-fold the minimal hemoglobin concentrations required for bacterial growth. This observation also supports the fact that HasA functions extracellularly in a soluble form [30, 39].

Heme Internalization

Only the heme but not the apo-protein can be internalized in the cell. The heme is too large to diffuse through the outer membrane, thus the translocation of heme across the outer membrane involves the interaction of the heme with a specific outer membrane receptor, in this case, HasR. The heme is then translocated from the outer membrane to the periplasm by an energy-dependent process which in most cases is TonB dependent and involves the formation of an ExbB-ExbD-HasB protein complex. In addition, this protein complex functions in both, the release of apo-HasA into the extracellular medium and in heme transport into the cytoplasm [15]. The heme is then transported from the periplasm to the cytoplasm by a specific periplasmic binding protein [17, 37].

Heme Utilization

Once in the cytoplasm, heme is delivered to heme oxygenase (HO). Heme oxygenase uses heme both as a substrate and a prosthetic group. It catalyzes the oxidative degradation of heme to biliverdin with the concomitant release of iron, and CO. The degradation of heme to biliverdin is shown in (Scheme 1) [47, 48]. This process involves three O_2 molecules and seven electrons. In the case of *Pseudomonas aeruginosa*, the seven electrons are transported from NADPH to a ferredoxin reductase (*pa*-FPR), and then to a ferredoxin (*pa*-Bfd) which then delivers the electrons to a heme oxygenase (*pa*-HO) [49].

The mechanism of heme degradation by heme oxygenase starts with the reduction of the ferric iron to form oxyferrous complex (Fe^{II}-O_2). The oxyferrous complex then accepts a proton and a second electron to form a ferric hydroperoxide intermediate. The ferric hydroperoxide species hydroxylates the heme α-meso-carbon to produce α-meso-hydroxyheme. A second O_2 is used to oxidize the α-meso-hydroxyheme to verdoheme with the concomitant release of CO. Finally the third O_2 molecule is inserted into the heme macrocycle, thereby cleaving the oxygen bridge to verdoheme. Then verdoheme is converted to biliverdin (BV) with the release of the heme-iron for subsequent metabolic use of the bacteria [16, 50].
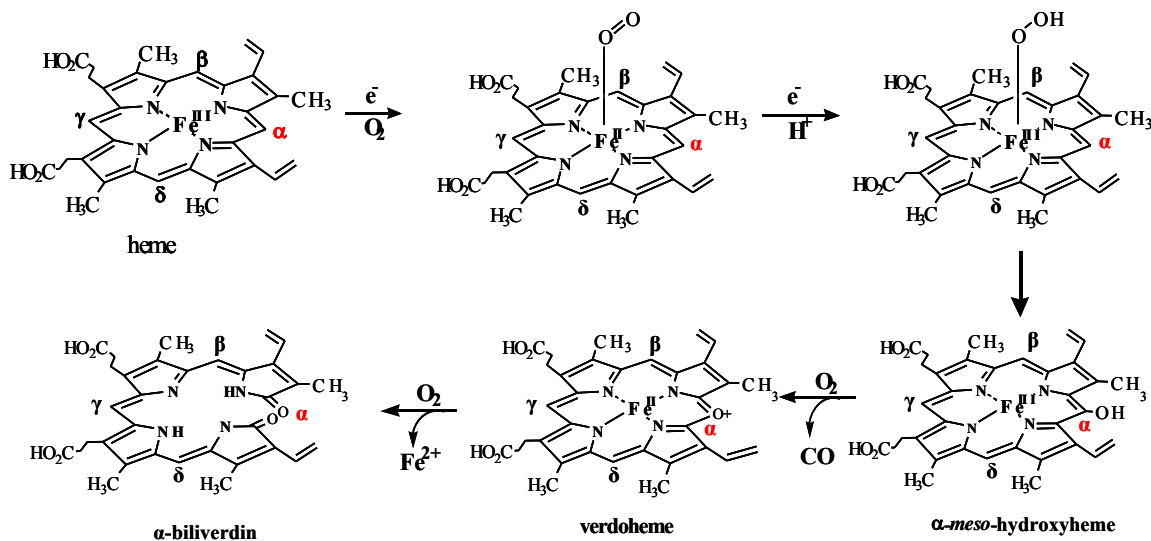
Scheme 1. Oxidative heme degradation catalyzed by heme oxygenase

Hemophores

Hemophores, constitute an independent, highly conserved family of small extracellular heme-binding proteins that do not share homology with any other known proteins. It is thought that hemophores are secreted into the extracellular medium during the early stages of infection when the amount of hemoglobin available is very low to outcompete other bacteria for the very low concentration of available heme-iron from the host animal [30]. Aside from *Pseudomonas aeruginosa,* the hemophore, HasA, has also been found in other gram-negative bacteria such as *Serratia marcescens* (HasA$_{SM}$) [16] which are responsible for urinary tract and wound infections in hospitals [51]; *Pseudomonas fluorescens* (HasA$_{PF}$) [52] which are found in blood isolates of patients who received blood transfusion [53, 54]; and *Yersinia pestis* (HasA$_{YP}$) [11] which is present in bacteria responsible for the bubonic, pneumonic and septicemic plague [55, 56]. The sequence alignments of HasA found in gram-negative bacteria are shown in Figure 3.

Hemophores lack an N-terminus secretion signal but possess secretion signal in the C-terminus [57]. The C-terminus signal of the hemophore is composed of a negatively charged amino acid followed by several hydrophobic residues (Figure 3). HasAp contains the motif, D-L-A-L-A-A. While, HasA$_{SM}$, HasA$_{PF}$ and HasA$_{YP}$ have E-L-L-A-A, D-W-A-L-A-A, and D-M-L-L-A-A, C-terminal motifs, respectively. In the extracellular medium, the hemophore undergoes proteolytic C-terminal cleavages. The cleavage presumably occurred due to the extracellular proteases secreted by the bacteria. HasAp undergoes multiple C-terminal proteolytic cleavage by removing

```
HasA_P      1 MSISISYSTTYSGWTVADYLADWSAYFGDVNHRPGQVVDGSNTGGFNPGP--FDGSQYAL
HasA_SM     1 MAFSVNYDSSFGGYSIHDYLGQWASTFGDVNHTNGN-VTDANSGGFYGGS--LSGSQYAL
HasA_PF     1 MTISVSYEAALGAYSVSDYLTDWALGFNTAGHGS------SNTGGFSNGS--LSGDQYST
HasA_YP     1 MSTTIQYNSNYADYSISSYLREWANNFGDIDQAP---AETKDRGSFSGSSTLFSGTQYAL


HasA_P     59 K-STASDAAFIAGG----DLHYTLFS------NPSHTLWGKLDSIALGDTLTG--GASSG
HasA_SM    58 SSTANQVTAFVAGG----NLTYTLFN------EPAHTLYGQLDSLSFGDGLSG--GDTSP
HasA_PF    53 HGANNSDYAFIADSNTSNGLHYVFNPALPASHNENHYLWGNLDNVQLGTGLGG--GNGSD
HasA_YP    61 GSSHSNPEGMIAEG----DLKYSFMP--------QHTFHGQIDTLQFGKDLATNAGGPSA


HasA_P    106 GYALDSQEVSFSNLGLDSPIAQG------RDG-TVHKVVYGLMSGDSSALQGQIDALLKA
HasA_SM   106 -YSIQVPDVSFGGLNLSSLQAQG------HDG-VVHQVVYGLMSGDTGALETALNGILDD
HasA_PF   111 -FTLDAFKVAFNGLDLSAAQGAG------RVGNDVQNVIYSLMQGNTSALETVLNNLLDD
HasA_YP   106 GKHLEKIDITFNELDLSGEFDSGKSMTENHQG-DMHKSVRGLMKGNPDPMLEVMKAKGIN


HasA_P    159 VDPSLSINSTFDQLAAAGVAHATPAAAAAEVGVVGVQELPHDLALAA
HasA_SM   158 YG--LSVNSTFDQVAAATA-------------VGVQHADSPELLAA
HasA_PF   164 FG--LSTANTFDEISAGLAAHAT--ATTTDVALVGVQDVAQDWALAA
HasA_YP   165 VDTAFKDLSIASQYPDSGYMSDAP-----MVDTVGVVDC-HDMLLAA
```

Figure 3. Amino acid sequence alignment of HasA proteins from *Pseudomonas aeruginosa* (HasAp), *Serratia marcescens* (HasA_SM), *Pseudomonas fluorescens* (HasA_PF) and *Yersinia pestis* (HasA_YP). The alignment was done using ClustalX [58]. The conserved heme ligands are shown in red and the C-terminus secretion signals are shown in blue.

15-21 amino acid residues (Figure 4). On the other hand, HasA_SM and HasA_PF undergo only single C-terminal cleavage by removing the last 12, and 21 residues, respectively (Figure 4) [52, 59]. Moreover, there is no mentioned in the literature if HasA_YF also undergoes C-terminal proteolytic cleavage. It was shown [30] that both uncleaved forms of HasAp and HasA_PF could not deliver heme to HasR_SM, but the cleaved form could. This shows that the extra amino acid residues at the C-terminus could have inhibited the heme transfer by steric hindrance thus preventing a direct

protein-protein interaction between HasR$_{SM}$ and HasAp. However, it cannot be determined which cleaved form of HasAp is biologically relevant [30]. In this research work, we also studied the difference between the full-length and truncated form of HasAp. This is discussed in Chapters 3 and 4.

```
            ↓↓↓↓          ↓
HasAp   1 MSISISYSTT..........QLAAAGVAHATPAAAAAEVGVVGVQELPHDLALAA 205


                                         ↓
HasASM  1 MAFSVNYDSS..........QVAAATA--------------VGVQHADSPELLAA 188


                                       ↓
HasAPF  1 MTISVSYEAA..........EISAGLAAHAT--ATTTDVALVGVQDVAQDWALAA 206
```
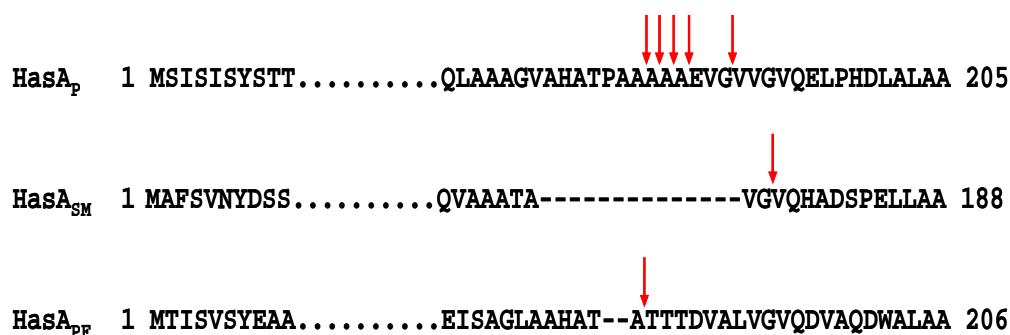
Figure 4. The C-terminal proteolytic cleavage sites of HasAp, HasA$_{SM}$ and HasA$_{PF}$ are indicated by red arrows. HasA$_{SM}$ and HasA$_{PF}$ have only one cleavage site. HasAp has five cleavage sites.

Structure of Hemophore

The first hemophore identified is from the human pathogen, *Serratia marcescens* (HasA$_{SM}$). HasA$_{SM}$ shares 50% identity with HasAp. The X-ray crystal structure of holo HasA$_{SM}$ has been elucidated (Figure 5) [60]. It is a monomeric globular protein that binds *b* heme with a stoichiometry of 1 [61]. The heme-iron is in the ferric form with a very low redox potential (-550 mV *vs*. standard hydrogen

electrode). This low negative redox potential value suggests that reduction of the heme iron is not favorable at aerobic conditions and the heme is not buried within the heme pocket [61]. The fact that HasA$_{SM}$ can take heme from other heme containing proteins suggests that it has a very high affinity for heme. The high heme affinity of the hemophore makes it very efficient in taking up heme from other heme-containing proteins in the extracellular medium. The affininity constant (K$_a$) of HasA$_{SM}$ to heme is 5.2 ($\pm$1.5) x 10^{10} M^{-1} which is considered as one of the highest reported for heme proteins [62].

The X-ray crystal structure of holo-HasA$_{SM}$ shows a unique alpha and beta fold. The four α-helices and the seven anti-parallel β-strands are packed on opposite sides. Two loops (L1 and L2) located at the interface of the α-helices and β-strands of the molecules hold the heme macrocycle [60, 63]. The heme prosthetic group is highly exposed to the solvent with an unusual His32-Tyr75 iron coordination (Figure 5). His32 is located in loop L1 and Tyr75 is in loop L2. The ferric iron is coordinated to the N$_\varepsilon$ of His32, while it is the O$_\eta$ of Tyr75 that coordinates it at the other side. In addition, two crystal structures at pH 4.6 and 8.0 [36] revealed that the phenolate group of Tyr75 forms a hydrogen-bond with the Nδ of His83, another residue close to the heme pocket which further stabilizes the Tyr75O$_\eta$-Fe bond. This was also observed in NMR studies carried out with a gallium (III)-protoporphyrin IX (*GaPPIX*) derivative of HasA$_{SM}$ to prevent the paramagnetic relaxation and resonance

shifts imparted by the heme-iron. His83Nδ1, which has a pKa of 9.7 stabilized the

Tyr75 coordinating conformation via hydrogen-bond [44]. In contrast, the structure at
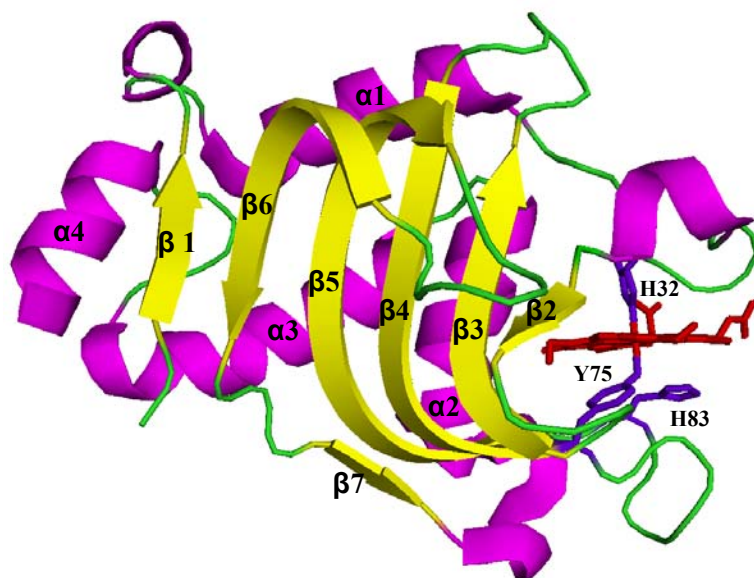
Figure 5. X-ray crystal structure of HasA of *Serratia marcescens* (PDB ID. 1DKO)
highlighting the elements of secondary structure. α-helices are shown in magenta, β-
sheets in yellow, loops in green, heme in red, and the axial ligands His32, Tyr75 and
alternate ligand, His83 in blue.

pH 6.5 showed that there is no H-bond between Tyr75 and His83, instead the Nδ1 of

His83 forms a hydrogen bond with a water molecule [45]. It has been shown by

Létoffé and coworkers [44] that in the absence of Tyr75, His83 can serve as an

alternate ligand. It can also be observed from the sequence alignment in Figure 3 of

the four hemophores that Tyr75 and His83 are conserved in proteins from four distinct bacteria. Thus, the unusual coordination and the flexibility of the heme binding site might give insights on the mechanisms of heme uptake and release. In an effort toward an understanding of this mechanism, in this research work we studied the heme coordination state and electronic structure of HasAp. This is discussed in Chapters 2 and 3.

The NMR structure of apo-HasA$_{SM}$ in solution (Figure 6B) display the same overall structure as that of the holo form except that loop L1 shows a wide conformational rearrangement relative to its position in the holo form as shown in Figure 6A [64]. That loop shows a 30 Å displacement of His32 in the apo form which suggests that apo-HasA is in an open conformation and it closes when it binds heme [64, 65]. This would imply that the upper loop (L1) is more flexible than the loop where Tyr75 and His83 are located. Furthermore, Wolff *et. al.* [64] carried out ^{15}N relaxation measurements to study the backbone dynamics of both the apo and holo forms of HasA$_{SM}$. They used *GaPPIX* as the prosthetic group of the hemophore to overcome the paramagnetic relaxation induced by the heme iron. The results showed some interesting insights on the heme binding and release mechanisms of the hemophore. They have proposed that heme binding occurs via an induced-fit process via loop L1 and they proposed that the flexibility of loop L1 is the one directing the heme binding and release mechanism [64].

The dynamics of L1 are likely necessary to form the closed form of the holo hemophore [64]. The heme binds primarily by the coordination of His32 to the heme iron and also to the Tyr75 ligand. In addition, the heme is also stabilized by the two
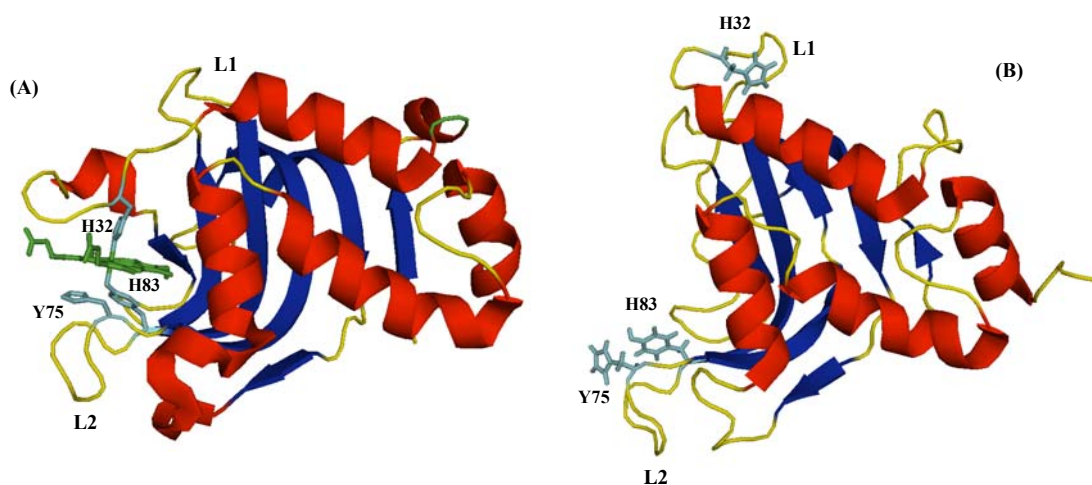
Figure 6. Comparison of the (A) Crystal structure of Holo-HasA$_{SM}$ (PDB ID. 1DKO); and (B) NMR structure of apo-HasA$_{SM}$ (PDB ID. 1YBJ) showing the elements of secondary structure. α-helices in red, β-sheet in blue, loops in yellow, heme in green and ligands in cyan. The apo-HasA$_{SM}$ is in an "open" conformation and the holo form is in a "close" conformation.

hydrogen bonds formed by His32 to Asn41 and Tyr137 located close to the heme pocket. Another two hydrogen bonds formed by His83, also contribute to the stability of the loops. Moreover, the propionate groups of the heme also interact to the

polypeptide by several hydrogen-bonds. It has been postulated by Arnoux, *et. al.* [45] that the formation of these hydrogen-bonds and the "propionate zip" is an essential step in the heme uptake and release mechanism of the hemophore.

Heme Uptake and Release Mechanisms of Hemophore

Work addressing the role of the distal ligands on the heme uptake and release mechanism of the hemophore has been reported. Caillet-Saguy *et. al.* [66] reported that the ^{1}H NMR spectrum of holo-HasA$_{SM}$ shows that the heme has two sets of resonances in a 70:30 ratio. This suggests that there are two heme orientations along the α-γ meso axis. The ^{1}H and ^{13}C NMR resonances also revealed that there is a chemical equilibrium between high-spin (S = 5/2) and low-spin (S = 1/2) species in solution. At higher temperature, the high-spin species is more populated than the low-spin species. The heme-iron could be pentacoordinated or hexacoordinated with an exogenous weak field water ligand, thus the high-spin state is favored [66]. In this research work, we determine the coordination state of HasAp at different temperatures by ^{13}C NMR spectroscopy as discussed in Chapter 3.

Deniau *et. al.* [62] constructed single, double, and triple mutants of the heme ligands of HasA$_{SM}$ to determine the role of these residues in heme binding using ITC. Interestingly, the mutation of the two axial ligands did not produce the same results on the heme binding affinity. The H32A and Y75A mutants resulted into a five-fold and 400-fold decrease in heme affinity, respectively. The results suggest that Tyr75 is a stronger ligand than His32. On the other hand, H83Q and H83A mutants gave

150-fold and 260-fold decrease in heme affinity, respectively. It has been observed that the axial ligands make a very uneven contribution to heme binding which could imply that Tyr75 is located in a more flexible loop than His32 [62]. This result is in contrast to the apo-HasA$_{SM}$ NMR structure and to the dynamic study [64] which showed that His32 is located in a more flexible loop than Tyr75. It can also be noted in this thermodynamic study that there is a much greater loss of heme affinity in His83A than in His32A HasA$_{SM}$ mutants. Hence, His83 is important in heme binding even though it is not directly coordinated to the heme iron. Therefore, it has been concluded that the Tyr75/His83 pair has an important implication in the heme uptake and release mechanism.

On the other hand, Raman spectroscopic studies [67] of the wild type and single mutants CO-complexes revealed that the His32 ligand was displaced by CO instead of Tyr75 unlike some proteins with His/Tyr coordination states. This supported the thermodynamics study [62] that Tyr75 is a stronger ligand than His32. The absence of hydrogen bond between His32 and CO demonstrates that there is another bonding interaction in the heme pocket which stabilized His32. Thus, Lukat-Rodgers *et. al.* [67], proposed that a similar dissociation state happen when heme is captured and delivered to the receptor.

Deniau *et. al.* [62] also determined that the heme affinity of the cleaved (without 12 C-terminal residues) and the uncleaved forms of HasA$_{SM}$ are the same. The affinity of HasA for heme is higher than that of HasR. It is interesting to note that HasA can transfer its heme to HasR, suggesting that this mechanism is driven by

direct protein-protein interaction. According to Létoffé *et. al.* [63], two independent β-strands, S51-T60 and G95-S107 of the HasA$_{SM}$ are involved in the interaction with its cognate receptor. In addition, Caillet-Saguy *et. al.* [66] proposed that during HasA$_{SM}$-HasR$_{SM}$ binding, HasA$_{SM}$ might become distorted in a way that the Tyr75-His83 hydrogen bond is broken and consequently weakened the Fe-Tyr75 bond.

The heme-iron in HasR$_{SM}$ is coordinated to two histidine ligands. Interestingly, mutation of the two histidines abolished the heme binding and heme transport, but did not affect HasA$_{SM}$ binding. Thus, it is concluded that the heme transfer from the hemophore to its receptor is not only driven by direct protein-protein interaction, but also depends on the bis-histine ligands of the receptor [46].

RESEARCH PROBLEM AND RATIONALE

Iron is an important nutrient for the opportunistic pathogen, *Pseudomonas aeruginosa* to efficiently colonize and infect a host animal [68, 69]. The poor bioavailability of iron in the host animal, however, presents a major problem. It is believed that in the early stages of infection when the iron concentration is very low, the heme acquisition system (*has*) available is activated and the hemophore, HasAp, is released into the extracellular medium to "steal" heme from heme containing proteins. A sensible way to prevent the colonization of the bacteria is to try to stop it in the early stages of infection before the host's immune system is weakened. Moreover, preventing heme-iron acquisition of the bacteria is important to stop

infection in the host animal. Insights gained on the understanding of the mechanism of how HasAp scavenge heme from heme proteins would provide opportunities to design drugs to inhibit the heme acquisition at the early stages of infection and thereby controlling the diseases associated with this pathogenic bacteria. Studying the structure-function relationship of this protein would also serve to understand the hemophores in general. Although the hemophore from *Serratia marcescens* has been structurally and biochemically characterized, there are still several questions that need to be addressed especially on the context of the mechanism of heme uptake.

In this context, this research work is aimed towards an understanding of the structure-function of the hemophore from *Pseudomonas aeruginosa*. The mechanism by which HasAp "steal" heme from other heme proteins is not known. Elucidation of this mechanism would entail studying the coordination state and electronic structure of the heme active site. One method that can be used to study the heme active site is ^{13}C NMR spectroscopy coupled with the biosynthetic preparation of ^{13}C-labeled heme to overcome the low natural abundance of ^{13}C [70, 71]. In Chapter 2, we developed a ^{13}C NMR spectroscopic method to differentiate the coordination state of high spin (S = 5/2) heme complex. Wild type sperm whale myoglobin and its H64V mutant were used as the hexa- and pentacoordinate high spin (S = 5/2) model heme complexes. The results showed that the magnitude of the ^{13}C chemical shifts of the core heme carbons can be employed as a simple diagnostic tool to determine the coordination state of the heme active sites, irregardless of the nature of the axial ligands. This

method was also used to determine the coordination state of a protein ShuT, a protein from *Shigella dysenteriae*.

In Chapter 3, this method was applied to determine the coordination state and electronic structure of the HasAp protein, along with other spectroscopic techniques, such as electronic absorption spectroscopy, and electron paramagnetic resonance (EPR). In addition, we did preliminary investigation by electronic absorption spectroscopy to determine if HasAp can capture heme regardless of the iron oxidation state through passive diffusion as reported for the HasA$_{SM}$. The rate of heme transfer from hemoglobin to HasAp was measured by stopped-flow spectroscopy. This chapter also reports the X-ray crystal structure of the truncated holo HasAp (without 21 C-terminal residues). Chapter 3 also reports the backbone amide assignments of the holo full-length and truncated HasAp as well as the truncated apo-HasAp by NMR. This was done by using triple resonance experiments and amino acid selective labeling of some residues affected by the paramagnetic relaxation of the heme-iron. Secondary structure assignments of the holo-HasAp full-length and truncated proteins were assigned using a combination of X-ray crystallography and NMR spectroscopy data. In addition, the difference between the apo and holo truncated HasAp was also determined. To probe the location of the tail in the structure in solution, ^{1}H-^{1}H NOE connectivities from the tail to the nearby residues were determined using 3D NOESY-HSQC NMR experiment. Conformational dynamics study of the holo truncated HasAp studied using the amide hydrogen-deuterium exchange experiment monitored by NMR is also presented in this chapter.

Chapter 4 describes the attempts to study the protein-protein interaction of HasAp and hemoglobin at the molecular level using the chemical shift perturbation analysis by NMR and by mapping of the binding interactions in the X-ray structure of HasAp.

REFERENCES

1. Berlutti, F., Morea, C., Battistoni, A., Sarli, S., Cipriani, P., Superti, F., Ammendolia, M. G., and Valenti, P., *Iron Availability Influences Aggregation, Biofilm Adhesion and Invasion of Pseudomonas aeruginosa and Burkholderia cenocepacia.* Int. J. Immunopathol. Pharmacol, 2005. **18**: p. 661-670.

2. Christensen, L.D., Moser, C., Jensen, P. O., Rasmussen, T. B., Christophersen, L., Kjelleberg, S., Kumar, N., Hoiby, N., Givskov, M., and Bjarnsholt, T., *Impact of Pseudomonas aeruginosa Quorum Sensing on Biofilm Persistence in an in Vivo Intraperitoneal Foreign-Body Infection Model.* Microbiology, 2007. **153**: p. 2312-2320.

3. Nouwens, A., Beatson, S. A., Whitchurch, C. B., Walsh, B. J., Schweizer, H. P., Mattick, J. S., and Cordwell, S. J., *Proteome Analysis of Extracellular Proteins Regulated by las and rhl quorum sensing systems in Pseudomonas aeruginosa PAO1.* Microbiology, 2003. **149**: p. 1311-1322.

4. Ochsner, U.A., Johnson, Z., and Vasil, M. L., *Genetics and Regulation of Two Distinct Haem-Uptake Systems, phu and has, in Pseudomonas aeruginosa.* Microbiology, 2000. **146**: p. 185-198.

5. Wang, C.Y., Jeng, J. S., Cheng, K. Y., Lee, L. N., Yu, C. J., Hsueh, P. R., and Yang, P. C., *Pandrug-Resistant Pseudomonas aeruginosa among Hospitalised Patients: Clinical Features, Risk-Factors and Outcomes.* Clin. Microbiol. Infect., 2006. **12**: p. 63-68.

6. Peng, X., Xu, C., Ren, H., Lin, X., Wu, L., and Wang, S., *Proteomic Analysis of the Scarcosine-Insoluble Outer Membrane Fraction of Pseudomonas*

aeruginosa Responding to Ampicillin, Kanamycin, and Tetracycline Resistance. J. Proteome. Res., 2005. **4**: p. 2257-2265.

7.   *Pseudomonas Infections.* [cited; Available from: http://www.healthatoz.com/healthatoz/Atoz/ency/pseudomonas_infections.jsp.

8.   Clarke, T.E., Tari, L. W., and Vogel, H. J., *Structural Biology of Bacterial Iron Uptake Systems.* Curr. Top. Med. Chem., 2001. **1**: p. 7-30.

9.   Braun, V., *Iron Uptake Mechanisms and Their Regulation in Pathogenic Bacteria.* J. Med. Microbiol., 2001. **291**: p. 67-79.

10. Létoffé, S., Ghigo, J. M., and Wandersman, C., *Iron Acquisition from Heme and Hemoglobin by a Serratia marcescens Extracellular Protein.* Proc. Natl. Acad. Sci., 1994. **91**: p. 9876-9880.

11. Rossi, M.-S., Fetherston, J. D., Létoffé, S., Carniel, E., Perry, R. D., and Ghigo, J. -M., *Identification and Characterization of the Hemophore-Dependent Heme Acquisition System of Yersinia pestis.* Infect. Immun., 2001. **69**: p. 6707-6717.

12. Vasil, M.L., *How We Learnt About Iron Acquisition in Pseudomonas aeruginosa: A Series of Very Fortunate Events.* Biometals, 2007. **20**: p. 587-601.

13. Wandersman, C., and Stojiljkovic, I., *Bacterial Heme Sources: The Role of Heme, Hemoprotein Receptors and Hemophores.* Curr. Opin. Microbiol., 2000. **3**: p. 215-220.

14. Ochsner, U.A., Vasil, A. I., and Vasil, M. L., *Role of the Ferric Uptake Regulator of Pseudomonas aeruginosa in the Regulation of Siderophores and Exotoxin A Expression: Purification and Activitiy on Iron-Regulated Promoters.* J. Bacteriol., 1995. **177**: p. 7194-7201.

15. Létoffé, S., Delepelaire, P., and Wandersman, C., *Free and Hemophore-Bound Heme Acquisitions Through the Outer Membrane Receptor HasR Have Different Requirements for the TonB-ExbB-ExbD Complex.* J. Bacteriol., 2004. **186**: p. 4067-4074.

16. Poole, K., and McKay, G. A., *Iron Acquisition and Its Control in Pseudomonas aeruginosa: Many Roads Lead To Rome.* Front. Biosci., 2003. **8**: p. 661-686.

17.   Ghigo, J.-M., Létoffé, S., and Wandersman, C., *A New Type of Hemophore-Dependent Heme Acquisition System of Serratia marcescens Reconstituted in Escherichia coli.* J. Bacteriol., 1997. **179**: p. 3572-3579.

18.   Binet, R., and Wandersman, C., *Cloning of the Serratia marcescens hasF Gene Encoding the Has ABC Exporter Outer Membrane Component: a TolC Analog.* Mol. Microbiol., 1996. **22**: p. 265-273.

19.   Arevalo-Ferro, C., Hentzer, M., Reil, G., Gorg, A., Kjelleberg, S., Givskov, M., Riedel, K., and Eberl, L., *Identification of Quorum-Sensing Regulated Proteins in the Opportunistic Pathogen Pseudomonas aeruginosa by Proteomics.* Envi. Microbiol., 2003. **5**: p. 1350-1369.

20.   Bottomley, M.J., Muraglia, E., Bazzo, R., and Carfi, A., *Molecular Insights into Quorum Sensing in the Human Pathogen Pseudomonas aeruginosa from the Structure of the Virulence Regulator LasR Bound to Its Autoinducer.* J. Biol. Chem., 2007. **282**: p. 13592-13600.

21.   Cornelis, P., and Aendekerk, S., *A New Regulator Linking Quorum Sensing and Iron Uptake in Pseudomonas aeruginosa.* Microbiology, 2004. **150**: p. 752-756.

22.   Williams, P., Winzer, K., Chan, W. C., and Camara, M., *Look Who's Talking: Communication and Quorum Sensing in the Bacterial World.* Phil. Trans, R. Soc. B, 2007. **362**: p. 1119-1134.

23.   Duan, K., and Surette, M. G., *Environmental Regulation of Pseudomonas aeruginosa PAO1 Las and Rhl Quorum-Sensing Systems.* J. Bacteriol., 2007. **189**: p. 4827-4836.

24.   Sandoz, K.M., Mitzimberg, S. M., and Schuster, M., *Social Cheating in Pseudomonas aeruginosa Quorum Sensing.* Proc. Natl. Acad. Sci., 2007. **40**: p. 15876-15881.

25.   Wagner, V.E., Gillis, R. J., Iglewski, B. H., *Transcriptome Analysis of Quorum-Sensing Regulation and Virulence Factor Expression in Pseudomonas aeruginosa.* Vaccine, 2004. **22S**: p. S15-S20.

26.   Schuster, M., and Greenberg, E. P., *A Network of Networks: Quorum Sensing Gene Regulation in Pseudomonas aeruginosa.* Int. J. Med. Microbiol., 2006. **296**: p. 73-81.

27. Fuqua, C., and Greenberg, E. P., *Census and Consensus in Bacterial Ecosystems: The LuxR-LuxI Family of Quorum-Sensing Transcriptional Regulators.* Nat. Rev. Mol. Cell Biol., 2002. **3**: p. 685-695.

28. Smith, R.S., and Iglewski, B. H., *P. aeruginosa Quorum-Sensing Systems and Virulence.* Curr. Opin. Microbiol., 2003. **6**: p. 56-60.

29. Juhas, M., Eberl, L., and Tummler, B., *Quorum-Sensing: The Power of Cooperation in the World of Pseudomonas.* Environ. Microbiol., 2005. **7**: p. 459-471.

30. Létoffé, S., Redeker, V., and Wandersman, C., *Isolation and Characterization of An Extracellular Haem-Binding Protein From Pseudomonas aeruginosa That Shares Function and Sequence Similarities with Serratia marcescens HasA Haemophore.* Mol. Microbiol., 1998. **28**: p. 1223-1234.

31. Izadi-Pruneyre, N., Wolff, N., Castagne, C., Czisch, M., Wandersman, C., Delepierre, M., and Lecroisey, A., *Backbone NMR Assignment and Secondary Structure of the 19kDa Hemophore HasA.* J. Biomol. NMR, 1999. **14**: p. 193-194.

32. Olson, J.C., and Ohman, D. E., *Efficient Production and Processing of Elastase and LasA by Pseudomonas aeruginosa Require Zinc and Calcium Ions.* J. Bacteriol., 1992. **174**: p. 4140-4147.

33. Vasil, M.L., and Ochsner, U. A., *The Response of Pseudomonas aeruginosa to Iron: Genetics, Biochemistry and Virulence.* Mol. Microbiol., 1999. **34**: p. 399-413.

34. Hantke, K., *Iron and Metal Regulation in Bacteria.* Curr. Opin. Microbiol., 2001. **4**: p. 172-177.

35. Baichoo, N., and Helmann, J. D., *Recognition of DNA by Fur: A Reinterpretation of the Fur Box Consensus Sequence.* J. Bacteriol., 2002. **184**: p. 5826-5832.

36. Bivelle, F., Cwerman, H., Létoffé, S., Rossi, M.-S., Drouet, V., Ghigo, J. M., and Wandersman, C., *Haemophore-Mediated Signalling in Serratia marcescens: A New Mode of Regulation for an Extra Cytoplasmic Function (ECF) Sigma Factor Involved in Haem Acquisition.* Mol. Microbiol., 2004. **53**: p. 1267-1277.

37.   Rossi, M.-S., Paquelin, A., Ghigo, J. -M., and Wandersman, C., *Haemophore-Mediated Signal Transduction Across the Bacterial Cell Envelope in Serratia marcescens: The Inducer and the Transported Substrate are Different Molecules.* Mol. Microbiol., 2003. **48**: p. 1467-1480.

38.   Cwerman, H., Wandersman, C., and Biville, F., *Heme and a Five-Amino-Acid Hemophore Region Form the Bipartite Stimulus Triggering the has Signalling Cascade.* J. Bacteriol., 2006. **188**: p. 3357-3364.

39.   Cescau, S., Cwerman, H., Létoffé, S., Delepelaire, P., Wandersman, C., and Biville, F., *Heme Acquisition by Hemophores.* Biometals, 2007. **20**: p. 603-613.

40.   Wolff, N., Sapriel, G., Bodenreider, C., Chaffotte, A., and Delepelaire, P., *Antifolding Activity of the SecB Chaperone is Essential for Secretion of HasA, a Quickly Folding ABC Pathway Substrate.* J. Biol. Chem., 2003. **278**: p. 38247-38253.

41.   Sapriel, G., Wandersman, C., and Delepelaire, P., *The SecB Chaperone is Bifunctional in Serratia marcescens: SecB is Involved in the Sec Pathway and Required for HasA Secretion by the ABC Transporter.* J. Bacteriol., 2003. **185**: p. 80-88.

42.   Delepelaire, P., and Wandersman, C., *The SecB Chaperone is Involved in the Secretion of the Serratia marcescens HasA Protein Through an ABC Transporter.* Embo J., 1998. **17**: p. 936-944.

43.   Debarbieux, L., and Wandersman, C., *Folded HasA Inhibits Its Own Secretion throught Its ABC Exporter.* Embo J., 2001. **20**: p. 4657-4663.

44.   Létoffé, S., Deniau, C., Wolff, N., Dassa, E., Delepelaire, P., Lecroisey, A., and Wandersman, C., *Haemophore-Mediated Bacterial Haem Transport: Evidence for a Common of Overlapping Site for Haem-Free and Haem-Loaded Haemophore on its Specific Outer Membrane Receptor.* Mol. Microbiol., 2001. **41**: p. 439-450.

45.   Arnoux, P., Haser, R., Izadi, N., Lecroisey, A., and Czjzek, M., *Functional Aspects of the Heme Bound Hemophore HasA By Structural Analysis of Various Crystal Forms.* Proteins, 2000. **41**: p. 202-210.

46. Izadi-Pruneyre, N., Huche, F., Lukat-Rodgers, G. S., Lecroisey, A., Gilli, R., Rodgers, K. R., Wandersman, C. and Delepelaire, P., *The Heme Transfer from the Soluble HasA Hemophore to Its Membrane-Bound Receptor HasR is Driven by Protein-Protein Interaction from a High to a Lower Affinity Binding Site.* J. Biol. Chem., 2006. **281**: p. 25541-25550.

47. Tenhunen, R., Marver, H., Pimstone, N. R., Trager, W. F., Cooper, D. Y., and Schmid, R., *Enzymatic Degradation of Heme. Oxygenative Cleavage Requiring Cytochrome P-450.* Biochemistry, 1972. **11**: p. 1716-1720.

48. Ortiz de Montellano, P.R., and Wilks, A., *Heme Oxygenase Structure and Mechanism.* Adv. Inorg. Chem., 2000. **51**: p. 359-402.

49. Wang, A., Zeng, Y. Han, H., Weeratunga, S., Morgan, B. N., Moenne-Loccoz, P., Schonbronn, E., and Rivera, M., *Biochemical and Structural Characterization of Pseudomonas aeruginosa Bfd and FPR: Ferredoxin NADP$^+$ Reductase and Not Ferredoxin Is the Redox Partner of Heme Oxygenase under Iron-Starvation Conditions.* Biochemistry, 2007. **46**: p. 12198-12211.

50. Ratliff, M., Zhu, W., Deshmukh, R., Wilks, A., and Stojiljkovic, I., *Homologues of Neisserial Heme Oxygenase in Gram-Negative Bacteria: Degradation of Heme by the Product of the pigA Gene or Pseudomonas aeruginosa.* J. Bacteriol., 2001. **183**: p. 6394-6403.

51. Hejazi, A., Falkiner, F. R., *Serratia Marcensces.* J. Med. Microbiol., 1997. **46**: p. 903-912.

52. Létoffé, S., Omori, K., and Wandersman, C., *Functional Characterization of the HasA$_{PF}$ Hemophore and Its Truncated and Chimeric Variants: Determination of a Region Involved in Binding to the Hemophore Receptor.* J. Bacteriol., 2000. **182**: p. 4401-4405.

53. Wei, B., Huang, T., Dalwadi, H., Sutton, C. L., Bruckner, D., and Braun, J., *Pseudomonas Fluorescens Encodes the Crohn's Disease-Associated I2 Sequence and T-Cell Superantigen.* Infect. Immun., 2002. **70**: p. 6567-6575.

54. Hseuh, P.-R., Feng, L. -J., Pan, H. -J. Chen, Y. -C., Sun, C. -C., Ho, S. -W., and Luh, K. -T., *Outbreak of Pseudomonas Fluorescens Bacteremia Among Oncology Patients.* J. Clin. Microbiol., 1998. **36**: p. 2914-2917.

55. Ryan, K.J., and Ray, C. G., *Sherris Medical Microbiology.* 4th ed. 2004: McGraw-Hill.

56.   Smiley, S.T., *Current Challenges in the Development of Vaccines by Pneumonic Plague.* Expert Rev. Vaccines, 2008. **7**: p. 209-221.

57.   Sapriel, G., Wandersman, C., and Delepelaire, P., *The N Terminus of the HasA Protein and the SecB Chaperone Cooperate in the Efficient Targeting and Secretion of HasA Via the ATP-Binding Cassette Transporter.* J. Biol. Chem., 2002. **277**: p. 6726-6732.

58.   Larkin, M.A., Blackshields, G., Brown, N. P., Chenna, R., McGettigan, P. A., McWilliam, H., Valentin, F., Wallace, I. M., Wilm, A., Lopez, R., Thompson, J. D., Gibson, T. J., and Higgins, D. G., *ClustalW and ClustalX Version 2.0.* Bioinformatics, 2007. **23**: p. 2947-2948.

59.   Izadi-Pruneyre, N., Wolff, N., Redeker, V., Wandersman, C., Delepierre, M., and Lecroisey, A., *NMR Studies of the C-Terminal Secretion Signal of the Haem-Binding Protein, HasA.* Eur. J. Biochem., 1999. **261**: p. 562-568.

60.   Arnoux, P., Haser, R., Izadi, N., Lecroisey, A., Delepierre, M., Wandersman, C., and Czjzek, M., *The Crystal Structure of HasA, A Hemophore Secreted by Serratia Marcescens.* Nat. Struct. Biol., 1999. **6**: p. 516-520.

61.   Izadi, N., Henry, Y., Haladjian, J., Goldberg, M. E., Wandersman, C., Delepierre, M., and Lecroisey, A., *Purification and Characterization of an Extracellular Heme-Binding Protein, HasA, Involved in Heme Iron Acquisition.* Biochemistry, 1997. **36**: p. 7050-7057.

62.   Deniau, C., Gilli, R., Izadi-Pruneyre, N., Létoffé, S., Delepierre, M., Wandersman, C., Briand, C., and Lecroisey, A., *Thermodynamics of Heme Binding to the HasA$_{SM}$ Hemophore: Effect of Mutations at Three Key Residues for Heme Uptake.* Biochemistry, 2003. **42**: p. 10627-10633.

63.   Létoffé, S., Debarbieux, L., Izadi, N., Delepelaire, P., and Wandersman, C., *Ligand Delivery by Haem Carrier Proteins: The Binding of Serratia marcescens Haemophore to Its Outer Membrane Receptor is Mediated by Two Distinct Peptide Regions.* Mol. Microbiol., 2003. **50**: p. 77-88.

64.   Wolff, N., Izadi-Pruneyre, N., Couprie, J., Habeck, M., Linge, J., Riepeng, W., Wandersman, C., Nilges, M., Delepierre, M., and Lecroisey, A., *Comparative Analysis of Structural and Dynamic Properties of the Loaded and Unloaded Hemophore HasA: Functional Implications.* J. Mol. Biol., 2008. **376**: p. 517-525.

65.   Cescau, S., Debarbieux, L., and Wandersman, C., *Probing the In Vivo Dynamics of Type I Protein Secretion Complex Association through Sensitivity to Detergent.* J. Bacteriol., 2007. **189**: p. 1496-1504.

66.   Caillet-Saguy, C., Delepierre, M., Lecroisey, A., Bertini, I., Piccioli, M., and Turano, P., *Direct-Detected ^{13}C NMR to Investigate the Iron(III) Hemophore HasA.* J. Am. Chem. Soc., 2006. **128**: p. 150-158.

67.   Lukat-Rodgers, G.S., Rodgers, K. R., Caillet-Saguy, C., Izadi-Pruneyre, N., and Lecroisey, A., *Novel Heme Ligand Displacement by CO in the Soluble Hemophore HasA and Its Proximal Ligand Mutants: Implications for Heme Uptake and Release.* Biochemistry, 2008.

68.   Martinez, J.L., Delgado-Iribarren, A., and Baquero, F., *Mechanisms of Iron Acquisition and Bacterial Virulence.* FEMS Microbiol. Rev., 1990. **75**: p. 45-56.

69.   Griffiths, E., *Iron and Bacterial Virulence - A Brief Overview.* Biometals, 1991. **4**: p. 7-13.

70.   Rivera, M., and Caignan, G. A., *Recent Developments in the ^{13}C NMR Spectroscopic Analysis of Paramagnetic Hemes and Heme Proteins.* Anal. Bioanal. Chem., 2004. **378**: p. 1464-1483.

71.   Rivera, M., and Walker, F. A., *Biosynthesis of Isotopically Enriched Protohemin IX.* Anal. Biochem., 1995. **230**: p. 295-302.

CHAPTER 2

^{13}C NMR Spectroscopy of Core Heme Carbons as a Simple Tool to Elucicate the Coordination State of Ferric High-Spin Heme Proteins

INTRODUCTION

Rapid elucidation of the coordination and spin state is desirable because the advent of genomics and proteomics has brought about the discovery of new and interesting heme proteins. Many of these new proteins are thought to act as heme transporter, heme degrading, or heme storage proteins and enzymes [1-4]. Detailed understanding of how these proteins acquire heme, bind it tightly, or pass it on to another protein, often starts with an understanding of the heme coordination state and heme electronic structure. Novel heme proteins exhibiting a high-spin state can be either five-coordinate, with only one protein-provided axial ligand, or six-coordinate, with one strong-field axial ligand and a weak-field sixth ligand that can be protein provided or exogenous.

Spectroscopic elucidation of the coordination state of high-spin heme proteins as five- or six-coordinate is not straightforward. In this context, it is noteworthy that recent studies have shown that the study of core porphyrin carbon chemical shifts is a powerful approach to determine the electronic structure of model ferrihemes [5-11] and heme active sites [11-14]. Observation and assignment of core porphyrin carbons can be more challenging than the observation and assignment of their protonated

counterparts because the proximity of core carbons to the heme iron makes their resonances more strongly affected by the unpaired electron. Nevertheless, efforts to detect, assign, and interpret core porphyrin carbon chemical shifts can be highly rewarding because relatively straightforward correlations permit one to gain valuable insights into the coordination state and electronic structure of ferrihemes [12, 15]. In this report, we demonstrate that detection of core porphyrin carbon resonances from high-spin ferriheme active sites can be made in a relatively straightforward manner and the magnitude of these shifts lead to unambiguous determination of the coordination state.

It has been known for quite some time that the most striking difference in the ^{1}H NMR spectra of five- and six-coordinate high-spin ferrihemes is the reversal in sign of the meso-H isotropic shift [16-18]. Thus, 6-coordinate ferrihemes exhibit meso-H resonances near 40 ppm, whereas the equivalent resonances in 5-coordinate ferrihemes occur near -25 ppm. The molecular orbital properties underlying this sign reversal brought about by heme coordination state are now fully understood [19] (discussed below). However, it is important to appreciate that perhaps the most important reason that this phenomenon has not been utilized to differentiate five- and six-coordinate high-spin ferriheme centers in proteins and enzymes is the extreme breadth of the meso-H resonances. This is illustrated in Figure 1 which allows comparison of the ^{1}H NMR spectrum of wild-type met sperm-whale myoglobin (sw-Mb) (Figure 1A) and that obtained from the corresponding H64V mutant (Figure 1B). In the ferric oxidation state, the heme iron of met-sw-Mb is six-coordinate high-spin,
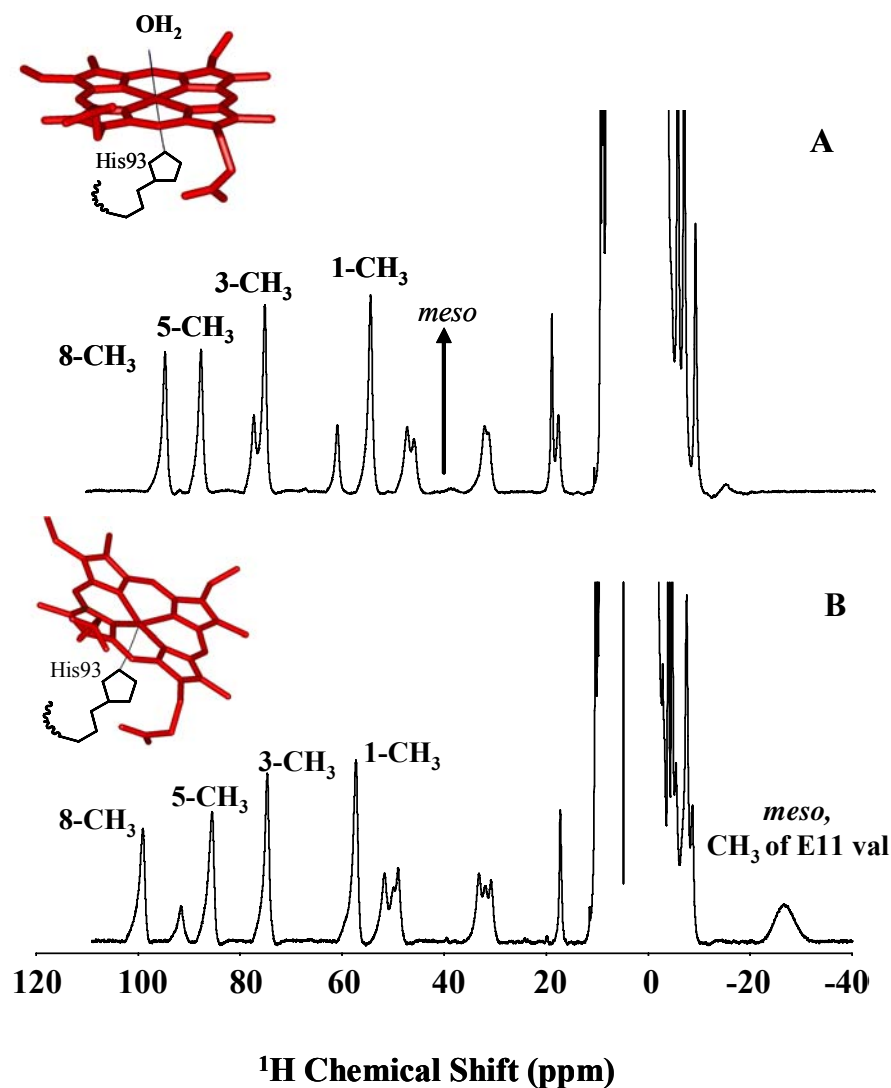
Figure 1. ^{1}H NMR spectra of hexacoordinate, wild-type sperm whale myoglobin (A) and pentacoordinate H64V sperm-whale myoglobin (B). The resonance assignments were obtained from ref. 17. Note the broad line width and consequent low intensity of the meso-H resonance in A. The corresponding resonance in B is buried under the methyl group of Val E11.

with proximal histidine (His-93) and a distal H_2O serving as axial ligands [17]. The distal H_2O ligand in Mb is hydrogen bonded to the N_ε atom of the distal histidine (His64); disruption of this hydrogen bond by the replacement of His-64 for Val results in a five-coordinate high-spin met-Mb (H64V-sw-Mb) devoid of the sixth H_2O ligand [20, 21].

La Mar and coworkers demonstrated that the meso-H resonce in the ^{1}H NMR spectrum of the H64V mutant (Figure 1B) is buried under the methyl resonance originating from Val E11, near -29 ppm. In comparison, the meso-H signal in the six-coordinate wild-type sw-Mb resonates near 40 ppm (Figure 1A). It is important to point out, however, that it is not trivial to assign meso-H resonances from high-spin ferrihemes because of the fast relaxation properties typical of $S = 5/2$ ferrihemes. Hence, although the magnitude of the meso-H shift is indicative of the coordination state in high-spin ferrihemes, the challenges associated with the assignment of very broad meso-H resonances render this approach impractical as an efficient method to establish coordination state. In this context, it is well-known that the relaxation rates of resonances affected by a paramagnetic center scale with the square of the magnitude of the gyromagnetic ratio [22, 23]. Hence, the effect of paramagnetism on ^{13}C relaxation is reduced ~16-fold with respect to ^{1}H, which results in narrower and therefore more readily observable ^{13}C resonances. We capitalized on this physical property to demonstrate that meso-carbon resonances from heme proteins are readily detected, thus providing a relatively straightforward spectroscopic diagnosis of the coordination state of high-spin ferric heme active sites.

EXPERIMENTAL PROCEDURES

General Methods

The recombinant pET29a plasmid harboring a gene coding for wild-type sperm whale myoglobin was a generous gift from Dr. Mark Hargrove, Iowa State University. The corresponding H64V mutation was carried out using the polymerase chain reaction (PCR) and the Quickchange Mutagenesis Kit from Stratagene (La Jolla, CA). Oligonucleotides were synthesized at the Biotechnology Support Facility, University of Kansas Medical Center and used without further purification. The mutagenic primers designed to introduce the H64V mutation are 5' – GCTTCTGAAGATCTGAAAAAA<u>GTT</u>GGTGTTACCGTGTTAACTGCC- 3' and 5' – GGCAGTTAACACGGTAACACC<u>AAC</u>TTTTTTCAGATCTTCAGAAGC -3'. The underlined codons represent mismatches introduced to generate the mutations. The recombinant construct was transformed into *Escherichia coli* XL1-Blue supercompetent cells for amplification. Once the mutation has been confirmed by sequencing, the recombinant DNA plasmid was transformed into *Escherichia coli* BL21 (DE3) GOLD cells for subsequent protein expression.

Expression and Purification of Wild-Type and Mutant Sperm Whale Mb Proteins

E. coli BL21(DE3)GOLD cells (Stratagene, La Jolla, CA) were used as the protein expression host. A single colony of freshly transformed cells was cultured overnight in 10 mL of Luria Bertani (LB) medium containing 50 μg/mL kanamycin.

The cells were subsequently subcultured into fresh 1 L LB-kanamycin medium and grown at 37 °C with continuous shaking at 225 rpm. Once the cell culture reached an optical density of 1.0, expression was induced by addition of isopropyl-β-D-thiogalactopyranose (IPTG) to a final concentration of 1 mM. Approximately 10 min after induction of protein synthesis, 17 mg of δ-aminolevulinic acid (ALA) and 100 mg of $FeSO_4 \bullet 7H_2O$ were added to each liter of cell culture. The cells were grown for an additional of 4-5 h at 30 °C and harvested by centrifugation. The harvested cells were resuspended and lysed and the soluble protein fraction was recovered using previously described protocols [24]. Ammonium sulfate was added to the supernatant (60% saturation, 2.4 M), and the resultant mixture was centrifuged at 23 500 rpm for 1 h. The supernatant was recovered and treated with 20 mM Tris buffer (pH 8.0) to bring the concentration of ammonium sulfate to 1.9 M. The resultant solution was loaded onto a phenyl Sepharose column (2.6 cm i.d. x 30 cm length) pre-equilibrated with 1.9 M ammonium sulfate in 20 mM Tris buffer (pH 8.0) and eluted with a solution of 0.9 M ammonium sulfate in 20 mM Tris buffer (pH 8.0). Fractions with an absorbance ratio (A_{280}/A_{410}) and (A_{280}/A_{395}) of <1.0 for wild type and H64V mutant, respectively were pooled, dialyzed extensively against phosphate buffer ($\mu=$ 0.10, pH 6.0) at 4 °C, concentrated by ultrafiltration, and loaded onto Sephadex G-50 column (2.6 cm i.d. x 90 cm length). Fractions with an absorbance ratio (A_{280}/A_{Soret}) of <0.5 were pooled and concentrated by ultrafiltration. Heme from Mb was extracted using Teale's method [25] to make apo-protein. The apo-Mb proteins were stored at -80 °C.

Expression and Purification of ShuT

The recently discovered heme protein from *Shigella dysenteriae* (ShuT) was expressed and purified as previously described [2]. Briefly, a 100 mL subculture of *E. coli* BL21 (DE3) plysS harboring pETShuT in LB-ampicillin (OD_{600} = 0.6) was used to inoculate 1 L cultures to an OD_{600} of 0.06. The cells were grown to an OD_{600} of 0.6-0.8 and induced with 1 mM isopropyl-*β*-D-thiogalactopyranose (IPTG); then, they were grown for an additional 4 h at 30 °C. The cells were harvested by centrifugation for 20 min at 6000 g in a Beckman JA-20 rotor. The cells were lysed at 4 °C by stirring in 50 mM sodium phosphate (pH 8.0) containing 100 mg of lysozyme/100 mL of cell lysate, 0.2 mM PMSF, and a protease inhibitor cocktail (Roche Diagnostics GmBH).

The periplasmic fraction was isolated by centrifugation at 3000 g for 30 min, and the resulting supernatant was again centrifuged at 6800 g for 30 min. the clarified solution was applied to an Ni-NTA agarose column (1 x 10 cm), and the protein was eluted in 20 mM Tris-HCl (pH 7.8) containing 250 mM imidazole and 300 mM NaCl, following previous wash steps (20 column volumes) in the same buffer containing 20 mM imidazole. The peak fractions, as judged by SDS-page, were pooled and dialyzed in 20 mM Tris-HCl (pH 7.5), concentrated to 10 mg/mL, and stored at -80 °C.

Preparation of Mb and ShuT Samples Reconstituted with ^{13}C-Labeled Heme

^{13}C-labeled *δ*-aminolevulinic acid (ALA) were prepared using a previously reported methodology [26] and were used as precursors for the biosynthetic

preparation of ^{13}C-labeled protoheme IX (heme) [12, 24, 27]. [5-^{13}C]-ALA was used to label heme at the meso (C_m) and α-pyrrole (C_α) positions, and [4-^{13}C]-ALA was used to label heme at the C_α and β pyrrole (C_β) carbons (see Figure 2). [13]C labeled heme is prepared by capitalizing on the fact that the first committed precursor in
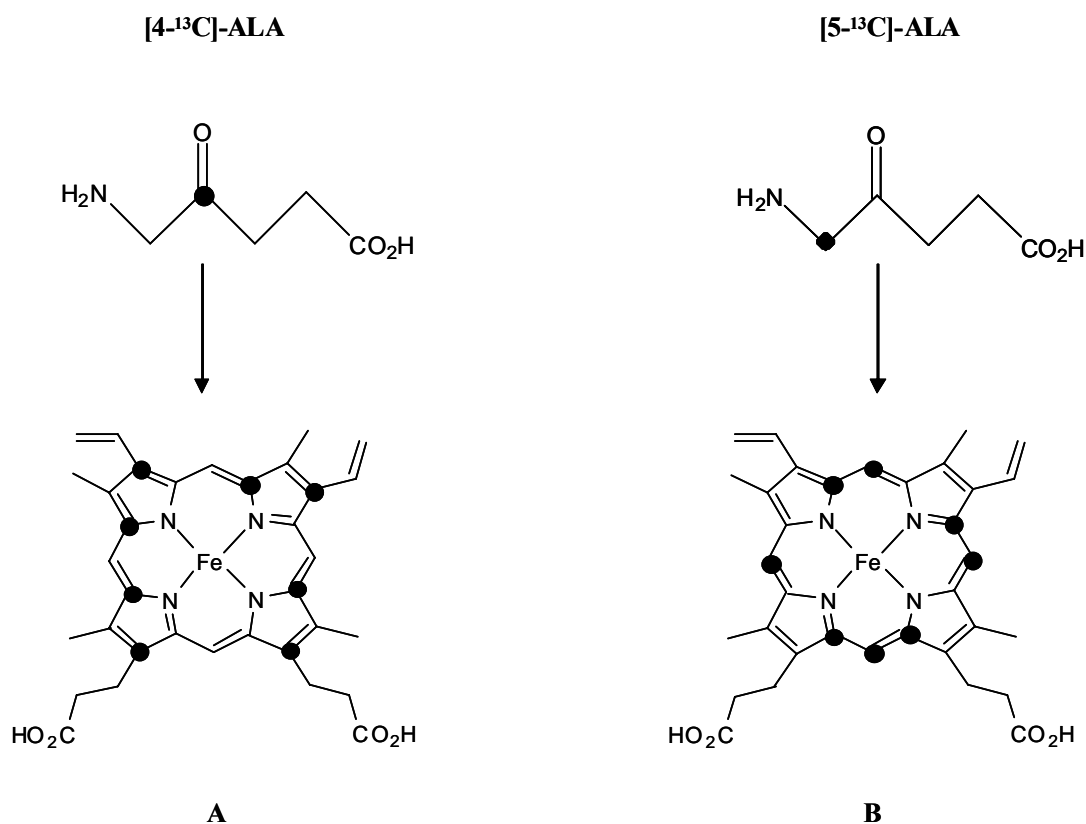
Figure 2. Heme labeled at the C_α and C_β positions was obtained using [4-^{13}C]-ALA as a precursor and heme labeled at the C_α and C_m positions was obtained from [5-^{13}C]-ALA.

40

heme biosynthesis is δ-aminolevulinic acid (ALA) [28, 29]. Hence, ^{13}C-labeled heme is biosynthesized in *E. coli* upon the addition of suitably ^{13}C-labeled ALA and trapped in the outer mitochondrial membrane cytochrome b_5 (OM cyt b_5) which is overexpressed in the bacterial host. The details of the biosynthetic protocol, which entails the expression and purification of OM cyt b_5 harboring ^{13}C-labeled heme, have been presented previously [24]. Reconstitution of the target protein with ^{13}C-labeled heme entails the removal of isotopically labeled macrocycle from OM cyt b_5, followed by the formation of the heme-target protein complex. ^{13}C-labeled heme is extracted from OM cyt b_5 with the methods reported previously [12, 30, 31]. In short, the addition of 15 mL of pyridine to 2.5 mL of 1 mM OM cyt b_5 in phosphate buffer ($\mu = 0.10$, pH 7.0), followed by the slow addition of chloroform, typically 10-15 mL, results in the precipitation of the polypeptide, leaving the pyridine hemochrome in solution. The latter is separated from the denatured polypeptide by centrifugation, allowed to equilibrate at room temperature, and then dried over anhydrous $MgSO_4$. The desiccant is separated by filtration, and the filtered pyridine/chloroform solution transferred to a round-bottom flask, where it is concentrated to dryness on a rotary evaporator. The solid is redissolved in 1.5 mL of DMSO, and the resultant solution is immediately used to reconstitute the target protein. In this study, ~2 μmol of Mb, H64V Mb or ShuT was reconstituted with a freshly prepared solution of ^{13}C-labeled heme until the A_{280}/A_{Soret} ratio no longer changed. The resultant solution was incubated at 4 °C overnight and then purified by size exclusion chromatography at the same temperature. The Mb-^{13}C-labeled heme complexes were purified in a Sephadex

G50 column (2.6 cm i.d. x 90 cm length), equilibrated and eluted with 10 mM phosphate buffer (pH 6.0). The ShuT-^{13}C labeled heme complex was purified in a Sephacryl S-100 column (2.6 cm i.d. x 90 cm length) also equilibrated and eluted with 10 mM phosphate buffer (pH 8.0). Fractions containing pure protein were concentrated in Amicon centrifugal concentrators to ~1 mL and transferred to smaller Centricon concentrators to exchange protein into deuterated buffer.

NMR Spectroscopy

^{1}H and ^{13}C spectra were acquired on a Varian Unity Inova spectrometer operating at a 599.74 MHz ^{1}H frequency and a 150.92 MHz ^{13}C frequency. The ^{1}H spectra were referenced to a residual water peak at 4.8 ppm and the ^{13}C spectra were referenced to an external solution of dioxane (60% v/v in D_2O) at 66.66 ppm. Proton spectra were acquired with presaturation of the residual water peak over 49 k data points, a spectral width of 125 kHz, a 200 ms acquisition time, no relaxation delay, and 1024 scans. The acquisition parameters used to obtain ^{13}C NMR spectra were given in the appropriate figure captions.

RESULTS AND DISCUSSION

Chemical Shift Characteristics of the High-Spin Core Heme Carbons

Wild type sperm whale Mb was reconstituted with hemin labeled with ^{13}C at the C_α and C_β positions (insert of Figure 3A) and with hemin labeled at the C_α and C_m
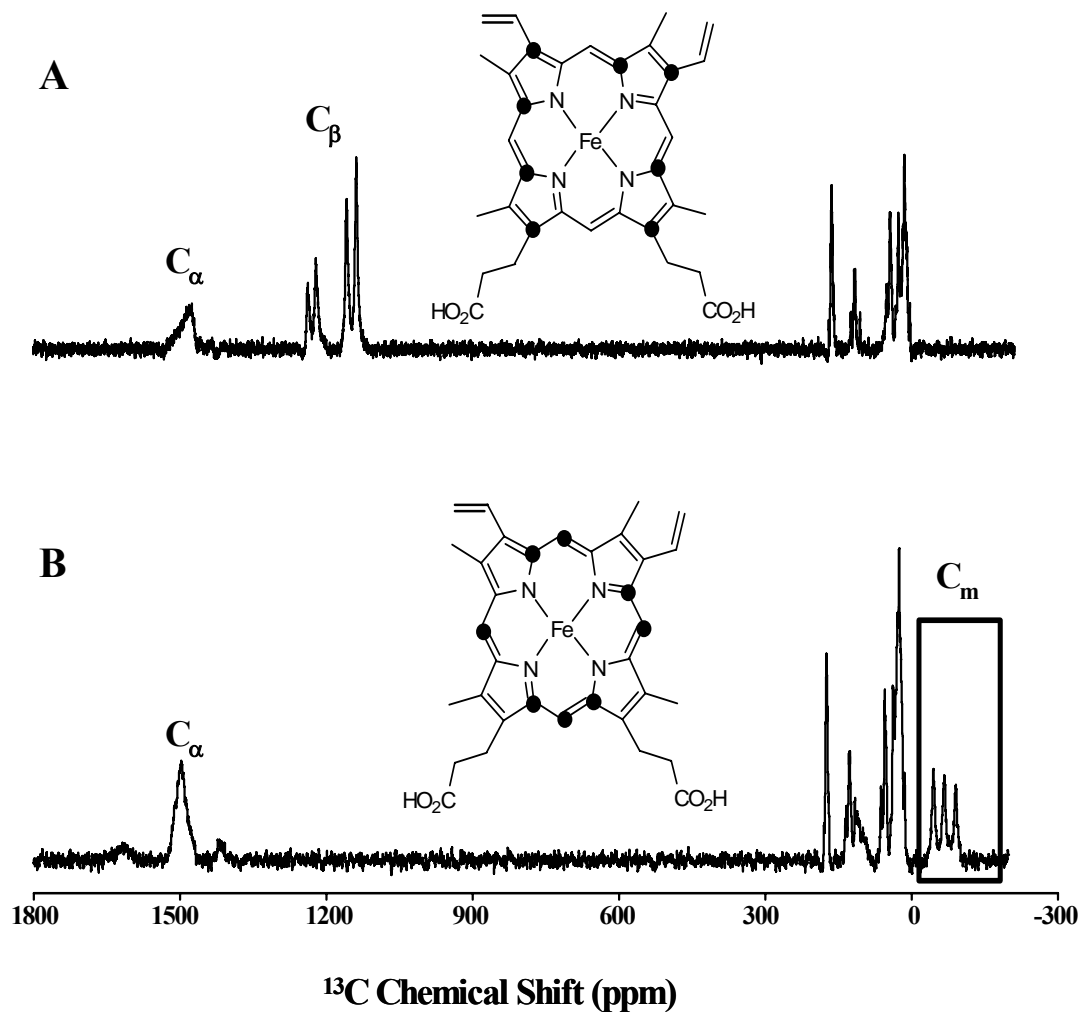
Figure 3. ^{13}C NMR spectra of wild type sperm whale myoglobin, pH 6.0, reconstituted with (A) heme labeled at the C_α and C_β positions and (B) heme labeled at the C_α and C_m positions. The spectra were obtained at 30 °C over 213 kHz, with 100 ms acquisition time, 20 ms relaxation delay, and 450 000 scans.

positions (insert of Figure 3B). The ^{13}C NMR spectrum in Figure 3A displays the paramagnetically affected resonances between 1100 and 1500 ppm, whereas the spectrum in Figure 3B shows a set of peaks centered near 1500 ppm and a second set of resonances (enclosed in a box) near -80 ppm. The ^{13}C labeling patterns in Figure 3A and B have in common the isotopic enrichment of C_α. It is therefore straightforward to conclude that resonances centered near 1500 ppm originate from C_α, resonances centered at ~1200 ppm originate from C_β and resonances near -80 ppm correspond to meso carbons.

A similar set of experiments was conducted with the H64V mutant, which is know to be pentacoordinated and high-spin [20, 21]. The spectrum shown in Figure 4A, obtained from a sample of H64V Mb reconstituted with heme labeled at the C_α and C_β positions, was acquired with a spectral window covering from -200 to 1200 ppm. This spectrum shows two sets of peaks originating from the heme: one near 800 ppm and the second at ~1000 ppm. The spectrum of H64V sw-Mb reconstituted with heme labeled at the C_α and C_m positions is shown in Figure 4B. In this spectrum, which was acquired with a spectral window covering from -200 to 1200 ppm, a set of peaks (enclosed in a box) centered near 250 ppm is apparent. However, when the spectrum was acquired using the same sample with a smaller spectral window (700-1400 ppm), a set of broad peaks centered near 1000 ppm became evident. These observations permit the straightforward assignment of the resonances at ~800 ppm to C_β, those near 1000 ppm to C_α, and the ones near 250 ppm to C_m.

The above-described observations indicate that hexa- and pentacoordinated
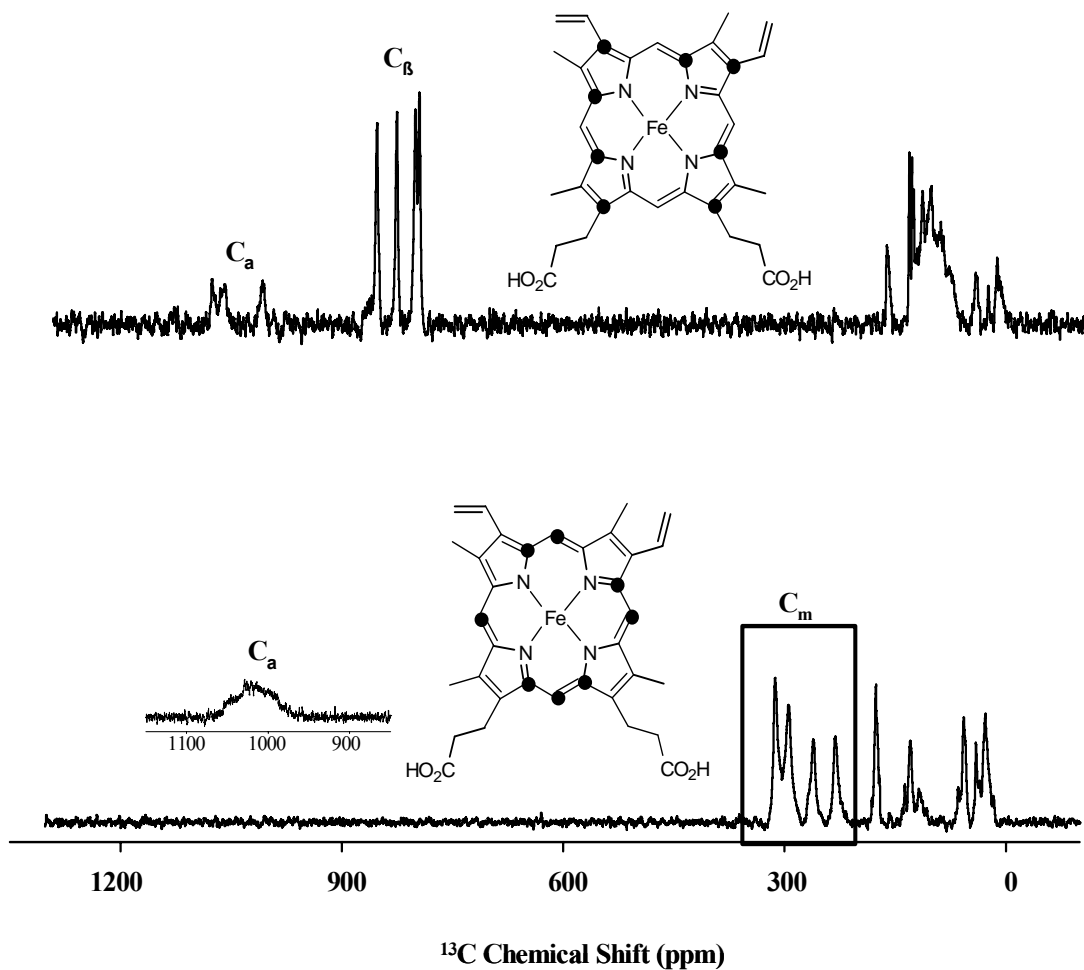
Figure 4. ^{13}C NMR spectra of the H64V mutant of sperm whale myoglobin at pH 6.0 reconstituted with (A) heme labeled at the C_α and C_β positions and (B) heme labeled at the C_α and C_m positions. The spectra were obtained at 30 °C over 213 kHz, with 100 ms acquisition time, 20 ms relaxation delay, and 450 000 scans.

Mb's exhibit distinct differences in the chemical shifts of their corresponding core carbons. Among these differences, those corresponding to C_m shifts stand out: C_m resonances from hexacoordinated Mb are centered at approximately -80 ppm (Figure 5A), whereas, the C_m resonances from pentacoordinated H64V sw-Mb occur near 250 ppm (Figure 5B). We propose that these chemical shift differences can be used as a diagnostic tool for the relatively straightforward determination of the coordination state of high-spin heme proteins. Two important properties make this approach readily applicable to this task: (i) C_m resonances from penta- and hexacoordinated heme active sites are relatively sharp and resonate relatively close to the typical diamagnetic range of ^{13}C resonances, which accounts for their relatively simple detection. This is in stark contrast with the difficult detection and assignment of the corresponding meso-^1H resonances, as has been illustrated in Figure 1. (ii) The electronic properties that give rise to the distinct C_m shifts are now well understood [19] and therefore provide a firm basis for consistent correlations between C_m shifts and heme coordination state. In short, five-coordinate ferrihemes place the metal out of the porphyrin plane, whereas in six-coordinate ferrihemes, the metal sits within the porphyrin plane. In high-spin ferrihemes (five- or six-coordinate), spin delocalization through σ-bonding interactions with the iron $d_{x^2-y^2}$ orbital is dominant [19] and results in very high spin densities at the C_α and C_β positions and therefore in large downfield C_α and C_β shifts [32, 33] (Figures 3 and 4). In addition, the out-of-plane displacement of the metal in five-coordinate ferrihemes promotes interactions between the metal d_{z^2} orbital and the porphyrin a_{2u} obital that are not possible in six-
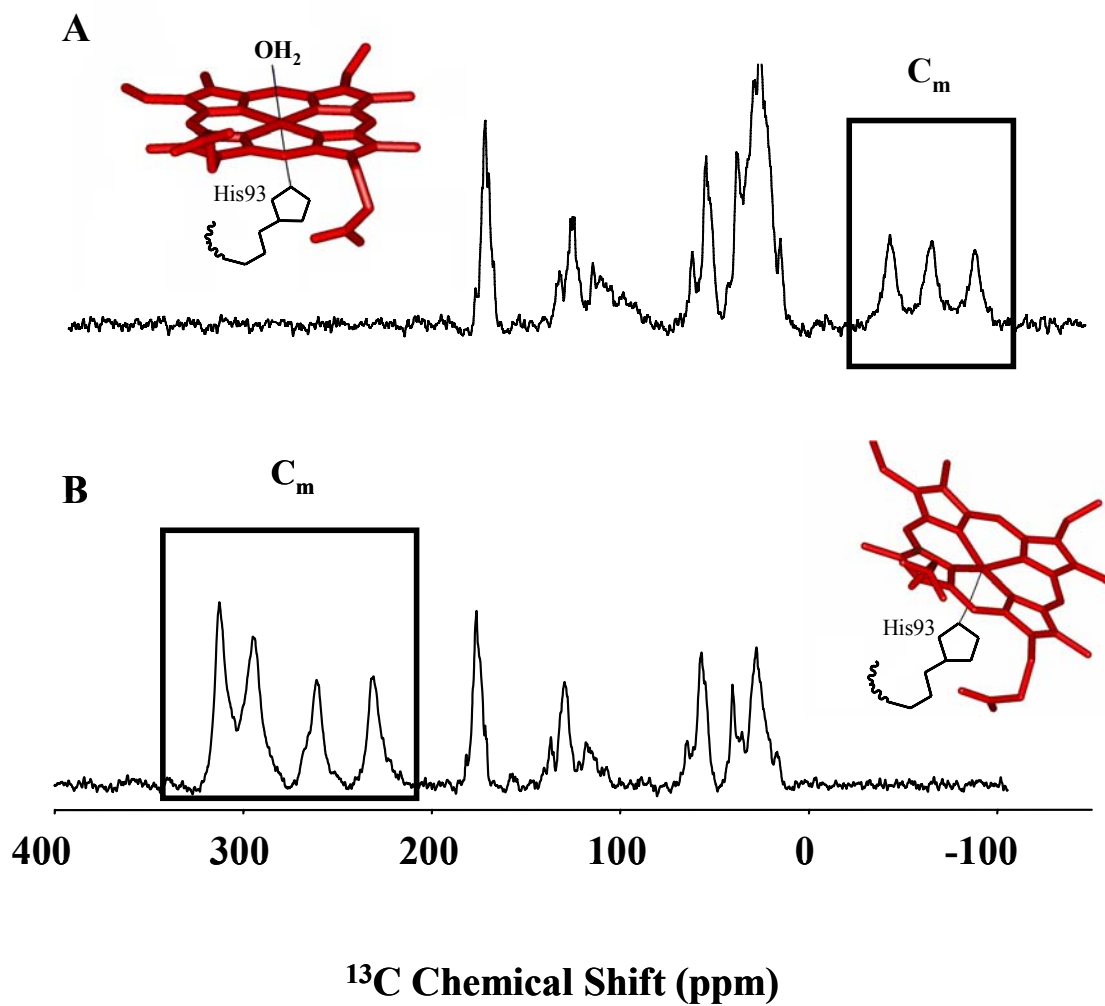
Figure 5. ^{13}C NMR spectra demonstrating the difference in the magnitude of meso-carbon chemical shifts obtained from (A) hexacoordinate high-spin sw-Mb and (B) pentacoordinate high-spin H64V-sw-Mb. The spectra were obtained at 30 °C over 84 kHz, with 100 ms acquisition time, 20 ms relaxation delay, and 110 000 scans.

coordinate high-spin ferrihemes [19]. These orbital interactions in five-coordinate ferrihemes allow delocalization of spin density from the porphyrin a_{2u} orbital into the metal $d_z{}^2$ orbital, thus placing positive unpaired electron density at C_m, which results in downfield C_m shifts. In this context, it is noteworthy that the C_m positions are located at the nodes of the σ-bonding system and therefore are insulated from direct σ-delocalization. Hence, interactions between the $d_z{}^2$ and a_{2u} orbitals in five-coordinate ferrihemes result in positive spin density at the meso positions and therefore downfield shifts ranging from 250 to 600 ppm (Figure 5B). In contrast, the placement of the iron in porphyrin plane in six coordinate ferrihemes prevents similar orbital interactions, thus leaving the C_m positions insulated from direct spin delocalization. The negative C_m shifts, -30 to -100 ppm (Figure 5A), are therefore a consequence of polarization from large spin density at the C_α position, which places negative spin density at the meso carbons.

Results from the DFT calculations also suggest that the porphyrin to iron-$d\pi$ (d_{xz} and d_{yz}) spin delocalization is more efficient in six- than in five-coordinate ferrihemes [33]. This phenomenon should be manifested in larger C_α and C_β shifts in six-coordinate complexes relative to the equivalent shifts in their five-coordinate counterparts. Indeed, spectra obtained from the six-coordinate Mb and from the five-coordinate H64V Mb (Figures 3 and 4) show that the C_α and C_β shifts corresponding to Mb are larger than those obtained from the the H64V mutant. This would suggest that the relative magnitude of the C_α and C_β shifts can be used to determine the coordination state of a ferriheme in an active site. However, the large chemical shifts

and broader lines of the C_α and C_β shifts makes this approach less practical than simply measuring the magnitude of the C_m shifts, which are significantly easier to observe. In the following discussion, we apply this concept to the determination of the coordination state of a recently discovered heme protein implicated in the heme uptake system of *S. dysenteriae* (ShuT) [2].

^{13}C NMR Analysis of the Coordination State of the Heme in ShuT.

ShuT is a 28.5 kDa monomeric periplasmic heme protein thought to be involved in transporting exogenously acquired heme across the periplasm of *S. dysenteriae* [4]. Exhaustive mutagenesis and spectroscopic (MCD and resonance Raman) studies have suggested that the ferriheme center in ShuT is five-coordinate, with Tyr-94 serving as the axial ligand [2]. We have used this recently discovered protein to illustrate the simplicity with which the coordination state of high-spin heme proteins can be elucidated using ^{13}C NMR spectroscopy.

A sample of ShuT was purified to homogeneity as described in the Experimental Methods. After purification, the sample of ShuT consisted of a mixture of molecules with and without heme in an approximate 1:1 ratio. A solution containing heme labeled at the meso carbons was added to a solution of ShuT to reconstitute labeled heme into those molecules devoid of heme. The resultant solution was purified from excess free heme and then concentrated for subsequent NMR analysis. A set of C_m resonances centered near 350 ppm in the ^{13}C NMR spectrum of this protein (Figure 6) demonstrates that ShuT harbors a five-coordinate ferric heme
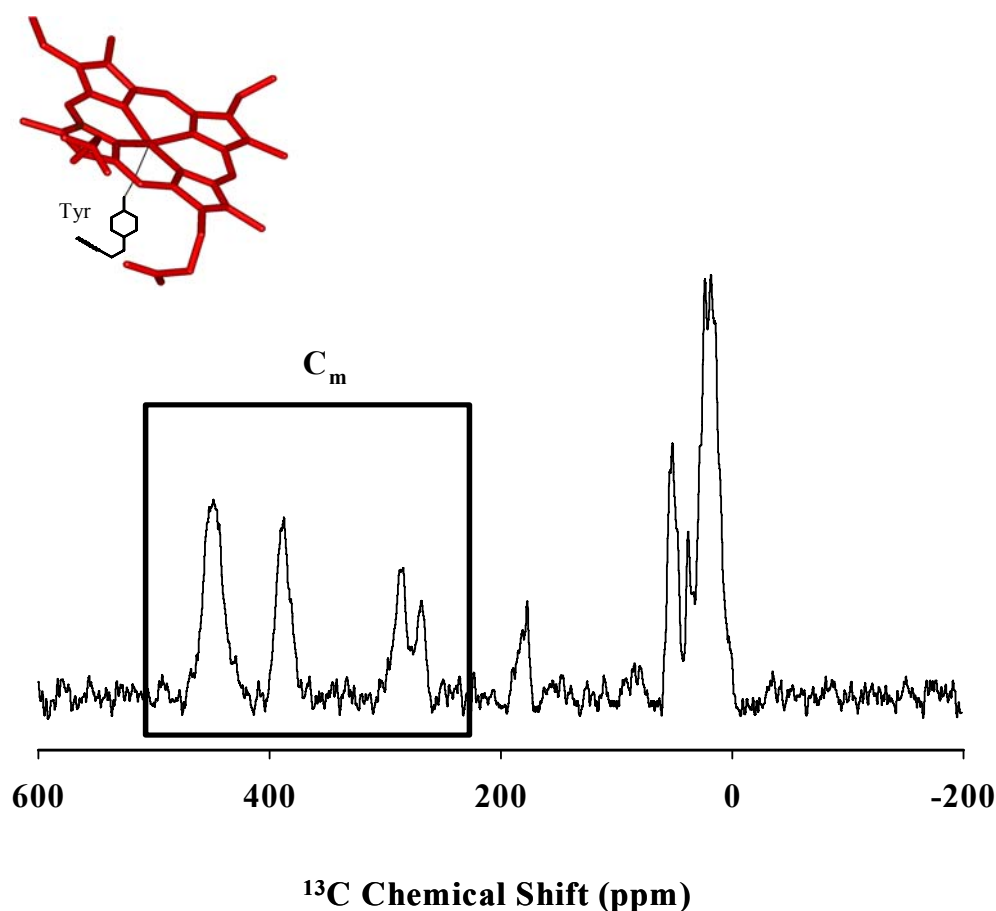
Figure 6. ^{13}C NMR spectrum of ShuT at pH 8.0 reconstituted with heme labeled at the C_α and C_m positions. The C_m chemical shifts centered at ~350 ppm unambiguously demonstrate that the ferriheme center in ShuT is pentacoordinate and high-spin. The spectrum was obtained with the aid of a cryoprobe in a Bruker instrument operating at 125.76 MHz (^{13}C-frequency) and 30 °C over 88 kHz, with 100 ms acquisition time, 20 ms relaxation delay, and 50 000 scans.

center. The spectrum was obtained in ~2 h from a 250 μL solution (2.0 mM) of ShuT using a cryoprobe. The relatively short analysis time required for the ShuT sample, which was labeled with ^{13}C heme to approximately a 50% enrichment level, underscores the simplicity and the potential of utilizing the C_m shift in the determination of coordination state of ferric heme centers in novel proteins. In comparison, spectroscopic methods commonly used to determine the coordination state of high-spin ferriproteins (MCD and resonance Raman) rely strongly on the availability of suitable model complexes for assignment and interpretation of the pertinent signals [2].

REFERENCES

1. Arnoux, P., Haser, R., Izadi, N., Lecroisey, A., Delepierre, M., Wandersman, C., and Czjek, M., *The Crystal Structure of HasA, a Hemophore Secreted by Serratia Marcescens.* Nat. Struct. Biol., 1999. **6**: p. 516-520.

2. Eakanunkul, S., Lukat-Rodgers, G. S., Sumithran, S., Ghosh, A., Rodgers, K. R., Dawson, J. H., and Wilks, A., *Characterization of the Periplasmic Heme-Binding Protein ShuT from the Heme Uptake System of Shigella dysenteriae.* Biochemistry, 2005. **44**: p. 13179-13191.

3. Hornung, J.M., Jones, H. A., and Perry, R. D., *The Hmu Locus of Yersinia pestis is Essential for Utilization of Free Haemin and Haem-Protein Complexes as Iron Sources.* Mol. Microbiol., 1996. **20**: p. 725-739.

4. Wyckoff, E.E., Duncan, D., Torres, A. G., Mills, M., Maase, K., and Payne, S. M., *Structure of the Shigella dysenteriae Haem Transport Locus and Its Phylogenetic Distribution in Enteric Bacteria.* Mol. Microbiol., 1998. **28**: p. 1139-1152.

5. Ikeue, T., Ohgo, Y., Yamaguchi, T., Takahashi, M., Takeda, M., and Nakamura, M., *Saddle-Shaped Six-Coordinate Iron(III) Porphyrin Complexes Showing a Novel Spin Crossover between S=1/2 and S=3/2 Spin States.* Angrew. Chem. Int. Ed., 2001. **40**: p. 2617-2620.

6. Ikeue, T., Ohgo, Y., Saitoh, T., Yamaguchi, T., and Nakamura, M., *Factors Affecting the Electronic Ground State of Low-Spin Iron(III) Porphyrin Complexes.* Inorg. Chem., 2001. **40**: p. 3423-3434.

7. Ikeue, T., Saitoh, T., Yamaguchi, T., Ohgo, Y., Nakamura, M., Takahashi, M., and Takeda, M., *Formation of Pure Intermediate Spin Complexes in Highly Nonplanar Iron(III) Porphyrins.* Chem. Commun., 2000: p. 1989-1900.

8. Nakamura, M., Hishino, A., Ikezaki, A., and Ikeue, T., *Chemical Shift of Meso-Carbon: A Powerful Probe to Determine the Coordination Structure and Electronic Configuration of Ferric Porphyrin Complexes.* Chem. Commun., 2003: p. 1862-1863.

9. Sakai, T., Ohgo Y., Ikeue, T., Takahashi, M., Takeda, M., and Nakamura, M., *Formation of the Intermediate-Spin Iron(III) Porphyrin Complexes with $(d_{xz},d_{yz})^3(d_{xy})^1(d_z^2)^1$ Electron Configuration.* J. Am. Chem. Soc., 2003. **125**: p. 13028-13029.

10. Rivera, M., Caignan, G. A., Astashkin, A. V., Raitsimring, A. M., Shokhireva, T. K., and Walker, F. A., *Models of the Low-Spin Iron(III) Hydroperoxide Intermediate of Heme Oxygenase: Magnetic Resonance Evidence for Thermodynamic Stabilization of the d(xy) Electronic State at Ambient Temperatures.* J. Am. Chem. Soc., 2002. **124**: p. 6077-6089.

11. Zeng, Y., Caignan, G. A., Bunce, R. A., Rodriguez, J. C., Wilks, A., and Rivera, M., *Azide-Inhibited Bacterial Heme Oxygenases Exhibit an S=3/2 $(d_{xz},d_{yz})^3(d_{xy})^1$ Spin State: Mechanistic Implications for Heme Oxidation.* J. Am. Chem. Soc., 2005. **127**: p. 9794-9807.

12. Rivera, M., and Caignan, G. A., *Recent Developments in the ^{13}C NMR Spectroscopic Analysis of Paramagnetic Hemes and Hemoproteins.* Anal. Bioanal. Chem., 2004. **378**: p. 1464-1483.

13. Caignan, G.A., Deshmukh, R., Zeng, Y., Wilks, A., Bunce, R. A., and Rivera, M., *The Hydroxide Complex of Pseudomonas aeruginosa Heme Oxygenase as a Model of the Low-Spin Iron(III) Hydroperoxide Intermediate in Heme Catabolism: ^{13}C NMR Spectroscopic Studies Suggest the Active Participation of the Heme in Macrocycle Hydroxylation.* J. Am. Chem. Soc., 2003. **125**: p. 11842-11852.

14. Rivera, M., Qiu, F., Bunce, R. A., and Stark, R. E., *Complete Isomer-Specific ^1H and ^{13}C NMR Assignments of the Heme Resonances of Rat Liver Outer Mitochondrial Membrane Cytochrome b$_5$.* J. Biol. Inorg. Chem., 1999. **4**: p. 87-98.

15. Mispelter, J., Momenteau, M., and Lhoste, J. M., *NMR Investigation of the Electric Properties and Magnetic States of Hemes and Hemoproteins: The S=2 State in Ferrous Porphyrins.* Biochimie, 1981. **63**: p. 911-914.

16. Kurland, R.J., Little, R. G., Davis, D. G., and Ho, C., *Proton Magnetic Resonance Study of High- and Low-Spin Hemin Derivatives.* Biochemistry, 1971. **10**: p. 2237-2246.

17. Rajarathnam, K., La Mar, G. N., Chiu, M. L., Sligar, S. G., Singh, J. P., and Smith, K. M., *^1H NMR Hyperfine Shift Pattern as Probe for Ligation State in High-Spin Ferric Hemoproteins: Water Binding in Metmyoglobin Mutants.* J. Am. Chem. Soc., 1991. **113**: p. 7886-7892.

18. Walker, F.A., *The Porphyrin Handbook*, ed. K.M. Kadish, Smith, K. M., Guilard, R. Vol. 5. 2000: Academic Press: New York. 81-183.

19. Cheng, R.-J., Chen, P. -Y., Lovell, T., Liu, T., Noodleman, L., and Case, D. A., *Symmetry and Bonding in Metalloporphyrins. A Modern Implementation for the Bonding Analyses of Five- and Six-coordinate High-Spin Iron(III)-Porphyrin Complexes Through Density Functional Calculation and NMR Spectroscopy.* J. Am. Chem. Soc., 2003. **125**: p. 6774-6783.

20. Ikeda-Saito, M., Hori, H., Anderson, L. A., Prince, R. C., Pickering, I. J., George, G. N., Sanders, C. R., Lutz, R., Mckelvey, E. J., and Mattera, R., *Coordination Structure of the Ferric Heme Iron in Engineered Distal Histidine Myoglobin Mutants.* J. Biol. Chem., 1992. **32**: p. 22843-22852.

21. Quillin, M.L., Arduini, R. M., Olson, J. S., and Philips, G. N., *High-Resolution Crystal Structures of Distal Histidine Mutants of Sperm Whale Myoglobin.* J. Mol. Biol., 1993. **234**: p. 140-155.

22. Banci, L., Bertini, I., and Luchinat, C., *Nuclear and Electronic Relaxation.* 1991: VCH: Weinheim, Germany.

23. Machonkin, T.E., Westler, W. M., and Markley, J. L., *(13)C[(13)C] 2D NMR: A Novel Strategy for the Study of Paramagnetic Proteins with Slow Electronic Relaxation Rates.* J. Am. Chem. Soc., 2002. **124**: p. 3204-3205.

24. Rivera, M., and Walker, F. A., *Biosynthetic Preparation of Isotopically Labeled Heme.* Anal. Biochem., 1995. **230**: p. 295-302.

25. Teale, F.W.J., *Cleavage of the Haem-Protein Link by Methylethylketone.* Biochim. Biophys. Acta, 1959. **35**: p. 543.

26. Bunce, R.A., Shiling, C. L., III, and Rivera, M., *Synthesis of [1,2-^{13}C]- and [2,3-^{13}C]-Labeled δ-Aminolevulinic Acid.* J. Labelled Compd. Radiopharm., 1997. **39**: p. 669-675.

27. Rodriguez-Maranon, M.J., Feng, Q., Stark, R. E., White, S. P., Zhang, X., Foundling, S. I., Rodriguez, V., Schilling, C. L., III, Bunce, R. A., and Rivera, M., *^{13}C NMR Spectroscopic and X-Ray Crystallographic Study of the Role Played by Mitochondrial Cytochrom b$_5$ Heme Propionates in the Electrostatic Binding to Cytochrome c.* Biochemistry, 1996. **35**: p. 16378-16390.

28. Warren, M.J., and Scott, A. I., *Tetrapyrrole Assembly and Modification into the Ligands of Biologically Functional Cofactors.* Trends Biochem. Sci., 1990. **15**: p. 486-491.

29. Scott, A.I., *How Nature Synthesizes Vitamin-B12 - a Survey of the Last 4 Billion Years.* Angew. Chem. Int. Ed. Engl., 1993. **32**: p. 1223-1243.

30. Caignan, G.A., Deshmukh, R., Wilks, A., Zeng, Y., Huang, H., Moenne-Loccoz, P., Bunce, R. A., Eastman, M. A., and Rivera, M., *Oxidation of Heme to β- and δ-Biliverdin by Pseudomonas aeruginosa as a Consequence of an Unusual Seating of the Heme.* J. Am. Chem. Soc., 2002. **124**: p. 14879-14892.

31. Zeng, Y., Deshmukh, R., Caignan, G. A., Bunce, R. A., Rivera, M., and Wilks, A., *Mixed Regioselectivity in the Arg-177 Mutants of Corynebacterium diphtheriae Heme Oxygenase as a Consequence of In-Plane Heme Disorder.* Biochemistry, 2004. **43**: p. 5222-5238.

32. Mao, J., Zhang, Y., and Oldfield, E., *Nuclear Magnetic Resonance Shifts in Paramagnetic Metalloporphyris and Metalloproteins.* J. Am. Chem. Soc., 2002. **124**: p. 13911-13920.

33. Walker, F.A., *Pulsed EPR and NMR Spectroscopy of Paramagnetic Iron Porphyrinates and Related Iron Macrocyles: How to Understand Patterns of Spin Delocalization and Recognize Radicals.* Inorg. Chem., 2003. **42**: p. 4526-4544.

CHAPTER 3

Structural and Spectroscopic Characterization of HasAp

INTRODUCTION

Many pathogenic bacteria have evolved specific heme uptake systems to acquire heme-iron from mammalian hosts. Heme uptake and utilization is a mechanism utilized by some pathogenic bacteria to overcome the highly restricted iron conditions encountered in the process of colonizing a mammalian host. Some pathogenic bacteria, such as the opportunistic bacteria, *Pseudomonas aeruginosa* are thought to overcome these challenging conditions by deploying multiple systems for iron uptake that are regulated by Fur, the **F**e **u**ptake **r**egulator [1]. These include the secretion of siderophores to bind and uptake Fe^{3+} via specific receptors [2, 3]. When iron is limited more severely, however, the global iron response associated with Fur-regulated genes includes the heme uptake systems *phu* (***P**seudomonas* **h**eme **u**ptake) and *has* (**h**eme **a**cquisition **s**ystem). The phu locus consists of a receptor gene (phuR) and the phuSTUVW operon encoding a typical ABC transporter. The second uptake system, *has*, consists of a heme receptor (hasR) and a protein that binds heme with high affinity, also known as the hemophore, HasAp [2]. In fact, it is thought that in the early stages of infection, before inflammation and damage ensues, the very low concentration of hemoglobin is overcome by the secretion of hemophores, which can "steal" heme from hemoglobin for subsequent delivery to HasR previous to

internalization. Once internalized to the cytoplasm heme is delivered to a heme oxygenase (*pa*-HO) for its degradation to biliverdin, thus facilitating release of the heme-iron for subsequent metabolic use [4].

To date, the only structurally characterized hemophore is that of *Serratia marcescens* (HasA$_{SM}$), which captures heme and delivers it to the receptor HasR$_{SM}$ [5]. In this organism HasR$_{SM}$ alone is able to take heme from hemoglobin but synergism with HasA$_{SM}$ increases the efficiency of heme uptake from hemoglobin at least 100-fold [6]. A gene encoding a similar protein (HasAp) in *P. aeruginosa* is upregulated under iron-limiting conditions [7]. HasAp, which shares approximately 50% identity with HasA$_{SM}$, is essential for *P. aeruginosa* uptake and utilization of hemoglobin iron [7]. Amino acid sequence alignment of HasAp and HasA$_{SM}$ is shown in Figure 1. Like HasA$_{SM}$, HasAp is secreted to the extracellular milieu where it undergoes C-terminal proteolytic cleavage [8], presumably by proteases also secreted by *P. aeruginosa*. However, whereas the growth of HasA$_{SM}$ mutants can be sufficiently rescued by addition of full-length or cleaved forms of the *S. marcescens* HasA to media where the only source of iron is hemoglobin, the growth of *P. aeruginosa* HasAp mutants can only be rescued by addition of truncated HasAp when hemoglobin is the sole source of iron [7]. These observations suggest that proteolytic cleavage of HasAp is important to activate this protein for heme uptake. In this context, it is also important to note that expression of most virulence factors in *P. aeruginosa* is not constitutive but is regulated in a cell density-dependent manner, *i. e.* quorum-sensing. This ensures that *P. aeruginosa* does not express pathogenic traits

```
HasA_P      1  MSISISYSTTYSGWTVADYLADWSAYFGDVNHRPGQVVDGSNTGGFNPGPFDGSQYALKS
HasA_SM     1  MAFSVNYDSSFGGYSIHDYLGQWASTFGDVNHTNGNVTD-ANSGGFYGGSLSGSQYAISS

HasA_P     61  TASDA-AFIAGGDLHYTLFSNPSHTLWGKLDSIALGDTLTGGASSGGYALDSQEVSFSNL
HasA_SM    60  TANQVTAFVAGGNLTYTLFNEPAHTLYGQLDSLSFGDGLSGGDTSP-YSIQVPDVSFGGL

HasA_P    120  GLDSPIAQGRDGTVHKVVYGLMSGDSSALQGQIDALLKAVDPSLSINSTFDQLAAA---G
HasA_SM   119  NLSSLQAQGHDGVVHQVVYGLMSGDTGALETALNGILD- -DYGLSVNSTFDQVAAATAVG

HasA_P    177  VAHA-TPAAAAAEVGVVGVQELPHDLALAA
HasA_SM   177  VQHADSPELLAA
```

Figure 1. Amino acid sequence alignment of HasA in *Pseudomonas aeruginosa* (HasAp) (A) and *Serratia marcescens* (HasA_SM) (B). Identical residues are shown in red. This alignment was prepared using ClustalW [9].

until the population has reached the critical density necessary to overwhelm the host defenses and establish an infection. It is therefore significant that a recent proteomics study revealed that among quorum-sensing regulated proteins in *P. aeruginosa*, several are involved in iron utilization, thus suggesting a link between quorum-sensing and the iron regulatory system [8]. Two of the up-regulatred proteins are the receptor phuR and the hemophore HasAp, which are components of each of the two heme uptake systems in *P. aeruginosa* (*phu* and *has*). Consequently, these observations indicate that hemoglobin utilization is one of the phenotypes controlled through quorum-sensing [8]. The same authors reported that a mass spectrometric proteomics analysis of the wild type *P. aeruginosa* (strain PAO1) revealed that the most abundant form of secreted HasAp is the processed form (wild type minus 21

amino acids). The multiple C-terminal cleavage sites of HasAp are shown in Figure 2. In contrast, similar analyses of quorum-sensing impaired mutants indicate that the most abundant form of HasAp is the full-length protein [8].

1   205
MSISISYSTTYS………..AAAAAEVGVVGVQELPHDLALAA

a   **15 residues**

b   **18 residues**

c   **19 residues**

d   **20 residues**

e   **21 residues**
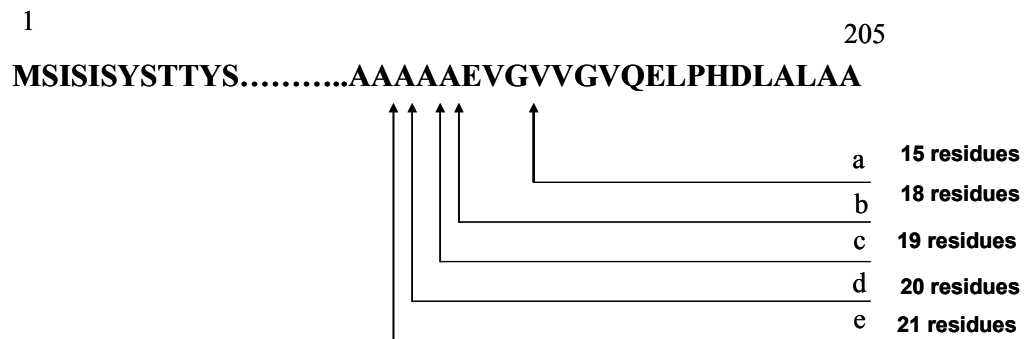
Figure 2. Multiple C-terminal cleavage sites of HasAp as indicated by the arrows.

Moreover, quorum-sensing impaired mutants show significantly reduced growth relative to wild type *P. aeruginosa* PAO1 in medium containing hemoglobin as the only source of iron. Growth, however, is rescued by supplementation with the quorum-sensing signal molecule N-acyl homoserine lactone (AHL), which indicates that the ability to utilize hemoglobin in *P. aeruginosa* is quorum-sensing controlled. It is therefore clear that genetic and proteomic studies converge on the idea that HasAp must be processed to function properly. These findings are significant because they indicate that production of functional (truncated) HasAp by *P. aeruginosa* is quorum-

sensing regulated [8]. These observations indicate that efforts aimed toward a molecular level understanding of hemoglobin utilization by the opportunistic *P. aeruginosa* should include the structural and biochemical characterization of the full-length and proteolyzed (truncated) forms of HasAp. In this work we have undertaken this task as a stepping stone to enhance current understanding of how this resilient microorganism can overcome the challenging low levels of iron encountered in the early stages of colonization (infection). An understanding of hemophore and hemoglobin interaction could give insights on the mechanism of heme uptake.

Analytical centrifugations methods were used to investigate the formation of a complex between $HasA_{SM}$ and hemoglobin [5]. These investigations led to the conclusion that a stable complex is not formed, although the formation of a transient complex could not be ruled out. Nevertheless, it was postulated that heme capture by $HasA_{SM}$ is thought to occur by passive transfer from hemoglobin to the hemophore, rather than by protein-protein interactions [5]. In this investigations leading to this report we used electronic absorption spectroscopy to assess the timescale of heme transfer. Secreted full-length HasAp is a 205 amino acid protein. Proteases also secreted by *P. aeruginosa* cleave its carboxy terminus at five different sites. It has been shown that the most abundant form of HasAp observed in the secretome of quorum-sensing impaired mutants of *P. aeruginosa* is the full-length protein. In contrast, the cleaved forms are more abundant in the secretome of wild type PAO1, with the most abundant form being that cleaved between residues 184 and 185 (full-length minus 21 C-terminal residues). Hence full-length HasAp and the species

consisting only of 184 residues, hereafter referred to as truncated HasAp, are the subjects of these studies. In this study, we attempt to understand the heme uptake and release mechanism of HasAp by using various techniques. This was primarily accomplished by elucidating the structure of HasAp both by X-ray crystallography and nuclear magnetic resonance (NMR) spectroscopy. The three-dimensional structure of holo truncated HasAp was determined by X-ray crystallography. The coordination and electronic structure of the heme active site is an important modulator of the physical, chemical and biochemical properties of heme proteins [10]. Various well-established techniques are widely used to study paramagnetic proteins [11]. Among these techniques, NMR spectroscopy has been proven to be a powerful tool to study heme proteins [11-14]. In this study we primarily use ^{13}C NMR spectroscopy coupled with the use of isotopically labeled-heme to study the heme active site to gain more insights on the heme uptake and release mechanisms. Besides ^{13}C NMR, complementary techniques such as electronic absorption spectroscopy, and electron paramagnetic resonance (EPR) were also employed to study the spin state and coordination of heme iron in HasAp. Moreover, to better understand the heme release and uptake mechanism of HasAp, it is also important to study its structure and dynamics in solution. In an attempt toward this goal, we report here the amide backbone amide resonance assignments of holo full-length, holo truncated and apo truncated forms of HasAp. These assignments were done on uniformly isotopic labeled HasAp using a combination of 2D and 3D NMR experiments [15], and amino acid selective labeled protein.

60

EXPERIMENTAL PROCEDURES

General Methods

The HasAp (PA3407) gene was synthesized and subcloned into pET11a vector by Celtek Genes (Nashville, TN). The genes were engineered with silent mutations introducing codons favored by *Escherichia coli* [16]. The restriction sites *Nde*I and *Bam*HI were constructed at the 5' and 3' ends of HasAp gene, respectively (Figure 3). The recombinant DNA plasmid harboring the HasAp gene was then transformed into *E. coli* BL21-GOLD (DE3) expression host cell (Stratagene, La Jolla, CA) for subsequent expression.

Site-Directed Mutagenesis

The truncated HasAp gene was contructed using the recombinant pET11a plasmid harboring the gene coding for HasAp (full-length form), polymerase chain reaction (PCR) and QuickChange™ mutagenesis kit from Stratagene (La Jolla, CA). The oligonucleotides were synthesized by Integrated DNA Technologies, Inc. and used without further purification. The primers were designed to have a melting temperature (Tm) greater than or equal to 78 °C. The sequences corresponding to the primers used are 5'-GCGACCCCGGCGGCGTAAGCGGCGGAAGTGGGC - 3' and 5'-GCCCACTTCCGCCGCTTACGCCGCCGGGGTCGC-3'. The underlined codons represent mismatches designed to introduce a stop codon where the protein cleavage was desired. The recombinant construct was transformed into *E. coli* XL1-Blue

5'   *Nde* I
GGG<u>CATATG</u> AGC ATT AGC ATT AGC TAT AGC ACC ACC TAT AGC GGC TGG ACC
        M   S   I   S   I   S   Y   S   T   T   Y   S   G   W   T

GTG GCG GAT TAT CTG GCG GAT TGG AGC GCG TAT TTT GGC GAT GTG AAC CAT
 V   A   D   Y   L   A   D   W   S   A   Y   F   G   D   V   N   H

CGT CCG GGC CAG GTG GTG GAT GGC AGC AAC ACC GGC GGC TTT AAC CCG GGC
  R   P   G   Q   V   V   D   G   S   N   T   G   G   F   N   P   G

CCG TTT GAT GGC AGC CAG TAT GCG CTG AAC AGC ACC GCG AGC GAT GCG GCG
  P   F   D   G   S   Q   F   A   L   K   S   T   A   S   D   A   A

TTT ATT GCG GGC GGC GAT CTG CAT TAT ACC CTG TTT AGC AAC CCG AGC CAT
 F   I   A   G   G   D   L   H   Y   T   L   F   S   N   P   S   H

ACC CTG TGG GGC AAA CTG GAT AGC ATT GCG CTG GGC GAT ACC CTG ACC GGC
 T   L   W   G   K   L   D   S   I   A   L   G   D   T   L   T   G

GGC GCG AGC AGC GGC GGC TAT GCG CTG GAT AGC CAG GAA GTG AGC TTT AGC
  G   A   S   S   G   G   Y   A   L   D   S   Q   E   V   S   F   S

AAC CTG GGC CTG GAT AGC CCG ATT GCG CAG GGC CGT GAT GGC ACC GTG CAT
 N   L   G   L   D   S   P   I   A   Q   G   R   D   G   T   V   H

AAA GTG GTG TAT GGC CTG ATG AGC GGC GAT AGC AGC GCG CTG CAG GGC CAG
 K   V   V   Y   G   L   M   S   G   D   S   S   A   L   Q   G   Q

ATT GAT GCG CTG CTG AAA GCG GTT GAT CCG AGC CTG AGC ATT AAC AGC ACC
 I   D   A   L   L   K   A   V   D   P   S   L   S   I   N   S   T

TTT GAT CAG CTG GCG GCG GCG GGC GTG GCG CAT GCG ACC CCG GCG GCG GCG
 F   D   Q   L   A   A   A   G   V   A   H   A   T   P   A   A   A

GCG GCG GAA GTG GGC GTG GTG GGC GTG CAG GAA CTG CCG CAT GAT CTG GCG
 A   A   E   V   G   V   V   G   V   Q   E   L   P   H   D   L   A
                     *Bam*H I   3'
CTG GCG GCG TAA <u>GGATCC</u>GGG
 L   A   A   -

Figure 3.   DNA and amino acid sequence of HasAp. The *Nde* I and *Bam*HI restriction endonuclease sites were constructed at the 5' and 3' ends, respectively, for subcloning.

supercompetent cells for amplification. Once the mutation had been confirmed by sequencing, the recombinant DNA plasmid was transformed into *E. coli* BL21 (DE3) GOLD cells for subsequent protein expression.

Protein Expression and Purification of Full-Length and Truncated HasAp

Protein Expression and Purification of Unlabeled Proteins

Protein samples were expressed using the recombinant pET11a plasmids harboring genes coding for the full-length (205 amino acids residues) and truncated (184 amino acid residues) HasAp. A single colony of freshly transformed cells was cultured for 12 h in 10 mL of Luria-Bertani (LB) medium containing 200 μg/mL of ampicillin. This culture was used to inoculate 1.0 L of M9 minimal medium (200 μg/mL ampicillin), which was then incubated with continuous shaking at 225 rpm. When the OD_{600} reached 0.80 − 0.90, the cells were centrifuged at 4000 rpm for 10 min. The cells were then resuspended and subcultured into 1.0 L of fresh minimal M9-ampicillin medium. After the OD_{600} reached 1.0, biosynthesis of the polypeptide was induced by addition of isopropyl-β-D-thiogalactopyranoside (IPTG) to a final concentration of 1 mM and the cells were cultured for 5 h at 30 °C, before they were harvested by centrifugation at 4000 rpm for 10 min. The cells were lysed by sonication as previously described [17] in 50 mM Tris-HCl (pH 7.8) containing 1 mM EDTA, and 1 mM phenylmethysulfonyl fluoride (PMSF). The cell suspension was then centrifuged at 23 500 rpm for 2 h. The cell debris was separated by ultracentrifugation and the soluble fraction was dialyzed against 20 mM Tris-HCl (pH

7.8) (3 x 4 L) at 4 °C. The protein was loaded into a Sepharose-Q Fast Flow column (2.6 cm i.d. x 15 cm length) pre-equilibrated with 20 mM Tris-HCl (pH 7.6). The protein was eluted with the same buffer with a linear gradient (50-500 mM) NaCl. Purity of the protein fractions were determined by SDS-PAGE and the best fractions were pooled. The apo-protein was subsequently reconstituted with hemin dissolved in DMSO. To this end, heme was added gradually to the protein solution until the absorbance ratio (A_{280}/A_{407}) no longer changed. The resultant solution was incubated at 4 °C and concentrated to a final volume of 2 - 3 mL using Amicon ultracentrifuge filter and further purified by size-exclusion chromatography in a Sephacryl S-200 column (2.6 cm i.d. x 90 cm length), equilibrated with 100 mM Tris-HCl and 100 mM NaCl (pH 7.6). Fractions with an absorbance ratio (A_{280}/A_{407}) < 0.35 were pooled, dialyzed against phosphate buffer (μ = 0.1, pH 7.0), concentrated by ultrafiltration, and stored at -20 °C.

Protein Expression and Purification of Labeled Proteins

Singly-(^{15}N) and doubly-labeled (^{15}N, ^{13}C) samples were expressed using the same procedure as the unlabeled proteins. When the OD_{600} reached 0.80 – 0.90, the cells were centrifuged at 4000 rpm for 10 min. The cells were then resuspended and subcultured in 1.0 L of fresh minimal M9-ampicillin medium that did not contain any nitrogen or carbon sources. After the OD_{600} reached 1.0, biosynthesis of the polypeptide was induced by addition of isopropyl-β-D-thiogalactopyranoside (IPTG) to a final concentration of 1 mM and 1 g of ^{15}NH$_4$Cl for producing [U-^{15}N]-HasAp.

For the [U-^{13}C, U-^{15}N]-HasAp labeled samples, 1 g of ^{15}NH$_4$Cl and 1.5 g of ^{13}C-labeled glucose were added during induction with IPTG.   The cells were then grown further for 5 h at 30 °C and harvested by centrifugation at 4000 rpm for 10 min. The harvested cells were resuspended and lysed by sonification. Cell lysis, protein purification and heme reconstitution of the singly (^{15}N) and doubly-labeled (^{15}N, ^{13}C)-samples were carried out using the same protocol for the unlabeled proteins described above.

Protein Expression and Purification of Selectively Labeled Proteins

The protocol used to prepare selectively labeled amino acid truncated HasAp was as previously described in [13, 18, 19] but with some minor changes. The M9 minimal medium was supplemented with the synthetic amino acids (g/L) prior to autoclaving, except for L-Trp (0.05) : L-Ala (0.5), L-Arg (0.4), L-Asn (0.4), L-Asp (0.4), L-Cys (0.05), L-Gln (0.4), L-Glu (0.65), Gly (0.55), L-His (0.1), L-Ile (0.23), L-Leu (0.23), L-Lys hydrochloride (0.42), L-Met (0.25), L-Phe (0.13), L-Pro (0.1), L-Ser (2.10), L-Thr (0.23), L-Tyr (0.17), and L-Val (0.23).

Expression of [^{15}N-Val]

In brief, 1.0 L of M9 minimal medium supplemented with all the amino acids except L-Val, was inoculated with 10 mL of the above mentioned *E. coli* BL21 GOLD (DE3) culture grown overnight. When the OD$_{600}$ reached a value of 1.0, biosynthesis of polypeptide was induced by adding isopropyl-β-D-thiogalactopyranoside (IPTG) to a final concentration of 1 mM, followed by the

addition of 0.23g [^{15}N-L-Val]. The cells were incubated for 5 h at 30 °C. Cell harvesting, lysis, protein purification and heme reconstitution were done as described above.

Expression of [^{15}N-Leu]

Expression of [^{15}N-Leu] truncated HasAp was carried out using the protocol similar to [^{15}N-Val] truncated HasAp except that the medium was devoid of L-Leu amino acid instead of L-Val. Moreover, 3 g of glucose instead of 2 g was used in the M9 medium. In addition, when the OD$_{600}$ reached 1.0, IPTG was added to induce the biosynthesis of the polypeptide followed by 55 mg of [^{15}N-L-Leu], 0.23g L-Ile, and 0.23g L-Val. It was observed in the previous expressions that both Ile and Val were also labeled together with Leu. Hence, these two amino acids were added to prevent isotopic scrambling. The cells were incubated for 5 h at 30 °C. Cell harvesting, lysis, protein purification and heme reconstitution were done as described above.

Expression of [^{15}N-Thr]

Expression of [^{15}N-Thr] truncated HasAp was carried out using the protocol similar to [^{15}N-Leu] except that the medium was devoid of L-Thr instead of L-Leu. During induction, IPTG was added followed by the addition of 55 mg [^{15}N-Thr], 0.55g Gly, and 2.10g L-Ser. It was necessary to supplement the medium with Gly and L-Ser to prevent the incorporation of ^{15}N labeled Gly and Ser residues as observed in

the previous expressions. Cell harvesting, lysis, protein purification and heme reconstitution were done as described above.

Expression of [^{15}N-Tyr]

Expression of [^{15}N-Tyr] truncated HasAp was carried out using the protocol similar to [^{15}N-Val] truncated HasAp except that the medium was devoid of ^{15}N-Tyr amino acid. In addition, when the OD$_{600}$ reached 1.0, IPTG was added to induce the biosynthesis of the polypeptide followed by 0.17g of [^{15}N-L-Tyr]. The cells were incubated for 5 h at 30 °C. Cell harvesting, lysis, protein purification and heme reconstitution were done as described above.

UV-Visible Absorption Spectroscopy

The electronic absorption spectra of both holo full-length and truncated HasAp were recorded in phosphate buffer ($\mu = 0.1$, pH 7.0) using an Ocean Optics UV-Vis spectrophotometer. Extinction coefficients of the proteins at 407 nm (ε_{407}) were measured as described previously [20]. In brief, a 100 μL of pyridine was added to a pure sample (900 μL) of holo HasAp in phosphate buffer ($\mu = 0.1$, pH 7.0) with an absorbance of 1.0. The pyridine will denature the protein and coordinate to the displaced heme. An excess of sodium dithionite was added to the solution to reduce the iron, after which the spectrum of the pyridine hemochrome was recorded. The protein concentration was calculated the using the reported extinction coefficient of the reduced ferrous pyridine-hemochrome and the Beer-Lambert Law. The average

protein concentration was calculated using extinction coefficients at the absorbance maxima of 418 nm, 555 nm and 525 nm are 170, 34.4, and 17.5 mM^{-1} cm^{-1}, respectively. The average protein concentration values were used to calculate the extinction coefficient of the protein at 407 nm. Three trials were performed per protein sample.

Sample Preparation

Preparation of Apo-protein

The extraction of heme was carried out using the cold-acid acetone treatment [6]. A 1.5 mL of 2.5 mM holo HasAp was added drop by drop with stirring into a 100 mL acid-acetone solution (0.2% V/V of 12M HCl) previously stored in -20 °C. The resultant solution turned red with the concomitant formation of white precipitate. The suspension was stirred for an additinal 10 min and then centrifuged at 2500 rpm for 1 min at 4 °C. The procedure was repeated again if the precipitate has some reddish color. The final precipitate was dissolved in 100 mL of 100 mM Tris-HCl buffer (pH 7.8) containing 7.0 M urea. The solution was then dialyzed against 100 mM Tris-HCl with 100 mM NaCl buffer (pH 7.8) (1 x 4 L) and then against phosphate buffer ($\mu = 0.1$, pH 7.0) (3 x 4 L) at 4 °C. After dialysis the protein was concentrated to 3 mL and loaded into a G50 size exclusion column pre-equilibrated with phosphate buffer ($\mu = 0.1$, pH 7.0). Protein fractions with > 90% apoprotein, as determined by the absence of the Soret peak at 407nm, were pooled and concentrated.

Preparation of Protein Harboring ^{13}C-Labeled Heme

[13]C-labeled δ-aminolevulinic acid (ALA) was used as the biosynthetic precursor for the preparation of ^{13}C-labeled protoporphyrin IX (heme) [21-23] . The ^{13}C-labeled hemes were synthesized and subsequently extracted from outer mitochondrial (OM) cytochrome b_5 using the methodology described in Chapter 2. Synthesis of [1,2-^{13}C]-ALA, [4-^{13}C]-ALA and [5-^{13}C]-ALA were previously described [21, 22]. [1,2-^{13}C]-ALA was used as precursor to label heme at the methyl, β-vinyls, propionate-β, and carbonyls (Figure 4A), while [4-^{13}C]- and [5-^{13}C]-ALA were used to label the core carbons: C_α and C_β, and C_α and C_m, positions, respectively (Figure 4B and C). After truncated apo-HasAp was reconstituted with a freshly prepared solution of ^{13}C-labeled heme, the resultant solution was incubated at 4 °C overnight and then purified in Sephacryl S-200 size exclusion column (2.6 i.d. cm x 90 cm. length). The fractions with high purity (A_{280}/A_{407}) ratio of < 0.35 were pooled and dialyzed in phosphate buffer ($\mu = 0.1$, pH 7.0). Fractions containing pure protein were concentrated in Amicon centrifugal concentrators to ~1 mL and transferred to smaller concentrators to exchange protein into deuterated buffer.

X-Ray Crystallography

Initial crystal growth screening conditions were carried out in the High Throughput Crystallization Screening Laboratory of Hauptman-Woodward Medical Research Institute (Buffalo, NY) [24]. This facility uses an automated liquid-handling system to set up 1536 microbatch-under-oil crystallization experiments and

plates are imaged before and after addition of the protein solution to the cocktails and every week thereafter for six weeks. The cocktail conditions and the images of the crystals are shown in Appendix 1. Twenty nine wells showed crystal growth after six weeks and 15 crystal growth conditions were optimized in our laboratory to obtain
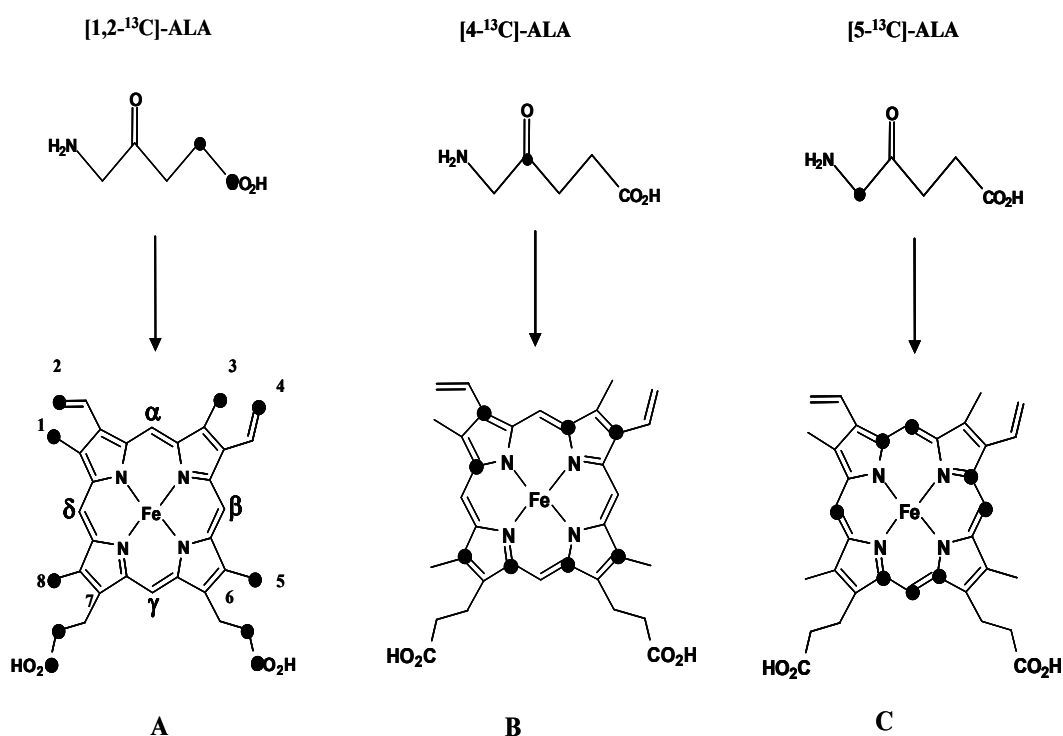
Figure 4. ^{13}C-labeling patterns obtained when protoporphyrin IX is biosynthesized from (A) [1,2-^{13}C]-ALA, (B) [4-^{13}C]-ALA, and (C) [5-^{13}C]-ALA.

good quality crystals suitable for X-ray diffraction. Crystals were grown using the hanging drop vapor diffusion method by mixing 5 μL of a 120 mg/mL solution holo HasAp with an equal volume of reservoir solution, containing 100 mM MES buffer (pH 6.5), 100 mM NH₄Cl, and 80% PEG 400. Under these conditions, holo truncated HasAp crystallizes as brown colored crystals (Figure 5) at 23 °C and takes 3 days to reach a size (1 mm length x 1 mm width x 1 mm depth) suitable for X-ray analysis.

Figure 5. Crystals of truncated holo-HasAp grown using the hanging drop method

NMR Spectroscopy

One-Dimensional NMR Spectroscopy

^{1}H NMR spectra were collected on a Varian Unity Inova spectrometer equipped with a triple resonance probe operating at a 599.74 MHz ^{1}H frequency. Proton spectra were acquired with presaturation of the residual water peak over 40 k data points, a spectral width of 100 kHz, a 200 ms acquisition time, 20 ms relaxation delay, and 1024 scans; spectra were referenced to a residual water peak at 4.80 ppm. The ^{13}C spectra were obtained on a Varian Unity Inova spectrometer equipped with a 5 mm broadband probe and operating at a frequency of 60.781 MHz ^{13}C frequency. The ^{13}C spectra were referenced to an external solution of dioxane (60% V/V in D_2O) at 66.66 ppm. The acquisition parameters used to obtain ^{13}C NMR spectra are given in the appropriate figure captions. One-dimensional ^{1}H and ^{13}C spectra were processed and analyzed with VNMRJ.

Two- and Three-Dimensional NMR Spectroscopy

The protein samples used for two- and three-dimensional NMR data collection were in phosphate buffer (μ = 0.1, 95% H_2O, 5% D_2O, pH 7.0). The protein concentrations were approximately 2.5 mM. All NMR experiments were performed at 32 °C unless otherwise noted in the figure captions. 2D and 3D NMR experiments [^{1}H-^{15}N-HSQC, HN(CO)CA, HNCA, CBCA(CO)NH, HNCACB and NOESY-HSQC] used to carry out the backbone assignment of holo HasAp, full-length and truncated, were carried out using Bruker Avance 800 spectrometer equipped with a 5

mm TXI ^{1}H-^{13}C/^{15}N/D xyz-gradient probe. The backbone assignments of truncated apo-HasAp were carried out using the same set of 2D and 3D NMR experiments obtained in the Varian Unity INOVA 600 spectrometer equipped with a triple-resonance z-axis gradient probe. While the three dimensional NMR experiments HNCO and (HCA)CO(CA)NH used for the sequential backbone assignment of holo proteins were carried out in the Varian Unity INOVA 600 spectrometer. Three-dimensional ^{15}N-separated NOESY-HSQC (110 ms mixing time) of the holo full-length HasAp was obtained at 305 K in a Bruker Avance 800 spectrometer. Specific parameters used for the NMR experiments are shown in the corresponding figure captions. The data were processed using NMRPipe [25] and analyzed with the program Sparky [26]. The chemical shifts were referenced directly and indirectly using the proton frequency of the DSS resonance at 0.00 ppm.

H/D Exchange Studies

Amide hydrogen-deuterium exchange experiments were carried out in the Varian Unity INOVA 600 spectrometer at 32 °C. Prior to the start of an H/D exchange experiment the [U-^{15}N]-holo truncated HasAp sample (2.5 mM) was exchanged in aqueous sodium phosphate buffer (μ = 0.10, pH 7.0). The aqueous solvent was eliminated by freeze-drying using Savant® Speed Vac Lyophilizer (Farmingdale, N. Y.) then resuspended in D$_2$O. The volume of D$_2$O added is equal to the volume of the protein sample prior to lyophilization. Sample prepared in this way showed identical UV-Vis and NMR spectroscopic characteristics to the sample shown

before lyophilization. The H/D exchange process was monitored immediately after the lyophilized protein was redissolved in D_2O. The exchange was followed as a function of time by following the time-dependent decrease of the amide cross-peaks with the aid of 2D ^1H-^{15}N HSQC [27]. The dead time between addition of D_2O to the lyophilized protein and the beginning of data acquisition was about 10 min. Total acquisition time for each HSQC spectrum was 20 min and spectra were taken every 20 min for 18 h, and every hour thereafter for a total of 32 h. Each HSQC spectrum was acquired at 32 °C using the Varian Unity INOVA 600 spectrometer. The HSQC spectra were taken over 8.4 kHz (^1H) and 2.2 kHz (^{15}N) spectral widths, with 4 scans per increment, 0.085 s acquisition time, 1.0 s relaxation delay and 1428 and 128 complex points for the ^1H, and ^{15}N dimensions, respectively. Exchange rate constants per residue (k_{ex}) were determined as described previously [28] by fitting the time-dependent decay of cross-peak intensities to a three parameter single exponential decay function using the program Sigma Plot version 2001, v.7.0. Sequence-specific intrinsic rate constants (k_{ch}), Gibbs free energy of exchange (ΔG_{HX}) and protection factors per residue were calculated using the spreadsheet provided in Dr. S. Walter Englander's website at http://hx2.med.upenn.edu/download.html. The spreadsheets were used with pD corrected values at 32 °C. The pH of the D_2O solution was measured immediately after data acquisition and corrected for the isotope effect using equation 1 [29].

$$(pD_{corrected} = pD_{read} + 0.4) \tag{1}$$

Heme Transfer Experiments

Preparation of Hb, Mb and HbO$_2$ Samples

Horse heart myoglobin and human hemoglobin were purchased from Sigma-Aldrich. Lyophilized myoglobin and hemoglobin were dissolved in phosphate buffer (μ = 0.10, pH 7.0). The insoluble part was removed by centrifugation and the solutions were purified in a Sephadex G-50 (2.6 i.d. cm x 90 cm. length) size exclusion column. Protein fractions with purity ratio < 0.25 at (A_{280}/A_{405}) and (A_{280}/A_{409}) for hemoglobin and myoglobin, respectively, were pooled and concentrated using Amicon ultracentrifuge filters to a final concentration of ~1.0 mL. Oxyhemoglobin (HbO$_2$) was prepared by adding molar excess of sodium dithionite to hemoglobin to reduce the ferric heme-iron to ferrous. This reaction was done inside a glove box. The sodium dithionite was then removed by passing the protein solution in a desalting column and the HbO$_2$ complex formed by subsequent exposure to air. Freshly prepared myoglobin, hemoglobin and oxyhemoglobin were used in the heme transfer experiments.

Heme Transfer Assay

The heme transfer assay was carried out at 37 °C using UV-Visible spectrophotometer. In brief, heme transfer experiments were carried out by mixing an excess of truncated apo-HasAp with respect to Hb, Mb and HbO$_2$ in phosphate buffer (μ = 0.1, pH 7.0) with stirring in a cuvette. The transfer of heme from holo-proteins

75

(Hb, Mb and HbO$_2$) to apo-HasAp were monitored by the emergence of the high-spin charge transfer band of holo HasAp at 616 nm as a function of time.

RESULTS AND DISCUSSION

Overexpression and Purification of HasAp

Both full-length and truncated apo-HasAp proteins were expressed under the same conditions. Luria-Bertani (LB) medium was first used to express the proteins. However, the expressed proteins contained > 50% heme content. The full length HasAp expressed using this medium have multiple C-terminal cleavages as determined by SDS-PAGE gel and mass spectrometry. Moreover, the cleaved and uncleaved forms were not separated by size exclusion chromatography. To circumvent this problem, M9 minimal medium not supplemented with FeSO$_4$ was used to grow the culture so as to inhibit the formation of heme containing HasAp. With the absence of iron in the culture medium, it took 12 h for the OD$_{600}$ to reach 1.0. After lysis, all the proteins were found in the supernatant. The proteins were purified using an anion exchange chromatography column. HasAp protein fractions were only 80% pure after ion exchange and they came out with 30% heme content. The fractions with the protein of interest as determined by SDS-PAGE gel were pooled and reconstituted with hemin. In the SDS-PAGE gel, the full-length and the truncated protein gave a band a little bit above and below 20 kDa, respectively (Figure 6). The protein was passed through a size exclusion column. The protein

76

purity was monitored by the ratio of A_{280}/A_{407}. The molecular weight of the full-length and the truncated HasAp forms were 20 773 and 18 761 kDa, respectively, as determined by mass spectrometry. The molecular weight also showed that both the full-length and truncated HasAp proteins were expressed without the start methionine residue.
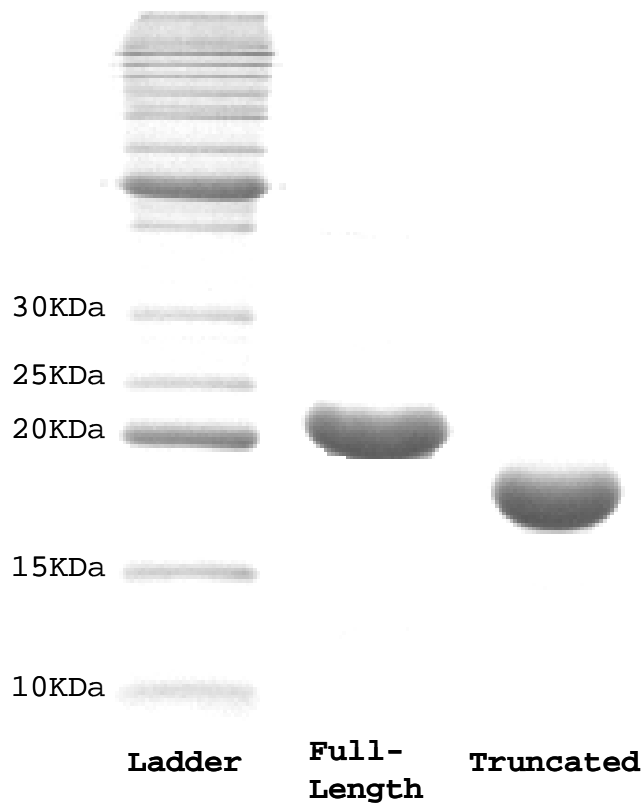
Figure 6. SDS PAGE of purified full-length and truncated HasAp. The molecular weight of full-length and truncated HasAp are 20 773 and 18 761 KDa, respectively.

Protein Crystallization

Protein crystallization is a trial-and-error process in which the protein is precipitated from its solution [30]. This process is characterized by a reversible equilibrium phenomenon driven toward the minimization of the free energy of the system [31]. This method aims to produce crystals free of contaminants and large enough to provide X-ray diffraction pattern. This diffraction pattern is then analyzed to solve the three-dimensional structure of the protein. Formation of crystals can be explained using the two-dimensional solubility diagram illustrating the protein concentration against the concentration of the precipitating agent as shown in Figure 7. The solubility curve separates the concentration space into two areas, the undersaturated and supersaturated state of a protein solution [30, 32, 33]. The area under the solubility curve is the undersaturation phase where crystals will not grow. The supersaturation phase is the area above the solubility curve and it is divided into three areas and this is where the protein crystallizes. In the metastable area, the rate of nucleation is slow that no crystal grows for a long time unless seed crystals are introduced. In the nucleation zone, supersaturation is large enough that crystal growth is observed. Lastly in the precipitation zone, supersaturation is large enough that protein molecules separates from the solution to form amorphous aggregates [34, 35].

Several methods are used to bring the protein solution into a supersaturation phase [32, 36]. In this work, the hanging drop diffusion method was used for protein
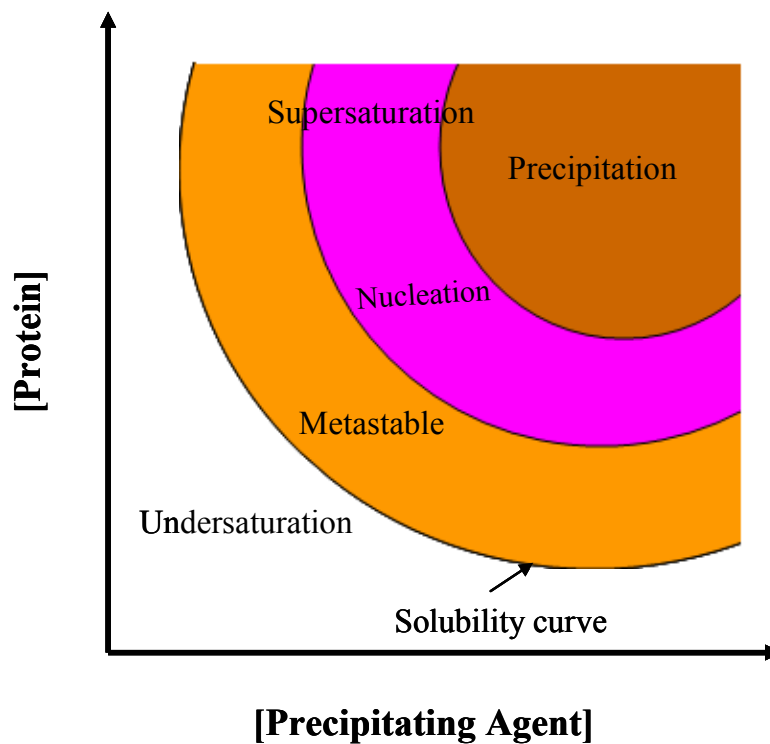
Figure 7. Schematic representation of a two-dimensional crystallization phase diagram.

crystallization (Figure 8). This technique uses vapor diffusion to promote crystal growth. A droplet containing the pure protein, buffer and precipitant solution is suspended over a reservoir like a hanging drop which contains higher concentrations of buffer and precipitants similar to the droplet [33]. The droplet contains a 1:1 ratio of the protein and the precipitants. Vapor equilibration between the droplet and reservoir is the driving force which causes the protein solution to reach the nucleation level to promote crystal growth.

Coverslip with protein solution (brown)

High-vacuum grease

Reservoir with
precipitant

Initial solution

Final solution
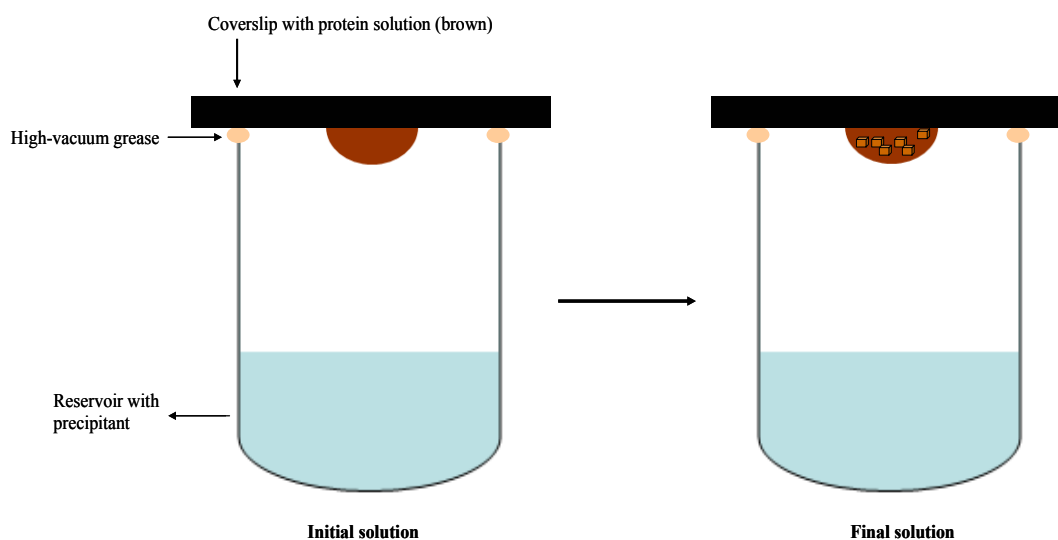
Figure 8. Schematic representation of the hanging drop diffusion vapor diffusion technique used in growing protein crystals.

X-ray Diffraction Analysis

Three-day old crystals of truncated holo-HasAp are shown in Figure 5. The truncated holo-HasAp protein crystallized with two monomers per asymmetric unit in space group P3(1). The overall structure was refined by Dr. Ernst Schönbrunn and coworkers to 1.7 Å resolution with a current R_{free} of 19.5%. The crystal is hexagonal, with unit cell a = b = 47.7 Å, and   c=141.29 Å; alpha = beta = 90 degrees, gamma = 120 degrees.

Secondary Structure of Truncated HasAp

The X-ray crystal structures of the two monomers of holo truncated HasAp is shown in Figure 9. Close inspection of the two crystals determined using the stride program [37] show that they both have the same secondary structure composition (Table 1). Analysis of the secondary structure content of the protein reveals that it is a member of the family of $\alpha\beta$ proteins, with 29% of the structure involved in α-helices and 34% in β-strands. The secondary structure (Figure 10) shows four α-helices and eight anti-parallel β-sheets, three 3_{10} –helix and 16 β-turns (types I, II, II', IV, VIb and VIII). The first β-sheet is connected to a three-residue 3_{10}-helix and α-helix 1, and interestingly, the following six antiparallel β-strands ($\beta2$ to $\beta7$) are adjacent in sequence and are connected by hairpins. The four α-helices ($\alpha1$-$\alpha4$) are packed against the aforementioned β-sheets, thus forming an "α-helix wall" opposite to the "β-sheet wall". The two 3_{10}-helices in the structure are 3_{10}-helix 1 (residues Thr9-Tyr11) which connects the first β-strand to the first α-helix. The second 3_{10}-helix (I125-D130) connects α-helix 2 and β-strand 6. 3_{10}-helices are only three or four residues long, compared with a mean of ten residues in a typical α-helix [38, 39], and are found at the N- or C-terminus of α-helices [40]. It is the fourth most common secondary motif in proteins and it is believed to be an intermediate in the α-helix folding and melting processes [40-43].
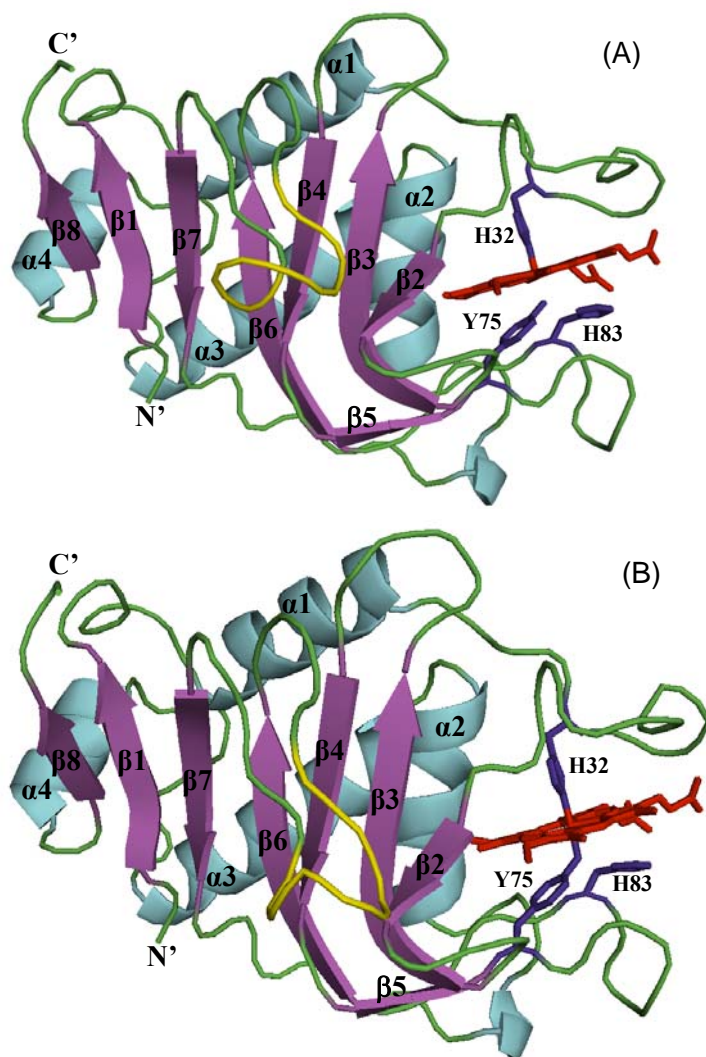
Figure 9. X-ray crystal structures of truncated HasAp (A) monomer A and (B) monomer B showing four α-helices (cyan), eight anti-parallel β-strands (magenta), loops (green), loop with high B-factor values (yellow), heme (red), and axial ligands (blue).

Table 1. Secondary Structure Comparison of Monomer A and B of Holo-HasAp
X-ray Crystal Structure Using The Program Stride [37].

Residue	Monomer A	Monomer B
Val16 - Phe27	Alpha Helix I	Alpha Helix I
Thr132 - Ser142	Alpha Helix II	Alpha Helix II
Ser145 - Val159	Alpha Helix III	Alpha Helix III
Phe169 - Ala175	Alpha Helix IV	Alpha Helix IV
Thr9 - Tyr11	3_{10} - Helix	3_{10} - Helix
Ile125 - Asp130	3_{10} - Helix	3_{10} - Helix
Ser4 - Ser8	Beta Sheet I	Beta Sheet I
Gly45 - Pro48	Beta Sheet II	Beta Sheet II
Asp52 - Lys59	Beta Sheet III	Beta Sheet III
Ala65 - Tyr75	Beta Sheet IV	Beta Sheet IV
Leu85 - Gly100	Beta Sheet V	Beta Sheet V
Tyr107 - Ser117	Beta Sheet VI	Beta Sheet VI
Leu121 - Ser123	Beta Sheet VII	Beta Sheet VII
Ala178 - Thr181	Beta Sheet VIII	Beta Sheet VIII
Tyr11 - Trp14	Turn I	Turn I
Arg33 - Gln36	Turn II	Turn II
Pro34 - Val37	Turn IV	Turn IV
Gly140 - Thr43	Turn IV	Turn IV
Phe46 - Gly49	Turn VI b	Turn VI b
Gly49 - Asp52	Turn I	Turn I
Gly53 - Tyr56	Turn VIII	Turn VIII
Ser60 - Ser63	Turn IV	Turn IV
Thr76 - Ser79	Turn II'	Turn II'
Ser79 - Ser82	Turn IV	Turn IV
Pro81 - Thr84	Turn IV	Turn IV
Gly100 - Ser103	Turn IV	Turn IV
Ala102 - Gly105	Turn IV	Turn IV
Leu109 - Gln112	Turn VIII	Turn VIII
Asp160 - Leu163	Turn I	Turn I
Ser164 - Ser167	Turn I	Turn I
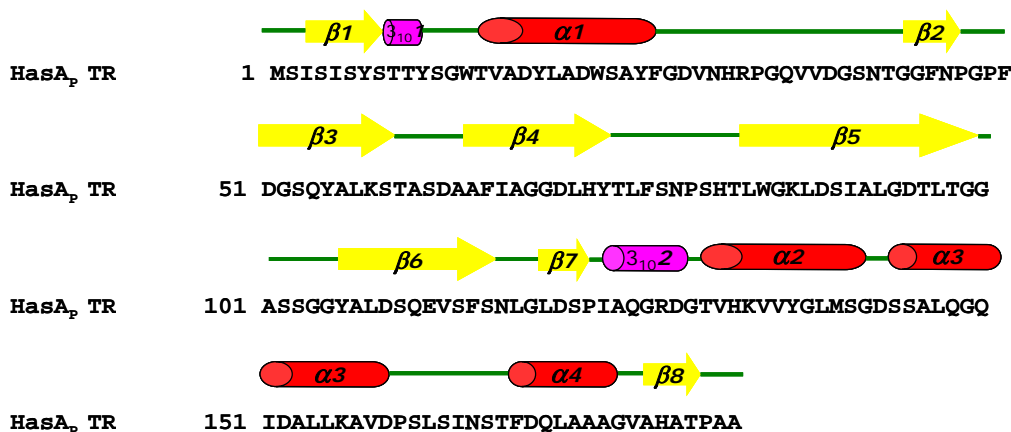
Figure 10. Secondary structure assignment of truncated HasAp using Stride [37]. The α-helices are in red, β-sheets in yellow, 3_{10}-helix in magenta and loops in green.

The X-ray crystal structure of HasAp looks very similar to that of HasA$_{SM}$ [44], which also looks like a fish with the heme pocket resembling a mouth biting the heme. These two proteins share > 50% sequence identity. A superimposed X-ray crystal structures of holo-HasA$_{SM}$ and HasAp (Figure 11) show that the polypeptide of truncated HasAp folds into the same αβ fold characteristic of HasA$_{SM}$ [44]. The heme is highly exposed to the solvent and it is contained within two extended loops: Loop 1 is located between α1 and β2 and contains one of the heme axial ligands, His32. The second extended loop is located between strands β5 and β6, and contains the other heme axial ligand, Tyr75. The carboxyl end of the second extended loop continues onto the bulk of the "β-sheet wall", thus the loops containing the heme can be thought of as flexible jaws hinged to the rigid β-sheet and α-helix

walls. In the structure of HasA$_{SM}$ electron density can be seen only to residue 174. In the structure of HasAp, electron density is seen for all 184 residues, which reveals a strand (β8, residues 178-181) parallel to β-1, thus extending the β-sheet wall by one strand, relative to the structure of HasA$_{SM}$.
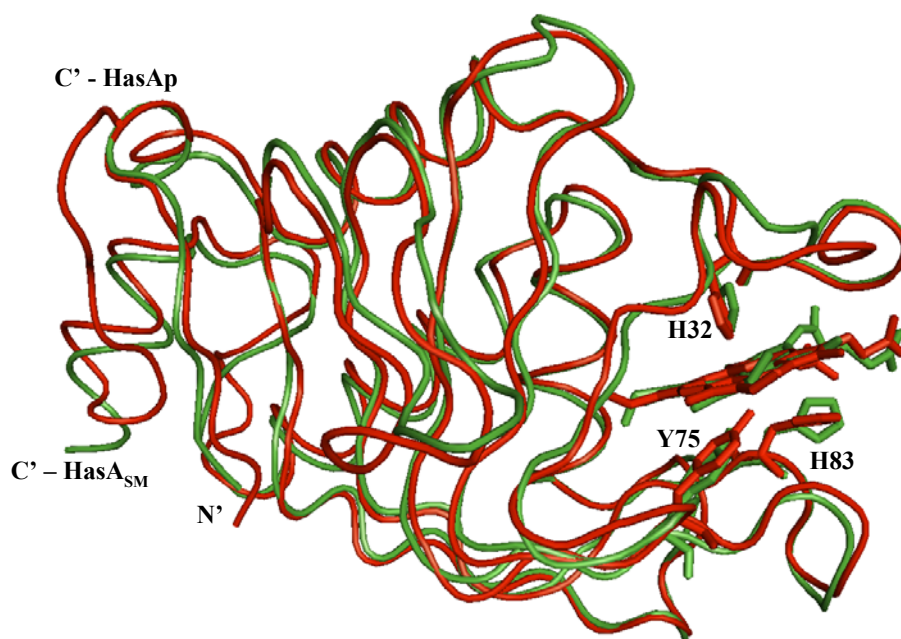
Figure 11. Superimposed X-ray crystals structures of Holo-HasAp (red) and Holo-HasA$_{SM}$ (green) (PDB ID. 1DKO).

As pointed out above, the heme is axially coordinated by a His32 and Tyr75, a coordination motif that is identical to that seen in the structure of HasA$_{SM}$, and in agreement with the conserved nature of these residues in hemophore sequences from distinct organisms [45]. The heme propionate groups interact with the polypeptide via hydrogen bonding and electrostatic interactions; the oxygen atoms of propionate A interact to form a salt bridge with the guanidinium group of Arg129, whereas the O1 atom of heme propionate D is hydrogen bonded to the NH of Gly35 on the opposite side of the heme plane. The heme prosthetic group in heme proteins binds to the polypeptide in two orientations that differ by a 180° rotation about the α-γ-meso axis, a phenomenon common to proteins when the heme is not bound covalently, *i.e.* cytochrome *b$_5$* [46, 47] and heme oxygenase [17]; these two heme isomeric forms of HasA$_{SM}$, which exist in 70:30 ratio have been observed in electron density maps of a 1.77 Å resolution structure [48] and solution NMR spectroscopic studies [49]. Analysis of heme electron density in HasAp, on the other hand, indicates that the heme is bound in only one orientation as shown in Figure 12. This conclusion is supported by observations made in the solution NMR spectroscopic studies described later in this chapter.

The hydrogen bonding network in the vicinity of the heme is also very similar in the HasA$_{SM}$ and HasAp structures. Notably, the orientation of the side chain of His83 places its Nδ within hydrogen bonding distance of the coordinated phenolate oxygen in Tyr75, a situation identical to that observed in the crystal structure of HasA$_{SM}$ [44], which was crystallized at pH 4.6. It is interesting that in a subsequent

investigation, crystals of HasA$_{SM}$ were grown at pH 4.6, 6.5, and 8.0 [48]. The structure of HasA$_{SM}$ obtained at pH 6.5 showed that the His83 side chain attains a
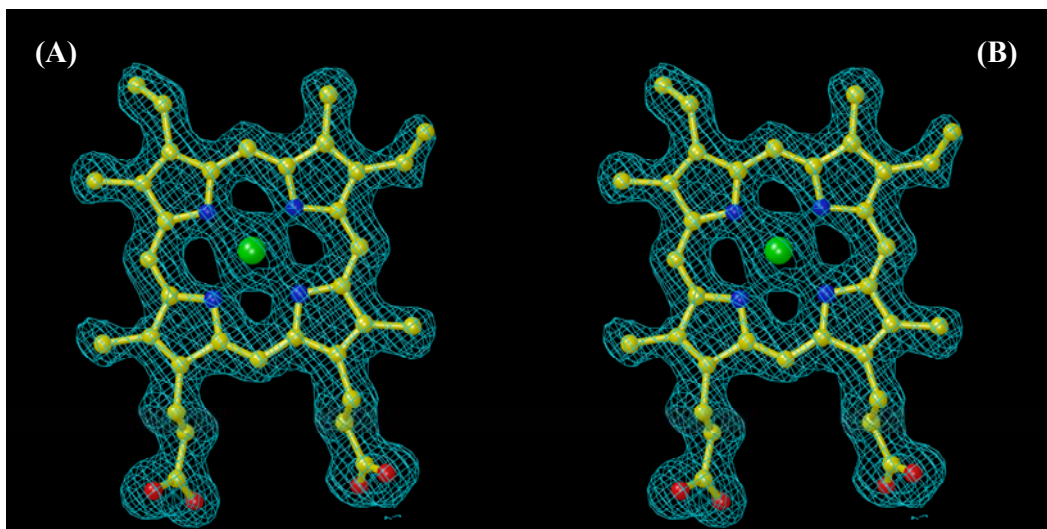
Figure 12. Electron density map of the heme active site of truncated HasAp crystal structure in (A) monomer A, and (B) monomer B. There is only one heme isomer in HasAp.

different conformation and is not hydrogen bonded to Tyr75. B factors for the heme in this structure were very high, thus the observation was interpreted to suggest that the loss of hydrogen bond between His83 Nδ and the phenolate of Tyr75 may facilitate heme acquisition and/or release [48]. It is therefore interesting that the structure of HasAp, obtained from crystals grown at pH 6.0, show low B-factors for the heme and a hydrogen bond between the coordinated Tyr75 phenolate oxygen and Nδ of His83. Thus a pH switch controlling the protonation state and concomitant

heme affinity in the hemophores does not seen to be operative when comparing the structures of HasAp and HasA$_{SM}$ obtained from crystals grown at similar pH values.

The internal order of the protein is reflected from B-factor values. The B-factors show thermal vibration, conformational disorder or static lattice disorder, or misorientation of the protein molecules [50]. This suggests that residues which exhibit high B-factor values are located in highly flexible and disordered loops. The calculated C$_\alpha$ B-factors of both HasAp monomers (Figure 13) show that residues 100-106 (GGASSGG) have B-factor values ranging from 29.42 to 51.58 A^2, while the average C$_\alpha$ B factor value is only 15.60 A^2. Ser103 shows the largest B-factor (51.58 A^2) among the residues in the protein. Inspection of the structure reveals that the loop containing residues 100-106 is a hairpin loop connecting β5 with β6 and is highly exposed to the solvent. This loop, which is colored yellow in Figure 9, faces outward and looks like the gills of the fish. Using the structural alignment in Figure 1, residues Gly100-Gly106 of HasAp correspond to Gly100-Pro105 of HasA$_{SM}$. It was observed by Létoffé *et. al*. [51] that these residues were involved in the interaction of HasA$_{SM}$ with HasR$_{SM}$. It is possible that the high flexibility of this loop allows it to change its conformation to bind with the cognate receptor to deliver the heme. In addition, residues A183 and A184 also have high B-factor values. This could also suggest that the tail is also a highly unstructured part of the protein. The flexibility of the tail could make HasAp easily accessible for: (1) binding with the ABC-transporter before

being secreted to the extracellular medium, and (2) proteases to cleave the C-terminal residues.
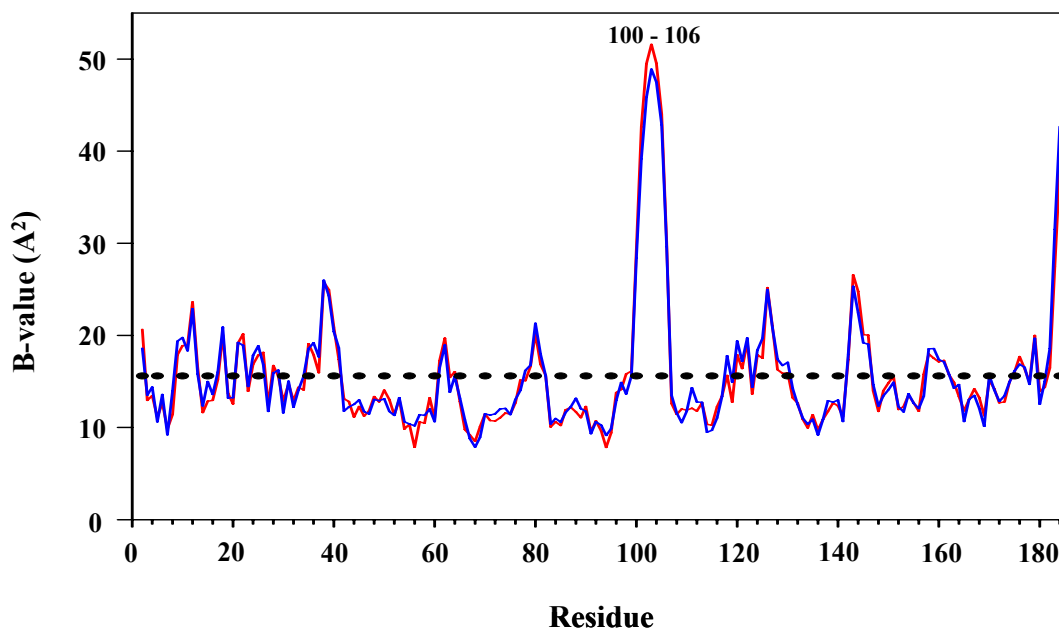
Figure 13. Per-residue plot of the C_α B-factor values of monomer A (red) and monomer B (blue). The average B-factor values of both monomers are shown in black dotted line. Residues 100 to 106 show high B-factor values.

Spin State of the Heme-Iron in HasAp

Electronic Absorption Spectroscopy

The electronic absorbance spectra of the holo full-length and truncated HasAp proteins show a Soret maximum at 407 nm with visible bands at 495, 540, 577, and 618 nm (inset of Figure 14). Their extinction coefficients at 407 nm (ε_{407}) is 77.67

mM^{-1} cm^{-1}. Typically, heme proteins exhibit characteristic electronic absorption bands in the visible region [52]. Moreover, high-spin species (S = 5/2) have Soret maxima between 405 to 410 nm while low-spin species (S = 1/2) have Soret maxima at longer wavelengths, between 415 to 425 nm. The electronic absorption spectrum of HasAp suggests that it is a high-spin species [53]. However, its alpha, beta and charge transfer bands do not show either fully high-spin or fully low-spin character. The alpha and beta bands at 577 and 540 nm, respectively, which are indicative of a fully low-spin species are not very prominent. Moreover, the bands at 495 and 616 nm correspond to a high-spin charge transfer band [52, 53]. The Soret peak and the visible bands strongly suggest that HasAp have both high-spin (S = 5/2) and low-spin (S = 1/2) characters.
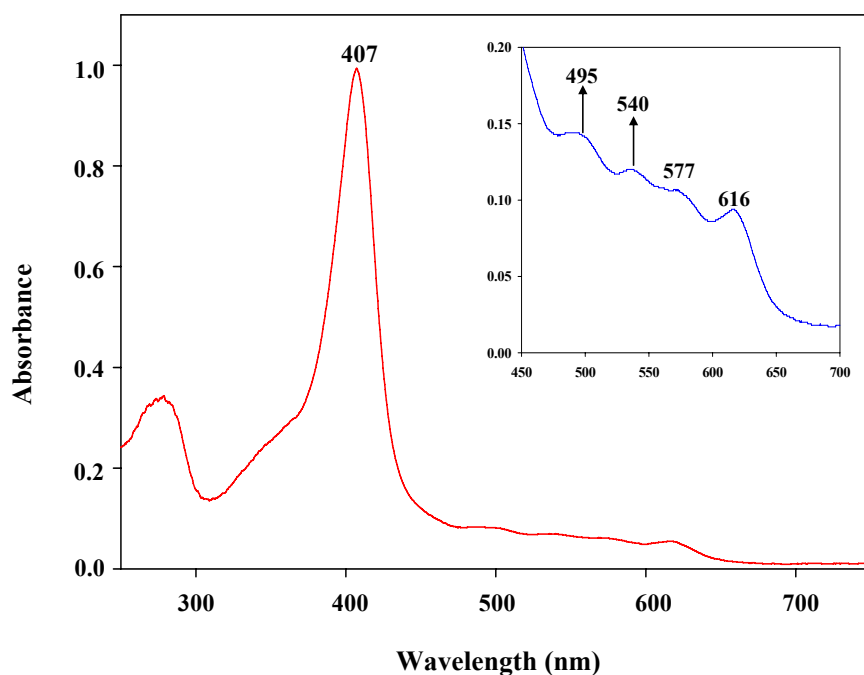
Figure 14. Electronic absorption spectrum of HasAp

90

¹H NMR Spectroscopy

The ¹H NMR spectra of both the holo full length and truncated HasAp are identical (Figure 15). The presence of only one set of resonances shows that there is only one heme conformation of HasAp in solution. This result also agrees with the X-ray crystal structure data (see above). The mean hyperfine shifts of the four methyl peaks in heme proteins has been used as an indicator of the spin state of the heme-iron [54, 55]. Heme methyl resonances of purely high-spin and low-spin species differ very dramatically from each other [54, 56-58]. The heme methyl resonances were identified as the three intense downfield resonances at 42.90, 38.40 and 29.64
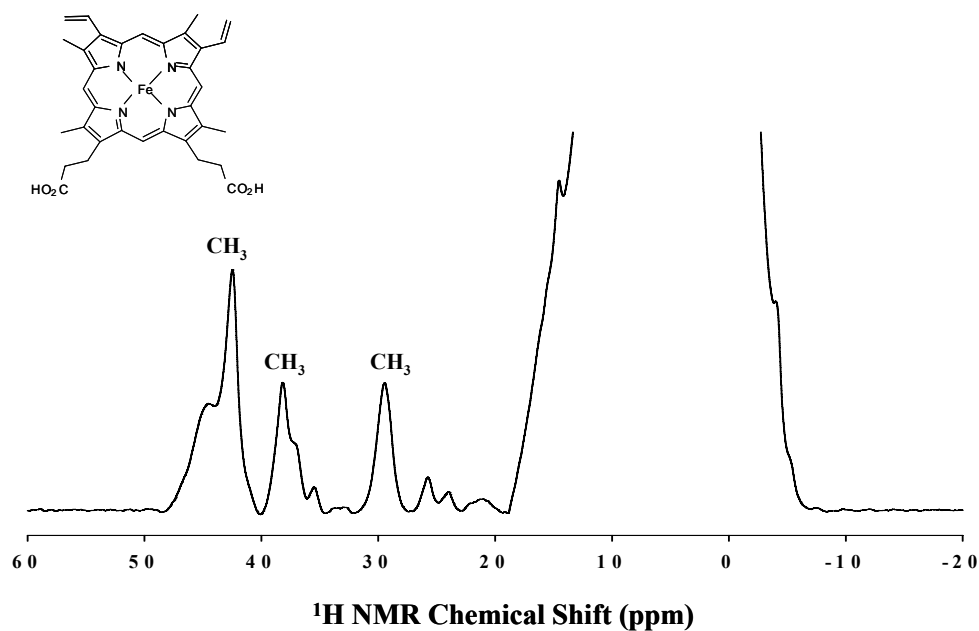
Figure 15. ¹H NMR spectrum of HasAp.

ppm. The most intense peak at 42.90 ppm contains two overlapping heme methyl resonances at 32 °C. The average ^{1}H chemical shift of the heme methyl resonances of high-spin (S = 5/2) met-myoglobin wild type and H64V mutants is ~80 ppm [59]. In comparison, the average chemical shift of the heme methyl resonances of HasAp is only 36.98 ppm. This average methyl chemical shift is too large for a low-spin species (S = 1/2). Thus, the ^{1}H NMR spectrum suggests an intermediate spin species (S = 3/2) or a mixture of high-spin (S = 5/2) and low spin (S = 1/2) species in fast exchange relative to the NMR timescale. These observations agree with the electronic absorption spectra of these proteins. From these results, we can conclude there is an equilibrium of high-spin (S = 5/2) and low-spin (S = 1/2) of HasAp in solution. It has been known that for a high-spin species, the meso-H isotropic shift [60-62] can be used as a probe to determine its coordination state. The meso-H for a penta- and hexacoordinate high-spin species resonates at ~ 40 ppm and -25 ppm, respectively. As shown in Chapter 2, broad meso-H peak render this approach inefficient. From the ^{1}H NMR data of HasAp shown in Figure 15, there is no way to determine its coordination state. There is no peak at approximately 40 ppm or -28 ppm. It has been reported [59, 63-68] that the chemical shift characteristics of the core heme carbons (C_α, C_β and C_m), more importantly the meso-carbons, can be used as a probe to determine the coordination state of heme iron. As mentioned in Chapter 2, the ^{13}C NMR approach is more practical in determining the coordination state of the heme-iron because the effect of paramagnetism of the relaxation of ^{13}C is ~ 16-fold lower

than the ^{1}H relaxation and this results in narrower and readily observable ^{13}C resonances.

^{13}C NMR Spectroscopy

To overcome the low natural abundance inherent to ^{13}C spectroscopy, heme-labeled with ^{13}C at appropriate positions was used to reconstitute truncated apo-HasAp. Heme derived from [1,2-^{13}C-ALA] was used to reconstitute apo-HasAp so the heme is labeled at the four methyls, two β-vinyls, two carbonyls, and two β-propionates (insert of Figure 16) [21]. The peaks with blue arterisks correspond to polypeptide peaks, which were determined from a sample of HasAp reconstituted with unlabeled heme. The [1,2-^{13}C]-ALA precursor should label 10 carbons in the heme macrocycle. However, in the spectrum (Figure 16) there are only 8 peaks originating from ^{13}C labeled carbons. Assignment of the ^{13}C peaks could not be accomplished using ^{1}H-^{13}C HMQC experiment because no signal was detected in the spectrum due to the fast relaxation of the ^{1}H resonances. However, La Mar and coworkers [69] reported that the 2,4 C$_\beta$-vinyls of met-aquo myoglobin resonate between 270 and 350 ppm. Hence, the peaks at 225 and 254 ppm were assigned as the 2, 4 C$_\beta$-vinyls. A closer look at the spectrum shows that the intense peak at ~200 ppm consists of two equivalent resonances, which have been assigned to the two carbonyls. The three peaks clustered between 30 and 45 ppm are due to the four methyls. The peak at 33 ppm has two overlapping methyl peaks. This leaves the two β-propionates unassigned. Hence, the two remaining peaks at 130 and 170 ppm are

assigned as the two β-propionates. Moreover, from Figure 16, it can be noted that there is only one heme isomer in HasAp.   This result agrees with information obtained from X-ray crystallography and ^{1}H NMR.
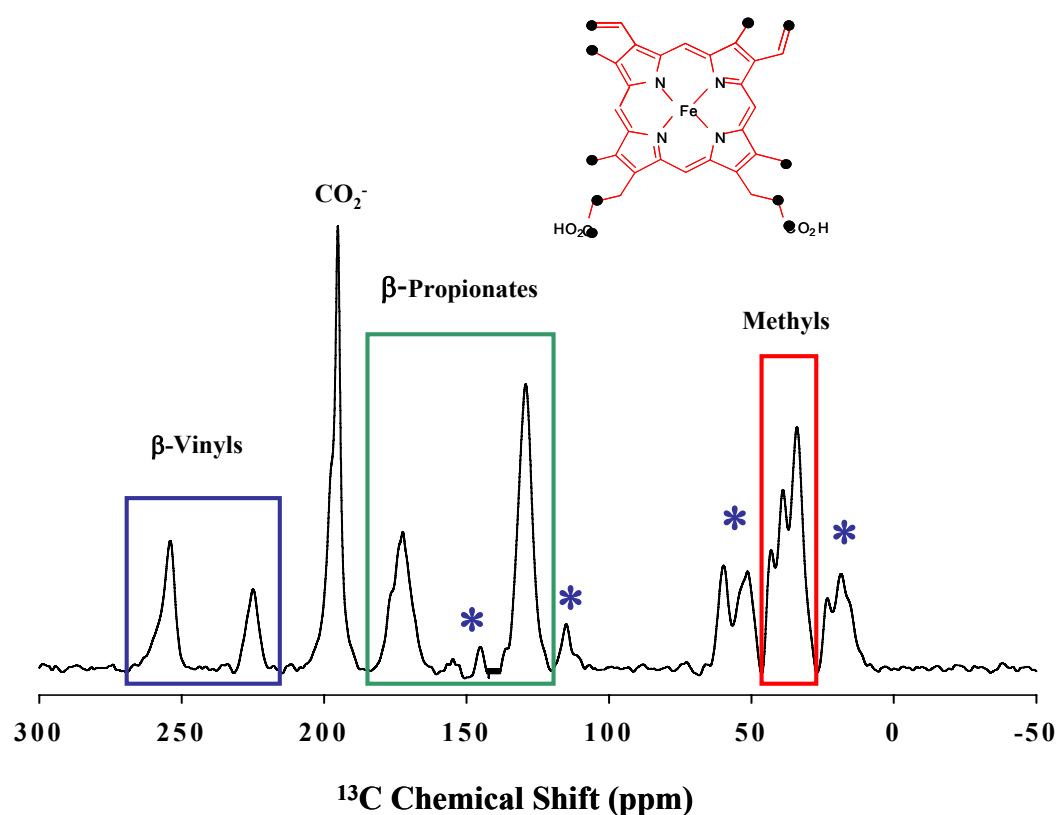
Figure 16. ^{13}C NMR spectrum of HasAp reconstituted with heme derived from [1,2-^{13}C]-ALA. The spectrum was obtained from a sample (2.5 mM) in phosphate buffer (pH 7.0) at 32 °C over 125 kHz, with 150 ms acquisition time, 20 ms relaxation delay and 100 000 scans at 150.821 MHz ^{13}C frequency. The polypeptide peaks are indicated by blue asterisks.

The protonated carbons of the heme would not be able to give much information on the electronic structure and coordination state of the heme-iron as much as the core porphyrin carbons. As mentioned earlier, the characteristic chemical shifts of the core carbons can be used as a probe to determine the coordination state and electronic structure of the heme. However, the close proximity of the core porphyrin carbons (C_α, C_β, and C_{meso}) to the heme iron makes them more strongly affected by the unpaired electron, which makes assigning them more challenging than assigning the protonated heme carbons [10]. Moreover, detection and assignment of core porphyrin carbons has provided straightforward correlations between ^{13}C-core chemical shifts and electronic structure of the heme [59, 68]. Several studies by NMR and density functional calculations (DFT) were reported to determine the electronic structure and coordination of the heme active sites [10, 22, 63, 70]. A method developed [59] and described in Chapter 2 on determining the coordination state of the high spin heme protein was developed to provide some insights on the electronic structure and coordination state of HasAp.

The meso-^{13}C chemical shifts have been shown to be a simple and reliable diagnostic tool to determine the coordination state of high-spin (S = 5/2) heme protein regardless of the axial ligands as described in Chapter 2. This method was also used to determine the coordination state of a heme transport protein, ShuT [20]. A summary of the ^{13}C chemical shift characteristics of the core carbons of the high-spin (S = 5/2) hexacoordinate and pentacoordinate sperm whale myoglobin complexes and

also the characteristic chemical shifts of the core carbons of low-spin species [10] are shown in Figure 17.

To determine the core porphyrin carbons chemical shifts, truncated HasAp samples were reconstituted with hemin labeled with ^{13}C at the C_α and C_β positions (insert of Figure 18A) and with hemin labeled at the C_α and C_m positions (insert of Figure 18B). The ^{13}C NMR spectrum in Figure 18A shows downfield paramagnetically affected resonances between 800 and 1100 ppm. While the spectrum in Figure 18B shows peaks between 1000 and 1100 ppm and another peak (enclosed in red box) at approximately -6 ppm. The common isotopic enrichment for both samples (Figures 18A and B) is C_α. Thus, the broad peaks centered at approximately 1050 ppm in Figures 18A and B can be straightforwardly assigned as the pyrrole C_α resonances. The four peaks between 900 to 950 ppm in Figure 18A are the four C_β resonances. Therefore, it is straightforward to conclude that the peak at -6.10 ppm in Figure 18B originates from the C_{meso} resonances. The downfield shifted C_α and C_β resonances indicate that the $d_{x^2-y^2}$ orbital of the iron is half-filled and this places a positive sigma spin density at the core carbons (C_α and C_β) [71-73]. The high spin density at the C_α and C_β positions leads to a conclusion that HasAp has more high-spin (S = 5/2) than low spin (S = 1/2) characteristics. It was also noted in Chapter 2 that pyrrole C_α and C_β chemical shifts (Figure 17) can also be used to differentiate the hexacoordinate from the pentacoordinate heme complex. Hexacoordinate complexes have C_α and C_β peaks at 1500 and 1250 ppm, respectively, whereas in pentacoordinate complexes they resonate at 1250 and 900
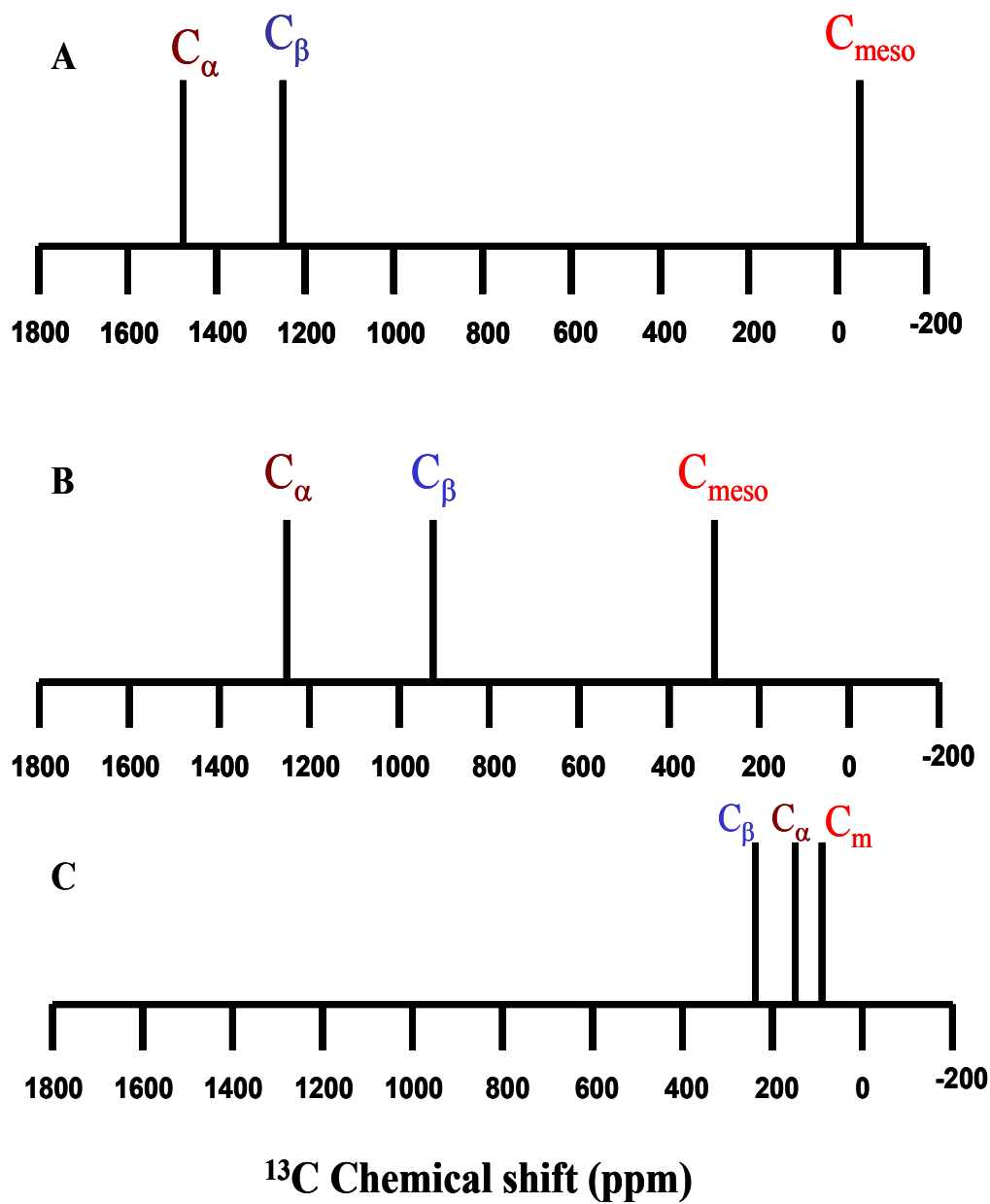
Figure 17. ^{13}C NMR chemical shift characteristics of the core carbons of (A) high-spin (S = 5/2) hexacoordinate; (B) high-spin (S = 5/2) pentacoordinate and (C) low-spin (S = ½) heme complexes. Adapted from [10, 59].
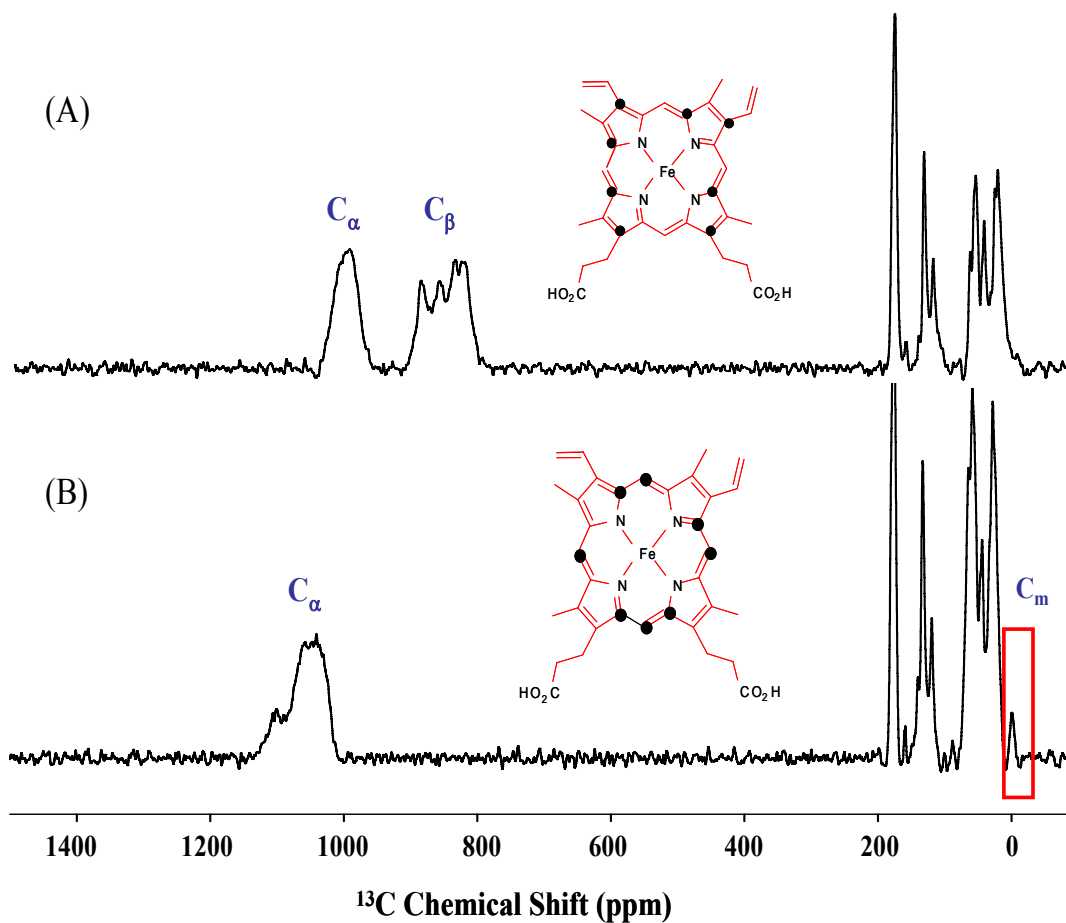
Figure 18. ^{13}C NMR spectra of HasAp, pH 7.0, reconstituted with (A) heme labeled at the C_α and C_β positions and (B) heme labeled at the C_α and C_m positions. The spectra were obtained at 32 °C over 213 kHz, with 100 ms acquisition time, 20 ms relaxation delay and 500 000 scans at 150.821 MHz ^{13}C frequency.

ppm, respectively, *i. e.* the pyrrole C_α and C_β chemical shifts of hexacoordinate heme complexes are more downfield shifted than their pentacoordinate counterparts. The pyrrole C_α and C_β chemical shifts of HasAp resonate at 1050 and 900 ppm, respectively. The C_α chemical shifts of HasAp are more upfield shifted compared to the C_α of the hexa- and pentacoordinate high-spin model heme complexes and the C_β has the same chemical shift as the pentacoordinate complex.

However, from the methodology developed in Chapter 2, it was emphasized that the magnitude of the ^{13}C-meso chemical shifts can provide a straightforward diagnostic tool to elucidate the coordination of the heme-iron. Hexacoordinate and pentacoordinate complexes exhibit ^{13}C-meso chemical shifts at approximately -80 and 250 ppm, respectively (Figure 17). The C_{meso} resonance at -6.10 ppm shows that the heme-iron in HasAp is hexacoordinate. However, the resonance is not as upfield as the purely high-spin hexacoordinate complex of sperm whale metmyoglobin (~80 ppm). An expanded spectrum of the C_{meso} resonance at 32 °C is shown in Figure 19. At closer inspection, the expanded spectrum shows that the single broad peak (-6.10 ppm) corresponding to the C_{meso} consists of several peaks. ^{13}C NMR spectra of HasAp reconstituted with heme labeled at the C_{meso} positions were also obtained at different temperatures. In Figure 19, it can be seen that at 37 ˚C, only one meso-carbon broad peak (-3.97 ppm) is observed. As the temperature is lowered, this peak moves upfield (indicated by red arrow) and new peaks show up. At 25 °C, the C_{meso} resonates at -6.95 ppm and a new small peak shows up at -15.53 ppm. As the temperature is lowered to 15, 10 and 5 °C, the C_{meso} peak shifts even more upfield. In
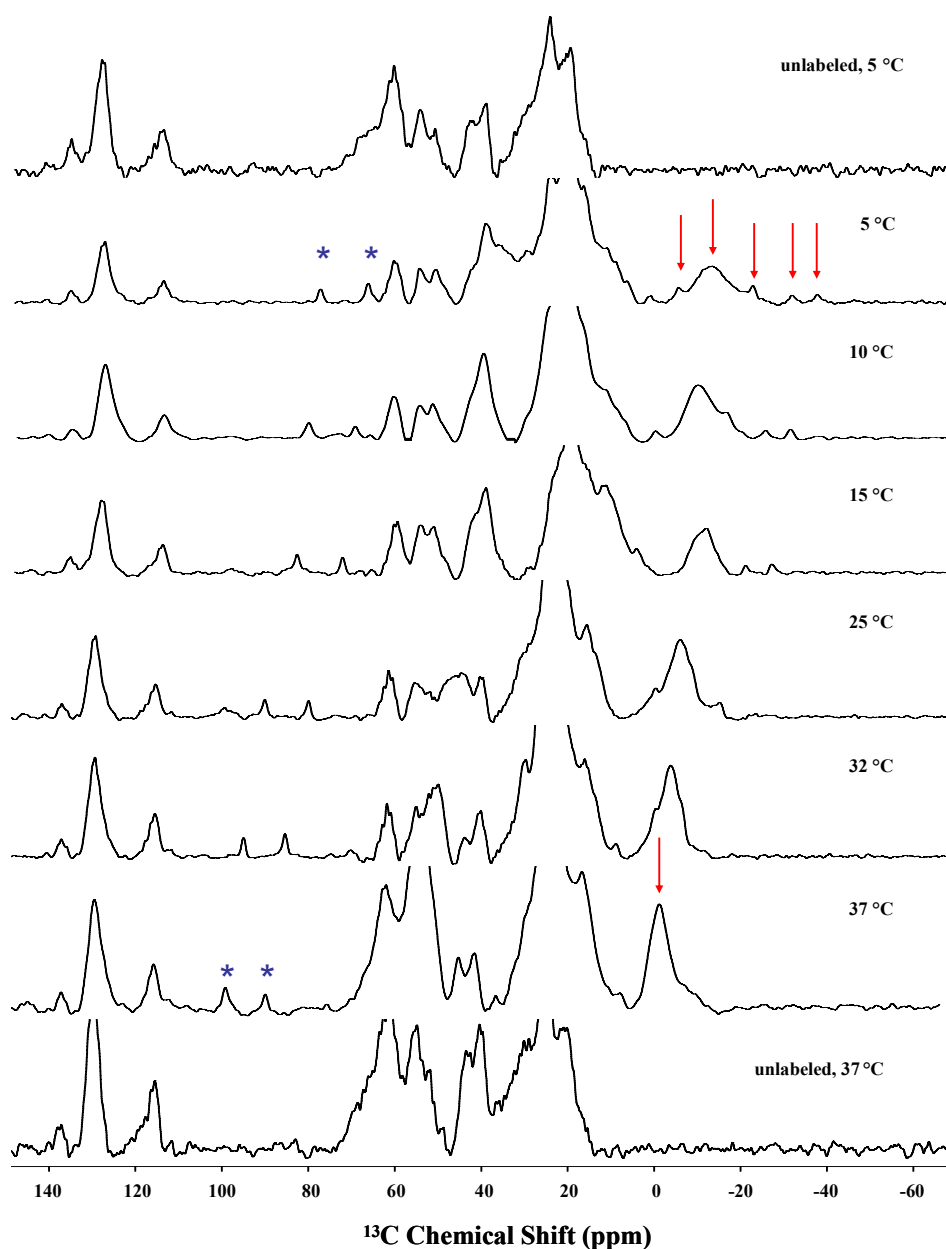
Figure 19. Expanded ^{13}C NMR spectra of HasAp in phosphate buffer ($\mu = 0.10$, pH 7.0 in D$_2$O) reconstituted with heme labeled at the C$_m$ positions. The spectra were obtained at different temperatures indicated above over 125 kHz, with 100 ms acquisition time, 20 ms relaxation delay, and 200 000 scans at 150.821 MHz ^{13}C frequency. The high-spin and low-spin ^{13}C-mesos are indicated with red arrows and blue asterisks, respectively.

100

addition, at 15 °C, there are two new small peaks and at 10 °C and 5 °C, there are three new peaks. The small peaks also shift upfield as the temperature is lowered and become more intense. This could imply that the species attains higher hexacoordinate character. Decreasing the temperature, however, shifts the meso-carbon resonances toward more negative values, which are characteristic of hexacoordinate high-spin heme centers. Comparison of spectra obtained with HasAp reconstituted with heme derived from 5-^{13}C-ALA spectra at different temperatures and spectra of HasAp reconstituted with unlabeled heme and identical acquisition parameters reveals that there are two sharp peaks resonating between 80-100 ppm which are not present in the unlabeled samples. As shown schematically in Figure 17C, the meso-carbon chemical shifts of low-spin hemes resonate near their diamagnetic region of 80 ppm [10]. Hence, the results suggest equilibrium of hexacoordinate high-spin and low-spin populations in slow exchange relative to the NMR time scale. We postulated that this hexacoordinate high-spin and low-spin equilibrium is due to the breaking and forming of the hydrogen-bond between the phenolate group of Tyr75 and Nδ of His83. To further prove the hydrogen-bond postulate, ^{13}C NMR spectra of HasAp with heme-labeled at the meso-carbon were obtained at different temperatures in 95% H_2O and 5% D_2O in order to compare them with the spectra in Figure 19, which were obtained in 100% D_2O. In principle, the hydrogen-bond between Tyr75 and His83 should be stronger in water solution than in D_2O because the hydrogen bond between His83 and Tyr75 would be abolished if hydrogen is replaced by deuterium. The ^{13}C NMR data obtained in H_2O solution are shown is Figure 20.

unlabeled, 5 °C

5 °C

25 °C

32 °C

37 °C

unlabeled, 37 °C

^{13}C Chemical Shift (ppm)
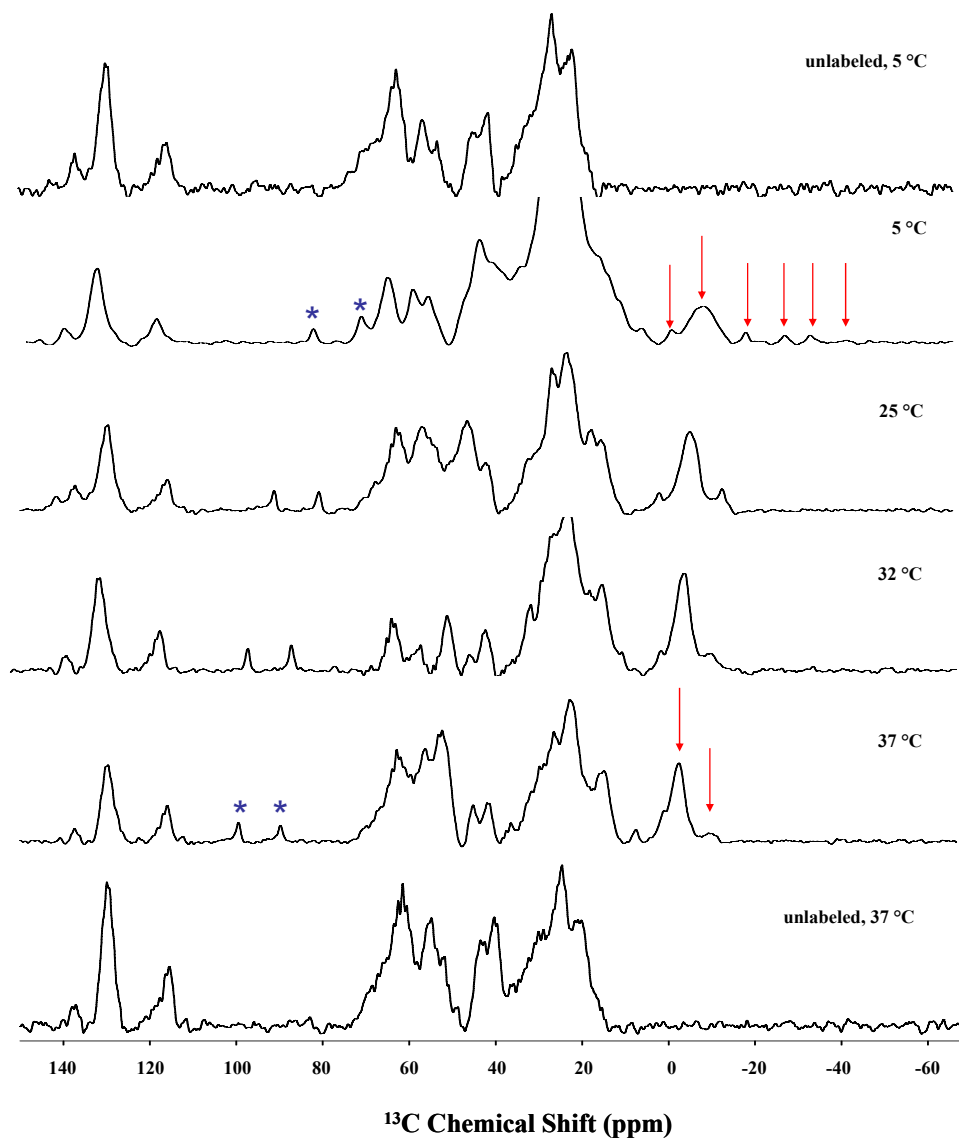
Figure 20. Expanded ^{13}C NMR spectra of HasAp in phosphate buffer ($\mu = 0.10$, pH 7.0 in 95% H_2O, 5% D_2O) reconstituted with heme labeled at the C_m positions. The spectra were obtained at different temperatures indicated above over 125 kHz, with 100 ms acquisition time, 20 ms relaxation delay, and 200 000 scans at 150.821 MHz ^{13}C frequency. The high-spin and low-spin ^{13}C-mesos are indicated with red arrows and blue asterisks, respectively.

The ^{13}C resonances of HasAp in H_2O are sharper and more intense than those in D_2O. It can also be observed that as temperature is lowered, new peaks show up, however, in H_2O new peaks start to show up at 37 ˚C. The meso-carbon resonances of both low-spin and high-spin species also move upfield as the temperature is lowered. The chemical shifts of the meso-carbons corresponding to the low-spin and high-spin species have been tabulated in Table 2. For the high-spin species, there are two meso-carbon chemical shifts in Table 2, one for the broad meso peak and the other for the most upfield shifted meso-carbon resonance. The meso-carbon chemical shift corresponding to the low-spin species is an average of the two observable meso peaks. It is noteworthy that the chemical shifts of the meso-carbon resonances from the low-spin species at different temperatures are identical in H_2O and in D_2O, despite the fact that they move upfield as the temperature is lowered. In striking contrast, the resonances corresponding to high-spin meso-carbons behave differently. From 25-37 °C, the broad meso-carbon is more upfield shifted in H_2O solution, but at 5 °C, it is more upfield shifted in D_2O. However, the chemical shifts of the most upfield shifted small peak in both solutions are more upfield shifted in H_2O solution. In fact, they start to show up at higher temperature and at 5 °C, the most upfield shifted meso-peak resonates at -40.19 ppm, which clearly suggests that there is a stronger hexacoordinate species at lower temperature in H_2O solution. The equilibrium of hexacoordinate high-spin and low-spin species in solution is likely brought about by the breaking and forming of the hydrogen-bond between Tyr75 and His83, as shown in Figure 21. The higher temperature could promote the breaking of the hydrogen-

Table 2. Chemical Shift Characteristics of Meso-Carbons at Different Temperatures

Temp. (°C)	D_2O		Low-Spin	H_2O		Low-Spin
	High-Spin			High-Spin		
5	-13.04	-39.82	72.11	-13.24	-40.19	72.37
10	-11.9	-33.44	75.23	-13.01	-35.18	75.28
15	-11.73	-28.19	78.55	-12.52	-29.89	78.65
25	-6.95	-15.53	84.64	-8.63	-16.18	84.64
32	-4.55		89.97	-6.95	-13.13	89.89
37	-3.97		93.64	-5.31	-12.75	93.62

bond between Tyr75 and His83 which makes Tyr75 a stronger field ligand and thus have a low-spin character. Whereas the formation of hydrogen-bond between Tyr75 and His83 makes Tyr75 a weaker field ligand, and weakens the field strength of the Tyr ligand, thus introducing high-spin character to the hexacoordinate complex. The changes in population of the two spin states in equilibrium serves as a sensitive probe of the effective axial field strength. The breaking and forming of hydrogen-bond which contributes to the two spin states of HasAp is in slow exchange relative to the NMR time scale.

The ^{13}C NMR spectra (Figure 22) of HasAp with heme labeled at the C_α and C_β positions were also taken at different temperatures to further prove the presence of equilibrium between hexacoordinate high-spin and low-spin species in solution. It should be expected that the C_α and C_β resonances should shift downfield as the temperature is lowered if a high-spin hexacoordinate species is populated. In contrast

to this expectation, the C_α (indicated by red arrows) and C_β (indicated by blue arrows) resonances are shifting upfield at lower temperatures. However, their chemical shift characteristics do not correspond to a fully low spin species [10]. Even at lower temperatures, the C_α and C_β resonances suggest that low spin species are being populated. The ^{13}C NMR results agree with the electronic absorbance spectrum that there is equilibrium of high-spin and low-spin species of HasAp in solution. At lower temperature, the high-spin species are still dominant as observed by the chemical

High Spin (S = 5/2)   Low Spin (S = 1/2)
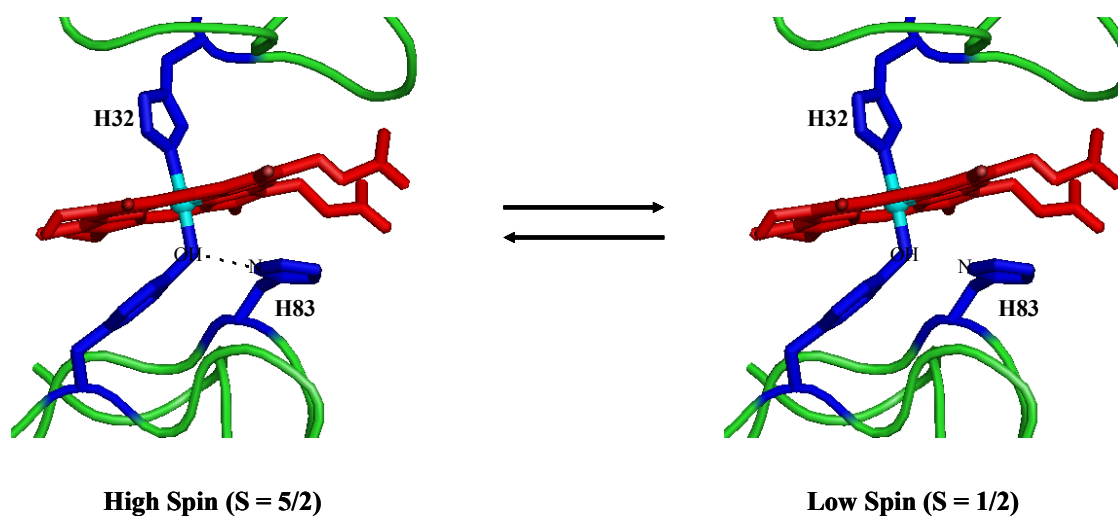
Figure 21. Illustration of the equilibrium of high-spin (S = 5/2) and low-spin (S = ½) hexacoordinate species of HasAp. The hydrogen bond between Tyr75 and His83 is shown in black dotted lines.
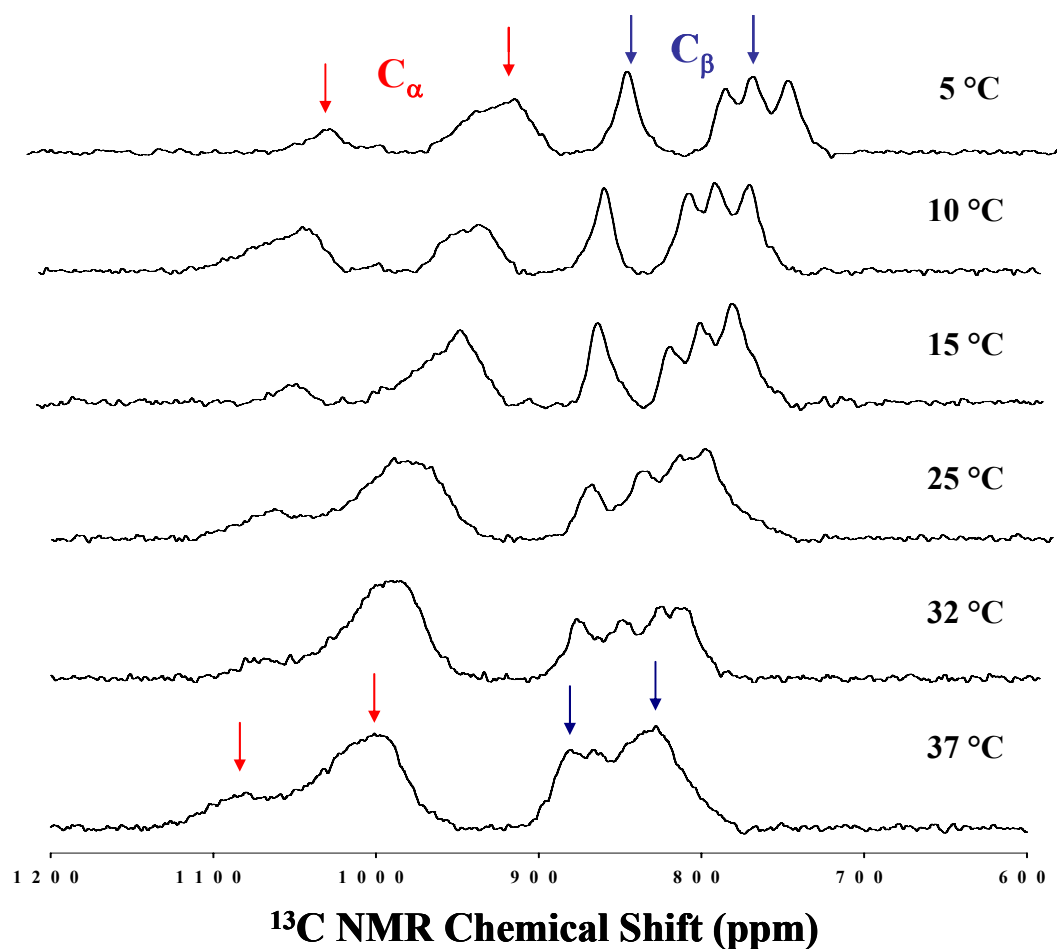
Figure 22. Expanded ^{13}C NMR spectra of HasAp at pH 7.0 reconstituted with heme labeled at the C_α and C_β positions. The C_α and C_β resonances are indicated with red and blue arrows, respectively. The spectra were obtained at different temperatures indicated above over 125 kHz, with 100 ms acquisition time, 20 ms relaxation delay, and 200 000 scans at at 150.821 MHz ^{13}C frequency.

shift characteristics of the C$_\alpha$ and C$_\beta$ resonances, but the low spin species are being populated. These results could lead to an understanding how HasAp takes up heme from hemoglobin and how it transfer heme to the cognate receptor. The axial ligand and/or His83 might play important roles in this process. The hydrogen-bond between Tyr75-His83 could make HasAp bind strongly with heme while the breaking of this bond might facilitate the release of heme to HasR. Hence, this hydrogen-bond may functionally be relevant in the context of uptake and release of heme in hemophores.

Electron Paramagnetic Resonance

The EPR spectra of HasAp at different pH is shown in Figure 23. At pH 5.8 and 7.0, it exhibits a rhombic low-spin signal with *g* values of 2.83, 2.20 and 1.71. In addition, it has a very weak high-spin signal (*g* = ~ 6) which is about ~10% with some distinguishing rhombicity. The EPR data also agree with the electronic absorption spectroscopy, ^{1}H and ^{13}C NMR results that there is a low-spin and high-spin equilibrium of HasAp in solution.

Heme Transfer Experiments

The heme transfer experiments aim to determine if apo-HasAp can capture heme from hemoglobin and myoglobin regardless of the heme iron redox state. Both methemoglobin and metmyoglobin have ferric heme iron, while oxyhemoglobin has a ferrous heme-iron. As shown in Figure 24, the Soret band of holo-HasAp,

methemoglobin, metmyoglobin and oxyhemoglobin are 407, 405 and 409, 415 nm, respectively. The difference in the Soret band of HasAp to the above-mentioned holo-
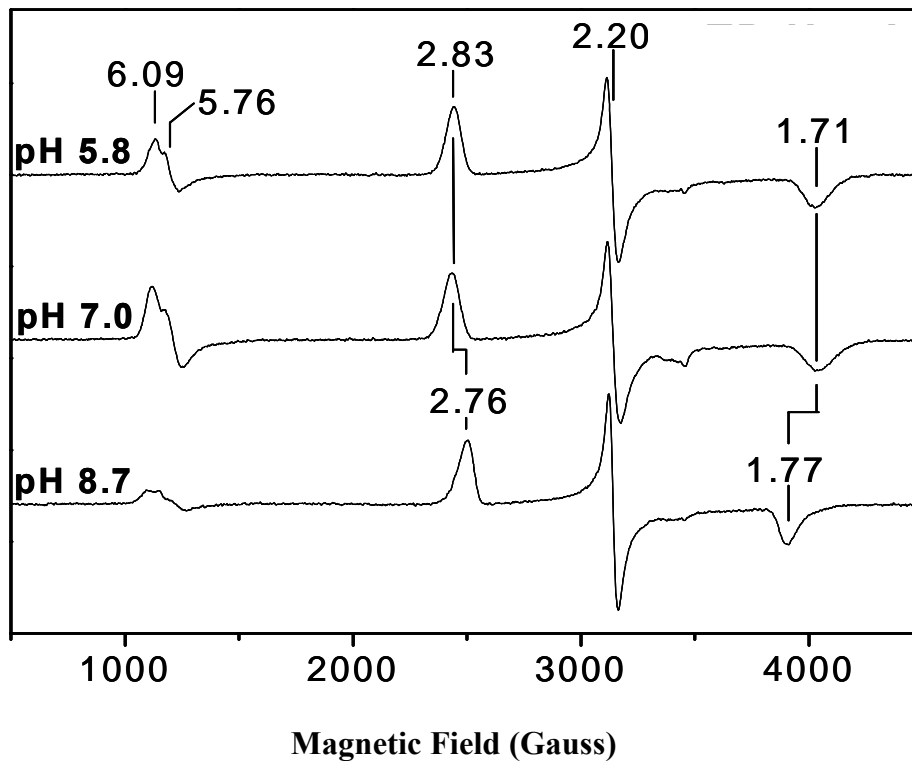
Figure 23 . EPR spectra of HasAp at different pH.

proteins is too small and it is hard to monitor the heme transfer using the Soret band. However, the high-spin charge transfer band of holo-HasAp at 616 nm (inset of Figure 24) is the only intense band which differs from the other proteins. Thus, the absorbance at this peak was used as a marker to monitor the heme transfer from holo-proteins to apo-HasAp.
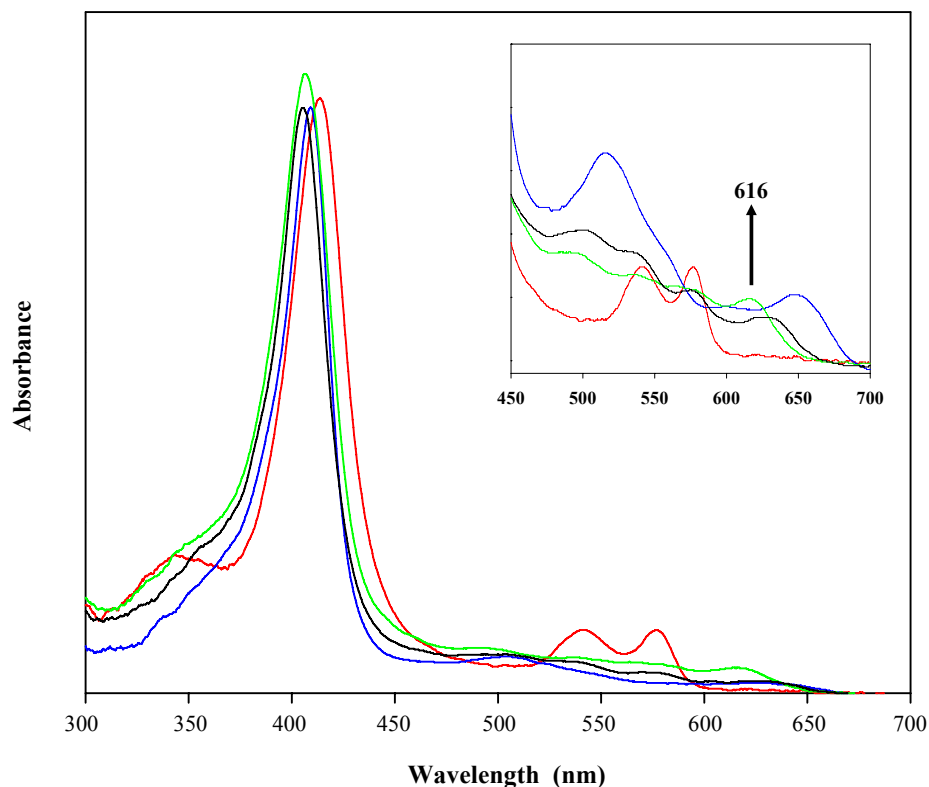
Figure 24. Electronic absorption spectra of oxyhemoglobin (red), methemoglobin (black), metmyoglobin (blue) and HasAp (green). The inset shows their visible bands. The high-spin charge transfer band of HasAp at 616 nm was used to monitor the heme transfer.

The heme transfer experiment from oxyhemoglobin to apo-HasAp is shown in Figure 25A. The black dotted line in the family of spectra in Figure 25A-C are the spectra of oxyhemoglobin, methemoglobin and metmyoglobin, respectively, before mixing with apo-HasAp. While, the red lines are the spectra taken 30 seconds after mixing of apo-HasAp with oxyhemoglobin, methemoglobin and metmyoglobin,

respectively. In Figure 25A, there is no noticeable change in visible spectra absorbances at 540 and 570 nm (inset of Figure 25A) as well as in the Soret bands at 415 nm. A 7 nm difference in the Soret band of HasAp and oxyhemoglobin would be slightly noticeable. The small decrease in the Soret absorbance is due to dilution after mixing of HasAp and oxyhemoglobin solution. The reaction was monitored for 2 hours. But the reaction was incubated for overnight. After 15 hours, the visible region shows bands characteristic of holo-HasAp and absence of low-spin marker bands of oxyhemoglobin. This could imply that heme is transferred to apo-HasAp when the heme is in the oxidized state. The autooxidation of methemoglobin would have facilitated the transfer.

There was also no heme transfer from metmyoglobin to apo-HasAp as observed in Figure 25B. The absorbances at the visible region did not change in 2 hours. However, after overnight incubation, heme transfer was observed as indicated by the change in the high-spin charge transfer bands. While in Figure 25C, it can clearly be observed that there is a fast heme transfer from methemoglobin to apo-HasAp. After 30 seconds of mixing apo-HasAp with methemoglobin, the high-spin charge transfer band shifts from 630 nm to 622 nm. Subsequent spectra show a complete shift to 616 nm. There is definitely a fast transfer of heme from methemoglobin to apo HasAp. The change at 616 nm in the heme transfer experiments is shown in Figure 26. From the results, it can be observed that both oxy hemoglobin and metmyoglobin did not show heme transfer to apo-HasAp or if there is any heme transfer, it is very slow. These experiments tell us that apo-HasAp can
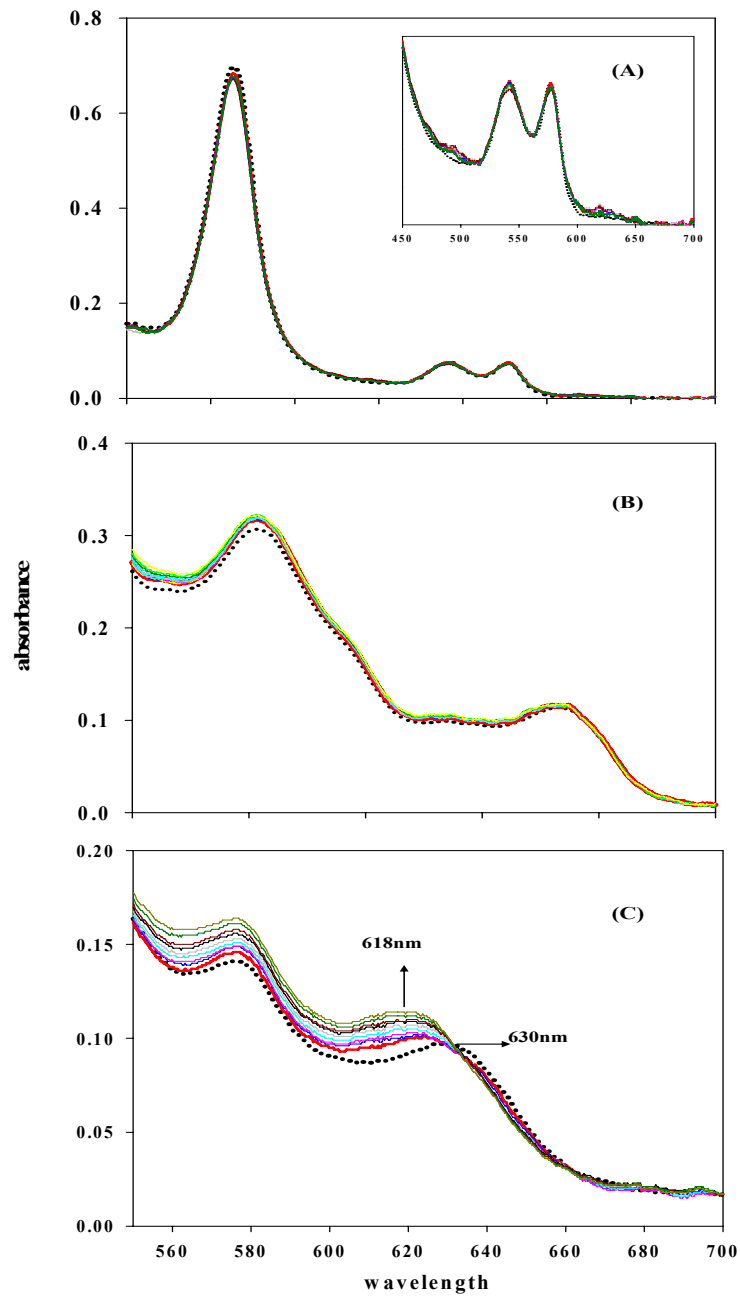
Figure 25. Heme transfer experiments from (A) oxyhemoglobin, (B) metmyoglobin and (C) methemoglobin to apo-HasAp.

capture heme from methemoglobin and not from oxyhemoglobin and metmyoglobin. In addition, the experiments also suggest that apo-HasAp can only take heme in the oxidized form as manifested in the oxyhemoglobin heme transfer experiment. It can take heme from metmyoglobin but very slow. This could lead us to conclude that apo-HasAp can "steal" heme from hemoglobin in the oxidized state by protein-protein interaction and not by passive diffusion. The protein-protein interaction of HasAp and methemoglobin is discussed in Chapter 4.
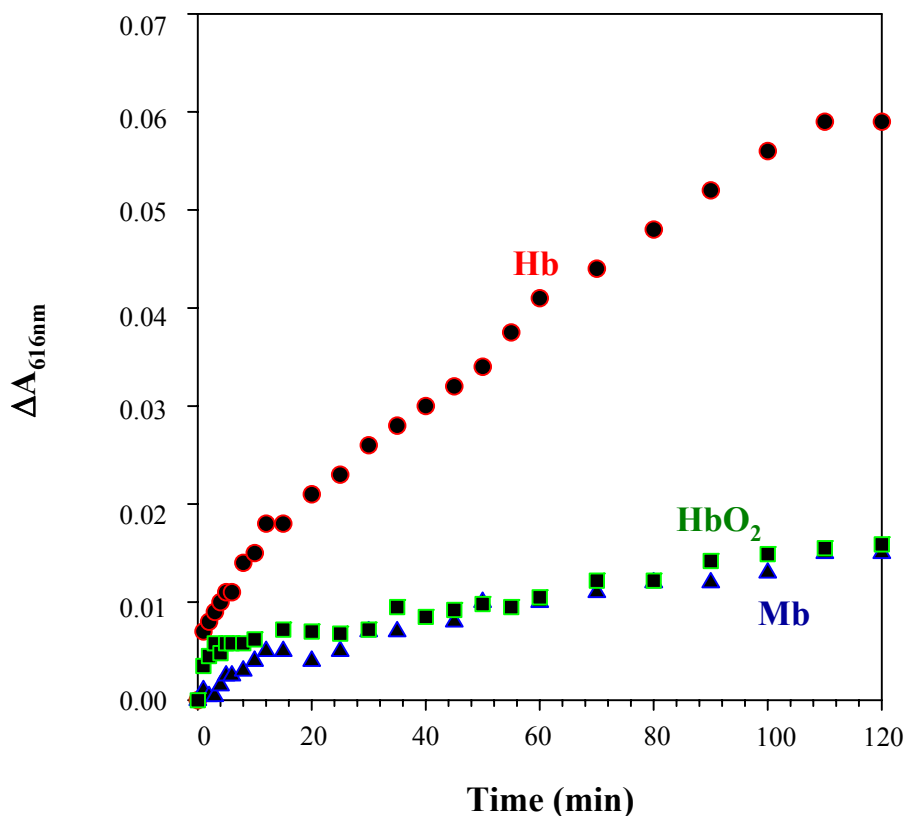
Figure 26. Heme transfer experiment from holo proteins (indicated above) to apo-HasAp. The heme transfer was monitored using the change in intensity at 616 nm with time.

However, the fast rate of heme transfer from hemoglobin to apo-HasAp cannot be monitored by UV-Visible spectroscopy. The kinetics of heme transfer experiments were done using stopped-flow spectroscopy at 37 °C with a 16:1 apo-HasAp to met-Hb ratio. The result showed a rapid formation of holo HasAp (Figure 27A). The time course at 616 nm appears to be biphasic with observed pseudo-first-order rate constants of 0.02 s^{-1} and 0.002 s^{-1} at 10 μM met-hHb (Figure 27B). The 0.02 s^{-1} observed rate is approximately two-orders of magnitude faster than the dissociation rate constant of met-Hb alone. The control experiments with equivalent amounts of bovine serum albumin show no significant spectra changes in the time
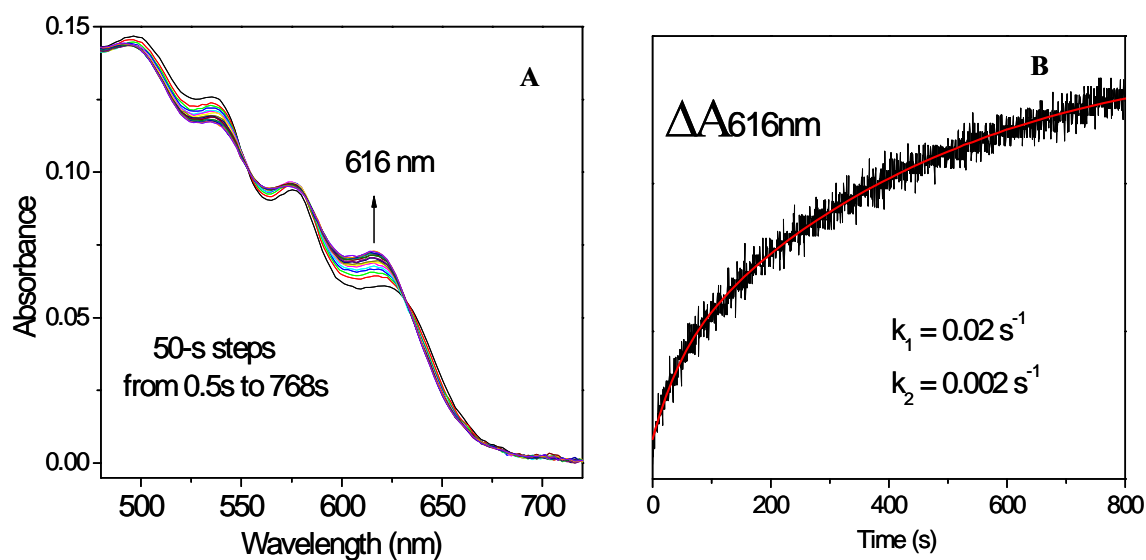
Figure 27. Heme transfer from hemoglobin to apo-HasAp monitored at 616 nm as a function of time (A) and the stopped flow experiment to determine the kinetics of heme transfer (B).

frame examined. These heme transfer experiments strongly suggests that apo-HasAp, can take heme only from methemoglobin and it takes the heme from hemoglobin before met-Hb dissociates in solutions. Thus, there is a likelihood of protein-protein interaction between apo-HasAp and met-Hb.

Amide Backbone Resonance Assignments

The ^{1}H-^{15}N HSQC spectra of holo full-length and truncated forms of HasAp (pH 7.0) taken at 32 °C are shown in Figures 28 and 29, respectively. The intensity of the cross-peaks and signal dispersion in both spectra are similar to each other. This is an indication that both the full-length and truncated ^{15}N-labeled samples are of good quality and labeling with deuterium is unnecessary for these samples. The full-length form is consists of 205 amino acid residues, while the truncated form has 184 residues. As observed in Figures 28 and 29, the cross-peaks corresponding to Gly35, Phe78 and Tyr138 (enclosed in black boxes) are not as intense as the rest of the residues. They are very weak but were assigned because correlations were found to the residues before and after them in the sequence. Overlayed spectra of holo full-length and truncated HasAp are shown in Figure 30. Not counting Pro198, 20 of the 21 residues in the carboxy tail of the full-length form exhibit cross-peaks. The 20 residues corresponding to the tail are located in a crowded region (enclosed in blue boxes). The two glycine residues (Gly191 and Gly193) are located upfield in the ^{15}N region. These assignments and the similarity in the spectra of full-length and truncated forms greatly simplified the assignment of resonances from the full-length
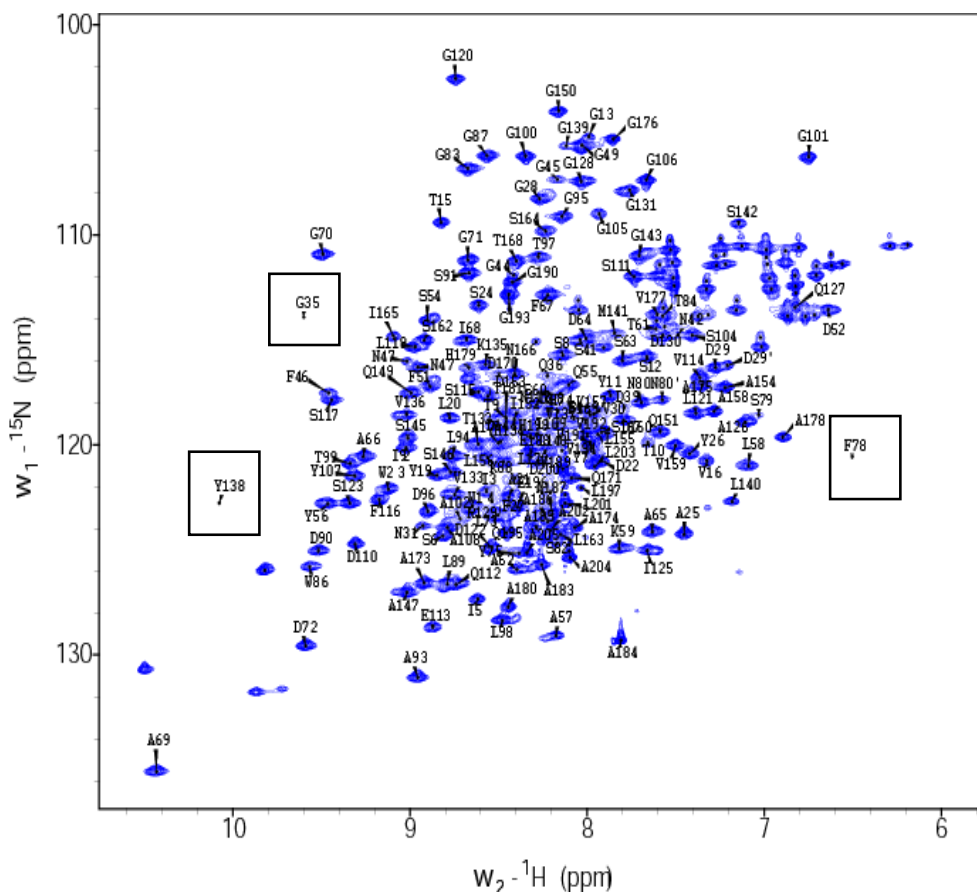
Figure 28. Fast ^{1}H{^{15}N} HSQC spectrum of holo full-length HasAp (2.8 mM in phosphate buffer, $\mu = 0.1$, pH 7.0, 5% D$_2$O) Weak resonances originating from G35, F78 and Y138 are enclosed in boxes. Spectrum was obtained at 305 K using a Bruker Avance 800 NMR spectrometer (see Experimental Procedures). Complex points, 256 (t_1) x 2048 (t_2); spectral width 3.4 kHz ($t1$) x 19.2 kHz ($t2$); 16 scans per increment; acquisition time 100 ms; recycle delay 1s.
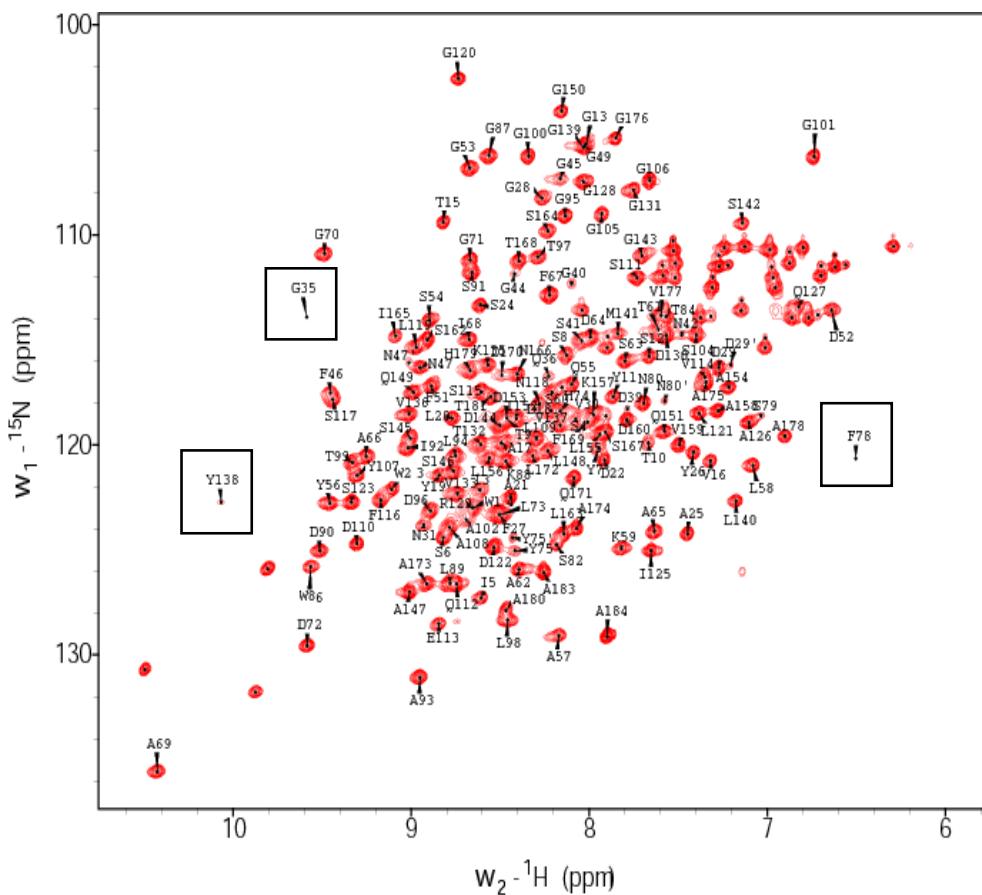
Figure 29. Fast $^1H\{^{15}N\}$ HSQC spectrum of holo truncated HasAp (2.8 mM in phosphate buffer, $\mu = 0.1$, pH 7.0, 5% D_2O) Weak resonances originating from G35, F78 and Y138 are enclosed in boxes. Spectrum was obtained at 305 K using a Bruker Avance 800 NMR spectrometer (see Experimental Procedures). Complex points, 256 (t_1) x 2048 (t_2); spectral width 3.4 kHz ($t1$) x 19.2 kHz ($t2$); 16 scans per increment; acquisition time 100 ms; recycle delay 1s.

form once the assignments for the truncated form had been obtained. The absence of heme isomerism in both forms of HasAp proteins as observed in the X-ray crystal structure and in the ^{1}H and ^{13}C NMR means that there should be only one cross-peak per residue. Interestingly Asp29, Asn47, and Asn80 display two cross-peaks each.
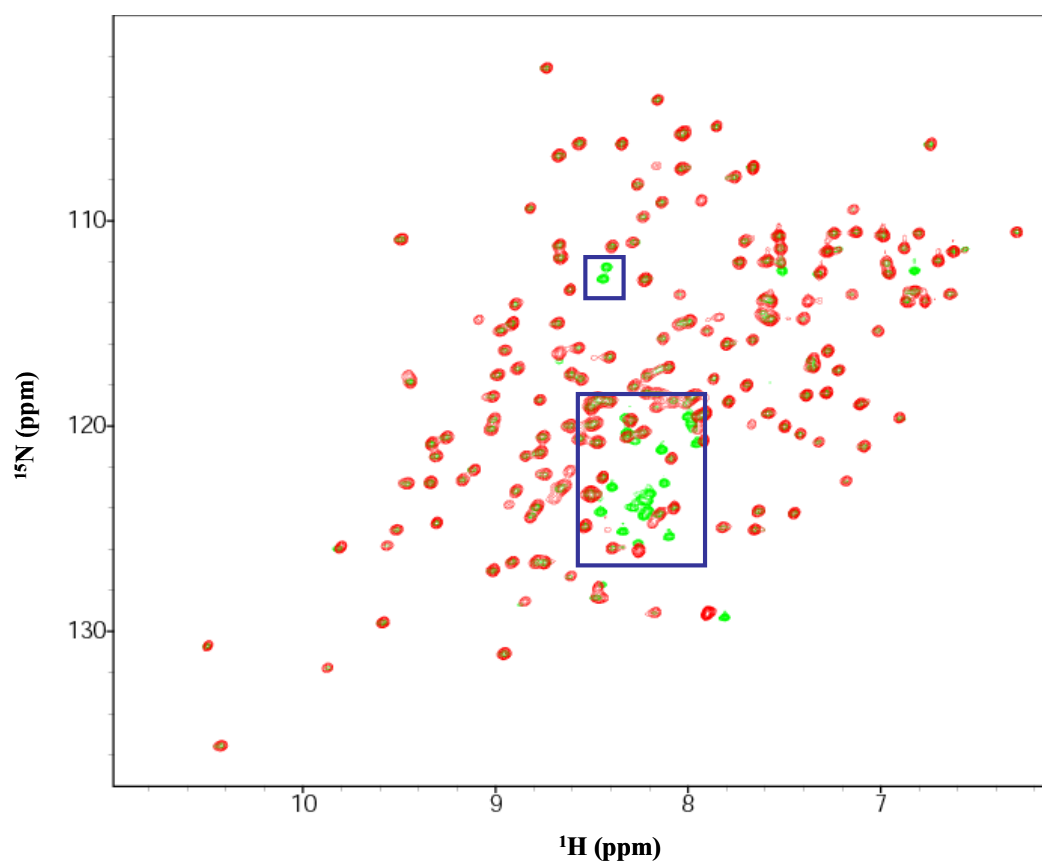
Figure 30. Fast ^{1}H{^{15}N} HSQC Spectra of (A) full-length (green) and (B) truncated (red) HasAp.

Conventional heteronuclear 2D and 3D NMR experiments performed with a sample of holo truncated [U-^{13}C, U-^{15}N]-HasAp allowed resonance assignment of a large majority of non-proline residues, with the exception of residues listed in Table 3. Most of these residues except for Ser2 and Ser103 are located < 9 Å from the heme iron, thus they are expected to be strongly influenced by the iron paramagnetism, which is manifested in weak or undetectable cross-peaks in the HSQC spectrum. These residues have been mapped on the X-ray crystal structure shown in Figure 31. No amide correlation connection was present to Ser2 because it is the first residue in the N-terminus, because, the start methionine codon was cleaved during expression. S103 is located in a loop and this residue has the highest B-factor value in the structure as determined by X-ray crystallography as discussed above. Thus, this residue was not seen because of its conformational disorder. The assignment of the above-mentioned residues in close proximity to the heme active site except for His32, Arg33, Thr76, and His83 were assigned with the aid of samples selectively labeled with ^{15}N-Leu, ^{15}N-Val, ^{15}N-Tyr or ^{15}N-Thr and 2D ^{1}H-^{15}N HSQC experiments tailored to detect fast relaxing signals [18, 74], in a manner similar that used for the assignment of fast relaxing signals in heme oxygenase from *Pseudomonas aeruginosa* [18]. The method was modified to prevent isotopic scrambling. Thus, 98% of the non-proline residues in both holo full-length and truncated HasAp forms were assigned using the combination of 3D NMR experiments and the selective labeling technique coupled with fast recycling ^{1}H-^{15}N HSQC. It should be noted that a cross-peak originating from axial ligand His32 or

Table 3. Distances of the Unassigned Residues from the Heme-Iron

Residue	Distance from heme-iron (Å)
His32	7.70
Arg33	6.92
Val37	8.10
Val38	9.29
Thr43	7.36
Thr76	8.01
Leu77	6.71
His83	6.52
Thr84	6.81
Leu85	7.92
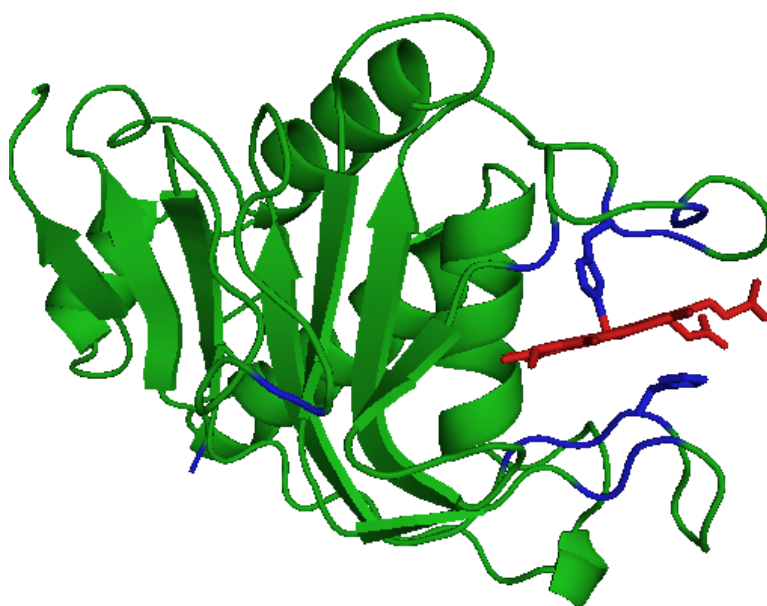
Figure 31. Unassigned residues using triple resonance NMR experiments are shown in blue. The heme is in red.

from His83, which in the crystal structure of HasA$_{SM}$ and HasAp forms a hydrogen bond to the phenolate oxygen of Tyr75, have not been identified. Selective labeling with His was not attempted due to cost considerations, thus it is not known whether the strategy would have facilitated the identification and sequential assignment of cross-peaks originating from these residues. Selective labeling with ^{15}N-Arg was not also attempted because it is not commercially available, hence Arg33 was not assigned. The backbone assignment of the truncated apo-HasAp was also assigned using the conventional 3D NMR experiments and only 89% of the non-proline residues were assigned. The ^{1}H-^{15}N spectrum is shown in Figure 32. Most of the residues not assigned are close to the N-terminus. Moreover, those residues in close proximity to the heme-iron were all assigned.

Triple Resonance NMR Assignments

The triple-resonance (3D) NMR experiments for sequential backbone assignments of proteins (See Table 4) are based on the ability to transfer magnetization through NMR active nuclei using *J*-couplings. The nomenclature of 3D NMR experiments is very descriptive. Names of nuclei used for magnetization transfer during the indirect evolution periods are listed in the order of their use. The nuclei whose frequency are not detected but are used in magnetization transfer are shown in parenthesis [75]. The signals in triple resonance experiments are dispersed in three dimensions so the spectra are distributed in a cube instead of a plane. 2D slices are taken from the 3D cube along the ^{15}N dimension. This is illustrated in
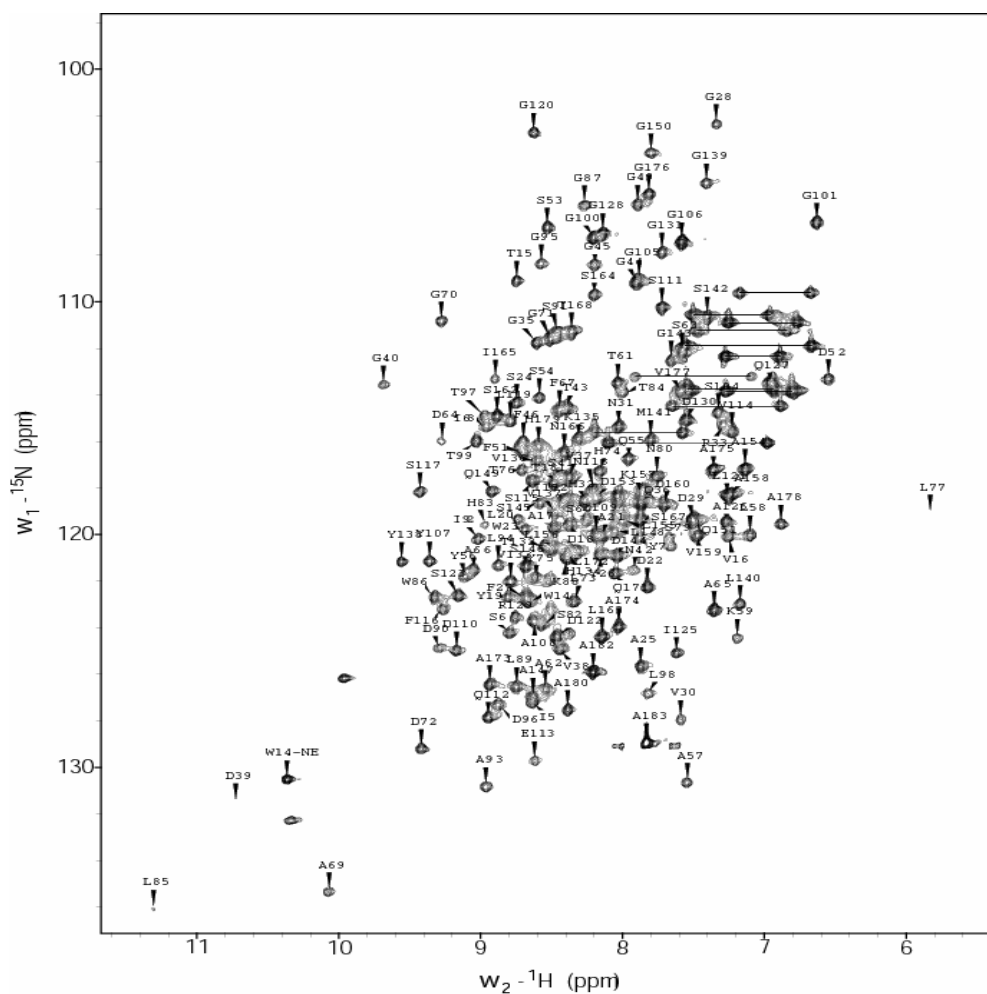
Figure 32. Fast $^1\text{H}\{^{15}\text{N}\}$ HSQC spectrum of apo truncated HasAp. Spectra were recorded on a Varian Unity INOVA 600 NMR Spectrometer. Acquisition parameters were as follows: (A) Complex points, 128 (t_1) x 1632 (t_2); spectral width, 2.4 kHz (t_1) x 9.60 kHz (t_2); acquisition time, 85 ms; recycle delay, 1 s; 32 scans.

Table 4, the nuclei whose frequencies are detected are encircled in blue and nuclei whose frequencies are used for magnetization transfer are encircled in red. A summary of the 3D NMR experiments and their correlations is shown in Table 5. The HNCA experiment is the prototype of all triple resonance experiments. This experiment employs out-and-back coherence transfer. This experiment correlates the amide ^{1}H and ^{15}N with the aid of the intraresidue ^{13}C$^\alpha$ through a single bond ($^1J_{NC}{}^\alpha$ = 7-11 Hz). The magnetization is first transferred from the amide proton to the directly attached nitrogen atom. Then the magnetization is transferred to the ^{13}C$^\alpha$. This experiment also gives sequential connectivities by transferring magnetization to the preceding ^{13}C$^\alpha$ via two interresidue bonds ($^2J_{NC}{}^\alpha$) [75-78]. Hence, in the HNCA experiment the ^{13}C$^\alpha$ of any given residue and that of its preceding residue can be assigned. It may be possible to assign the protein backbone exclusively with an HNCA experiment. However, sometimes sequential assignments with HNCA are ambiguous because of the frequency overlap or the degeneracies of the intraresidue and interresidue C$^\alpha$.

To overcome this ambiguity, a complementary experiment to HNCA was employed. This 3D experiment, HN(CO)CA, provides assignments only for the ^{13}C$^\alpha$ of the preceding residue (See Table 4). The HN(CO)CA experiment is specifically designed for sequential correlations between the ^{15}N and ^{1}H chemical shifts of a given residue and the preceding ^{13}C$^\alpha$ shifts via the intervening ^{13}CO nucleus by means of the ^1J(NH), ^1J(N,CO) and ^1J(CA,CO) coupling constants [76, 79, 80].

Table 4. Magnetization Transfer Observed in 3D NMR Experiments

Experiment	Magnetization Transfer
HNCA	
HN(CO)CA	
CBCA(CO)NH	
HNCACB	
HNCO	

Table 5. Triple Resonance Experiments Used for Sequential Backbone Assignment

Experiment	Observed Correlations	*J* Couplings
HNCA	$^1H^N_i - {^{15}}N_i - {^{13}}C^\alpha_i$	$^1J_{NH}$
	$^1H^N_i - {^{15}}N_i - {^{13}}C^\alpha_{i-1}$	$^1J_{NC^\alpha}$
		$^2J_{NC^\alpha}$
HN(CO)CA	$^1H^N_i - {^{15}}N_i - 13C^\alpha_{i-1}$	$^1J_{NH}$
		$^1J_{NCO}$
		$^1J_{C^\alpha CO}$
CBCA(CO)NH	$^1H^N_i - {^{15}}N_i - {^{13}}C^\beta_{i-1}$	$^1J_{CH}$
		$^1J_{C^\alpha C^\beta}$
		$^1J_{C^\alpha CO}$
		$^1J_{NCO}$
		$^1J_{NH}$
HNCACB	$^1H^N_i - {^{15}}N_i - {^{13}}C^\alpha_i/C^\alpha_{i-1}$	$^1J_{NH}$
	$^1H^N_i - {^{15}}N_i - {^{13}}C^\beta_i/C^\beta_{i-1}$	$^1J_{C^\alpha N}$
		$^1J_{CC}$
		$^2J_{C^\alpha N}$
HNCO	$^1H^N_i - {^{15}}N_i - {^{13}}CO_{i-1}$	$^1J_{NH}$
		$^1J_{NCO}$

Moreover, ambiguity from the $^{13}C^{\alpha}$ resonances can be further resolved by looking at the beta carbons ($^{13}C^{\beta}$). Basically, most of the $^{13}C^{\alpha}$ of most in HasAp were assigned by the combination of HN(CO)CA and HNCA experiments.

The $^{13}C^{\beta}$ were assigned using CBCA(CO)NH and HNCACB experiments. These experiments are considered to be the workhorse for backbone assignments. Both experiments provide similar set of data. The HNCACB experiment provides both intra- and interresidue connections, whereas, CBCA(CO)NH provides only interresidue connections (See Table 4). HNCACB correlates the ^{1}H and ^{15}N amide resonances with those of the interresidue $^{13}C^{\alpha}$ and $^{13}C^{\beta}$ resonances by means of the ^{1}J(NH), $^{1,2}J$(N,CA) and optional ^{1}J(CA,CB) coupling constants [81, 82]. In the HNCACB spectrum, at any given amide proton frequency, four peaks can be observed: two positive $^{13}C^{\alpha}$ cross-peaks and two negative $^{13}C^{\beta}$ cross-peaks, which correspond to the $^{13}C^{\alpha}$ and $^{13}C^{\beta}$ of a given residue and its preceding residue. Proline residues can interrupt the chain because they do not have amide protons. In principle, HNCACB can provide the assignments for both $^{13}C^{\alpha}$ and $^{13}C^{\beta}$, but frequency overlap and degeneracies of resonances can also be a problem like in HNCA. CBCA(CO)NH can help overcome this ambiguity by providing assignments of the $^{13}C^{\alpha}$ and $^{13}C^{\beta}$ peaks of the preceding residue (See Table 4). This experiment correlates the ^{1}H and ^{15}N resonances of a given residue to both $^{13}C^{\alpha}$ and $^{13}C^{\beta}$ of the preceding residue [75, 76]. In this spectrum, positive and negative peaks can be observed due to the $^{13}C^{\alpha}$ and $^{13}C^{\beta}$ resonances, respectively.

Overall, the amide backbone assignments were accomplished with the use of the above described triple resonance NMR experiments. However, there were still some ambiguities in the assignment. Two more experiments were done to resolve these ambiguities. These two experiments are HNCO and (HCA)CO(CA)NH. The HNCO experiment correlates crucial sequence backbone connectivities between the amide ^{1}H and ^{15}N of a given amino acid to the carbonyl (^{13}CO) resonance of the preceding residue by means of ^1J(NH) and ^1J(N,CO) coupling constants ^1J(NH) and ^1J(N,CO) coupling constants [75, 78, 79]. The HNCO provides the assignment of the ^{13}CO of the previous residues while (HCA)CO(CA)NH provides the connectivity to both intra- and interresidue ^{13}CO. Majority of the resonances were assigned using the above-mentioned 3D NMR experiments. The chemical shifts for N-H, ^{15}N, ^{13}C$^{\alpha}$, ^{13}C$^{\beta}$, and ^{13}C' of full-length and truncated holo HasAp and truncated apo-HasAp are summarized in Appendix 2, 3 and 4, respectively.

Assignment of Leu 77 and Leu85

Leu77 and Leu85 could not be assigned with the aid of the 3D spectra described above. Leu77 and Leu85 are located 6.71 and 7.92 Å, respectively from the heme-iron. The ^{1}H-^{15}N HSQC spectrum of ^{15}N-Leu-HasAp acquired with conditions typically utilized to study diamagnetic proteins (Figure 33A), shows 16 cross peaks, that is, one less cross-peak than the number of Leu residues in the sequence. All these cross-peaks, except the weak signal at δ (^{1}H) = 7.3 ppm δ (^{15}N) = 123 ppm (enclosed in circle) had been previously assigned with the aid of 3D heteronuclear experiments.
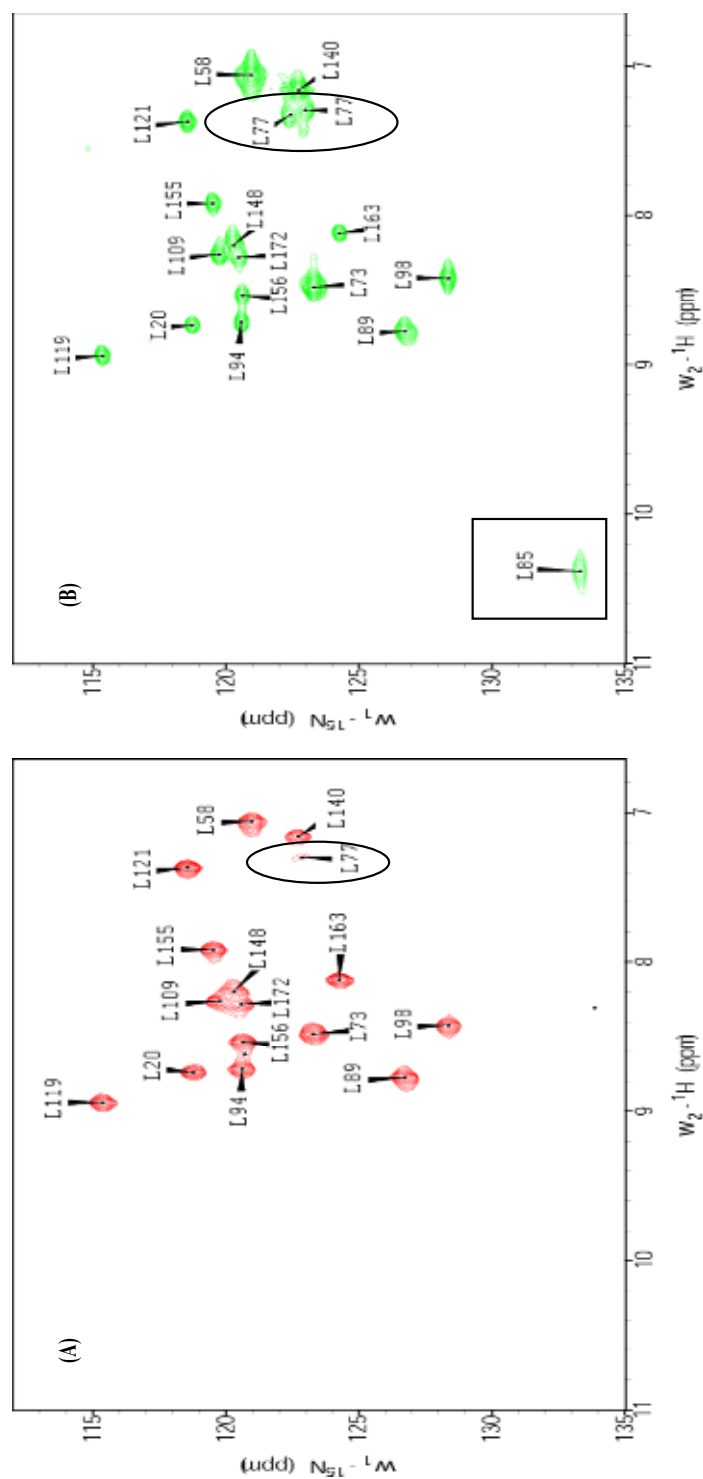
Figure 33. ^{1}H{^{15}N} HSQC spectra of [^{15}N-Leu]-HasAp. Spectra were recorded on a Varian Unity INOVA 600 NMR Spectrometers. Acquisition parameters were as follows: (A) Complex points, 128 ($t1$) x 1632 ($t2$); spectral width, 2.4 kHz ($t1$) x 9.60 kHz ($t2$); acquisition time, 85 ms; recycle delay, 1 s; 32 scans. (B) Complex points, 128 ($t1$) x 1050 ($t2$); spectral width, 3.6 kHz ($t1$) x 15 kHz ($t2$); acquisition time, 35 ms; recycle delay, 50 ms; 256 scans.

In comparison, an HSQC spectrum acquired with rapid pulse repetition from the same ^{15}N-Leu-HasAp sample (Figure 33B) exhibits a cross-peak with a large downfield ^{1}H and ^{15}N shifts, at δ (^{1}H) = 10.4 ppm and δ (^{15}N) = 133 ppm, respectively. This cross-peak was sequentially assigned to Leu85 using information obtained from the suite of 3D spectra collected to obtain sequential assignments. Thus, the fact that strip plots taken from ^{1}H-^{13}C slices at the ^{15}N frequencies of the amide N-H cross-peak in question and the N-H cross-peak of W86 share a C^β correlation (Figure 34) in the CBCA(CO)NH and HNCACB assigns the N-H cross-peak in question to Leu85. It is important to note that in retrospect the Leu85 cross-peak can also be observed as a very weak signal in a HSQC spectrum acquired with standard conditions and a sample of uniformly ^{15}N-labeled HasAp. In absence of the information provided by the HSQC spectrum acquired with a sample of [^{15}N-Leu]-HasAp and fast pulse recycling, however, this cross-peak could have been easily overlooked. It is also noteworthy that the non-assigned weak signal at δ (^{1}H) = 7.2 ppm and δ (^{15}N) = 125 ppm in the HSQC spectrum acquired with standard conditions (Figure 33A) is a well-defined cross-peak in the spectrum acquired with fast repetition. In fact, this signal, which is attributed by default to Leu77, is a double cross-peak, indicating that Leu-77 is present in at least two conformations in HasAp.

Assignment of Val 37 and Val 38

Valine 37 and 38 are located 8.10 and 9.29 Å, respectively from the heme-iron. The HSQC spectrum of ^{15}N-Val-HasAp acquired with standard conditions

(Figure 35A) displays 8 cross-peaks corresponding to previously assigned Val residues. All the alanines were also labeled. However, the intensities of the ^{15}N-Ala are lower compared to ^{15}N-Val. Moreover, all alanine amide resonances were assigned, so new peaks observed can be safely assigned as valine residues. In comparison, the HSQC spectrum acquired with the same sample but with fast pulse
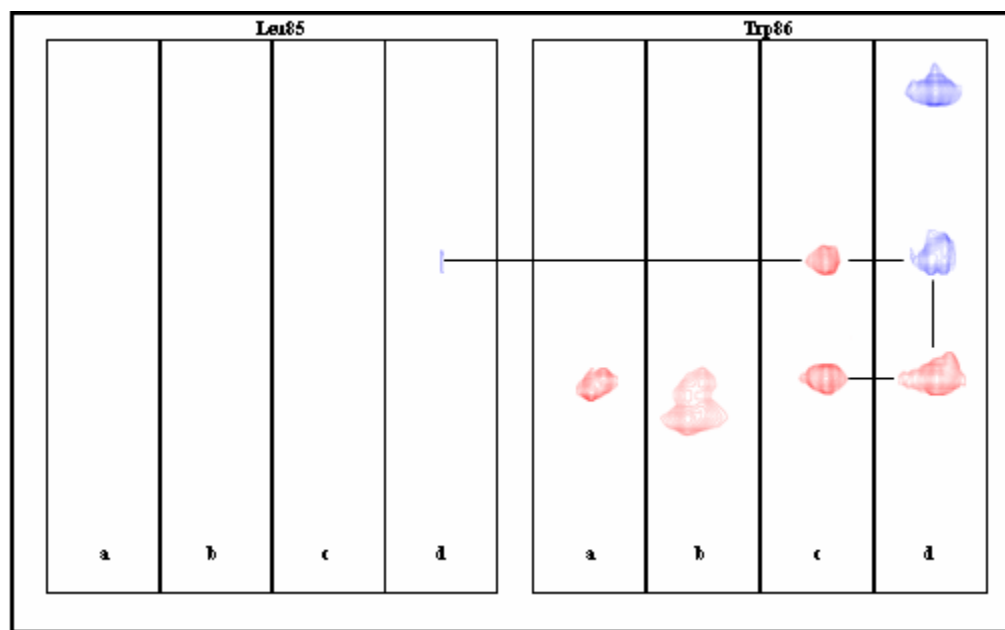
Figure 34. Strip plots taken at ^{1}H$_N$ amide resonance frequencies corresponding to residues Leu85 and Trp86. The panels shown are sections of HN(CO)CA (a), HNCA (b), CBCA(CO)NH (c) and HNCACB (d) spectra collected with holo truncated HasAp sample. Straight lines connect resonances exhibiting sequential intra- (^{13}C$_i$) and/or inter-residue (^{13}C$_{i-1}$) correlations with the corresponding amide ^{1}H$_N$. Cross-peaks in HNCACB spectra shown in red were phased positive (^{13}C$^\alpha$s) and exhibit a 180° phase difference relative to those shown in blue (^{13}C$^\beta$s).
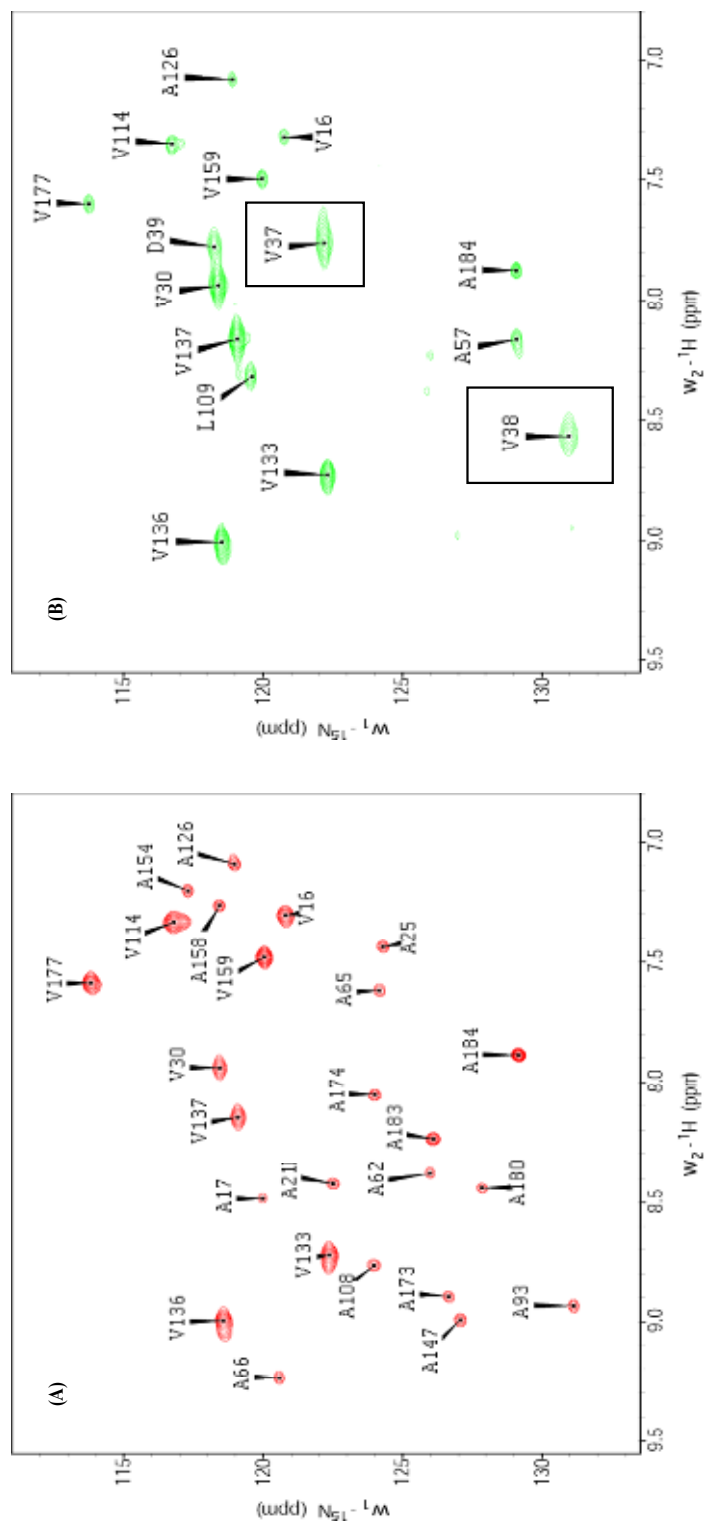
Figure 35. $^1H\{^{15}N\}$ HSQC spectra of [^{15}N-Val]-HasAp. Spectra were recorded on a Bruker Avance 800 (A) and Varian Unity INOVA 600 (B) NMR Spectrometers. Acquisition parameters were as follows: (A) Complex points 256 (*t1*) x 2048 (*t2*); spectral width, 3.4 kHz (*t1*) x 19.2 kHz (*t2*); acquisition time, 100 ms; recycle delay, 1 s; 16 scans. (B) Complex points, 128 (*t1*) x 1050 (*t2*); spectral width, 3.6 kHz (*t1*) x 15 kHz (*t2*); acquisition time, 35 ms; recycle delay, 50 ms; 256 scans.

130

repetition exhibits 10 cross-peaks corresponding to valine resonances (Figure 35B); the signal at δ (^{1}H) = 7.8 ppm and δ (^{15}N) = 122 ppm corresponds to Val37 because it has C$^\alpha$ and C$^\beta$ correlations to the preceding residue, Gln36, with the aid of CBCA(CO)NH and HNCACB data, as described above. Thus, the broad peak in Figure 35B at δ (^{1}H) = 8.6 ppm and δ (^{15}N) = 131 ppm corresponds to Val38.

Assignment of Thr 43 and Thr84

The three unassigned threonines, Thr43, 76 and 84 are located 7.36, 8.01 and 6.81 Å from the heme-iron. Isotopic scrambling with glycine and serine was overcome by supplementing the medium with those ^{15}N-Gly and ^{15}N-Ser together with the ^{15}N-Thr during induction with IPTG. In the normal HSQC spectrum (Figure 36A), only one new cross-peak corresponding to Thr shows up. This peak is at δ (^{1}H) = 7.5 ppm and δ (^{15}N) = 114 ppm besides Thr61. It is a fairly intense cross-peak and it is not surprising that it was not observed in the HSQC spectrum of the fully labeled ^{15}N-sample because this cross-peak overlapped with Asp30. This peak beside Thr61 was assigned as Thr84 because in its HN(CO)CA and HNCA spectra, it has C$^\alpha$ which corresponds to a histidine. Moreover, the HNCACB also has C$^\alpha$ and C$^\beta$ corresponding to a histidine. It cannot be Thr43 or Thr76 because it does not have correlations with Asn42 or Tyr75. Moreover, it was hard to assign this cross-peak without the aid of selective labeling because the preceding residue, His83 was not assigned and no correlation was observed with Leu85. In the fast pulse recycling HSQC (Figure 36B), one very broad peak located δ (^{1}H) = 6.8 ppm and δ (^{15}N) = 106
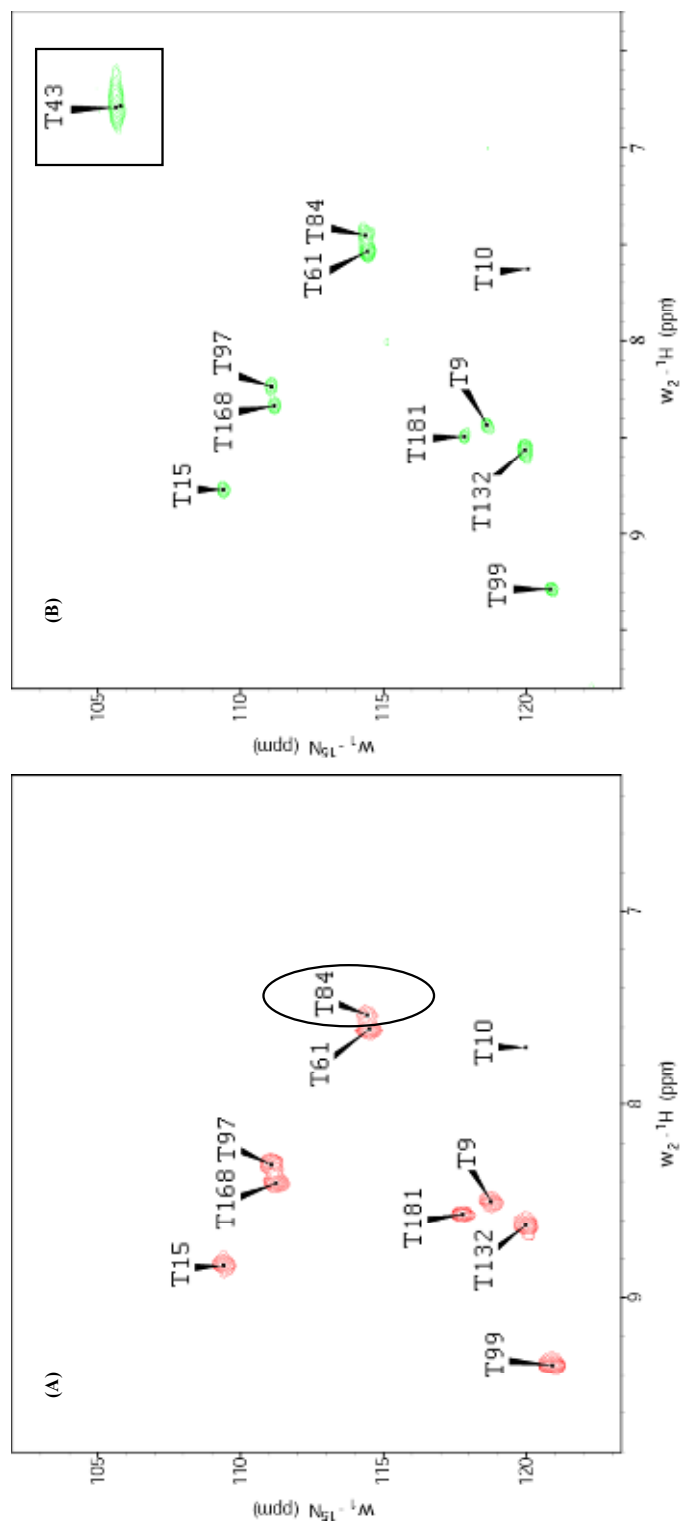
Figure 36. ^{1}H{^{15}N} HSQC spectra of [^{15}N-Thr]-HasAp. Spectra were recorded on a Varian Unity INOVA 600 NMR Spectrometers. Acquisition parameters were as follows: (A) Complex points, 128 (*t1*) x 1632 (*t2*); spectral width, 2.4 kHz (*t1*) x 9.60 kHz (*t2*); acquisition time, 85 ms; recycle delay, 1 s; 32 scans. (B) Complex points, 128 (*t1*) x 1050 (*t2*); spectral width, 3.6 kHz (*t1*) x 15 kHz (*t2*); acquisition time, 35 ms; recycle delay, 50 ms; 256 scans.

ppm can be observed. This peak has C^α correlations to Asn42 and C^α and C^β correlations to Gly44. Therefore, it is assigned as Thr43. However, this leaves Thr76 unassigned.

Assignment of Tyr 75

HasAp was also labeled with ^{15}N-Tyr in an effort to confirm the sequential assignment of the Tyr75 axial ligand. It is located 9.15 Å from the heme-iron. Isotopic scrambling with phenylalanine, glutamine and aspartate residues was observed when HasAp was expressed with ^{15}N-labeled Tyr. However, their intensities are lower compared to the tyrosine residues. Results from these experiments confirmed the assignment of Tyr75 and drew attention to the fact that several residues near the heme are conformationally disordered, as indicated by the presence of more than one cross-peak per residue in HSQC spectra. For example, the HSQC spectrum of ^{15}N-Tyr HasAp suggested the presence of two cross-peaks originating from Tyr138 (Figure 37A-B). The peak at δ (^{1}H) = 10 ppm and δ (^{15}N) = 123 ppm had been assigned to Tyr138 but the smaller peak with very weak intensity had been overlooked. Upon additional analysis, it was shown that the lower intensity cross-peak can be sequentially assigned to Tyr138, thus demonstrating that this residue is conformationally disordered. The HSQC spectra (Figure 37A-B) also suggest that the axial ligand Tyr75 exhibits two cross-peaks. The most intense peak had been assigned sequentially, whereas the low intensity signal had been previously overlooked. The clear presence of more than one cross-peak in Tyr75, Leu77 and Tyr138 prompted us
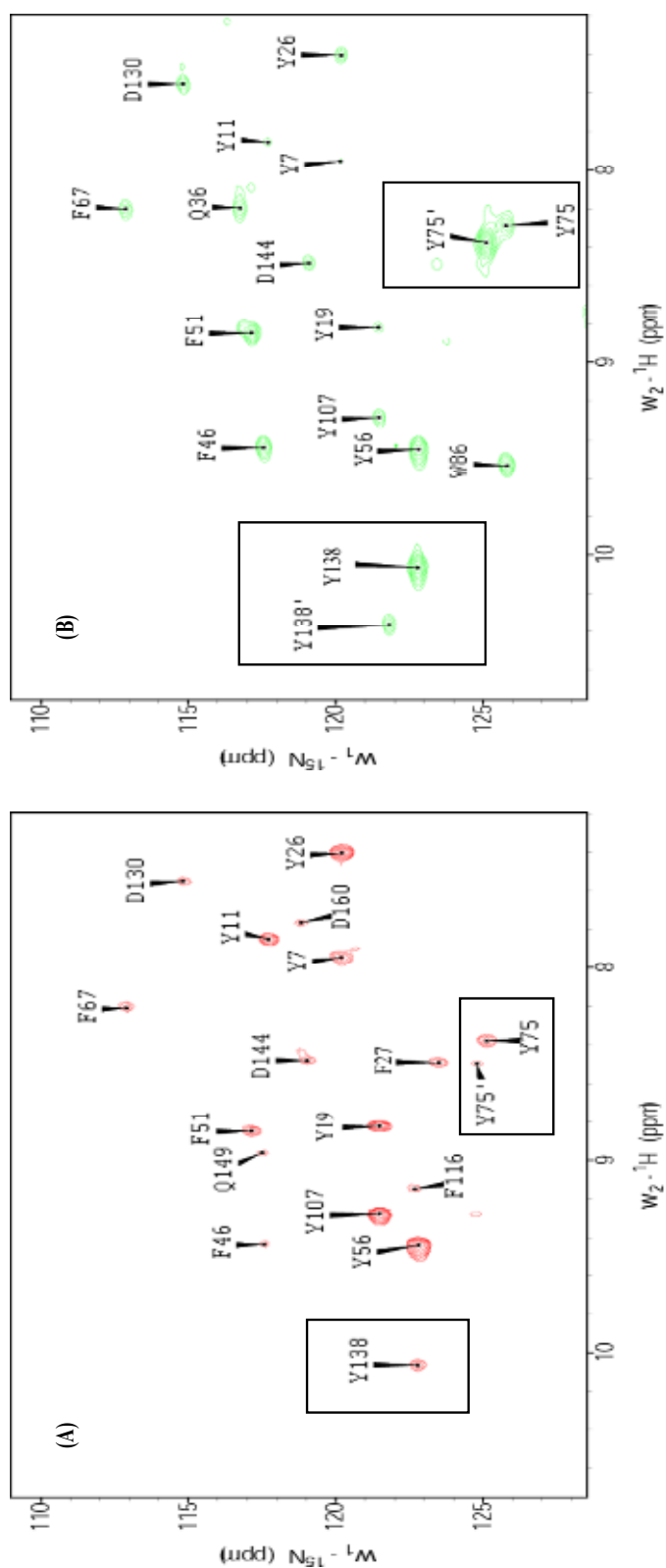
Figure 37. $^1H\{^{15}N\}$ HSQC spectra of [^{15}N-Tyr]-HasAp. Spectra were recorded on a Varian Unity INOVA 600 NMR Spectrometers. Acquisition parameters were as follows: (A) Complex points, 128 (*t1*) x 1632 (*t2*); spectral width, 2.4 kHz (*t1*) x 9.60 kHz (*t2*); acquisition time, 85 ms; recycle delay, 1 s; 32 scans. (B) Complex points, 128 (*t1*) x 1050 (*t2*); spectral width, 3.6 kHz (*t1*) x 15 kHz (*t2*); acquisition time, 35 ms; recycle delay, 50 ms; 256 scans.

134

to investigate and find the presence of conformational disorder in a number of residues in HasAp.

Fast Recycling HSQC of HasAp

It can be observed in the fast recycling HSQC spectra of both full-length and truncated fully labeled ^{15}N-HasAp samples shown in Figure 38 and 39, respectively, that there are several residues that exhibit two cross-peaks. The results which are summarized in tabular form in Appendix 5 and in pictorial form in Figure 40 indicate that most of these residues which have double peaks are located in the extended loop containing His32, in the hairpin containing Tyr75 and in helix α2 and strand β2, both of which form the "back wall" of the heme pocket, are disordered conformationally. This conformational agility may contribute to endow HasAp with its ability to capture heme from hemoglobin and then deliver it to the HasR receptor.

On the other hand, Gly35, Phe78 and Tyr138 (enclosed in black boxes) which where pointed out to be very weak in the HSQC spectra in Figures 28 and 29 are now more intense and broad. Morever, two new peaks were observed in the fast recycling ^{1}H-^{15}N-HSQC spectrum of both full-length and truncated HasAp as seen in Figures 38 and 39 enclosed in green boxes. These peaks could be His32 and His83, however, no cross-peak can be found in all the 3D NMR spectra to sequentially assign these cross-peaks. Comparison of the full-length and truncated HasAp acquired with normal and fast recycling HSQC also revealed that there are some peaks that are benefited by the short acquisition time which means that these residues relax faster than the rest of the residues. Mapping these residues in the X-ray crystal structure of
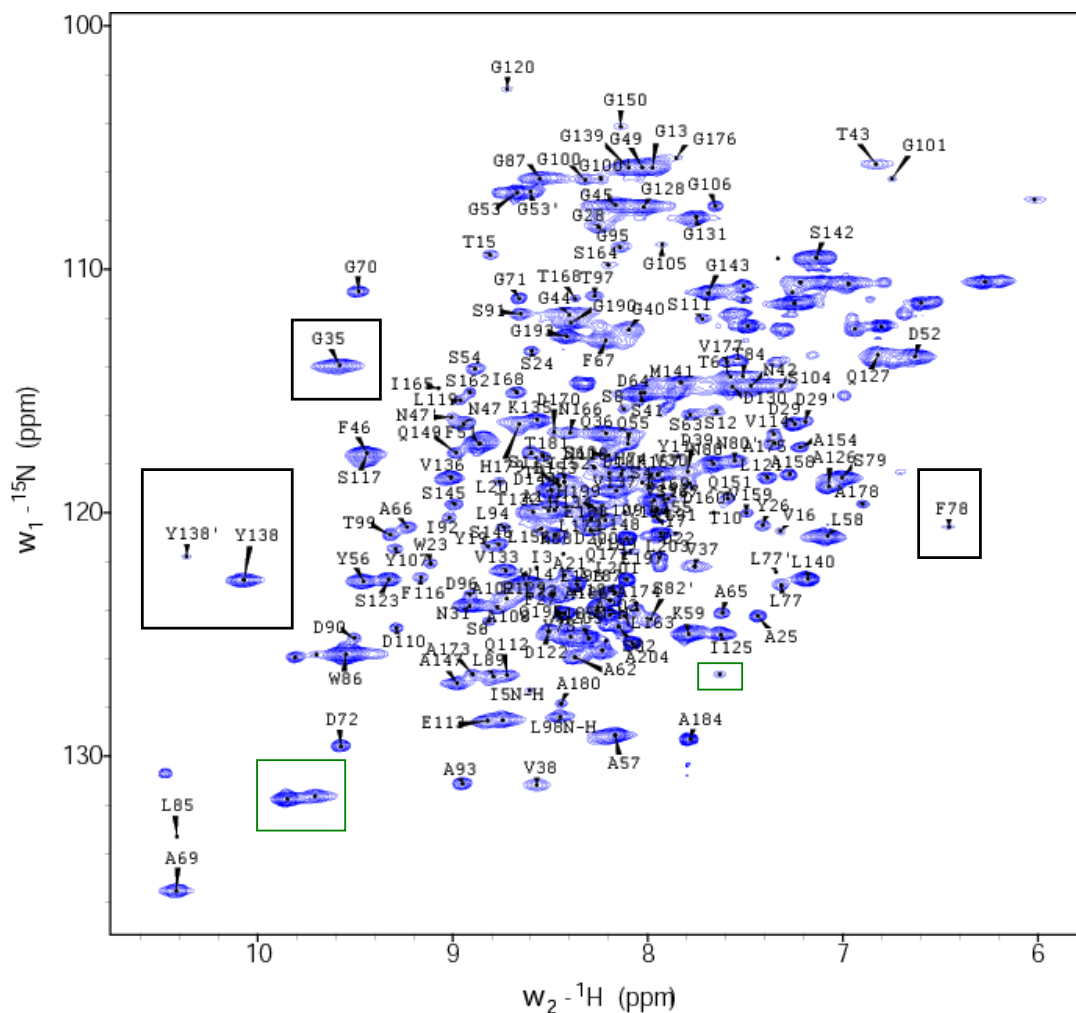
Figure 38. Fast recycling $^1H\{^{15}N\}$ HSQC spectrum of holo full-length HasAp (2.8 mM in phosphate buffer, $\mu = 0.1$, pH 7.0, 5% D_2O). G35, F78 and Y138 resonances are enclosed in boxes. They are broader and more intense in the fast recycling HSQC shown above compared to the HSQC spectrum obtained in Figure 28. Spectrum was recorded on a Varian Unity INOVA 600 NMR Complex points, 128 (t_1) x 1632 (t_2); spectral width, 2.4 kHz (t_1) x 9.60 kHz (t_2); acquisition time, 35 ms; recycle delay, 1 s; 128 scans.

Figure 39. Fast recycling ^{1}H{^{15}N} HSQC spectrum of holo truncated HasAp (2.8 mM in phosphate buffer, μ = 0.1, pH 7.0, 5% D$_2$O). G35, F78 and Y138 resonances are enclosed in boxes. They are broader and more intense in the fast recycling HSQC shown above compared to the HSQC spectrum obtained in Figure 28. Spectrum was recorded on a Varian Unity INOVA 600 NMR Complex points, 128 (t_1) x 1632 (t_2); spectral width, 2.4 kHz (t_1) x 9.60 kHz (t_2); acquisition time, 35 ms; recycle delay, 1 s; 128 scans.

HasAp (Figure 41) shows that these residues are located less than 11 Å from the heme-iron. Clearly resonances from these residues are affected by the paramagnetic heme-iron which enhances relaxation and causes broadening of the signals.
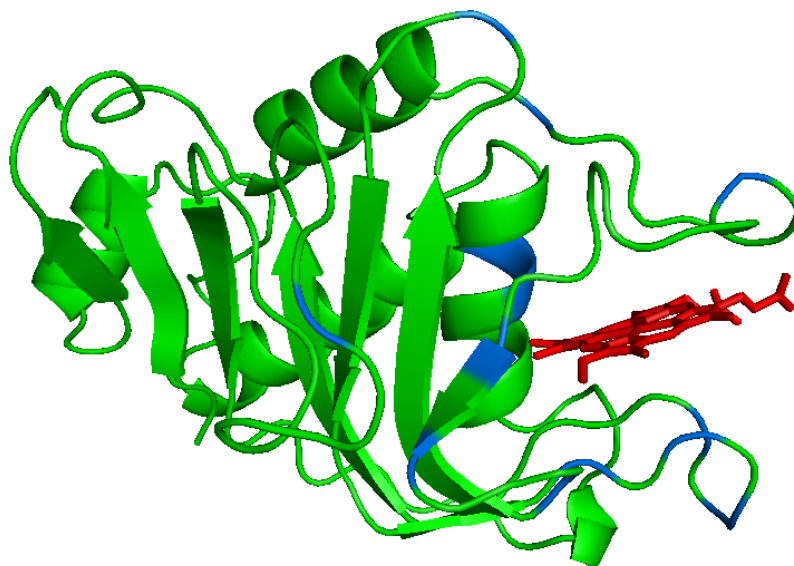
Figure 40. Residues which exhibit double cross-peaks in the fast recycling HSQC are highlighted in marine. The heme is in red.

Secondary Structure Identification of HasAp by NMR

The elements of secondary structure of HasAp can be identified by using the Chemical Shift Index (CSI) method of Wishart *et. al.* [83, 84]. Chemical shifts of
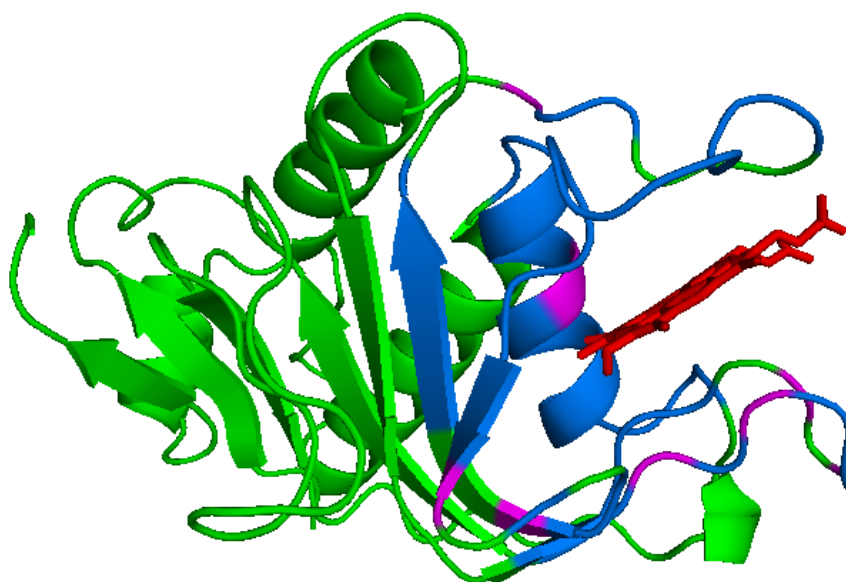
Figure 41. Residues which are affected by the paramagnetic relaxation of the heme iron as observed in the fast recycling HSQC are highlighted in blue and magenta. The residues in magenta show double resonance in the spectrum. Residues not affected by heme paramagnetism are shown in green. The heme is in red.

NMR active nuclei depend on several factors such as proximity to polar groups, presence of aromatic rings, bond hybridization states, local electronic distributions and magnetic anisotropies. Thus, chemical shifts depend on the structural environment and they can give structural information [84]. Wishart *et. al.* [83] developed useful empirical rules, called CSI, which is based on the observation that there is a relationship between $^1H^\alpha$, $^{13}C^\alpha$, $^{13}C^\beta$ or $^{13}C'$ chemical shifts and protein secondary structure. The CSI approach has become a standard procedure in the NMR

based structural characterization of proteins and is considered as a quick and reliable method for determining the elements of secondary structure in proteins [85-89]. It has been observed in essentially all 20 amino acids that the C^α and the carbonyls chemical shifts are downfield and upfield shifted, respectively, when they are located in the α-helices and in β-strands, relative to their positions in random coil. While, the C^β resonances are upfield and downfield shifted when located in the α-helices and β-strands, respectively [83, 88, 90, 91]. Strong correlation between protein secondary structure and C^α, C^β and C' chemical shifts suggests that these can be used for determining the secondary structure of the protein [83]. From these observations, the chemical shift approach was developed as a tool for assigning the secondary structure of the protein [83, 92].

The CSI concept consists of two parts. In the first part, chemical-shift index values (-1, 0, 1) are assigned to each residues based on their chemical shifts. Wishart *et. al.* [83] tabulated the $^{13}C^\alpha$, $^{13}C^\beta$ and $^{13}C'$ chemical shift reference values for each amino acid. If the observed chemical shift for $^{13}C^\alpha$ and $^{13}C'$ is higher than the range for that amino acid in random coils, it is marked as "+1". In the same way, if the value is within the range or below the range for that amino acid, it is marked as "0" or "-1", respectively. The same chemical index values are also applied for $^{13}C^\beta$, but the shifts are opposite from those observed in $^{13}C^\alpha$ and $^{13}C'$. In the second part, the secondary structures are assigned based on the values and local "densities" of these chemical-shift indices. For both $^{13}C^\alpha$ and $^{13}C'$, a consecutive group of four or more "+1's" not interrupted by a "0" or "-1" is considered a helix. A consecutive group of

three or more "-1's" not interrupted by "1" and "0" is considered a β-strand. All other regions not assigned as α-helix or β-strand is considered to be "coils". For the $^{13}C^\beta$ index values, a consecutive group of four or more "1's" not interrupted by "1" or "0" is considered a β-strand. The $^{13}C^\beta$ chemical shift index can only be used to identify β-sheets [83].

The chemical shift index ($^{13}C^\alpha$, $^{13}C^\beta$ and $^{13}C'$) versus the residue number of holo full-length and truncated HasAp are shown in Figures 42 and 43. The CSI were analyzed using the tool designed by Wishart *et. al.* [83] described above. The consensus chemical shift index of $^{13}C^\alpha$, $^{13}C^\beta$ and $^{13}C'$ for both proteins was calculated using the Chemical Shift Index software version 2.0 downloaded from the website of PENCE/CIHR-Group Joint Software Center of the University of Alberta at http://www.bionmr.ualberta.ca/bds/software/csi/latest/csi.html. The consensus CSI calculated using the software reveals four α-helices and 5 β-strands in the structure of holo full-length and truncated HasAp. Comparison of the secondary structures calculated using the consensus CSI and the X-ray structure are tabulated in Table 6. From Table 6, it can be noted that the α-helices for both the X-ray and CSI data are almost the same. However, in the X-ray structure there are 8 β-strands, while in the CSI there are only 5 β-strands. Closer inspection of the CSI based from the $^{13}C^\beta$ data which give more information about the β-strands in the structures revealed that there are 8 β-strands in the structure of both holo full-length and truncated HasAp. Moreover, since the X-ray crystal structure of the full-length HasAp does not show

141
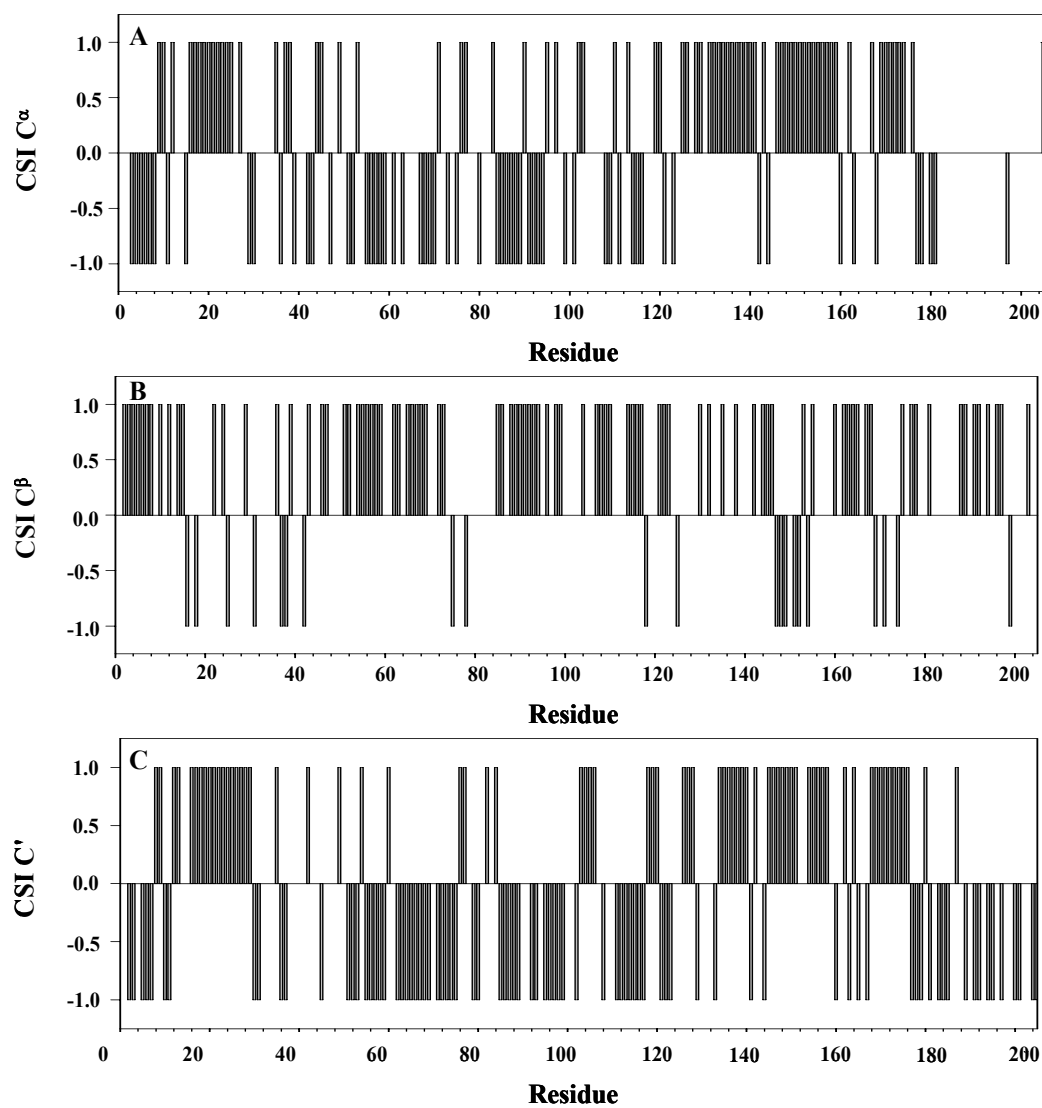
Figure 42. Chemical shift index (CSI) of holo full-length HasAp determined using (A) $^{13}C^{\alpha}$, (B) $^{13}C^{\beta}$, and (C) $^{13}C'$ chemical shifts.
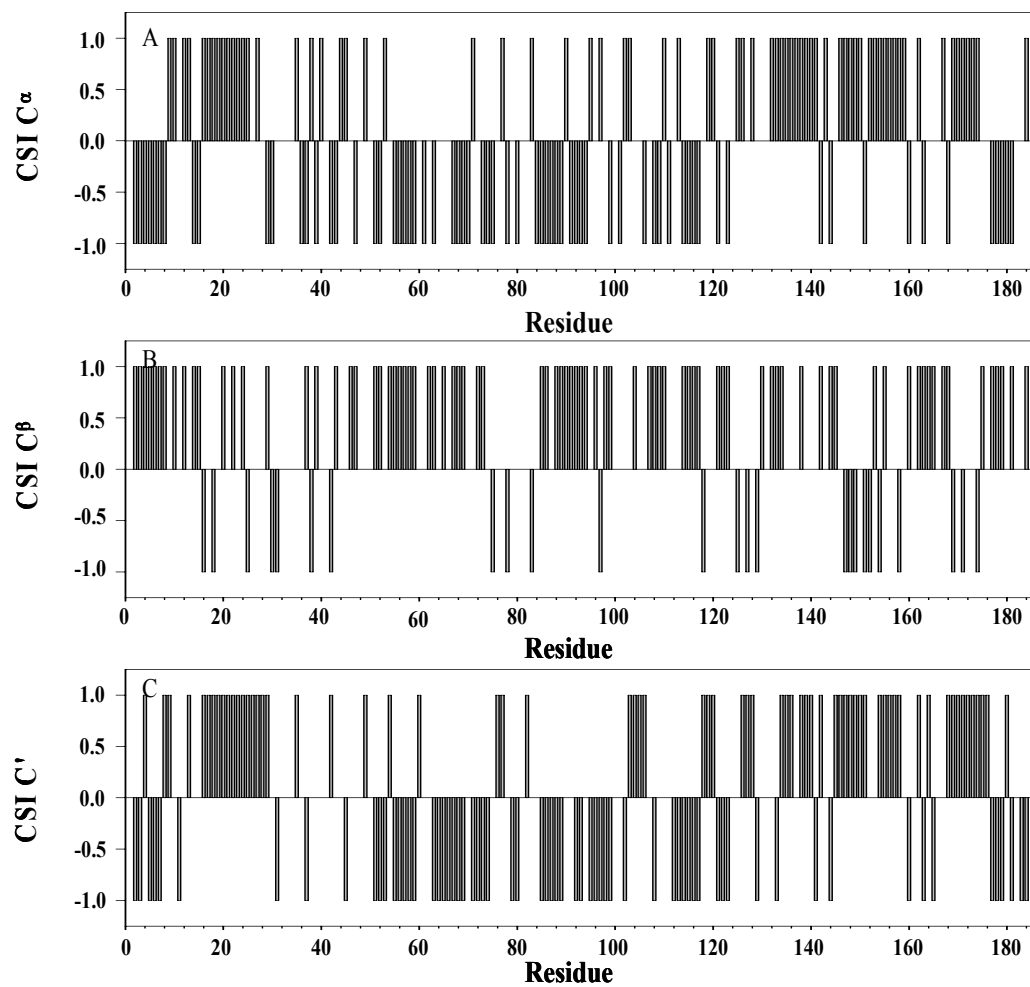
Figure 43. Chemical shift index (CSI) of holo truncated HasAp determined using (A) $^{13}C^{\alpha}$, (B) $^{13}C^{\beta}$, and (C) $^{13}C'$ chemical shifts.

the last 21 carboxy residues, it can be concluded that this part of the protein is highly dynamic and disordered. These residues were assigned using the triple resonance experiments and based from the CSI results shown in Figure 42, this part of the protein is not classified as α-helix or β-strands. It is a loop or a random coil. Thus, it can be concluded that both the X-ray and CSI results agree with each other.

Table 6. Comparison of the Elements of Secondary Structures of HasAp by X-Ray and NMR

Secondary Structure	Residues		
	X-Ray[a]	Full-Length CSI[b]	Truncated CSI[b]
Helix	Val16-Phe27	Val16-Tyr26	Val16-Tyr26
	Thr132-Ser142	Lys135-Leu140	His134-Leu140
	Ser145-Val159	Ser146-Gly150	Ala147-Gln151
		Ala154-Ala158	Ala154-Ala158
	Phe169-Ala175	Phe169-Ala174	Phe169-Gly176
Strand	Ser4-Ser8	Ser2-Ser8	Ile3-Ser8
	Gly45-Pro48		
	Asp52-Lys59	Gln55-Lys59	Gln55-Lys59
	Ala65-Tyr75	Phe67-Gly70	Ile68-Gly70
	Leu85-Gly100	Leu85-Lys89	Leu85-Leu94
		Ser91-Leu94	
	Tyr107-Ser117	Val114-Ser117	Val114-Phe116
	Leu121-Ser123		
	Ala178-Thr181		

[a] Secondary structure as determined by the Stride program [37]
[b] Secondary structure as determined by the consensus CSI program

Structure of the Carboxy Tail of Full-Length HasAp

As observed in the ^{1}H-^{15}N HSQC of the full-length HasAp shown in Figure 44A, the peaks corresponding to the 21 C-terminal residues of the tail (enclosed in black boxes) are more intense than the rest of the residues in the protein. A closer inspection of the 1D slices shown at the right-hand side and bottom of the spectrum in Figure 44A taken at cross-peak originating from Ala187 δ (^{1}H) = 8.20 ppm and δ (^{15}N) = 123 ppm, it can be observed that the 1D ^{1}H and ^{15}N peaks originating from Ala187 are sharper and more intense than those observed for the other residues with ^{15}N frequency also at 123 ppm. The 1D peaks of Ala187 as well as the other residues of the tails have narrower linewidths and more intense peaks compared to rest of the residues of the protein. This suggests that the resonances coming from those NHs are relaxing much faster compared to the rest of the residues thereby resulting in sharper peaks. In other words, the residues in the tail have different relaxation property than the rest of the protein. These resonances appear to be in slow exchange in the NMR time scale compared to the rest of the protein, which results in more intense and sharper peaks. While the rest of the residues in the protein have broader linewidths and shorter relaxation time, T_2, compared to the tail. The line width of an NMR signal depends on the transverse relaxation time, T_2, which is the inverse of the relaxation time (R = $1/T_2$). T_2 relaxation is measured by the half-height linewidth of the Lorentzian lineshaped peak, ($\Delta v_{\frac{1}{2}} = 1/\pi T_2^*$) [93].

The spin relaxation times, T_1 and T_2 are related to the Nuclear Overhauser Effect (NOE) [94]. NOE is used for structural studies because it can provide data on
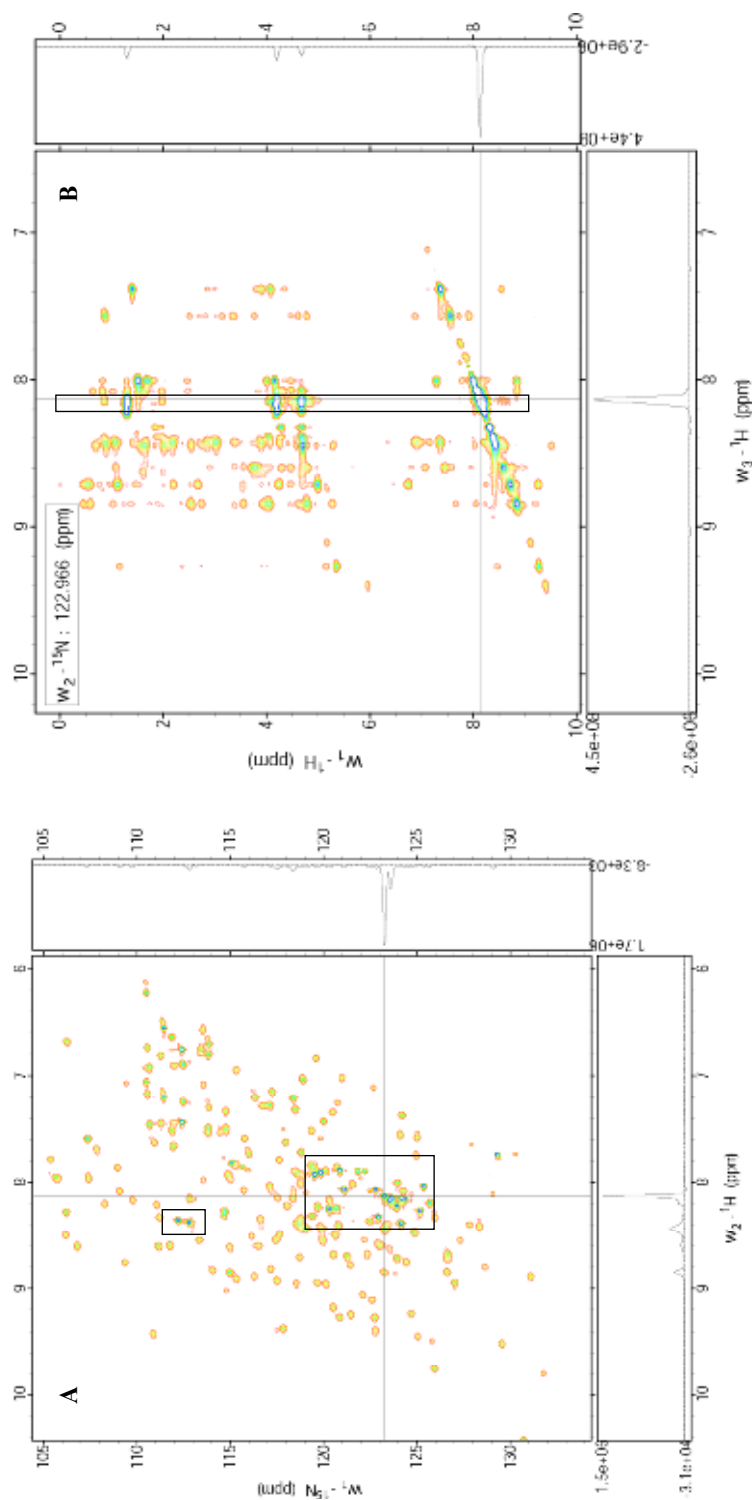
Figure 44. ¹H-¹⁵N HSQC spectrum (A) and ¹H-¹H 2D slice of 3D NOESY-HSQC spectrum of holo truncated HasAp. 1D-traces shown at the right-hand side and bottom of each spectrum are taken at cross-peaks originating from Ala187. NOE cross-peaks corresponding to Ala187 are enclosed in black rectangle.

internuclear distances which is directly correlated to the molecular conformation of the protein. The NOE intensity is directly propotional to $1/r^6$, with r being the distance between the protons. NOE correlation between two hydrogen atoms depends on the distance between them, typically, approximately 5 Å or less from one another. The NOE correlates hydrogen atoms of proteins which are close in space due to tertiary structure but not necessarily close in amino acid sequence. In globular proteins, large numbers of NOEs are observed due to several pairs of hydrogen atoms in close proximity in space from each other. This is one of the most important information NOE can provide for structure determination [93, 94].

In 3D NOESY-HSQC experiment, the NOESY experiment is extended by an HSQC step. The signals are dispersed into three dimensions (^{1}H-^{15}N-^{1}H). Data acquisition starts after the HSQC step instead of at the end of the NOESY mixing time. Magnetization is transferred from the first nucleus to the next one during the mixing time. Mixing time employs two magnetization transfer processes: dipolar interaction (NOE) and scalar coupling [94]. Figure 44B shows the ^{1}H-^{1}H 2D slice at δ (^{15}N) = 123 ppm out of the 3D NOESY-HSQC spectrum taken with 110 ms mixing time. In the two dimensional spectrum, the diagonal signals divide the spectrum in two equal halves. There are several symmetrical cross signals observed along the diagonal line. These cross signals originate from nuclei that exchanged magnetization during the mixing time. Hence, they are indicative of the interaction between nuclei and give important NOE information. From Figure 44B, Ala187 peak which is marked with the cross lines shows fewer cross-peak signals (shown in black

box) which suggests that it does not have many NOE correlations with other residues in the protein. This could be because the NH of Ala187 is far in space from the rest of the residues or it could be because the NH is very dynamic and the NOE cannot be build during the mixing time. As observed in Figure 44A, Ala187 also relaxes slower compared to the other residues at the same ^{15}N frequency. Moreover, few or no NOEs were also observed for the other non-proline residues in the tail. The few NOE cross-peaks observed could be attributed the intramolecular proton or to the protons preceding or after Ala187. It can be concluded that these part of the full-length protein is highly dynamic and disordered. This result also agrees with the X-ray and CSI data reported above.

To further show that there are indeed few NOEs observed in the carboxy terminus of the protein, we compared the NOE cross peaks observed in Leu73 which is also along the same ^{15}N frequency as Ala187. In the ^{1}H-^{15}N HSQC shown in Figure 45A, the ^{1}H and ^{15}N slices of Leu73 are shown in the bottom and right-hand side, respectively. The 1D peaks are broader and less intense compared to Ala187. In addition, the ^{1}H-^{1}H 2D slice from the 3D NOESY-HSQC spectrum is shown in Figure 45B. Several NOE cross peaks originating from Leu73 are observed (enclosed in black box), suggesting that this residue is close in space to a number of residues in the protein structure compared to Ala187. In fact, this is also observed for a majority of residues, except those located in the carboxy tail. Thus, the NOESY-HSQC experiment tells us that the 21 residues which composed the carboxy tail are indeed far in distance to the rest of the residues in the tail or that they are very dynamic and
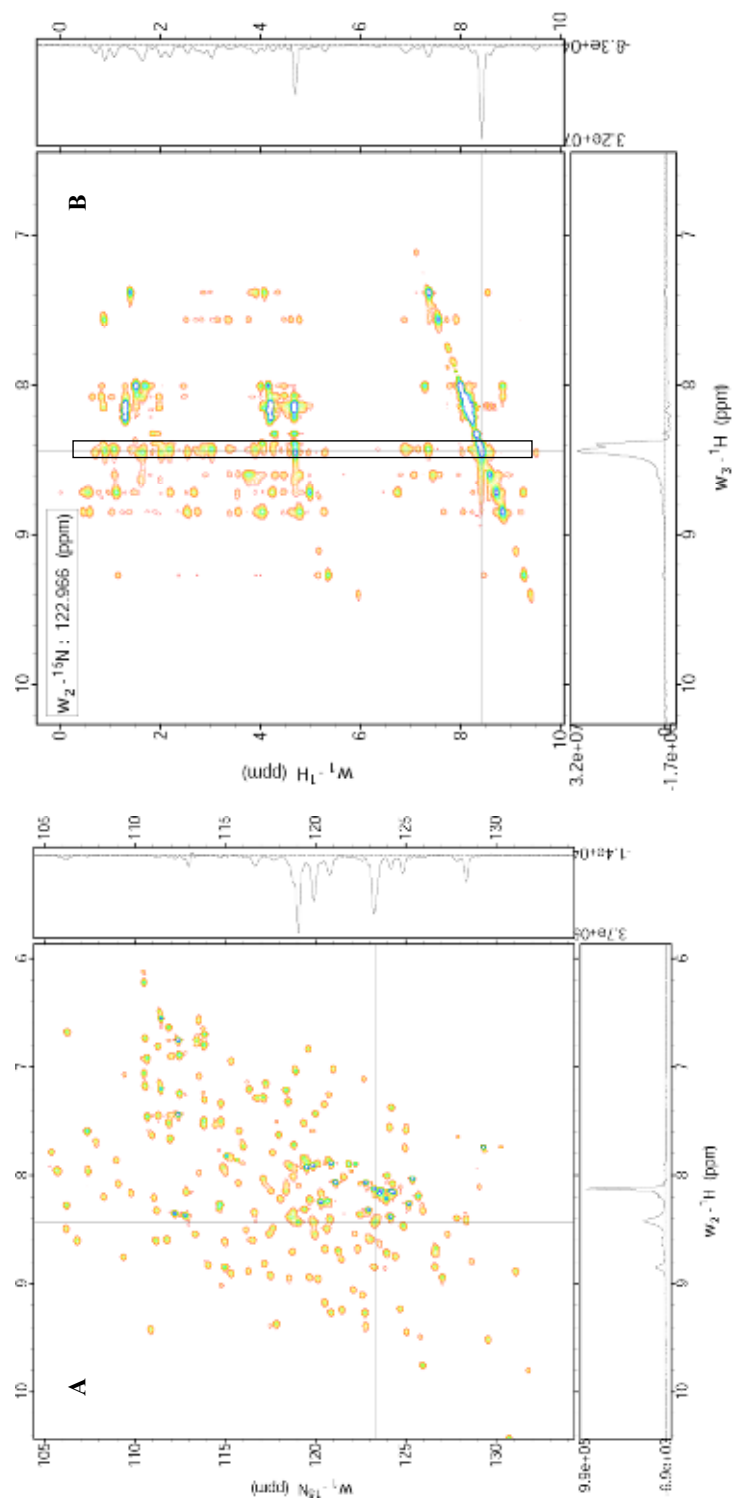
Figure 45. ^{1}H-^{15}N HSQC spectrum (A) and ^{1}H-^{1}H 2D slice of 3D NOESY-HSQC spectrum of holo truncated HasAp. 1D-traces shown at the right-hand side and bottom of each spectrum are taken at cross-peaks originating from Leu73. NOE cross-peaks corresponding to Leu73 are enclosed in black

149

cannot be detected in the NOE correlations.

Difference Between Apo and Holo Truncated HasAp

It is important to determine if there is conformational difference between the physiologically relevant truncated apo-HasAp and its heme loaded counterpart. The ^{1}H-^{15}N HSQC spectrum of apo truncated HasAp is shown in Figure 32. The presence and absence of heme in the protein could promote structural and conformational differences that could provide insights on the heme uptake and release mechanism of HasAp. The conformational difference between the apo and holo truncated HasAp were determined using the chemical shift perturbation analysis. This is commonly used to determine residues in the protein which undergo change in chemical environment as a result of protein-protein interaction [95]. The magnitude of the amide chemical shift perturbation that occur upon binding of heme in the protein was used as an indicator to identify the regions of the protein experiencing change in chemical environment as a result of the presence of heme. The magnitude of the chemical shift perturbation was calculated using the weighted average chemical shift difference of the ^{15}N nuclei and amide ^{1}H. The per-residue chemical shift perturbation is plotted in Figure 46A. The arithmetic mean of all perturbations is 0.25 ppm. The region between Gly28 to Thr43 showed large perturbations. Among the residues in the protein, Asp39 showed the highest chemical shift perturbation (1.69 ppm). These perturbations are mapped in the holo truncated HasAp structure shown in Figure 46B; regions of the protein which exhibit chemical shift perturbation larger than the
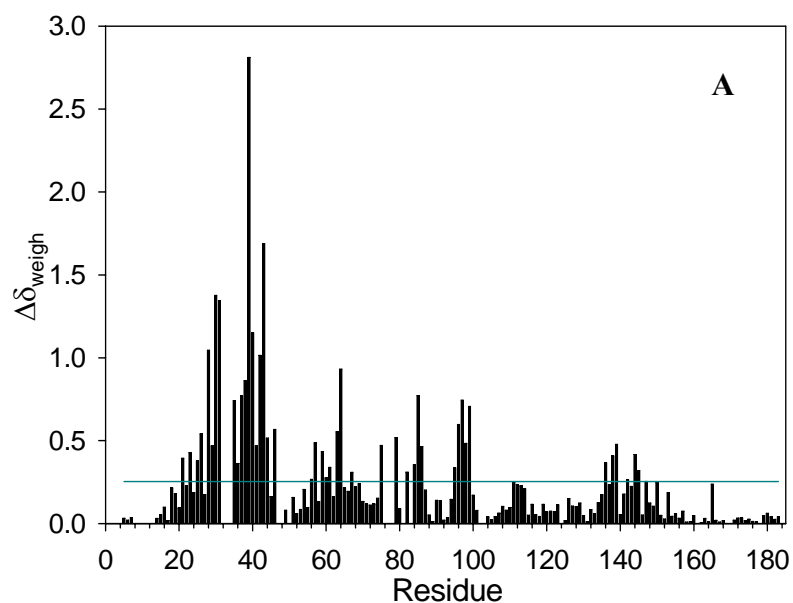
Figure 46. (A) Per-residue plot of the chemical shift difference between apo and holo truncated HasAp calculated using the weighted average amide chemical shift , $\Delta\delta_{ave} = \{[(\Delta\delta 1_H)^2 + (\Delta\delta 15_N/5)^2]/2\}^{1/2}$. The horizontal line represents the average difference of all residues (0.25). (B) The weighted average amide chemical shift differences are mapped onto the structure of holo truncated HasAp. Residues which exhibit differences in the range of $0.25 < \Delta\delta_{ave} < 0.80$ are highlighted in cyan, and those which exhibit the largest difference ($\Delta\delta_{ave} > 0.80$) are highlighted in red.

arithmetic mean of all perturbation (0.25 ppm) but ≤ 0.80 are colored in cyan. While, residues exhibiting largest chemical shift perturbation (> 0.80) are colored in red. Residues with chemical shift perturbation lower than the arithmetic mean are colored in white.

It can be observed from Figure 46B that residues which are perturbed are located in $\alpha 1$, $\alpha 2$, $\beta 2$, $\beta 3$, $\beta 4$, and in the two extended loops where the heme ligands are located. Interestingly, residues which exhibit chemical shift perturbation are concentrated on one part of the protein, close to the heme pocket. Residues with the largest chemical shift perturbations shown in red are located in the long extended loop which connects $\alpha 1$ and $\beta 2$ and this is the loop where His32 is located. These results suggest that this region of the protein experiences different conformations in both apo and holo state, but the other regions of the protein far from the active site are the same in both forms. The results also agree with the NMR structure of apo-HasA$_{SM}$ [96]. The NMR structure of apo-HasA$_{SM}$ is in an open conformation and its holo structure is in closed conformation. Hence, in HasAp it could also be the same since these two proteins share 50% identity. This open conformation may make HasAp more active in taking the heme from hemoglobin and when it takes the heme, the loops closed to secure the heme inside. This open and close conformation could also suggest that there is a different dynamics in both apo and holo HasAp. The dynamic property of holo truncated HasAp was studied by H/D exchange experiments.

Hydrogen-Deuterium Exchange Experiment of HasAp

Hydrogen/Deuterium (H/D) exchange experiment is a phenomenon wherein the amide backbone protons in the peptide bond of a protein are exchanged by deuterium. By changing the solvent from H_2O to D_2O, the exchange process can be followed. The H/D exchange in holo-HasAp was followed by HSQC as a function of time. As the amide protons exchange with deuterium, the signals in the HSQC spectrum decay with time. This experiment gives information of all the residues in the protein at the same time. Basically, the H/D exchange experiment gives information on the exchange rate of hydrogen with deuterium and this reflects the accessibility of the particular amide to the solvent [28, 97, 98] as well as the dynamics of the protein[18]. Hence, amide protons forming hydrogen bonding interactions with other residues and those that are buried within the hydrophobic core will exchange slowly than the residues not forming hydrogen bonding interaction and exposed to the solvent. The rate constants for H/D exchanged for each residue were calculated by fitting the time-dependent decay of the cross-peak intensity to a three-parameter single exponential decay (Figure 47) using eq 2 [99].

$$I(t) \; = \; I_\infty + A \, \exp(-k_{ex}t) \tag{2}$$

where I(t) is the intensity of the cross-peak at time t, I_∞ is the cross-peak intensity at infinite time, A is the amplitude of the exchange curve, and k_{ex} is the experimental N-H exchange rate constant of each residue in the protein. Protection factors (P) allow the quantitative comparison of the H/D exchange rate of the residues in the protein.

Protection factors were calculated using eq 3 [97, 98] where k_{ch} is the sequence-specific intrinsic rate constants of each residues and k_{ex} is described above.

$$P = k_{ch}/k_{ex} \qquad (3)$$
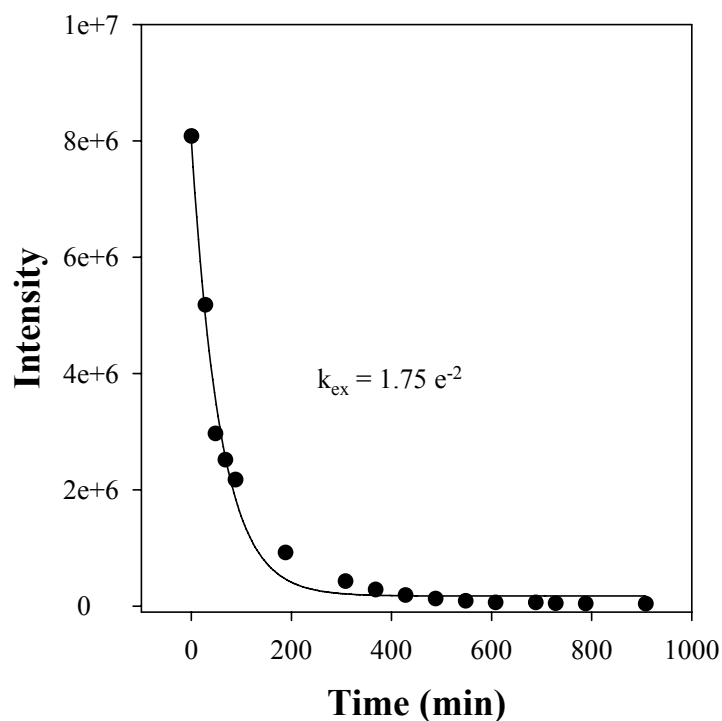
Figure 47. H/D exchange rate constant determination for residue Asp52 in holo truncated HasAp at pD 7.58. The line represents the fit of equation 2 to the experimental data.

The H/D experiment was monitored for 32 hours. Exchange rates (k_{ex}) for 30% of the residues were not obtained because rates are too fast to observe

experimentally. Per-residue plot of the logarithm of the protection factors is shown in Figure 48 and the results are mapped on the structure of HasAp shown in Figures 49A-D. As observed in Figures 49A and C, the residues with k_{ex} too fast to measure (yellow) are mostly concentrated in the loops: loops where the heme axial ligands (His32 and Tyr75) are located; hairpin loops which connect the antiparallel beta sheets, β3 and β4, and β6 and β7; extended loop connecting 3_{10}-helix 2 and β7 and in the last 5 C-terminal residues (ATPAA). Those residues with high B-factor values mentioned earlier have k_{ex} too fast to measure. Moreover, α3, α4, 3_{10}-helix 2, β7 and β8 were susceptible to H/D exchange as shown in Figures 49A and C colored in
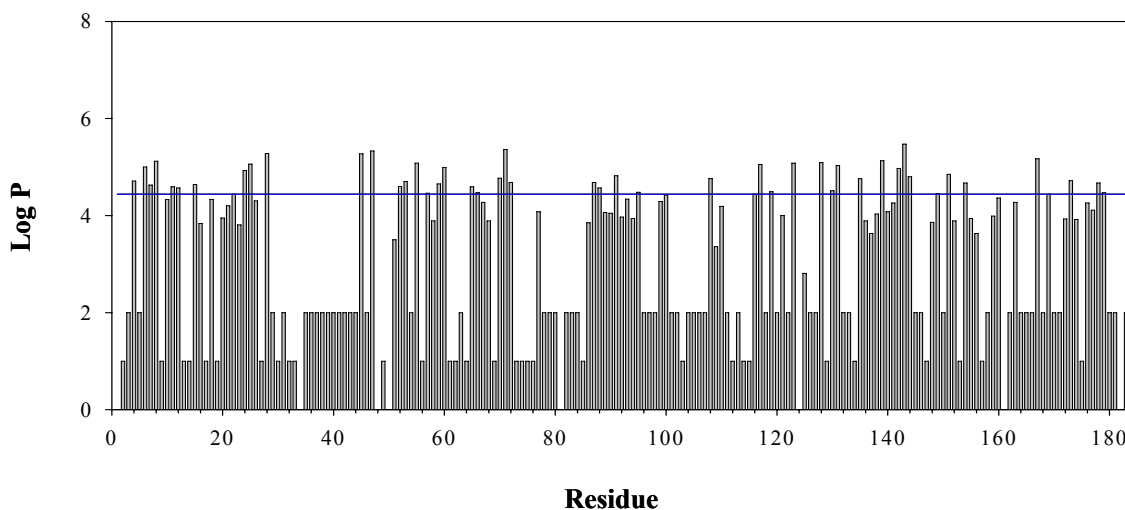
Figure 48. Per-residue protection factors obtained from amide H/D exchange experiment of truncated holo HasAp. A value of log P = 1 was given to residues not included in the analysis due to either lack of assignment or peak overlap and a value of log P = 2 was arbitrarily given to residues exhibiting exchange rates too fast to be measure. The horizontal line represents the average log P of all residues.

yellow and cyan. This result suggests that this region of the protein is dynamic. β4-β6 have lower protection factors values and α1, α2 and β3 have combination of residues which are less and highly protected by deuterium exchange. A closer look at the surface structures of the protein in Figures 49B and D shows overall the protein is highly dynamic as suggested by the results that there are more residues with k_{ex} too fast too measure (yellow) and with lower protection factor values (cyan) combined
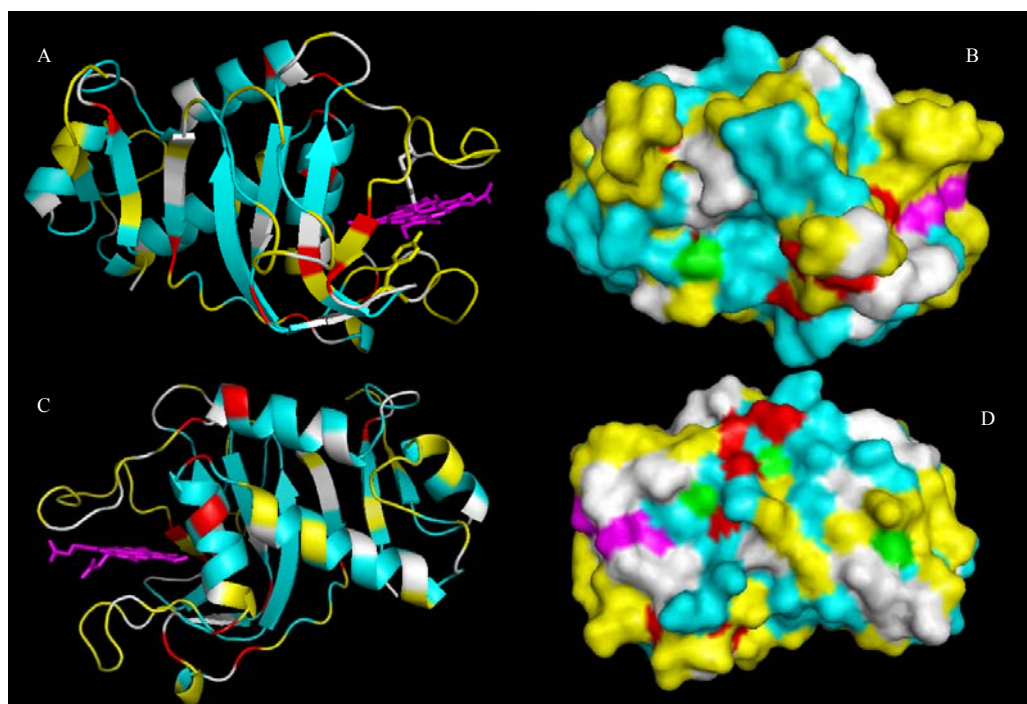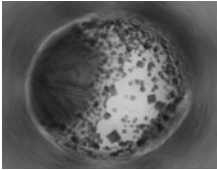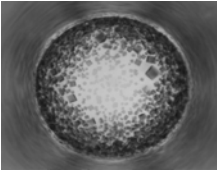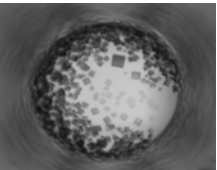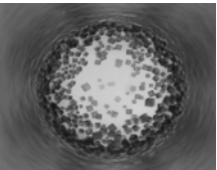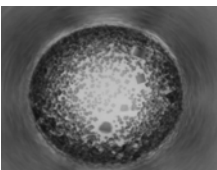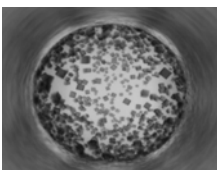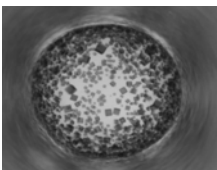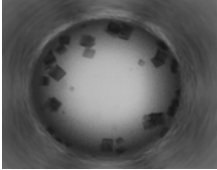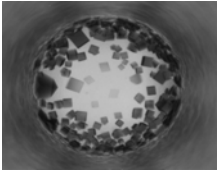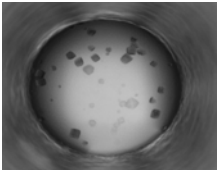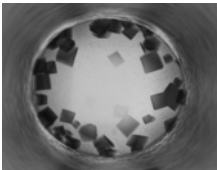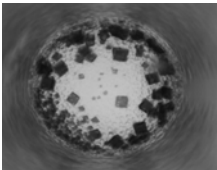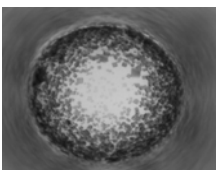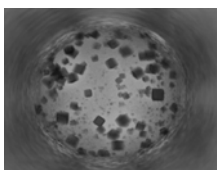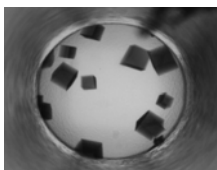
Figure 49. Stereoview (A and C) and surface structure (B and D) of holo truncated HasAp highlighting residues with high protection factor values in red, with low protection values in cyan, residues with k_{ex} too fast to measure in yellow, residues not included in the analysis due to lack of assignment or peak overlap in white and the heme in magenta.
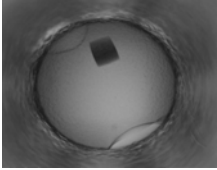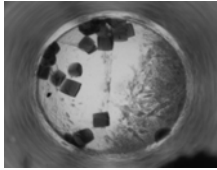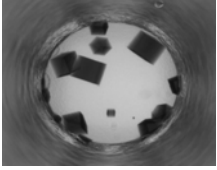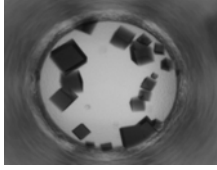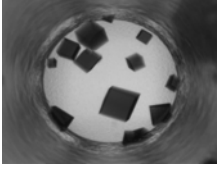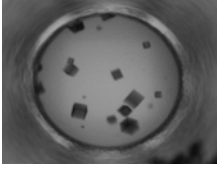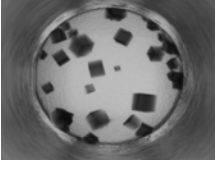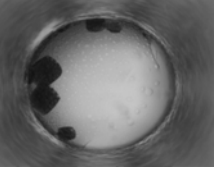
than residues which are highly protected (red). Interestingly, most of these fast exchanging residues are located close to the heme active site, in the loops and C-terminus. In comparison, in general the α-helices are more protected than the β-sheets and majority of the residues which are protected are glycine. Overall, the residues which were susceptible to hydrogen-deuterium exchange are located in the surface of the protein. The H/D exchange experiment suggests HasAp is a highly dynamic protein.
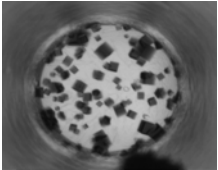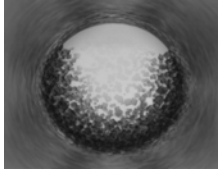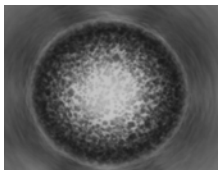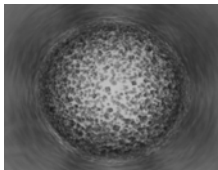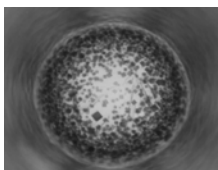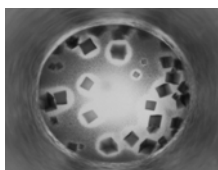
APPENDICES

Appendix 1. Protein Crystallization conditions

Crystal	Plate #	Salt	Conc.	Buffer	Conc.	pH	Solvent	Conc.
	520	KSCN	0.1M	Tris	0.1M	8	PEG8000	40% W/V
	551	NH_4NO_3	0.1M	Tris	0.1M	8	PEG4000	20% W/V
	582	KBr	0.1M	Tris	0.1M	8	PEG4000	20% W/V
	587	KCl	0.1M	Tris	0.1M	8	PEG4000	20% W/V
	602	$NaNO_3$	0.1M	Tris	0.1M	8	PEG4000	20% W/V
	644	$KC_2H_3O_2$	0.1M	Tris	0.1M	8	PEG4000	40% W/V
	664	RbCl	0.1M	Tris	0.1M	8	PEG4000	40% W/V

Crystal	Plate #	Salt	Conc.	Buffer	Conc.	pH	Solvent	Conc.
	699	NH_4Cl	0.1M	Tris	0.1M	8	PEG1000	20% W/V
	734	KSCN	0.1M	Tris	0.1M	8	PEG1000	20% W/V
	735	RbCl	0.1M	MES	0.1M	6	PEG1000	20% W/V
	743	$NaNO_3$	0.1M	Tris	0.1M	8	PEG1000	20% W/V
	745	$Na_2S_2O_3$	0.1M	Tris	0.1M	8	PEG1000	20% W/V
	761	NH_4SCN	0.1M	Tris	0.1M	8	PEG1000	20% W/V
	818	NaCl	0.1M	Tris	0.1M	8	PEG1000	40% W/V
	840	NH_4Br	0.1M	Tris	0.1M	8	PEG400	40% V/V

Crystal	Plate #	Salt	Conc.	Buffer	Conc.	pH	Solvent	Conc.
	842	NH_4Cl	0.1M	MES	0.1M	6	MES	40% V/V
	849	$(NH_4)_2SO_4$	0.1M	MOPS	0.1M	7	PEG400	40% V/V
	888	NaBr	0.1M	Tris	0.1M	8	PEG400	40% V/V
	893	$NaNO_3$	0.1M	Tris	0.1M	8	PEG400	40% W/V
	911	NH_4SCN	0.1M	Tris	0.1M	8	PEG400	40% V/V
	918	NH_4Cl	0.1M	Tris	0.1M	8	PEG400	80% V/V
	947	KCl	0.1M	Tris	0.1M	8	PEG400	80%V/V
	951	KH_2PO_4	0.1M	Sodium acetate	0.1M	5	PEG400	20% V/V

Crystal	Plate #	Salt	Conc.	Buffer	Conc.	pH	Solvent	Conc.
	976	$Li_2SO_4.H_2O$	0.1M	Tris	0.1M	8	PEG400	60% V/V
	1187			Tris	0.1M	9	PEG6000	10% W/V
	1193			Tris	0.1M	8	PEG6000	20% W/V
	1199			Tris	0.1M	8	PEG6000	30% W/V
	1389			Tris	0.1M	8.5	PEG3350	25% W/V
	1425		0.20M	Tris	0.1M	8.5	PEG3350	25% W/V

Appendix 2. Backbone Assignment of Holo Full-Length HasAp

Residue	^1H_N	$^{15}N_H$	$^{13}C^\alpha$	$^{13}C^\beta$	^{13}CO
Met1					
Ser2			57.80	64.51	171.20
Ile3	8.57	122.24	61.61	38.74	171.89
Ser4	8.08	118.76	56.67	65.08	174.15
Ile5	8.62	127.37	60.01	42.84	174.88
Ser6	8.82	124.36	56.42	65.24	172.63
Tyr7	7.98	120.15	55.07	41.32	172.54
Ser8	8.14	115.73	57.02	63.68	177.45
Thr9	8.46	118.71	65.61	68.68	176.06
Thr10	7.66	119.88	65.82	69.48	174.64
Tyr11	7.87	117.66	58.73	38.18	175.09
Ser12	7.66	115.81	63.47	64.34	175.25
Gly13	7.99	105.33	45.07		175.00
Trp14	8.65	122.90	57.44	29.15	176.21
Thr15	8.82	109.40	60.19	70.93	175.52
Val16	7.33	120.77	66.64	30.80	178.40
Ala17	8.50	119.92	55.63	18.98	179.51
Asp18	8.22	118.38	57.41	39.70	179.97
Tyr19	8.85	121.46	63.59	39.09	176.85
Leu20	8.78	118.72	58.18	41.76	179.45
Ala21	8.44	122.50	55.55	18.79	180.32
Asp22	7.92	120.77	58.04	42.78	178.33
Trp23	9.12	122.13	63.41	28.76	178.56
Ser24	8.61	113.34	63.04	64.02	176.88
Ala25	7.45	124.26	54.53	18.18	178.78
Tyr26	7.42	120.43	58.40	38.55	177.86
Phe27	8.50	123.35	61.47	39.20	176.64
Gly28	8.27	108.27	44.99		176.72
Asp29	7.28	116.33	51.54	42.84	177.96
Asp29'	7.21	116.21	51.43	42.95	177.86
Val30	7.96	118.55	61.51	31.00	176.31
Asn31	8.93	123.86	53.33	36.07	172.58
His32					
Arg33					
Pro34			65.94	32.43	177.42

Residue	^1H_N	$^{15}N_H$	$^{13}C^\alpha$	$^{13}C^\beta$	^{13}CO
Gly35	9.60	113.92	46.05		174.95
Gln36	8.22	116.73	54.18	30.95	175.08
Val37	7.81	122.27	65.40	29.49	173.92
Val38	8.60	131.25	65.67	29.69	176.61
Asp39	7.79	118.25	52.37	41.93	177.20
Gly40	8.11	112.50	45.63		173.86
Ser41	8.04	115.00	58.92	63.28	174.11
Asn42	7.49	114.77	51.12	36.31	176.28
Thr43	6.85	105.65	58.20	71.88	
Gly44	8.41	111.92	45.97		173.75
Gly45	8.17	107.36	45.97		170.42
Phe46	9.46	117.54	57.58	44.22	176.12
Asn47	8.96	116.31	49.00	43.02	175.20
Asn47'	9.02	116.02	49.00	43.02	175.19
Pro48			65.72	34.60	179.70
Gly49	8.03	105.74	46.46		176.28
Pro50			64.67	34.38	177.66
Phe51	8.89	117.22	56.80	40.74	170.85
Asp52	6.64	113.56	51.98	45.95	174.82
Gly53	8.67	106.84	47.35		171.28
Ser54	8.90	114.08	58.17	63.98	176.77
Gln55	8.11	117.14	54.67	37.30	175.22
Tyr56	9.46	122.81	57.51	42.40	172.15
Ala57	8.18	129.09	49.54	24.04	174.32
Leu58	7.09	121.01	54.17	45.27	174.39
Lys59	7.82	124.95	53.88	34.82	174.31
Ser60	8.22	117.56	57.64	63.30	174.77
Thr61	7.61	114.47	62.17	68.50	174.75
Ala62	8.40	125.95	52.45	21.18	176.53
Ser63	7.80	116.00	56.94	66.37	172.39
Asp64	8.01	114.94	54.67	41.33	175.78
Ala65	7.63	124.14	52.87	19.88	175.26
Ala66	9.26	120.57	52.24	25.21	174.16
Phe67	8.22	112.85	55.30	44.27	172.88
Ile68	8.68	115.00	60.78	42.31	176.28

Residue	^1H_N	$^{15}N_H$	$^{13}C^\alpha$	$^{13}C^\beta$	^{13}CO
Ala69	10.43	135.57	50.42	20.88	175.13
Gly70	9.49	110.91	43.63		173.75
Gly71	8.67	111.20	46.71		171.60
Asp72	9.59	129.59	54.64	41.64	173.68
Leu73	8.50	123.35	54.52	47.11	176.09
His74	8.17	118.44	56.49	31.57	173.66
Tyr75	8.41	125.14	53.22	34.06	173.65
Thr76			64.91		176.31
Leu77	7.32	123.00	58.42	41.80	179.14
Phe78	6.51	120.57	57.82	38.59	175.30
Ser79	7.03	118.60	57.86	63.03	170.58
Asn80	7.69	117.98	51.47	39.40	173.73
Asn80'	7.56	117.91	51.31	39.40	173.62
Pro81			62.53	32.85	176.40
Ser82	8.17	124.71	58.09	63.27	174.83
His83			57.94		174.83
Thr84	7.57	113.86	62.27	68.61	176.29
Leu85	10.42	133.39	54.68	46.18	174.29
Trp86	9.57	125.82	55.45	30.42	172.17
Gly87	8.57	106.22	43.37		172.16
Lys88	8.47	120.82	54.78	34.75	175.12
Leu89	8.79	126.62	54.06	46.17	172.91
Asp90	9.52	125.06	55.03	44.85	176.71
Ser91	8.67	111.80	56.97	66.74	173.55
Ile92	9.02	120.14	59.79	42.32	172.69
Ala93	8.96	131.10	50.88	21.53	174.70
Leu94	8.76	120.52	53.67	43.17	176.77
Gly95	8.14	109.12	47.19		171.14
Asp96	8.90	123.18	53.77	45.32	174.06
Thr97	8.28	111.04	64.78	65.17	172.64
Leu98	8.48	128.37	55.29	43.13	176.48
Thr99	9.34	120.89	60.23	72.03	173.64
Gly100	8.35	106.24	45.14		173.40
Gly101	6.75	106.29	43.70		173.78

Residue	^1H_N	$^{15}N_H$	$^{13}C^\alpha$	$^{13}C^\beta$	^{13}CO
Ala102	8.72	123.54	55.52	19.37	174.43
Ser103			59.93	63.19	175.01
Ser104	7.41	114.79	57.77	63.83	174.48
Gly105	7.93	109.00	45.51		174.16
Gly106	7.67	107.39	44.32		174.38
Tyr107	9.31	121.48	58.77	41.16	175.73
Ala108	8.79	123.96	51.54	22.38	174.62
L109	8.30	119.68	52.91	43.35	176.99
Asp110	9.31	124.74	56.74	41.60	177.49
Ser111	7.74	112.00	55.98	63.13	173.14
Gln112	8.74	126.66	56.67	30.00	175.16
Glu113	8.87	128.70	58.68	30.70	175.28
Val114	7.36	116.81	60.36	37.61	173.65
Ser115	8.61	117.49	56.34	66.08	172.39
Phe116	9.17	122.62	56.19	42.07	174.15
Ser117	9.44	117.86	57.73	65.61	172.83
Asn118	8.28	118.09	53.85	37.18	175.65
Leu119	8.97	115.34	57.32	42.10	178.74
Gly120	8.74	102.57	47.27		174.94
Leu121	7.39	118.52	54.73	42.88	176.22
Asp122	8.54	124.90	53.97	43.71	175.93
Ser123	9.34	122.78	56.26	66.91	172.36
Pro124			61.88	32.67	177.40
Ile125	7.66	125.05	64.75	36.26	176.44
Ala126	7.11	118.93	53.99	19.02	178.98
Gln127	6.83	113.45	56.75	29.46	177.44
Gly128	8.03	107.46	46.39		175.02
Arg129	8.66	123.07	57.17	29.66	174.77
Asp130	7.57	114.80	54.61	41.86	177.01
Gly131	7.76	107.87	45.91		173.13
Thr132	8.62	119.97	67.34	69.08	175.17
Val133	8.75	122.37	69.33	31.31	176.47
His134	8.49	119.86	62.64	31.38	178.35
Lys135	8.57	116.18	61.26	33.14	181.44
Val136	9.02	118.57	66.77	31.83	178.22

Residue	^1H_N	$^{15}N_H$	$^{13}C^\alpha$	$^{13}C^\beta$	^{13}CO
Val137	8.17	119.10	67.68	32.11	176.86
Tyr138	10.08	122.77	62.56	40.27	179.69
Tyr138'	10.40	121.81	62.59	40.17	179.51
Gly139	8.12	105.76	48.30		176.33
Leu140	7.18	122.71	58.52	41.38	179.13
Met141	7.84	114.69	59.91	33.39	174.96
Ser142	7.15	109.47	56.39	63.69	174.23
Gly143	7.71	111.00	47.05		173.67
Asp144	8.51	119.08	52.51	42.29	175.52
Ser145	9.01	119.68	58.83	64.18	175.19
Ser146	8.77	121.29	62.35	63.42	177.11
Ala147	9.02	127.05	55.63	17.41	180.91
Leu148	8.24	120.33	58.50	41.02	177.82
Gln149	8.99	117.52	60.99	29.16	177.78
Gly150	8.16	104.10	47.32		177.05
Gln151	7.59	119.38	57.56	27.69	178.05
Ile152	8.41	118.78	64.59	36.73	177.24
Asp153	8.46	118.75	59.19	42.84	177.18
Ala154	7.22	117.27	55.39	18.15	181.17
Leu155	7.94	119.51	58.01	42.89	180.16
Leu156	8.56	120.61	58.17	41.42	178.48
Lys157	7.98	118.58	58.69	32.93	178.30
Ala158	7.28	118.41	53.73	18.39	179.37
Val159	7.50	120.03	65.67	31.83	176.62
Asp160	7.79	118.83	52.49	44.22	173.93
Pro161			64.60	32.17	176.80
Ser162	8.92	115.01	60.00	64.09	174.53
Leu163	8.15	124.29	53.97	43.54	174.75
Ser164	8.24	109.81	58.26	67.58	175.01
Ile1165	9.09	114.83	62.38	39.04	174.10
Asn166	8.41	116.63	53.67	39.21	174.79
Ser167	7.92	119.41	60.33	64.41	173.17
Thr168	8.40	111.25	60.01	71.51	176.88
Phe169	8.01	118.94	64.32	36.12	177.70

Residue	^1H_N	$^{15}N_H$	$^{13}C^\alpha$	$^{13}C^\beta$	^{13}CO
Asp170	8.50	116.71	57.63	41.23	180.09
Gln171	8.09	121.58	59.21	28.10	180.18
Leu172	8.32	120.59	57.52	41.51	179.40
Ala173	8.92	126.59	54.84	18.64	182.15
Ala174	8.07	123.95	54.90	17.66	178.93
Ala175	7.35	117.16	52.27	20.41	177.61
Gly176	7.85	105.44	45.72		174.47
Val177	7.60	113.80	62.16	33.13	173.52
Ala178	6.90	119.64	48.81	24.40	175.20
His179	8.67	116.34	55.35	32.32	172.53
Ala180	8.45	127.73	50.72	19.53	178.57
Thr181	8.56	117.69	59.24	69.32	172.37
Pro182			63.16	32.27	176.70
Ala183	8.26	125.71	52.42	19.50	174.60
Ala184	7.81	129.34	52.39	19.50	176.25
Ala185	8.29	123.97	52.36	19.66	177.24
Ala186	8.22	123.65	52.83	19.44	177.27
Ala187	8.20	123.30	52.57	19.53	177.61
Glu188	8.32	120.34	56.57	30.47	176.34
Val189	8.14	121.16	62.68	32.84	176.56
Gly190	8.42	112.25	45.35		173.69
Val191	7.98	119.90	62.49	33.10	175.30
Val192	8.00	119.57	62.67	32.91	176.41
Gly193	8.44	112.84	45.43		173.70
Val194	7.98	119.90	62.46	32.90	176.07
Gln195	8.46	124.19	55.86	29.86	175.43
Glu196	8.40	122.97	56.60	30.70	175.82
Leu197	8.04	122.05	53.17	43.02	176.54
Pro198			63.23	32.22	178.20
His199	8.32	119.63	56.44	30.70	174.82
Asp200	8.28	120.73	54.54	41.15	175.87
Leu201	8.13	122.79	55.67	42.46	176.11
Ala202	8.21	124.11	52.78	19.09	177.47
Leu203	7.95	120.84	55.26	42.68	176.80
Ala204	8.10	125.38	52.59	19.61	175.90
Ala205	8.34	125.16	54.06	19.68	175.12

Appendix 3. Backbone Assignment of Holo Truncated HasAp

Residue	^1H_N	$^{15}N_H$	$^{13}C^\alpha$	$^{13}C^\beta$	^{13}CO
Met1					
Ser2			57.41	64.18	171.30
Ile3	8.61	122.19	61.42	38.61	171.96
Ser4	8.08	118.78	56.35	65.07	174.26
Ile5	8.61	127.30	59.91	42.78	174.97
Ser6	8.82	124.44	56.30	65.18	172.68
Tyr7	7.95	120.15	54.72	41.23	172.54
Ser8	8.13	115.73	56.87	63.85	177.41
Thr9	8.46	118.74	65.38	68.27	176.18
Thr10	7.67	119.92	65.57	69.52	174.75
Tyr11	7.87	117.70	58.54	38.07	175.12
Ser12	7.66	115.79	63.08	64.14	175.30
Gly13	7.99	105.38	46.12		175.09
Trp14	8.64	122.89	56.97	29.13	176.26
Thr15	8.82	109.40	59.93	70.72	175.61
Val16	7.32	120.77	66.43	30.71	178.47
Ala17	8.49	119.91	55.47	18.77	179.58
Asp18	8.21	118.37	57.43	39.64	180.10
Tyr19	8.84	121.46	63.33	39.14	176.89
Leu20	8.77	118.73	58.10	41.69	179.53
Ala21	8.44	122.51	55.35	18.35	180.42
Asp22	7.92	120.73	57.75	42.73	178.38
Trp23	9.11	122.12	63.22	28.61	178.70
Ser24	8.61	113.34	62.80	64.49	177.01
Ala25	7.45	124.25	54.35	18.05	178.90
Tyr26	7.42	120.36	58.41	38.30	177.99
Phe27	8.50	123.33	61.29	38.87	176.81
Gly28	8.27	108.24	44.78		176.81
Asp29	7.27	116.34	51.50	42.75	178.10
Asp29'	7.21	116.20	51.32	42.65	177.86
Val30	7.98	118.58	61.24	30.98	176.41
Asn31	8.93	123.82	53.00	35.77	172.60
His32					
Arg33					
Pro34			65.80	32.45	177.52

Residue	^1H_N	$^{15}N_H$	$^{13}C^\alpha$	$^{13}C^\beta$	^{13}CO
Gly35	9.59	113.91	45.88		175.03
Gln36	8.23	116.73	53.97	30.68	175.21
Val37	7.84	122.30	58.41	33.54	173.90
Val38	8.59	131.02	65.40	29.45	176.66
Asp39	7.79	118.31	52.21	41.81	177.21
Gly40	8.10	112.33	45.76		173.89
Ser41	8.04	115.05	58.83	63.27	174.17
Asn42	7.48	114.77	51.00	36.16	176.40
Thr43	6.83	105.68	59.99	71.93	175.63
Gly44	8.42	111.86	45.77		173.65
Gly45	8.16	107.33	45.88		170.48
Phe46	9.45	117.53	57.21	44.19	176.16
Asn47	8.95	116.32	48.99	42.83	175.20
Asn47'	9.01	116.08	48.93	42.53	175.20
Pro48			65.43	34.47	179.77
Gly49	8.02	105.74	46.25		176.30
Pro50			64.59	34.24	177.73
Phe51	8.89	117.21	56.63	40.58	170.93
Asp52	6.64	113.58	51.76	45.84	174.87
Gly53	8.67	106.81	47.24		171.37
Ser54	8.90	114.06	58.02	64.04	176.84
Gln55	8.10	117.12	54.47	37.21	175.26
Tyr56	9.46	122.79	57.19	42.34	172.17
Ala57	8.17	129.09	49.28	23.90	174.35
Leu58	7.08	120.99	54.05	45.11	172.63
Lys59	7.82	124.93	53.80	34.68	174.46
Ser60	8.21	117.51	57.78	63.34	174.89
Thr61	7.61	114.50	61.97	68.45	174.77
Ala62	8.39	125.95	52.42	21.04	176.64
Ser63	7.80	116.01	56.73	66.23	172.45
Asp64	7.99	114.88	54.44	41.24	175.89
Ala65	7.63	124.12	52.71	19.76	175.26
Ala66	9.25	120.55	51.99	19.63	174.23
Phe67	8.22	112.87	55.05	44.11	172.94
Ile68	8.67	114.98	60.64	42.24	176.35

Residue	^1H_N	$^{15}N_H$	$^{13}C^\alpha$	$^{13}C^\beta$	^{13}CO
Ala69	10.42	135.58	50.22	20.80	175.20
Gly70	9.49	110.90	43.51		173.83
Gly71	8.67	111.19	46.45		171.68
Asp72	9.58	129.57	54.29	41.52	173.74
Leu73	8.50	123.33	54.31	46.98	176.15
His74	8.16	118.41	54.74	31.57	173.71
Tyr75	8.42	125.06	52.39	34.50	
Tyr75'	8.43	124.44	52.59	34.50	
Thr76				68.39	176.31
Leu77	7.31	122.94	58.17	41.41	179.14
Leu77'	7.32	122.24	58.48	41.52	179.14
Phe78	6.50	120.65	56.83	38.34	175.30
Ser79	7.04	118.61	57.68	62.91	170.57
Asn80	7.69	118.02	51.38	39.24	173.70
Asn80'	7.58	117.91	51.22	39.04	173.70
Pro81			61.40	32.31	176.51
Ser82	8.18	124.75	58.13	63.37	174.80
His83			57.70	28.88	174.87
Thr84	7.57	113.90	62.03	68.39	
Leu85	10.42	133.40	53.99	45.50	174.31
Trp86	9.56	125.83	55.21	30.31	172.23
Gly87	8.56	106.24	43.20		172.22
Lys88	8.47	120.79	54.58	34.59	175.17
Leu89	8.78	126.61	53.78	46.10	172.93
Asp90	9.51	125.05	54.84	44.74	176.80
Ser91	8.66	111.78	56.74	66.65	173.59
Ile92	9.02	120.14	59.56	42.12	172.76
Ala93	8.95	131.10	50.71	21.44	174.79
Leu94	8.75	120.52	53.51	43.21	176.83
Gly95	8.14	109.10	46.98		171.18
Asp96	8.89	123.15	53.58	45.19	174.11
Thr97	8.29	111.05	64.49	65.30	172.56
Leu98	8.46	128.36	55.16	43.11	176.54
Thr99	9.33	120.84	60.01	71.96	173.67
Gly100	8.34	106.24	44.98		173.37
Gly101	6.74	106.28	43.52		173.82

Residue	$^{1}H_N$	$^{15}N_H$	$^{13}C^{\alpha}$	$^{13}C^{\beta}$	^{13}CO
Val137	8.16	119.08	67.59	31.58	176.94
Tyr138	10.07	122.74	62.14	39.91	179.78
Tyr138'	10.38	121.80	62.31		179.78
Gly139	8.10	105.75	48.21		176.38
Leu140	7.18	122.68	58.22	41.27	179.24
Met141	7.84	114.72	59.62	33.42	175.03
Ser142	7.14	109.44	56.11	63.63	174.32
Gly143	7.70	110.98	46.92		173.77
Asp144	8.50	119.07	52.24	42.15	175.52
Ser145	9.01	119.68	58.61	64.06	175.19
Ser146	8.76	121.26	62.13	63.23	177.21
Ala147	9.01	127.03	55.52	17.37	181.05
Leu148	8.23	120.30	58.22	40.94	177.92
Gln149	8.99	117.51	60.73	28.73	177.83
Gly150	8.16	104.10	47.14		177.11
Gln151	7.58	119.36	47.17	27.46	178.15
Ile152	8.41	118.76	64.52	36.68	177.29
Asp153	8.46	118.74	58.98	42.76	177.24
Ala154	7.22	117.27	55.10	18.12	181.26
Leu155	7.94	119.51	57.83	42.98	180.27
Leu156	8.56	120.63	57.86	41.28	178.55
Lys157	7.98	118.58	58.47	32.78	178.43
Ala158	7.28	118.39	53.51	18.25	179.51
Val159	7.50	120.01	65.36	31.71	176.69
Asp160	7.79	118.81	52.17	43.95	173.90
Pro161			64.45	32.05	176.85
Ser162	8.91	115.00	59.81	63.91	174.57
Leu163	8.14	124.26	53.75	43.44	174.87
Ser164	8.23	109.82	58.02	67.53	175.13
Ile1165	9.09	114.82	62.09	39.05	174.17
Asn166	8.41	116.64	53.43	39.07	174.81
Ser167	7.91	119.41	60.19	64.38	173.25
Thr168	8.39	111.24	59.76	71.41	176.96
Phe169	8.01	118.91	64.17	36.01	177.77

Residue	^1H_N	$^{15}N_H$	$^{13}C^\alpha$	$^{13}C^\beta$	^{13}CO
Asp170	8.49	116.68	57.40	41.01	180.21
Gln171	8.09	121.59	59.11	27.99	180.33
Leu172	8.32	120.54	57.30	41.41	179.49
Ala173	8.91	126.64	54.66	18.60	182.28
Ala174	8.07	123.99	54.76	17.64	179.04
Ala175	7.35	117.02	52.09	20.36	177.68
Gly176	7.85	105.38	45.59		174.54
Val177	7.60	113.85	62.09	33.07	173.63
Ala178	6.90	119.61	48.66	24.32	175.35
His179	8.67	116.46	54.99	31.76	172.52
Ala180	8.47	127.89	50.55	19.40	178.68
Thr181	8.55	117.72	59.05	69.08	172.40
Pro182			62.93	32.17	176.76
Ala183	8.26	126.09	52.33	19.42	174.57
Ala184	7.90	129.16	53.70	20.08	176.20

Appendix 4. Backbone Assignment of Apo Truncated HasAp

Residue	^1H_N	$^{15}N_H$	$^{13}C^\alpha$
Met1			
Ser2			
Ile3			
Ser4			
Ile5	8.65	127.18	59.92
Ser6	8.81	124.28	56.29
Tyr7	7.89	120.15	54.66
Ser8			
Thr9			
Thr10			
Tyr11			
Ser12			
Gly13			
Trp14	8.68	122.88	57.03
Thr15	8.76	109.08	60.03
Val16	7.26	120.10	66.35
Ala17	8.49	119.73	55.39
Asp18	8.38	119.56	57.38
Tyr19	8.82	122.74	63.35
Leu20	8.75	119.35	58.31
Ala21	8.16	120.11	55.02
Asp22	7.83	122.32	58.52
Trp23	8.70	119.81	63.57
Ser24	8.76	114.36	63.54
Ala25	7.88	125.69	54.82
Tyr26	8.16	120.89	57.00
Phe27	8.69	122.72	60.93
Gly28	7.35	102.41	46.28
Val30	7.60	128.01	63.83
Asn31	8.04	115.40	54.67
His32	8.28	118.57	59.67
Arg33	7.30	115.31	52.91
Pro34			

Residue	^1H_N	$^{15}N_H$	$^{13}C^\alpha$
Gly35	8.61	111.72	45.43
Gln36	7.88	118.66	55.05
Val37	8.38	117.54	60.16
Val38	8.45	124.92	61.72
Asp39	10.74	131.50	53.99
Gly40	9.69	113.58	46.40
Ser41			
Asn42			
Thr43	8.40	114.58	61.97
Gly44	7.91	109.17	44.95
Gly45	8.21	108.42	44.21
Phe46	8.72	116.14	58.46
Asn47			
Pro48			
Gly49	7.90	105.82	46.36
Pro50			
Phe51	8.70	116.41	51.00
Asp52	6.56	113.33	52.00
Gly53	8.54	106.79	47.64
Ser54	8.60	114.17	58.15
Gln55	7.97	116.78	54.16
Tyr56	9.12	121.85	57.72
Ala57	7.56	130.70	48.83
Leu58	7.11	120.04	54.76
Lys59	7.20	124.48	53.21
Ser60	8.26	119.34	58.00
Thr61	8.04	113.50	62.60
Ala62	8.55	126.68	52.32
Ser63	7.59	112.18	56.33
Asp64	9.28	116.05	54.18
Ala65	7.36	123.30	53.48
Ala66	9.06	121.55	51.30
Phe67	8.46	114.69	55.31
Ile68	8.97	115.40	61.11

Residue	^1H_N	$^{15}N_H$	$^{13}C^\alpha$
Ala69	10.09	135.37	50.24
Gly70	9.29	110.80	43.66
Gly71	8.52	111.54	46.56
Asp72	9.43	129.27	54.45
Leu73	8.35	122.94	54.29
His74	8.17	117.28	54.56
Tyr75	8.63	121.88	55.56
Thr76	8.72	117.24	63.09
Leu77	5.86	119.25	57.00
Phe78			
Ser79	7.68	120.10	65.61
Asn80	7.77	117.50	58.27
Pro81			
Ser82	8.58	123.90	59.30
His83	8.97	119.60	57.94
Thr84	8.01	113.89	62.99
Leu85	11.32	136.10	54.00
Trp86	9.33	122.74	55.45
Gly87	8.28	105.84	43.59
Lys88	8.40	121.06	54.91
Leu89	8.76	126.56	53.65
Asp90	9.30	124.90	55.11
Ser91	8.47	111.28	56.77
Ile92	9.03	120.22	58.95
Ala93	8.98	130.88	50.61
Leu94	8.88	121.33	53.83
Gly95	8.58	108.36	47.65
Asp96	8.89	127.33	54.38
Thr97	8.99	114.94	68.53
Leu98	7.82	126.84	54.22
Thr99	9.04	116.04	59.88
Gly100	8.21	107.22	45.22
Gly101	6.64	106.55	43.62

Residue	^1H_N	$^{15}N_H$	$^{13}C^\alpha$
Ala102			
Ser103			
Ser104	7.34	114.79	57.66
Gly105	7.89	109.04	45.37
Gly106	7.59	107.43	43.93
Tyr107	9.37	121.16	59.20
Ala108	8.63	123.75	51.29
Leu109	8.20	120.01	52.87
Asp110	9.18	125.02	57.03
Ser111	7.73	110.24	55.82
Gln112	8.95	127.87	56.44
Glu113	8.63	129.79	58.69
Val114	7.24	115.61	60.32
Ser115	8.65	117.68	56.26
Phe116	9.27	123.25	56.05
Ser117	9.44	118.16	57.62
Asn118	8.22	118.08	53.78
Leu119	8.80	115.18	57.19
Gly120	8.64	102.73	47.41
Leu121	7.27	118.36	54.46
Asp122	8.47	124.40	54.05
Ser123	9.17	122.68	55.82
Pro124			
Ile125	7.63	125.10	64.41
Ala126	7.28	119.46	54.11
Gln127	6.97	113.46	56.72
Gly128	8.15	107.05	46.65
Arg129	8.77	123.58	57.15
Asp130	7.56	115.13	54.60
Gly131	7.74	107.86	45.68
Thr132	8.56	120.48	66.88
Val133	8.80	122.07	69.02
His134	8.40	120.82	62.21
Lys135	8.32	115.92	60.85
Val136	8.61	116.83	66.49

Residue	^1H_N	$^{15}N_H$	$^{13}C^\alpha$
Val137	8.49	119.08	67.14
Tyr138	9.57	121.19	61.42
Gly139	7.42	104.90	48.21
Leu140	7.18	123.04	58.25
Met141	7.81	115.92	59.24
Ser142	7.41	110.61	57.43
Gly143	7.67	112.50	46.28
Asp144	8.05	120.93	52.76
Ser145	8.59	118.63	57.72
Ser146	8.69	121.41	63.08
Ala147	8.64	127.01	55.32
Leu148	8.06	119.86	58.28
Gln149	8.93	118.14	60.64
Gly150	7.81	103.63	47.42
Gln151	7.50	119.51	57.43
Ile152	8.41	118.45	63.88
Asp153	8.19	118.43	58.98
Ala154	7.15	117.17	55.23
Leu155	8.01	119.43	57.88
Leu156	8.51	120.60	58.02
Lys157	7.88	118.34	58.37
Ala158	7.25	118.26	53.63
Val159	7.48	120.03	65.45
Asp160	7.72	118.73	52.34
Pro161			
Ser162	8.89	114.95	59.84
Leu163	8.15	124.41	53.89
Ser164	8.21	109.67	58.21
Ile1165	8.92	113.33	62.31
Asn166	8.42	116.53	53.57
Ser167	7.89	119.38	60.17
Thr168	8.37	111.26	59.92
Phe169			

Residue	^1H_N	$^{15}N_H$	$^{13}C^\alpha$
Asp170			
Gln171	8.06	121.72	59.12
Leu172	8.33	120.69	57.43
Ala173	8.95	126.47	54.86
Ala174	8.04	123.98	54.84
Ala175	7.37	117.20	52.27
Gly176	7.83	105.34	45.98
Val177	7.61	113.90	62.08
Ala178	6.89	119.57	48.94
His179	8.60	116.22	55.16
Ala180	8.40	127.56	50.79
Thr181	8.50	117.80	59.11
Pro182			
Ala183	8.22	125.92	52.46
Ala184	7.84	128.98	53.79

Appendix 5. ^{1}H and ^{15}N Chemical Shifts of Residues with Double Peaks

Residue	Full-Length		Truncated	
	^{1}H	^{15}N	^{1}H	^{15}N
Asp29	7.28	116.33	7.27	116.34
Asp29'	7.21	116.21	7.21	116.20
Gln36	8.22	116.73	8.23	116.73
Gln36'	8.14	116.75	8.12	116.74
Gly45	8.17	107.36	8.16	107.33
Gly45'	8.27	107.39	8.23	107.40
Asn47	8.96	116.31	8.95	116.32
Asn47'	9.02	116.02	9.01	116.08
Phe51	8.89	117.22	8.89	117.21
Phe51'	8.84	116.89	8.82	116.89
Ala62	8.40	125.95	8.39	125.95
Ala62'	8.33	125.78	8.31	125.85
Tyr75	8.41	125.14	8.42	125.06
Tyr75'	8.42	124.60	8.43	124.44
Leu77	7.32	123.00	7.31	122.94
Leu77'	7.34	122.44	7.34	122.43
Ser79	7.03	118.60	7.00	118.57
Ser79'	6.71	118.33	6.68	118.36
Asn80	7.69	117.98	7.69	118.02
Asn80'	7.56	117.91	7.58	117.91
Ser82	8.17	124.71	8.18	124.75
Ser82'	7.99	124.38	7.97	124.41
Gly100	8.35	106.24	8.34	106.24
Gly100'	8.24	106.30	8.24	106.28
Tyr138	10.08	122.77	10.07	122.74
Tyr138'	10.40	121.81	10.38	121.80
Gly139	8.12	105.76	8.10	105.75
Gly139'	8.18	105.89	8.17	105.82

REFERENCES

1. Ochsner, U.A., Johnson, Z., and Vasil, A. I., *Genetics and Regulation of Two Distinct Haem-Uptake Systems, phu and has, in Pseudomonas aeruginosa.* Microbiology, 2000. **146**: p. 185-198.

2. Wandersman, C., and Delepelaire, P., *Bacterial Iron Sources: From Siderophores to Hemophores.* Annu. Rev. Microbiol., 2004. **58**: p. 611-647.

3. Genco, C.A., and Dixon, D. W., *Emerging Strategies in Microbial Haem Capture.* Mol. Microbiol., 2001. **39**: p. 1-11.

4. Ratliff, M., Zhu, W., Deshmukh, R., Wilks, A., and Stojiljkovic, I., *Homologues of Neisserial Heme Oxygenase in Gram-Negative Bacteria: Degradation of Heme by the Product of the pigA Gene of Pseudomonas aeruginosa.* J. Bacteriol., 2001. **183**: p. 6394-6403.

5. Létoffé, S., Nato, F., Goldberg, M. E., and Wandersman, C., *Interactions of HasA, a Bacterial Haemophore with Haemoglobin and with Its Outer Membrane Receptor HasR.* Mol. Microbiol., 1999. **33**: p. 546-555.

6. Ghigo, J.M., Létoffé, S., and Wandersman, C., *A New Type of Hemophore-Dependent Heme Acquisition System of Serratia Marcescens Reconstituted in Escherichia coli.* J. Bacteriol., 1997. **179**: p. 3572-3579.

7. Létoffé, S., Redeker, V., and Wandersman, C., *Isolation and Characterization of an Extracellular Haem-Binding Protein from Pseudomonas aeruginosa that Shares Function and Sequence Similarities with Serratia Marcescens HasA Haemophore.* Mol. Microbiol., 1998. **28**: p. 1223-1224.

8. Arevalo-Ferro, C., Hentzer, M., Reil, G., Gorg, A., Kjelleberg, S., Givskov, M., Riedel, K., and Eberl, L., *Identification of Quorum-Sensing Regulated Proteins in the Opportunistic Pathogens Pseudomonas aeruginosa by Proteomics.* Environ. Microbial., 2003. **5**: p. 1350-1369.

9. Larkin, M.A., Blackshields, G., Brown, N. P., Chenna, R., McGettigan, P. A., McWillian, H., Valentin, F., Wallace, I. M., Wilm, A., Lopez, R., Thompson, J. D., Gibson, T. J., and Higgins, D. G., *Clustal W and Clustal X Version 2.0.* Bioinformatics, 2007. **23**: p. 2947-2948.

10. Rivera, M., and Caignan, G. A., *Recent Developments in the ^{13}C NMR Spectroscopic Analysis of Paramagnetic Hemes and Heme Proteins.* Anal. Bioanal. Chem., 2004. **378**: p. 1464-1483.

11. Machonkin, T.E., Westler, W. M., and Markley, J. L., *Paramagnetic NMR Spectroscopy and Density Functional Calculations in the Analysis of the Geometric and Electronic Structures of Iron-Sulfur Proteins.* Inorg. Chem., 2005. **44**: p. 779-797.

12. Bertini, I., Turano, P., Vila, A. J., *Nuclear Magnetic Resonance of Paramagnetic Metalloproteins.* J. Chem. Rev., 1993. **93**: p. 2833-2932.

13. Cheng, H., Westler, W. M., Xia, B., Oh, B. -H., and Markley, J. L., *Protein Expression, Selective Isotope Labeling, and Analysis of Hyperfine-Shifted NMR Signals of Anabaena 7120 Vegetative [2Fe-2S] Ferredoxin.* Arch. Biochem. Biophys., 1995. **316**: p. 619-634.

14. Bertini, I., Luchinat, C., and Rosato, A., *The Solution Structure of Paramagnetic Metalloproteins.* Adv. Inorg. Chem., 1999. **47**: p. 251-282.

15. Lian, L.-Y., and Middleton, D. A., *Labeling Approaches for Protein Structural Studies by Solution-State and Solid-State NMR.* Prog. NMR Spectrosc., 2001. **39**: p. 171-190.

16. Ikemura, T., *Codon Usage and tRNA Content in Unicellular and Multicellular Organisms.* Mol. Biol. Evol., 1985. **2**: p. 13-34.

17. Caignan, G.A., Deshmukh, R., Wilks, A., Zeng, Y., Huang, H., Moenne-Loccoz, P., Bunce, R. A., Eastman, M. A., and Rivera, M., *Oxidation of heme to β- and δ-biliverdin by Pseudomonas aeruginosa Heme Oxygenase as a Consequence of an Unusual Seating of the Heme.* J. Am. Chem. Soc., 2002. **124**: p. 14879-14892.

18. Rodriguez, J.C., Wilks, A., and Rivera, M., *Backbone NMR Assignments and H/D Exchange Studies on the Ferric Azide- and Cyanide-Inhibited Forms of Pseudomonas aeruginosa Heme Oxygenase.* Biochemistry, 2006. **45**: p. 4578-4592.

19. Cheng, H., and Markley, J. L., *NMR Spectroscopic Studies of Paramagnetic Proteins: Iron Sulfur Proteins.* Annu. Rev. Biophys. Biomol. Struct., 1995. **24**: p. 209-237.

20. Eakanunkul, S., Lukat-Rodgers, G. S., Sumithran, S., Ghosh, A, Rodgers, K. R., Dawson, J. H., and Wilks, A., *Characterization of the Periplasmic Heme-Binding Protein ShuT from the Heme Uptake System of Shigella dysenteriae.* Biochemistry, 2005. **44**: p. 13179-13191.

21.   Rivera, M., and Walker, F. A., *Biosynthesis of Isotopically Enriched Protohemin IX.* Anal. Biochem., 1995. **230**: p. 295-302.

22.   Rivera, M., Qiu, F., Bunce, R. A., Stark, R. E., *Complete Isomer-Specific ^1H and ^{13}C NMR Assignments of the Heme Resonances Arising from Both Isomeric Forms of Rat Liver Outer Mitochondrial Membrane Cytochrome b_5.* J. Biol. Inorg. Chem., 1999. **4**: p. 87-98.

23.   Bunce, R.A., Shilling, C. L., and Rivera, M., *Synthesis of [1,2-^{13}C]- and [2,3-^{13}C]-Labeled δ-Aminolevulinic Acid.* J. Labelled Compd. Radiopharm., 1997. **39**: p. 669-675.

24.   Luft, J.R., Collins, R. J., Fehrman, N. A., Lauricella, A. M., Veatch, C. K., and DeTitta, G. T., *A Deliberate Approach to Screening for Initial Crystallization Conditions of Biological Macromolecules.* J. Struct. Biol., 2003. **142**: p. 170-179.

25.   Delaglio, F., Grzesiek, S., Vuister, G. W., Zhu, W., Pfeifer, J. and Bax, A., *NMRPipe: A Multidimensional Spectral Processing System Based on UNIX Pipes.* J. Biol. NMR, 1995. **6**: p. 277-293.

26.   Goddard, T.D., and Kneller, D. G., *Sparky 3*: University of California, San Francisco, CA.

27.   Kay, L.E., Keifer, P., and Saarinen, T., *Pure Absorption Gradient Enhanced Heteronuclear Single Quantum Correlation Spectroscopy with Improved Sensitivity.* J. Am. Chem. Soc., 1992. **114**: p. 10663-10665.

28.   Simeonov, M., Altuve, A., Massiah, M. A., Wang, A., Eastman, M. A., Benson, D. R., and Rivera, M., *Mitochondrial and Microsomal Ferric b_5 Cytochromes Exhibit Divergent Conformational Plasticity in the Context of a Common Fold.* Biochemistry, 2005. **44**: p. 9308-9319.

29.   Glasoe, P.K., and Long, F. A., *Use of Glass Electrodes to Measure Acidities in Deuterium Oxide.* J. Phys. Chem., 1960. **64**: p. 188-190.

30.   Drenth, J., *Principles of Protein X-Ray Crystallography.* 3rd ed. 2007: Springer.

31.   Weber, P.C., *Physical Principles of Protein Crystallization.* Adv. Prot. Chem., 1991: p. 1-36.

32.   Ducruix, A., and Giege, R., *Crystallization of Nucleic Acids and Proteins. A Practical Approach.* 1992: Oxford University Press, New York.

33. Messerschmidt, A., *X-Ray Crystallography of Biomacromolecules*. 2007: Wiley-VCH.

34. Asherie, N., *Protein Crystallization and Phase Diagrams.* Methods, 2004. **34**: p. 266-272.

35. Saridakis, E., and Chayen, N. E., *Systematic Improvement of Protein Crystals by Determining the Supersolubility Curves of Phase Diagrams.* Biophys. J., 2003. **84**: p. 1218-1222.

36. McPherson, A., *Crystallisation of Biological Macromolecules*. 1999: Cold Spring Harbor Press, New York.

37. Heinig, M., Frishman, D., *STRIDE: A Web Server for Secondary Structure Assignment from Known Atomic Coordinates of Proteins.* Nucl. Acids Res., 2004. **32**: p. W500-2.

38. Rohl, C.A., and Doig, A. J., *Models for the 3_{10}-Helix/Coil, p-Helix/Coil, and a-Helix/3_{10}-Helix/Coil Transitions in Isolated Peptides.* Protein Sci., 1996. **5**: p. 1687-1696.

39. Barlow, D.J., and Thornton, J. M., *Helix Geometry in Proteins.* J. Mol. Biol., 1988. **201**: p. 601-619.

40. Crisma, M., Saviano, M., Moretto, A., Broxterman, Q. B., Kaptein, B., and Toniolo, C., *Peptide $\alpha/3_{10}$-Helix Dimorphism in the Crystal State.* J. Am. Chem. Soc., 2007. **129**: p. 15471-15473.

41. Freitas, M.S., Gaspar, L. P, Lorenzoni, M., Almeida, F. C., Tinoco, L. W., Almeida, M. S., Maia, L. F., Degreve, L., Valente, A. P., and Silva, J. L., *Structure of the Ebola Fusion Peptide in a Membrane-Mimetic Environment and the Interaction with Lipid Rafts.* J. Biol. Chem., 2007. **282**: p. 27306-27314.

42. Shea, J.E., Brooks, C. L., *From Folding Theories to Folding Proteins: A Review and Assessment of Simulation Studies of Protein Folding and Unfolding.* Annu. Rev. Phys. Chem., 1995. **52**: p. 499-535.

43. Milhauser, G.L., *Views of Helical Peptides: A Proposal for the Position of 3_{10}-Helix along the Thermodynamic Folding Pathway.* Biochemistry, 1995. **34**: p. 3873-3877.

44. Arnoux, P., Haser, R., Izadi, N., Lecroisey, A., Delepierre, M., Wandersman, C., and Czjek, M., *The Crystal Structure of HasA, a Hemophore Secreted by Serratia marcescens.* Nature Struct. Biol., 1999. **6**: p. 516-520.

45. Rosi, M.S., Fetherston, J. D., Letoffe, S., Perry, R. D., and Ghigo, J. M., *Identification and Characterization of the Hemophore-Dependent Heme Acquisition System of Yersinia Pestis.* Infect. Immun., 2001. **69**: p. 6707-6717.

46. Rivera, M., Barillas,-Mury, C., Christensen, K. A., Little, J. W., Wells, M. A., and Walker, F. A., *Gene Synthesis, Bacterial Expression, and ^{1}H NMR Spectroscopic Studies of the Rat Outer Mitochondrial Membrane Cytochrome b_5.* Biochemistry, 1992. **31**: p. 12233-12240.

47. Lee, K.B., Jun, E., La Mar, G. N., Rezzano, I. N., Ravindra, K. P., Smith, K. M., Walker, F. A., and Buttlaire, D. H., *Influence of Heme Vinyl- and Carboxylate-Protein Contacts on Structure and Redox Properties of Bovine Cytochrome b_5.* J. Am. Chem. Soc., 1991. **113**: p. 3576.

48. Arnoux, P., Haser, R., Izadi-Pruneyre, N., Lecroisey, A., and Czjek, M., *Functional Aspects of the Heme Bound Hemophore HasA by Structural Analysis of Various Crystal Forms.* Proteins: Struct. Funct., Genet., 2000. **41**: p. 202-210.

49. Caillet-Saguy, C., Delepierre, M., Lecroisey, A., Bertini, I., Piccioli, M., and Turano, P., *Direct-Detected ^{13}C NMR to Investigate the Iron (III) Hemophore HasA.* J. Am. Chem. Soc., 2006. **128**: p. 150-158.

50. Yoshizaki, I., Sato, T., Igarashi, N., Natsuisaka, M., Tanaka, N., Komatsu, H., and Yoda, S., *Systematic Analysis of Supersaturation and Lysozyme Crystal Quality.* Acta Cryst., 2001. **D57**: p. 1621-1629.

51. Létoffé, S., Debarbieux, L., Izadi, N., Delepelaire, P., and Wandersman, C., *Ligand Delivery by Haem Carrier Proteins: The Binding of Serratia marcescens Haemophore to Its Outer Membrane Receptor is Mediated by Two Distinct Peptide Regions.* Mol. Microbiol., 2003. **50**: p. 77-88.

52. Perutz, M.F., *Structure and Function of Haemoglobin I. A Tentative Atomic Model of Horse Oxyhaemoglobin.* J. Mol. Biol., 1965. **13**: p. 646-668.

53. IIzuka, T., and Yonetani, T., *Spin Changes in Hemoproteins.* Advan. in Biophys., 1970. **1**: p. 157-182.

54.   Walker, F.A., Simonis, U., *Proton NMR Spectroscopy of Model Hemes.* Magnetic Resonance, ed. L.J.a.R. Berliner, J. Vol. 12. 1993: Plenum, New York. 133-274.

55.   La Mar, G.N., ed. *Biological Application of Magnetic Resonance.* ed. R.G. Shulman. 1979, Academic Press, New York. 305-344.

56.   La Mar, G.N., Krishnamoorthi, R., Smith, K. M., Gersonde, K., and Sick, H., *Proton Nuclear Magnetic Resonance Investigation of the Conformation-Dependent Spin Equilibrium in Azide Ligated Monomeric Insect Hemoglobins.* Biochemistry, 1983. **22**: p. 6239-6246.

57.   Cutnell, J.D., La Mar, G. N. and Kong, S. B., *Proton Nuclear Magnetic Resonance Study of the Relaxation Behavior of Kinetic Lability of Exchangeable Protons in the Heme Pocket of Cyanometmyoglobin.* J. Am. Chem. Soc., 1981. **103**: p. 3567-3572.

58.   Kong, S.B., Cutnell, J. D., and La Mar, G. N., *Proton Nuclear Magnetic Resonance Study of the Dynamic Stability of the Heme Pocket of Soybean Leghemoglobin a. Exchange Rates for the Labile Proton of the Proximal Histidyl Imidazole.* J. Biol. Chem., 1983. **258**: p. 357-370.

59.   Alontaga, A.Y., Bunce, R. A., Wilks, A., and Rivera, M., ^{13}C *NMR Spectroscopy of Core Heme Carbons as a Simple Tool to Elucidate the Coordination State of Ferric High-Spin Heme Proteins.* Inorg. Chem., 2006. **45**: p. 8876-8881.

60.   Walker, F.A., *The Porphyrin Handbook*, K.M. Kadish, Smith, K. M., Guilard, R., Editor. 2000, Academic Press: New York. p. 81-183.

61.   Kurland, R.J., Little, R. G., Davis, D. G., and Ho, C., *Proton Magnetic Resonance Study of High- and Low-Spin Hemin Derivatives.* Biochemistry, 1971. **10**: p. 2237-2246.

62.   Rajarathnam, K., La Mar, G. N., Chiu, M. L., Sligar, S. G., Singh, J. P., and Smith, K. M., ^1H *NMR Hyperfine Shift Pattern as Probe for Ligation State in High-Spin Ferric Hemoproteins: Water Binding in Metmyoglobin Mutants.* J. Am. Chem. Soc., 1991. **113**: p. 7886-7892.

63.   Zeng, Y., Caignan, G. A., Bunce, R. A., Rodriguez, J. C., Wilks, A., and Rivera, M., *Azide-Inhibited Bacterial Heme Oxygenase Exhibit an S=3/2 $(d_{xz},d_{yz})^3$ $(d_z^2)^1$ Spin State: Mechanistic Implications for Heme Oxidation.* J. Am. Chem. Soc., 2005. **127**: p. 9794-9807.

64. Ikeue, T., Ohgo, Y., Saitoh, T., Yamaguchi, T., and Nakamura, M., *Saddle-Shaped Six-Coordinate Iron(III) Porphyrin Complexes Showing a Novel Spin Crossover between S=1/2 and S=3/2 Spin States.* Angrew. Chem. Int. Ed., 2001. **40**: p. 2617-2620.

65. Ikeue, T., Ohgo, Y., Yamaguchi, T., Takahashi, M., Takeda, M., and Nakamura, M., *Factors Affecting the Electronic Ground State of Low-Spin Iron(III) Porphyrin Complexes.* Angew. Chem. Int. Ed., 2001. **40**: p. 2617-2620.

66. Ikeue, T., Saitoh, T., Yamaguchi, T., Ohgo, Y., Nakamura, M., Takahashi, M., and Takeda, M., *Formation of Pure Intermediate Spin Complexes in Highly Nonplanar Iron (III) Porphyrins.* Chem. Commun., 2000: p. 1989-1990.

67. Sakai, T., Ohgo, Y., Ikeue, T., Takahashi, M., Takeda, M., and Nakamura, M., *Formation of the Intermediate-Spin Iron (III) Porphyrin Complexes with $(d_{xz},d_{yz})^3 (d_{xy})^1 (d_{z^2})^1$ Electronic Configuration.* J. Am. Chem. Soc., 2003. **125**: p. 13028-13029.

68. Nakamura, M., Hoshino, A., Ikezaki, A., and Ikeue, T., *Chemical Shift of Meso-Carbon: A Powerful Probe to Determining the Coordination Structure and Electronic Configuration of Ferric Porphyrin Complexes.* Chem. Commun., 2003: p. 1862-1863.

69. Sankar, S.S., La Mar, G. N., Smith, K. M., and Fujinari, E. M., *^{13}C-NMR Study of Labeled Vinyl Groups in Paramagnetic Myoglobin Derivatives.* Biochim. Biophys. Acta, 1987. **912**: p. 220-229.

70. Caignan, G.A., Deshmukh, R., Zeng, Y., Wilks, A., Bunce, R. A., and Rivera, M., *The Hydroxide Complex of Pseudomonas aeruginosa Heme Oxygenase as a Model of the Low-Spin (III) Hydroperoxide Intermediate in Heme Catabolism: ^{13}C NMR Spectroscopic Studies Suggest the Active Participation of the Heme in Macrocycle Hydroxylation.* J. Am. Chem. Soc., 2003. **125**: p. 11842-11852.

71. Mao, J., Zhang, Y., and Oldfield, E., *Nuclear Magnetic Resonance Hyperfine Shifts in Paramagnetic Metalloporphyrins and Metalloproteins.* J. Am. Chem. Soc., 2002. **124**: p. 13911-13920.

72. Cheng, R.-J., Chen, P. -Y., Lovell, T., Liu, T., Noodleman, L., Case, D. A., *Symmetry and Bonding in Metalloporphyrins. A Modern Implementation for the Bonding Analyses of Five- and Six-Coordinate High-Spin Iron (III)-Porphyrin Complexes Through Density Functional Calculation and NMR Spectroscopy.* J. Am. Chem. Soc., 2003. **125**: p. 6774-6783.

73.   Walker, F.A., *Pulsed EPR and NMR Spectroscopy of Paramagnetic Iron Porphyrinates and Related Iron Macrocycles: How to Understand Patterns of Spin Delocalization and Recognize Radicals.* Inorg. Chem., 2003. **42**: p. 4526-4544.

74.   Machonkin, T.E., Westler, W. M., and Markley, J. L., *Strategy for the Study of Paramagnetic Proteins with Slow Electronic Relaxation Rates by NMR Spectroscopy: Application to Oxidized Human [2Fe-2S] Ferredoxin.* J. Am. Chem. Soc., 2004. **126**: p. 5413-5426.

75.   Cavanagh, J., Fairbrother, W. J., Palmer III, A. R., and Skelton, N. J., *Protein NMR Spectroscopy Principles and Practice.* 1996: Academic Press.

76.   Grzesiek, S., and Bax, A., *Correlating Backbone Amide and Side Chain Resonances in Larger Proteins by Multiple Relayed Triple Resonance NMR.* J. Am. Chem. Soc., 1992. **114**: p. 6291-6293.

77.   Farmer, B.T., Venters, R. A., Spicer, L. D., Wittekind, M. G., and Muller, L., *A Refocused and Optimize HNCA: Increased Sensitivity and Resolution in Large Macromolecules.* J. Biol. NMR, 1992. **2**: p. 195-202.

78.   Kay, L.E., Ikura, M., Tschudin, R., and Bax, A., *Three-Dimensional Triple-Resonance NMR Spectroscopy of Isotopically Enriched Proteins.* J. Magn. Reson., 1990. **89**: p. 496-514.

79.   Grzesiek, S., and Bax, A., *Improved 3D Triple-Resonance NMR Techniques Applied to a 31 kDa Protein.* J. Magn. Reson., 1992. **96**: p. 432-440.

80.   Bax, A.a.I., M., *An Efficient 3D NMR Technique for Correlating the Proton and ^{15}N Backbone Amide Resonances with the a-Carbon of the Preceding Residue in Uniformly $^{15}N/^{13}C$ Enriched Proteins.* J. Biol. NMR, 1991. **1**: p. 99-104.

81.   Uhrinova, S., Uhrin, D., Nairn, J., Price, N. C., Fothergill-Gillmore, L. A., and Barlow, P. N., *Backbone Assignment of Double Labelled 23.7 kDa Phosphoglycerate Mutase from Schizosaccharomyces pombe.* J. Biomol. NMR, 1997. **10**: p. 309-310.

82.   Muhandiram, D.R., and Kay, L. E., *Gradient Enhanced Triple Resonance Three-Dimensional NMR Experiments with Improved Sensitivity.* J. Magn. Reson., 1994. **B103**: p. 203-216.

83.   Wishart, D.S., and Sykes, B. D., *The C-13 Chemical Shift Index - A Simple Method for the Identification of Protein Secondary Structure Using C-13 Chemical Shift Data.* J. Biol. NMR, 1994. **4**: p. 171-180.

84.   Wishart, D.S., and Sykes, B. D., *Chemical Shift as a Tool for Structure Determination.* Meth. Enzymol., 1994. **239**: p. 363-392.

85.   Williamson, M.P., *Secondary-Structure Dependent Chemical Shifts in Proteins.* Biopolymers, 1990. **29**: p. 1428-1431.

86.   Gross, K.-H., and Kalbitzer, H. R., *Distribution of Chemical Shifts in ^{1}H Nuclear Magnetic Resonance Spectra of Proteins.* J. Magn. Reson., 1988. **76**: p. 87-99.

87.   Mielke, S.P., and Krishnan, V. V., *An Evaluation of Chemical Shift Index-Based Secondary Structure Determination in Proteins: Influence of Random Coil Chemical Shifts.* J. Biomol. NMR, 2004. **30**: p. 143-153.

88.   Wishart, D.S., Sykes, B. D., and Richards, F. M., *Relationship between Nuclear Magnetic Resonance Chemical Shift and Protein Secondary Structure.* J. Mol. Biol., 1991. **222**: p. 311-333.

89.   Wishart, D.S., Sykes, B. D. and Richards, F. M., *Simple Techniques for the Quantification of Protein Secondary Structure by H-1 NMR Spectroscopy.* FEBS Lett., 1991. **293**: p. 72-80.

90.   Saito, H., *Conformation-Dependent ^{13}C Chemical Shifts: A New Means of Conformational Characterization as Obtained by High-Resolution Solid State NMR.* Magn. Reson. Chem., 1986. **24**: p. 835-845.

91.   Spera, S., and Bax, A., *Emperical Correlation between Protein Backbone Conformation and C-Alpha and C-Beta C-13 Nuclear Magnetic Resonance Chemical Shifts.* J. Am. Chem. Soc., 1991. **113**: p. 5490-5492.

92.   Wishart, D.S., Sykes, B. D., and Richards, F. M., *The Chemical Shift Index: A Fast and Simple Method for the Assignment of Protein Secondary Structure through NMR Spectroscopy.* Biochemistry, 1992. **31**: p. 1647-1651.

93.   Claridge, T.D.W., *High-Resolution NMR Techniques in Organic Chemistry.* 1999: Pergamon.

94.   Wuthrich, K., *NMR of Proteins and Nucleic Acids.* 1986: Wiley-Interscience.

95.   Zuiderweg, E.R.P., *Mapping Protein-Protein Interactions in Solution by NMR Spectroscopy.* Biochemistry, 2002. **41**: p. 1-7.

96.   Wolff, N., Izadi-Pruneyre, N., Couprie, J., Habeck, M., Linge, J., Riepeng, W., Wandersman, C., Nilges, M., Delepierre, M., and Lecroisey, A., *Comparative Analysis of Structural and Dynamic Properties of the Loaded and Unloaded Hemophore HasA: Functional Implications.* J. Mol. Biol., 2008. **376**: p. 517-525.

97.   Hvidt, A., and Nielsen, S. O., *Hydrogen Exchange in Proteins.* Adv. Protein Chem., 1966. **21**: p. 288-380.

98.   Bai, Y., Milne, J. S., Mayne, L., and Englander, S. W., *Protein Stability Parameters Measured by Hydrogen Exchange.* Proteins: Struct. Funct., Genet., 1994. **20**: p. 4-14.

99.   Swint-Kruse, L., and Robertson, A. D., *Temperature and pH Dependences of Hydrogen Exchange and Global Stability for Ovomucoid Third Domain.* Biochemistry, 1996. **35**: p. 107-147.

CHAPTER 4

Chemical Shift Perturbation Mapping of the Protein-Protein Interaction of HasAp with Hemoglobin

INTRODUCTION

Iron is an essential nutrient for almost every living organism including the gram-negative bacteria [1-3]. However, free soluble iron is not available under biological conditions [4, 5]. Under iron starvation conditions, the gram-negative bacteria *Pseudomonas aeruginosa* uses different iron uptake mechanisms to scavenge iron from the host animal [6]. A major source of iron in the host is heme [7] which are bound in heme proteins such as hemoglobin, transferrin, and lactoferrin [2, 8-10] and approximately 95% of the heme are bound in hemoglobin [11]. The heme acquisition system (*has*) is one of the mechanism by which this bacteria "steal" heme from the host animal. The *has* system involves the secretion of a hemophore, HasAp, into the extracellular medium using the type I secretion pathway (TISS) [12-15]. HasAp is believed to "steal" heme from hemoglobin and then delivers the heme to the cognate receptor, HasR for subsequent deliver into the cytosol. The mechanism of heme uptake of HasAp from hemoglobin has not been understood. Létoffé *et al.* [14, 16] reported that the hemophore, from *Serratia marcescens* (HasA$_{SM}$) takes the heme from hemoglobin by passive diffusion as determined by analytical ultracentrifugation technique. However, we have presented in Chapter 3 using electronic absorbance

spectroscopy and stopped-flow analysis that there is a likelihood of protein-protein interaction between HasAp and hemoglobin. To further proved this, we attempted to determine the proposed HasAp-hemoglobin interaction at the molecular level using a combination of X-ray crystallography and NMR spectroscopy to specifically determine which regions of HasAp are involved in heme uptake from hemoglobin. This study would further give more insights on how hemophores in general scavenge heme from hemoglobin. The X-ray crystal structure of holo truncated HasAp and the amide backbone assignments of holo full-length and truncated and apo truncated HasAp are reported in Chapter 3.

One of the powerful techniques used to determine weak protein-protein interaction in solution at the molecular level is NMR [17-22]. In comparison to other biochemical techniques available, the high sensitivity of the chemical shifts [23] upon structural rearrangements and ligand binding makes the chemical shift perturbation mapping a practical method to determine protein-protein interaction ([22, 24-27]. In brief, the ^{1}H-^{15}N HSQC spectrum of the uniformly ^{15}N-labeled protein is monitored as function of added unlabeled protein and the perturbations of the chemical shifts of each residue in the protein are recorded [22, 24]. Hence, the resonances which undergo environmental or chemical changes as manifested by the perturbation of the chemical shifts of the nuclei [22, 24, 28, 29] are mapped onto the three-dimensional X-ray crystal structure of the protein to determine the putative binding interface [18]. Basically, chemical shift mapping can be used to determine the binding interface and the kinetics of binding between the two proteins. If the protein-protein interaction is

weak, the free and bound proteins are in fast chemical exchange and only one set of resonances is observed [30]. If the interaction is strong, two sets of resonances are observed which are in slow exchange, one for the free protein and one for the bound-protein [31, 32]. For the intermediate exchange regime, the resonances becomes broad [33] and may disappear in the HSQC spectrum.

EXPERIMENTAL PROCEDURES

General Methods

The recombinant pET11a plasmid harboring the genes coding for wild-type cleaved and uncleaved HasAp were transformed into *Escherichia coli* BL21-GOLD (DE3) expression host cell (Stratagene, La Jolla, CA) for subsequent expression. Gene synthesis, subcloning, site-directed mutagenesis, and bacterial transformations were carried out as described in Chapter 3.

Expression and Purification of Uniformly ^{15}N-Labeled HasAp

A single colony of freshly transformed E. coli BL21-GOLD (DE3) cells as cultured for 12 h in 10 mL of LB-medium containing 100 μg/mL of ampicillin. The cells were subsequently subcultured into fresh M9-minimal medium and grown at 37 °C with continuous shaking at 225 rpm. Once the OD$_{600}$ reached 0.80 − 0.90, the

culture was transferred to centrifuge bottles and centrifuged at 4000 rpm for 10 m. The supernatant was discarded, and the cells were resuspended in a small volume of M9-minimal ampicillin medium that did not contain ammonium chloride as nitrogen source. After the OD_{600} reached 1.0, biosynthesis of the polypeptide was induced by addition of isopropyl-β-D-thiogalactopyranoside (IPTG) to a final concentration of 1 mM and 1 g of $^{15}NH_4Cl$ for producing [U-^{15}N]-HasAp. The cells were then grown further for 5 h at 30 °C and harvested by centrifugation at 4000 rpm for 10 min. The harvested cells were resuspended and lysed by sonification. Cell lysis, protein purification and heme reconstitution of the uniformly ^{15}N-labeled HasAp were carried out using the same protocol described in Chapter 3.

Preparation of Apo Truncated HasAp

The extraction of heme was carried out using the cold-acid acetone treatment. A 1.5 mL of 2.5 mM holo ^{15}N-labeled truncated HasAp was added drop by drop with stirring into a 100 mL acid-acetone solution previously stored in -20 °C. The solution contains 0.2 % V/V of 12 M HCl. After addition, the solution turned red with the formation of white precipitate. The solution was kept stirring for 10 min after addition of the protein and then centrifuged at 2500 rpm for 1 min at 4 ºC. The procedure was repeated again if the precipitate has some reddish color. The final precipitate was dissolved in 100 mL of 100 mM Tris-HCl buffer (pH 7.8) containing 7.0 M urea. The solution was then dialyzed against 100 mM Tris-HCl with 100 mM NaCl buffer (pH 7.8) (1 x 4 L) and then against phosphate buffer (μ = 0.1, pH 7.0) (3 x 4 L) at 4

°C. After dialysis, the protein was concentrated to 3 mL and loaded into a G50 size exclusion column pre-equilibrated with phosphate buffer (μ = 0.1, pH 7.0). Protein fractions with > 90% apo protein, as determined by the absence of the Soret peak at 407 nm, were pooled and concentrated.

Preparation of Hemoglobin Samples

Lyophilized human hemoglobin (Sigma) was dissolved in phosphate buffer (μ = 0.10, pH 7.0). The insoluble part was removed by centrifugation. The soluble part was purified in Sephacryl S-200 size exclusion column. Protein fractions with purity ratio (A_{280}/A_{406}) < 0.25 were pooled and concentrated using Amicon ultracentrifuge filter to a final concentration of ~1 mL. Freshly prepared human hemoglobin was used in the titration experiments. The cyanomethemoglobin (HbCN) was prepared by adding the appropriate volume of 1 M NaCN stock solution to a solution of HasAp to achieve a 20-fold excess concentration of ligand relative to the concentration of HasAp in solution.

NMR Sample Preparation

The titration experiments were performed as follows. Uniformly ^{15}N-labeled holo full-length and truncated HasAp (2.5 mM) samples were titrated with incremental 0.083 molar equivalence of met-hemoglobin with respect to HasAp at a time to a final molar ratio of 1:1.25 of ^{15}N-labeled holo HasAp to unlabeled hemoglobin. ^{1}H-^{15}N HSQC NMR spectrum was taken before the titration and after

each titration. A stock solution of 3.5 mM of hemoglobin was used in the titration experiments. Both HasAp and hemoglobin were in the same phosphate buffer ($\mu = 0.1$, pH 7.0). The NMR samples contained 5% D_2O in sodium phosphate buffer. The titration experiment for apo HasAp and HbCN were carried out in the same way as described for the holo HasAp, however, incremental addition of 0.25 molar equivalence of HbCN was titrated each time to a final molar ratio of 1:0.75 of ^{15}N-labeled apo-HasAp to unlabeled HbCN.

NMR Spectroscopy

NMR experiments were performed at 305 K on a Bruker Avance 800 spectrometer equipped with a 5 mm TXI [1]H-^{13}C/^{15}N/D xyz-gradient probe. Fast ^{1}H-^{15}N-HSQC spectra [34] were collected over a 19.2 kHz (^{1}H) and 3.4 kHz (^{15}N) spectral widths; with 32 scans per increment; 2048 (^{1}H) and 256 (^{15}N) complex points; 100 ms acquisition time; and 1 s relaxation delay. ^{1}H-^{15}N-HSQC spectra were processed using NMRPipe [35] and analyzed with Sparky [36]. The interaction between HasAp and hemoglobin were determined using chemical shift perturbation analyses [22].

RESULTS AND DISCUSSION

The fact that heme from hemoglobin is captured very rapidly by apo-HasAp suggest specific interactions amongst the two proteins that lead to facile transfer of

the heme from one molecule to the other. This fast transfer precludes most experimental approaches aimed at mapping the surface of interaction between these proteins. To better understand how HasAp takes the heme from hemoglobin, it is highly significant to determine protein-protein interaction between HasAp and hemoglobin at the molecular level. In addition, it is also important to determine if the cleavage of the last 21-amino acid residues in the tail is biologically relevant in terms of heme capture from hemoglobin. The protein-protein interaction between the holo full-length, holo truncated HasAp, and apo truncated HasAp with hemoglobin were carried out using NMR spectroscopy. ^{1}H-^{15}N HSQC spectra were recorded using uniformly ^{15}N-labeled HasAp in combination with unlabeled hemoglobin, in this way we can only monitor the residues in HasAp that are affected. This entailed assigning the amide backbone of HasAp. The assignment of the N-H resonances of HasAp at 32 °C were carried out using a combination of 2D and 3D NMR experiments and amino acid selective labeling techniques described in Chapter 3. 98% of the residues in holo full-length and truncated HasAp were assigned, while only 89% of residues in apo HasAp were assigned. These assignments were used to determine the protein-protein interaction between HasAp and hemoglobin by mapping the chemical shift perturbation in the X-ray crystal structure of holo truncated HasAp. Hence, interaction is viewed on the HasAp perspective.

NMR Spectral Changes Observed Upon Addition of Hemoglobin to Holo HasAp

It has been shown in the proteomics study of Arevalo-Ferro *et. al.* [37] that cleaved HasAp appears to be the physiologically active form based from the 2D gel electrophoresis data. In this study, we determined the protein-protein interaction between holo full-length and truncated HasAp with hemoglobin. It has been shown in Chapter 3 that heme transfer from hemoglobin to HasAp is very fast and to circumvent the problem of fast heme transfer, holo HasAp was used in this experiment to determine the binding sites of interaction of HasAp with hemoglobin. The interaction was monitored by the chemical shift perturbation of the N-H cross-peaks in the ^{1}H-^{15}N HSQC spectra. Cross-peaks affected by the titration can be categorized in three groups: (1) Cross-peaks that do not show appreciable chemical shift perturbation ($\Delta\delta_{avg}$), (2) cross-peaks that shift as the titration progresses; the perturbations in this category are in fast exchange, *i.e.*, $\Delta\delta_{max} < k_{ex}$, and (3) cross-peaks that decrease in intensity and disappear as the titration progresses; the perturbations in this category are in the intermediate exchange regime, where $\Delta\delta_{max}$ ~k_{ex}. The results of holo full-length and truncated HasAp interaction with hemoglobin are summarized in the per-residue plot of average chemical shift perturbations depicted in Figure 1A and B, respectively, where residues in categories 1 and 2 are represented by positive bars and residues in category 3 by negative bars; absence of a bar for a particular residue indicates either a proline residue, lack of assignment, or peak overlap that prevent its analysis. From Figure 1, it can be observed that the same residues in both full-length and truncated HasAp are perturbed and also the residues

which disappeared are also the same. The results suggest that the binding sites for both are conserved. Moreover, it can also be observed that the magnitude of the chemical shift perturbations in the truncated protein is larger compared to the full-length form and this indicates that the truncated form is likely to be the physiologically relevant form of HasAp.

The per-residue chemical shift perturbations in category 2 of both full-length and truncated HasAp upon titration with hemoglobin were mapped in the structure of HasAp with green indicating $\Delta\delta_{avg} < 0.02$, white $0.02 > \Delta\delta_{avg} < 0.03$, yellow $0.03 > \Delta\delta_{avg} < 0.04$, orange $0.04 > \Delta\delta_{avg} < 0.05$, and red $\Delta\delta_{avg} > 0.05$; resonances in category 3 were mapped in marine. As shown in Figures 2 and 3, it can be observed that indeed the perturbed regions of the protein are the same for both full-length and truncated HasAp but the magnitude of perturbation in the truncated protein is larger as shown by the color coding schemes. Significant chemical shift perturbations were observed in several areas of HasAp upon binding with hemoglobin. Together, these residues comprise an extended surface that has been illustrated in white, yellow, orange, and red in Figures 2 and 3. In particular, $\alpha2$ is the most perturbed region of the protein. For both full-length and truncated HasAp, Trp23 in $\alpha2$ is the most perturbed residue and from the surface structure of the protein (Figure 4A and B), Trp23 is situated inside a cavity and not on surface of the protein. A π-π stacking with another aromatic residue of hemoglobin could have caused this interaction. Moreover, hairpin loops in close proximity to $\alpha1$ are also perturbed. These are the hairpin loops connecting $\alpha1$ and $\beta1$, $\beta6$ and $\beta7$, and $\beta3$ and $\beta4$. Some parts of $\alpha4$,
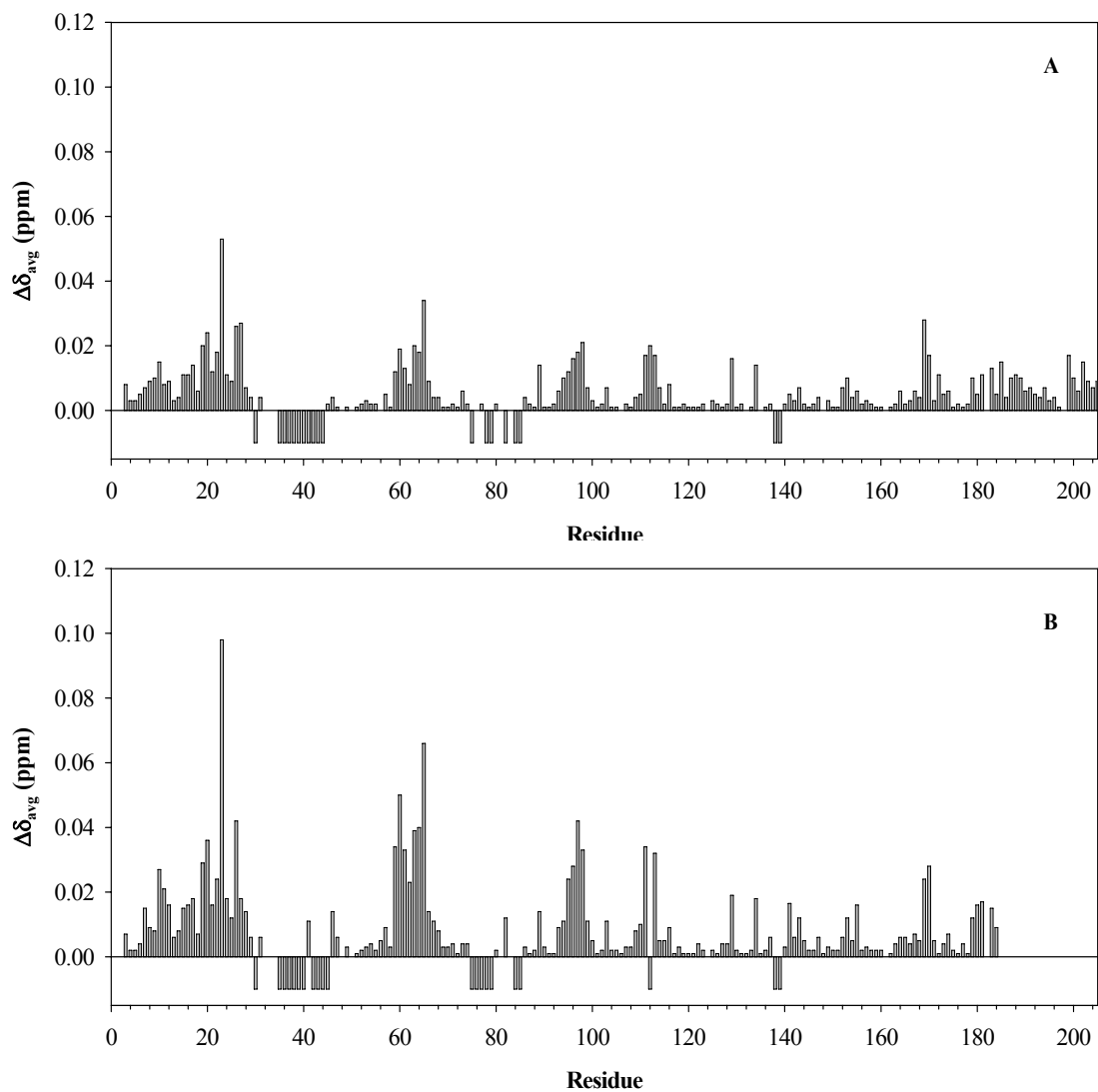
Figure 1. Per-residue chemical shift perturbation plot of holo full-length (A) and truncated HasAp (B) upon binding with hemoglobin measured using the weighted average ^{1}H and ^{15}N shifts and was calculated with the expression $\Delta\delta_{avg} = \{[(\Delta\delta 1_H)^2 + (\Delta\delta 15_N/5)^2]/2\}^{1/2}$.
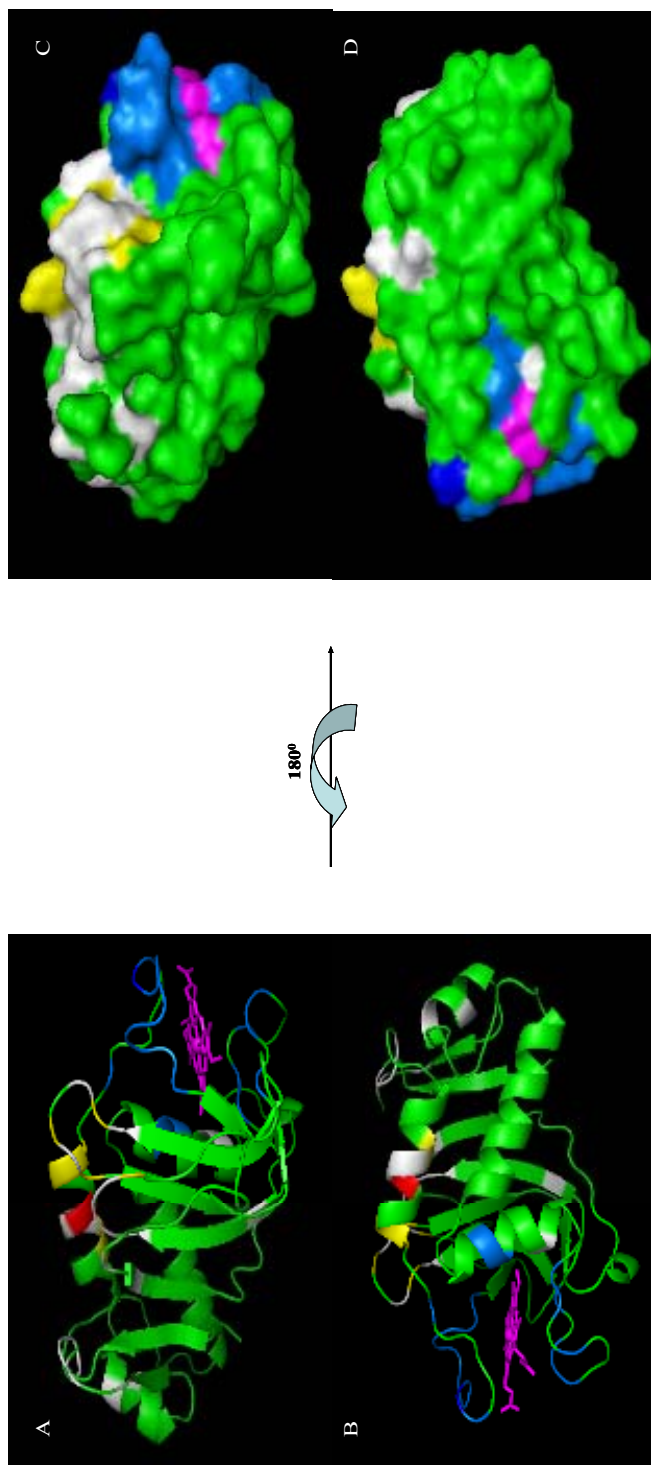
Figure 2. Chemical shift perturbation analyses calculated with the expression $\Delta\delta_{avg} = \{[\Delta\delta_{1H})^2 + (\Delta\delta_{15N}/5)^2]/2\}^{\frac{1}{2}}$ of holo full-length HasAp upon binding with hemoglobin are mapped onto the structure (A and B) and on the molecular surface (C and D) of holo HasAp. The two views are rotated 180° about the x-axis. Residues found to exhibit largest perturbations ($\Delta\delta_{avg} > 0.05$) are in red, those exhibiting perturbation in the range ($0.03 > \Delta\delta_{avg} < 0.04$) are in orange, those with perturbations ($0.04 > \Delta\delta_{avg} < 0.05$) are yellow, and those which exhibit the lowest perturbations ($\Delta\delta_{avg} < 0.04$) are in white. Residues which were not perturbed are in green. Residues which exhibit perturbations ($\Delta\delta_{avg} < 0.02$) are in white. Residues which were not perturbed are in green. Residues which disappear are in marine. The heme is in magenta.
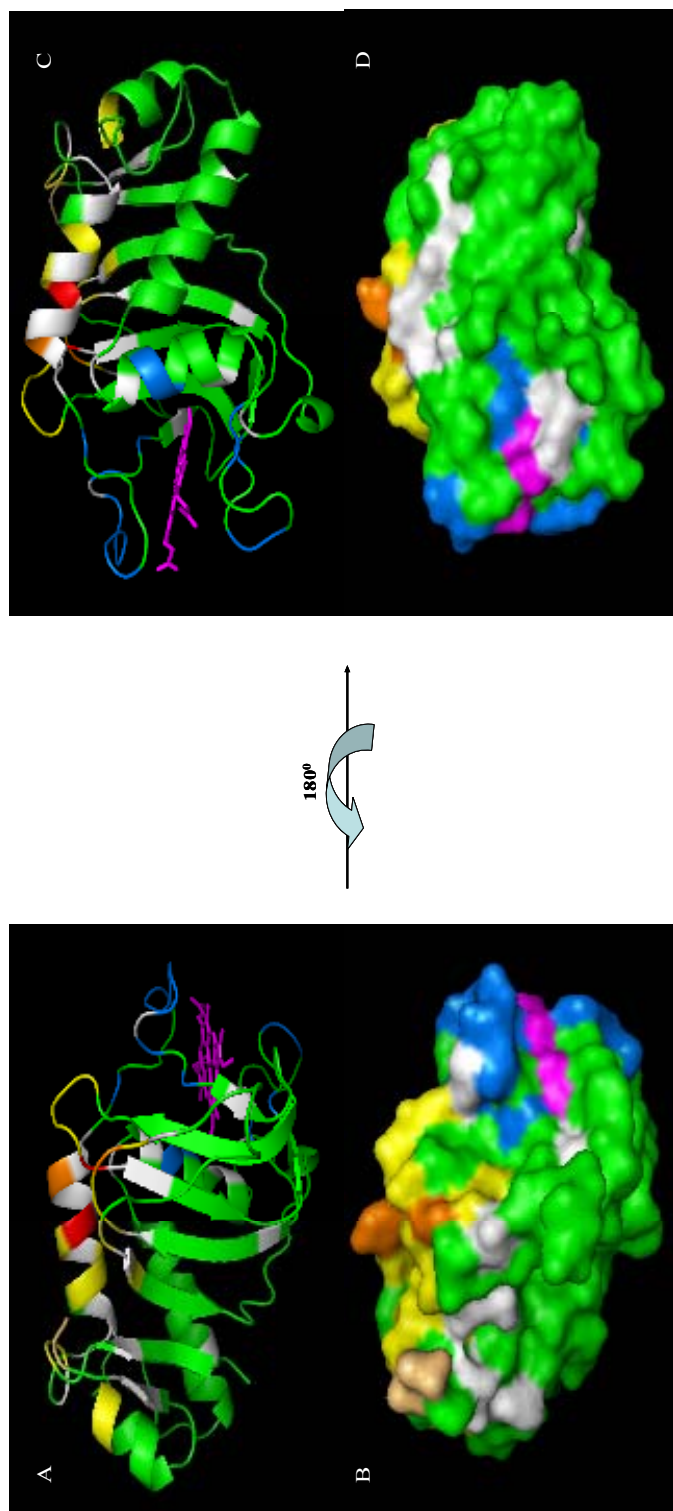
Figure 3. Chemical shift perturbation analyses calculated with the expression $\Delta\delta_{avg} = \{[\Delta\delta 1_H)^2 + (\Delta\delta 15_N/5)^2]/2\}^{\frac{1}{2}}$ of holo truncated HasAp upon binding with hemoglobin are mapped onto the structure (A and B) and on the molecular surface (C and D) of holo HasAp. The two views are rotated 180° about the x-axis. Residues found to exhibit largest perturbations ($\Delta\delta_{avg} > 0.05$) are in red, those exhibiting perturbation in the range ($0.03 > \Delta\delta_{avg} < 0.04$) are in orange, those with perturbations ($0.04 > \Delta\delta_{avg} < 0.05$) are yellow, and those which exhibit the lowest perturbations ($\Delta\delta_{avg} < 0.02$) are in white. Residues that are not perturbed are in green. Residues which disappear are in marine. The heme is in magenta.

201
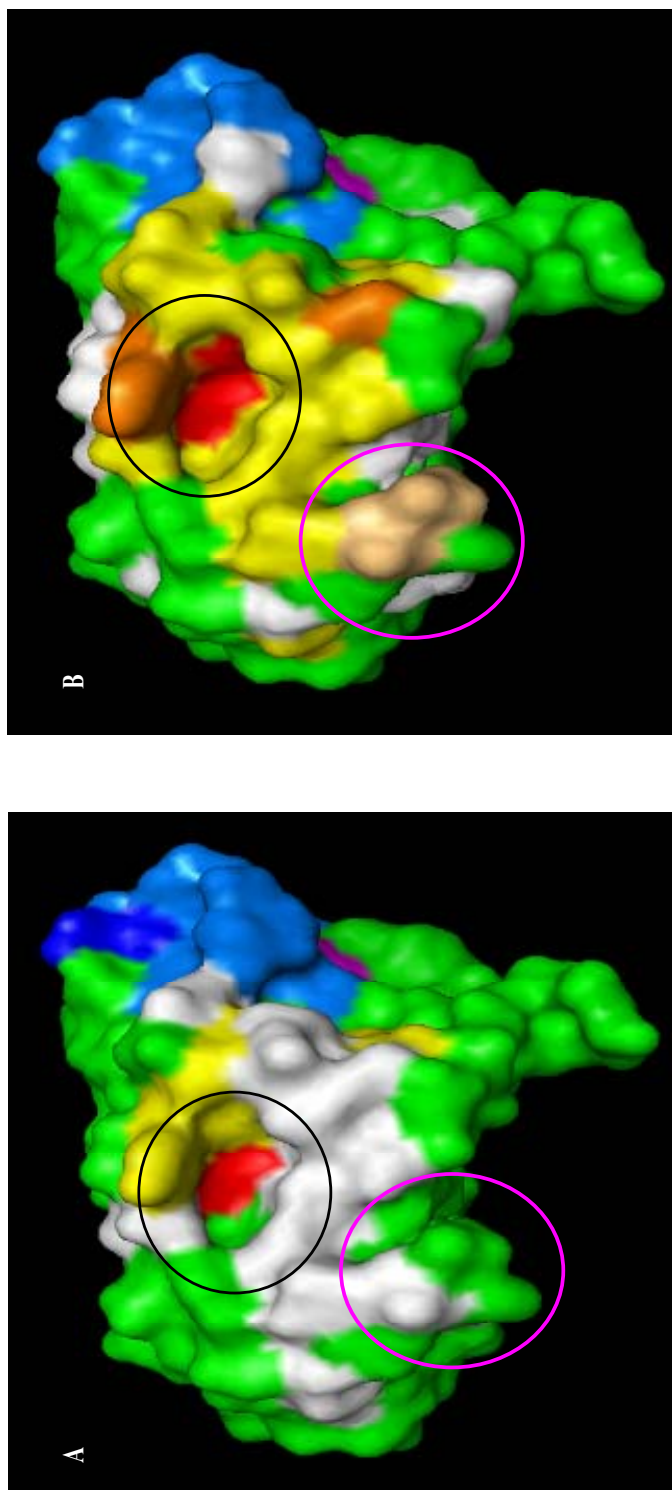
Figure 4. Mappping of chemical shift perturbation of holo full-length (A) and holo truncated (B) HasAp upon binding with hemoglobin. The most perturbed residue, Trp23 in both proteins are shown in red enclosed in black circle. The residues in the C-terminus are enclosed in the magenta circle. It is located close to the binding site.

β1, β2, β4-β8 are also perturbed. In addition, the residues in the tail are also perturbed. The marked difference in the magnitude of the chemical shift perturbation in full-length and truncated HasAp is also clearly observed in the titration curves (Figure 5). Upon incremental titration of 0.083 molar equivalence of hemoglobin with respect to HasAp, the residues in truncated HasAp showed larger perturbation compared to the residues in the full-length protein. This is clearly shown in Figure 5 with 5 residues (Y11, L20, W23 and Y26) as examples.

The surface structures in Figures 2-3 C and D shows that the bulk of the perturbed area of the protein is concentrated on the upper area of the protein. While, the bottom part are not affected shown in green. On the other hand, the back part of the protein where the α-helices are situated (Figures 2-3 C and D) shows that it is less perturbed than the other side. The results suggest that hemoglobin binds on the upper part of the protein and the interaction of hemoglobin to both full-length and truncated HasAp are the same but it binds more tightly in the truncated form than in the full-length form. As also observed in Figure 4A and B, the residues in the tail are also perturbed which could suggest that these residues interact with hemoglobin. Residues A180-A205 in the full-length HasAp were also perturbed but they cannot be mapped on the structure of truncated HasAp. A closer inspection of the structure of truncated HasAp could suggest that the tail could be speculated to be located somewhere on top of α1 and this could prevent the efficient interaction of hemoglobin with HasAp. Furthermore, the residues in the tail of the full-length protein is dynamic as reported in Chapter 3 and this mobility of the tail could also prevent the interaction with

hemoglobin. The tail may pose as a steric hindrance with hemoglobin interaction. Hence, it could be one of the reasons the tail is cleaved in the extracellular medium so it can efficiently take heme from hemoglobin.

As shown in Figures 2-3, the residues in category 3 are concentrated in the heme pocket. These residues are found in the long extended loop where the axial heme ligand His32 is situated and in the loop where the other axial ligand Tyr75 is located and also in $\alpha 2$ at the back of the heme. As has been pointed out above, resonances in category 3 do not exhibit chemical shift perturbations. Rather, the intensity of these resonances decreases as the titration progresses with most resonances disappearing before the titration is over. It is noteworthy that most of the
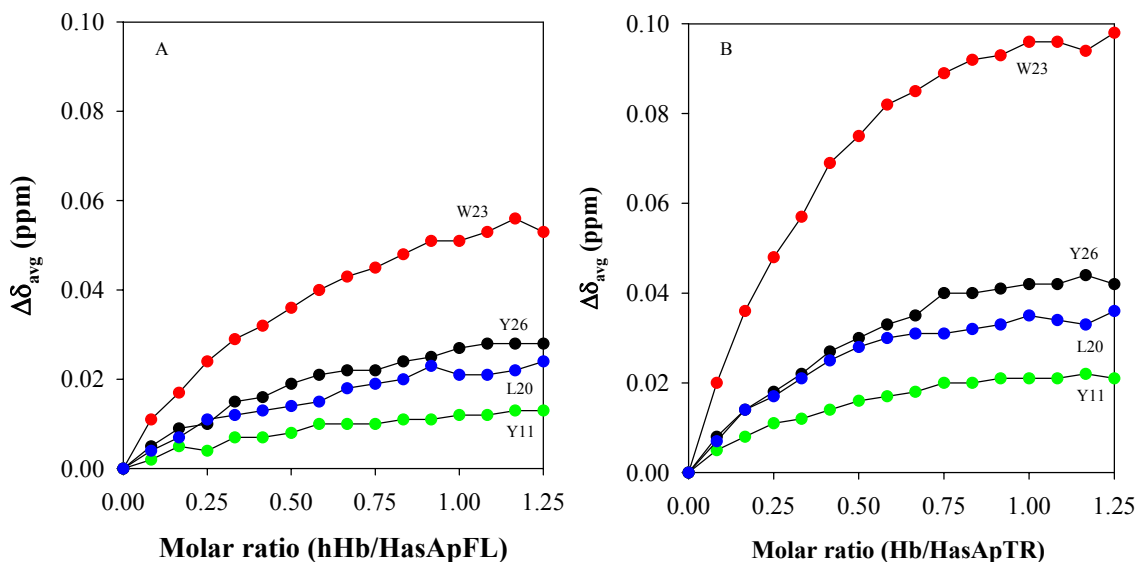

Figure 5. Titration curve of residues Y11, L20, W23, and Y26 obtained upon titration of hemoglobin into holo full-length (A) and truncated (B) HasAp.

residues highlighted in marine in Figure 2-3 exhibit multiple cross-peaks in HSQC spectra acquired with fast pulse repetition and only a weak cross-peak in HSQC spectra recorded with standard conditions. This means that resonances from these residues are affected by their proximity to the heme-iron (fast relaxation) and by conformational disorder (multiple cross-peaks). Although it is clear that disappearance of these resonances during the titration is a consequence of exchange in the intermediate timescale, the nature of the exchange can be a consequence of at least two different phenomena: (a) exchange between hemoglobin-bound and free forms of HasAp or (b) exchange between conformers that is brought to the intermediate timescale via interactions with hemoglobin. Hence, if line broadening is brought about by exchange between hemoglobin-bound and free forms, the surface colored in marine may be considered as directly interacting with hemoglobin. Alternatively, if resonance broadening is a consequence of changes in rate of conformer interconversion, the surface in marine may not interact directly with hemoglobin. If this is the case, it is interesting that binding to hemoglobin would promote changes in conformational dynamics in loop harboring His32, which is closest to the area of interaction in HasAp and in the hairpin containing the other axial ligand, Tyr75, which is on the opposite side of the heme. From titration study of holo full-length and truncated HasAp with hemoglobin, it can be concluded that there is protein-protein interaction between these two proteins. Hence, in the following experiment we tried to determine the binding sites of hemoglobin in apo truncated HasAp.

NMR Spectral Changes Observed Upon Addition of HbCN to Apo-HasAp

From the results above, it appears that the truncated form is likely to be the biologically relevant form of HasAp. Thus, we attempted to determine the protein-protein interaction between truncated apo-HasAp and hemoglobin. To prevent the transfer of heme from hemoglobin to apo-HasAp, cyanomethemoglobin was used instead of methemoglobin. The titration experiment is similar to the experiment described above for holo HasAp and hemoglobin. U-^{15}N labeled apo-HasAp and unlabeled cyanomethemoglobin were used in the experiment. 89% of the backbone amide of apo-HasAp was assigned as described in Chapter 3. The per-residue plot of the chemical shift perturbations of apo-HasAp upon binding with hemoglobin is shown in Figure 6. It can be observed that residues Val38 is the most perturbed residue in apo-HasAp. In addition, V37 and Asp64 also exhibit large chemical shift perturbations. The data in Figure 6 suggests that there are less residues which are affected by hemoglobin binding in apo-HasAp than in holo-HasAp, but the magnitude of chemical shift perturbation shown by Val38 is two-fold higher than the residue which showed the largest perturbation in holo truncated HasAp. The superimposed ^{1}H-^{15}N HSQC spectra of apo-HasAp with increasing addition of HbCN illustrating the chemical shift perturbations of Val37, Val38 and Asp64 resonances are shown in Figure 7. It can be observed that there is a marked movement of the N-H cross-peaks of the three residues mentioned as shown by the arrows. The magnitude of the chemical shift perturbations of all the residues affected in apo-HasAp upon titration with HbCN were mapped in the structure of holo-HasAp (Figure 8) using the same

color coding scheme as described above. The residues colored in red (Val37, Val38 and Asp64) are resonances which exhibit large chemical shift perturbation. Val37 and
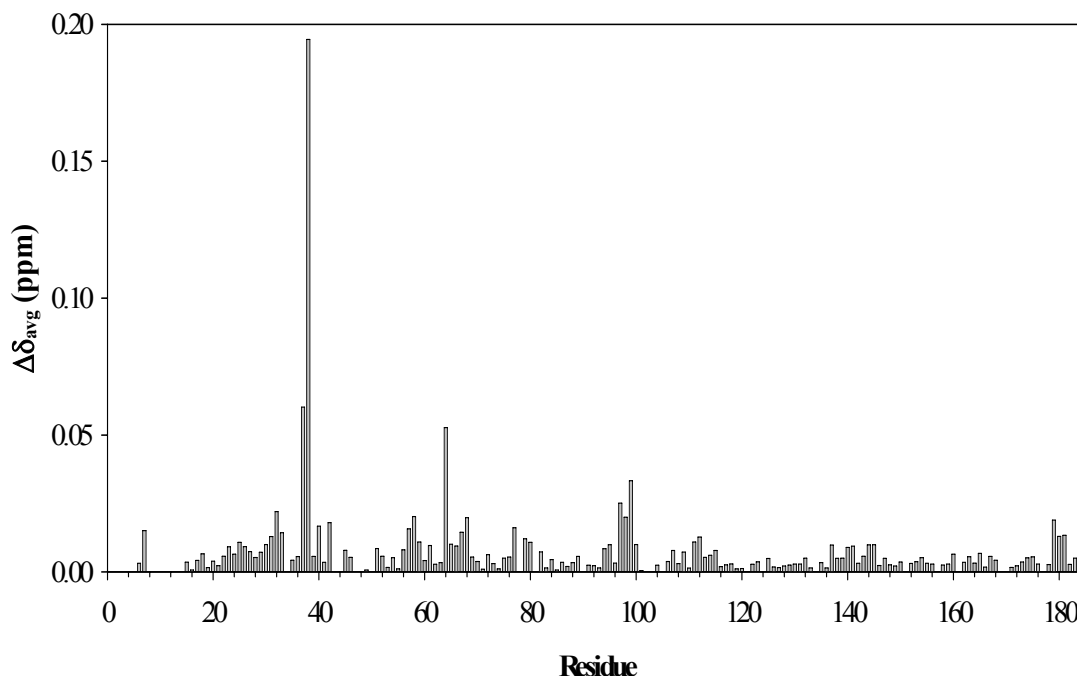
Figure 6. Per-residue chemical shift perturbation plot of apo-HasAp upon binding with HbCN measured using the weighted average ^{1}H and ^{15}N shifts and was calculated with the expression $\Delta\delta_{avg} = \{[(\Delta\delta1_H)^2 + (\Delta\delta15_N/5)^2]/2\}^{1/2}$.

Val38 are both located in the extended loop where His32 is located. While Asp64 is located in a hairpin loop connecting β3 and β4 and this is close to α1. The rest of the residues which were perturbed are located in the loop where Tyr75 is located, carboxyl end of β2, hairpin loop connecting β6 and β7, and in β8. The results of the

hemoglobin titration experiments with apo- and holo-HasAp showed that there are more residues in the holo form that were perturbed. Moreover, in holo HasAp, $\alpha 1$ is the region of the secondary structure where residues which exhibit the large perturbations are located, whereas in apo-HasAp, it is in the loop where His32 is located. It can be noted that in holo-HasAp Val37 and Val38 disappeared and their intensity in the HSQC spectra were very weak to start with. However, both results agree that the back part of the protein where the α-helices are located are not involved in the interaction. Moreover, in both apo and holo titration experiments, it can be noted that the upper part of the protein are perturbed upon hemoglobin binding. This could suggest that this is the area which interacts with hemoglobin. Interestingly, as shown in Figure 8B and D, Val37 and Val38 are situated on top of the heme (magenta). This also suggests that the heme pocket of apo-HasAp is highly involved in heme uptake from hemoglobin. Based from the results it can be speculated that the loop where His32 is located interacts with hemoglobin to take the heme with Val37 and Val38 as the two residues that are directly involved and this leads to a conformation change of the structure of the protein with the upper part of the protein going to a "closed" conformation upon heme binding.
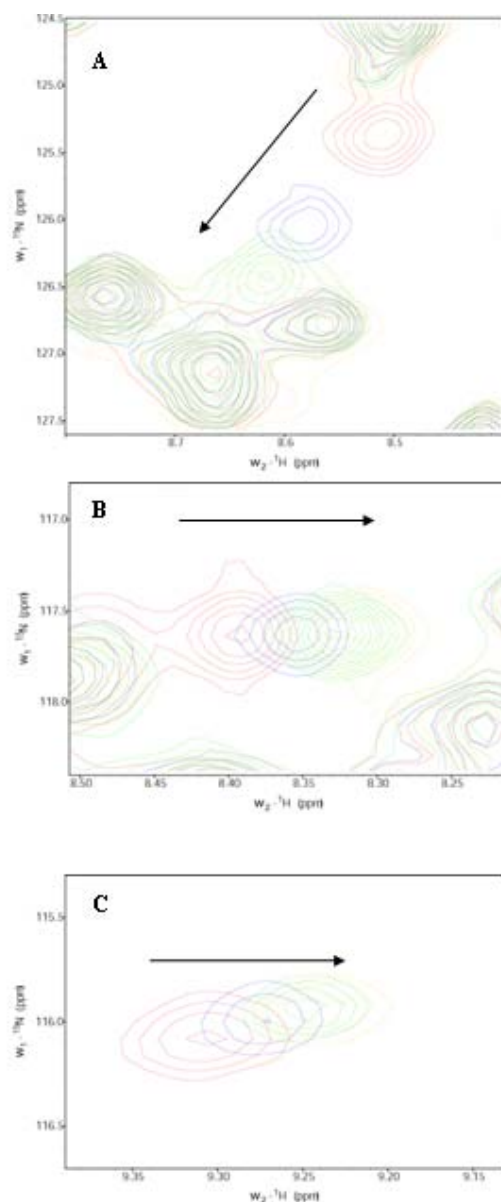
Figure 7. Superimposed ^{1}H-^{15}N HSQC spectral regions of apo-HasAp upon titration with increasing amounts of HbCN. The red, blue, green and yellow cross-peaks represent the resonances with 0, 0.25, 0.50 and 0.75 equivalent addition of HbCN. The spectral regions shown highlights (A) Val38, (B) Val37 and (C) Asp64 which showed large chemical shift perturbation as indicated by the black arrows.
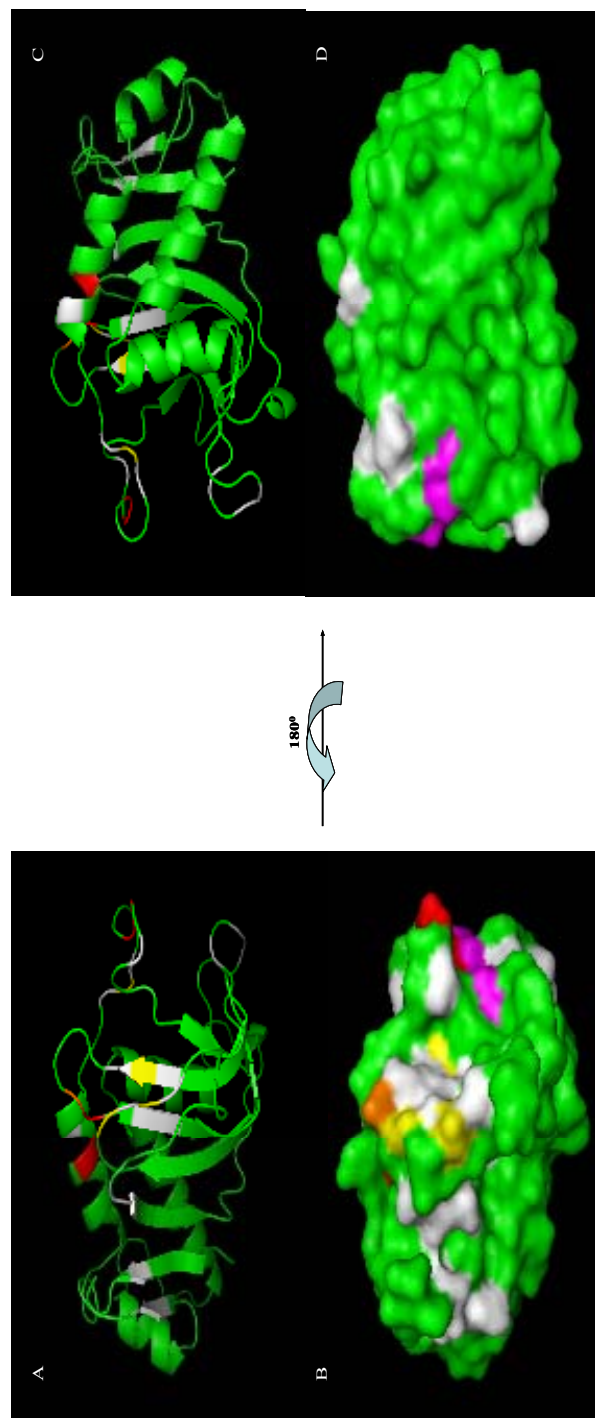
Figure 8. Chemical shift perturbation analyses calculated with the expression $\Delta\delta_{avg} = \{[\Delta\delta_{1H}]^2 + (\Delta\delta_{15N}/5)^2]/2\}^{\frac{1}{2}}$ of apo- HasAp upon binding with hemoglobin are mapped onto the structure (A and C) and on the molecular surface (C and D) of holo HasAp. The two views are rotated 180° about the x-axis. Residues found to exhibit largest perturbations ($\Delta\delta_{avg} > 0.05$) are in red, those exhibiting perturbation in the range ($0.03 > \Delta\delta_{avg} < 0.04$) are in orange, those with perturbations ($0.04 > \Delta\delta_{avg} < 0.05$) are yellow, and those which exhibit the lowest perturbations ($\Delta\delta_{avg} < 0.02$) are in white. Residues which were not perturbed are in green. Residues which disappear are in marine. The heme is in magenta.

210

REFERENCES

1. Arnoux, P., Haser, R., Izadi, N., Lecroisey, A., and Czjzek, M., *Functional Aspects of the Heme Bound Hemophore HasA by Structural Analysis of Various Crystal Forms.* Proteins: Struct. Funct. Genet., 2000. **41**: p. 202-210.

2. Ochsner, U.A., Johnson, Z., and Vasil, M. L., *Genetics and Regulation of Two Distinct Haem-Uptake Systems, phu and has, in Pseudomonas aeruginosa.* Microbiology, 2000. **146**: p. 185-198.

3. Clarke, T.E., Tari, L. W., and Vogel, H. J., *Structural Biology of Bacterial Iron Uptake Systems.* Curr. Top. Med. Chem., 2001. **1**: p. 7-30.

4. Weinberg, E.D., *Iron and Infection.* Microbiol. Rev., 1978. **42**: p. 45-60.

5. Arnoux, P., Haser, R., Izadi, N., Lecroisey, A., Delepierre, M., Wandersman, C., and Czjzek, M., *The Crystal Structure of HasA, a Hemophore Secreted by Serratia marcescens.* Nat. Struct. Biol., 1999. **6**: p. 516-520.

6. Deniau, C., Gilli, R., Izadi-Pruneyre, N., Létoffé, S., Delepierre, M., Wandersman, C., Briand, C., and Lecroisey, A., *Thermodynamics of Heme Binding to the HasA$_{SM}$ Hemophore: Effect of Mutations at Three Key Residues for Heme Uptake.* Biochemistry, 2003. **42**: p. 10627-10633.

7. Wandersman, C., and Stojiljkovic, I., *Bacterial Heme Sources: The Role of Heme, Hemoprotein Receptors and Hemophores.* Curr. Opin. Microbiol., 2000. **3**: p. 215-220.

8. Crosa, J.H., *Signal Transduction and Transcriptional and Posttranscriptional Control of Iron-Regulated Genes in Bacteria.* Microbiol. Mol. Biol. Rev., 1997. **61**: p. 319-336.

9. Payne, S.M., *Iron Acquisition in Microbial Pathogenesis.* Trends Microbiol., 1993. **1**: p. 66-69.

10. Litwin, C.M.a.C., S. B., *Role of Iron in Regulation of Virulence Genes.* Clin. Microbiol. Rev., 1993. **6**: p. 137-149.

11. Otto, B.R., Verweij-van Vught, A. M., and MacLaren, D. M., *Transferrins and Heme-Compounds as Iron Sources of Pathogenic Bacteria.* Crit. Rev. Microbiol., 1992. **18**: p. 217-233.

12.   Létoffé, S., Deniau, C., Wolff, N., Dassa, E., Delepelaire, P., Lecroisey, A., and Wandersman, C., *Haemophore-Mediated Bacterial Haem Transport: Evidence for a Common or Overlapping Site for Haem-Free and Haem-Loaded Haemophore on its Specific Outer Membrane Receptor.* Mol. Microbiol., 2001. **41**: p. 439-450.

13.   Létoffé, S., Ghigo, J. M., and Wandersman, C., *Secretion of the Serratia marcescens HasA Protein by an ABC Transporter.* J. Bacteriol., 1994. **176**: p. 5372-5377.

14.   Cescau, S., Cwerman, H., Létoffé, S., Delepelaire, P., Wandersman, C. and Biville, F., *Heme Acquisition by Hemophores.* Biometals, 2007. **20**: p. 603-613.

15.   Wandersman, C., and Delepelaire, P., *Bacterial Iron Sources: From Siderophores to Hemophores.* Annu. Rev. Microbiol., 2004. **58**: p. 611-647.

16.   Létoffé, S., Nato, F., Goldberg, M. E., and Wandersman, C., *Interactions of HasA, a Bacterial Haemophore, with Haemoglobin and with its Outer Membrane Receptor HasR.* Mol. Microbiol., 1999. **33**: p. 546-555.

17.   Hamel, D.J., Zhou, H., Starich, M. R., Byrd, R. A., and Dahlquist, F. W., *Chemical-Shift-Perturbation Mapping of the Phosphotransfer and Catalytic Domain Interaction in the Histidine Autokinase CheA from Thermotoga maritima.* Biochemistry, 2006. **45**: p. 9509-9517.

18.   Rajagopal, P., Waygood, E. B., Reizer, J., Saier Jr., M. H., and Klevit, R. E., *Demonstration of Protein-Protein Interaction Specificity by NMR Chemical Shift Mapping.* Protein Sci., 1997. **6**: p. 2624-2627.

19.   Shi, Y., and Wu, J., *Structural Basis of Protein-Protein Interaction Studied by NMR.* J. Struct. Funct. Genomics, 2007. **8**: p. 67-72.

20.   Bonvin, A.M., Boelens, R., and Kaptein, R., *NMR Analysis of Protein Interactions.* Curr. Opin. Chem. Biol., 2005. **9**: p. 501-508.

21.   Vaynberg, J., and Qin, J., *Weak Protein-Protein Interactions as Probed by NMR Spectroscopy.* Trends Biotechnol., 2006. **24**: p. 22-27.

22.   Zuiderweg, E.R.P., *Mapping Protein-Protein Interactions in Solution by NMR Spectroscopy.* Biochemistry, 2002. **41**: p. 1-7.

23.   Wishart, D.S., and Nip, A. M., *Protein Chemical Shfit Analysis: A Practical Guide.* Biochem. Cell Biol., 1998. **76**: p. 153-163.

24. Schumann, F.H., Riepl, H., Maurer, T., Gronwald, W., Neideg, K. -P., and Kabiltzer, H. R., *Combined Chemical Shift Changes and Amino Acid Specific Chemical Shift Mapping of Protein-Protein Interactions.* J. Biomol. NMR, 2007. **39**: p. 275-289.

25. Rodriguez, J.C., Wilks, A., and Rivera, M., *Backbone NMR Assignments and H/D Exchange Studies on the Ferric Azide- and Cyanide-Inhibited Forms of Pseudomonas aeruginosa Heme Oxygenase.* Biochemistry, 2006. **45**: p. 4578-4592.

26. Wagner, G., Pardi, A., and Wuthrich, K., *Hydrogen Bond Length and Proton NMR Chemical Shifts in Proteins.* J. Am. Chem. Soc., 1983. **105**: p. 5948-5949.

27. Li, H., Yamada, H., and Akasaka, K., *Effect of Pressure on Individual Hydrogen Bonds in Proteins. Basic Pancreatic Trypsin Inhibitor.* Biochemistry, 1998. **37**: p. 1167-1173.

28. Pellecchia, M., Montgomery, D. H., Stevens, S. Y., Vander Kooi, C. W., Feng, E. H., Gierasch, L. M., and Zuiderweg, E. R. P., *Structural Insights into Substrate Binding by the Molecular Chaperone DnaK.* Nat. Struct. Biol., 2000. **7**: p. 298-303.

29. Stevens, S.Y., Sanker, S., Kent, C., and Zuiderweg, E. R. P., *Delineation of the Allosteric Mechanism of Cytidylyltransferase Exhibiting Negative Cooperativity.* Nat. Struct. Biol., 2001. **8**: p. 947-952.

30. Hall, D.A., Vander Kooi, C. W., Stasik, C. N., Stevens, S., Y., Zuiderweg, E. R. P., and Matthews, R. G., *Mapping the Interactions between Flavodoxin and Its Physiological Partners Flavodoxin Reductase and Cobalamin-Dependent Methionine Synthase.* Proc. Natl. Acad. Sci. U.S.A., 2001. **98**: p. 9521-9526.

31. Williamson, R.A., Carr, M. D., Frenkiel, T. A., Feeney, J., and Freedman, R. B., *Mapping the Binding Site for Matrix Metalloproteinase on the N-Terminal Domain of the Tissue Inhibitor of Metalloproteinases-2 by NMR Chemical Shift Perturbation.* Biochemistry, 1997. **36**: p. 13882-13889.

32. Muskett, F.W., Frenkiel, T. A., Feeney, J., Freedman, R. B., Carr, M. D., and Williamson, R. A., *High Resolution Structure of the N-Terminal Domain of Tissue Inhibitor of Metalloproteinases-2 and Characterization of Its Interaction Site with Matrix Metalloproteinase-3.* J. Biol. Chem., 1998. **273**: p. 21736-21743.

33. Zuiderweg, E.R.P., Hamers, L. F., Rollema, H. S., De Bruin, S. H., and Hilbers, C. W., *^{31}P NMR Study of the Kinetics of Binding of Myo-Inositol Hexakisphosphate to Human Hemoglobin.* Eur. J. Biochem., 1981. **118**: p. 95-104.

34. Kay, L.E., Keifer, P., and Saarinen, T., *Pure Absorption Gradient Enhanced Heteronuclear Single Quantum Correlation Spectroscopy with Improved Sensitivity.* J. Am. Chem. Soc., 1992. **114**: p. 10663-10665.

35. Delaglio, F., Grzesiek, S., Vuister, G. W., Zhu, W., Pfeifer, J., and Bax, A., *NMRPipe: A Multidimensional Spectral Processing System Based on UNIX Pipes.* J. Biomol. NMR, 1995. **6**: p. 277-293.

36. Goddard, T.D., and Kneller, D. G., *Sparky 3*: University of California, San Francisco, CA.

37. Arevalo-Ferro, C., Hentzer, M., Reil, G., Gorg, A., Kjekkeberg, M. G., Reidel, K., and Eberl, L., *Identification of Quorum-Sensing Regulated Proteins in the Opportunistic Pathogen Pseudomonas aeruginosa by Proteomics.* Environ. Microbiol., 2003. **5**: p. 1350-1369.

CHAPTER 5

Summary

The gram-negative bacteria, *Pseudomonas aeruginosa* overcome iron starvation conditions by using two known distinct heme uptake mechanisms regulated by the Fe uptake regulator (Fur) [1-4]. One of the heme uptake mechanisms is the heme acquisition system (*has*) which constitutes a receptor, HasR and a heme-binding protein, HasAp [1]. HasAp is classified as hemophore secreted by *Pseudomonas aeruginosa* in response to iron limitation condition at the early stage of infection. Hemophores are secreted to the extracellular medium to scavenge free heme and heme from other heme proteins available from the host animal and deliver the heme to the specific outer membrane receptor, HasR for internalization into the bacterial cell [5, 6]. The mechanistic detail how HasAp takes heme from hemoglobin and its subsequent release of heme to the receptor is not fully understood. It is also interesting to note that HasAp undergoes C-terminal proteolytic cleavages at five different sites in the extracellular medium, whereas, hemophores from other gram-negative bacteria only undergo a single C-terminal proteolytic cleavage [7-9]. The structural and biochemical studies carried out with HasAp was aimed at elucidating the structure and function relationship of this protein. The significant difference between the full-length and truncated HasAp and the unusual His-Tyr coordination of hemophores could give some insights on how this heme scavenging proteins can take heme from hemoglobin. Thus, inhibitors can be designed to prevent the transfer of

heme from hemoglobin to HasAp and by doing this; infection can be prevented at the early stage of infection. In this research, we used a combination of bioanalytical techniques in the context of trying to understand the heme uptake mechanism of HasAp. The summary and findings that can be drawn based on our experimental results are summarized below.

1.   Structure of HasAp suggests heme uptake and release is due to different conformation and bonding interactions present in the apo and holo forms. The C-terminus of the full-length HasAp is highly unstructured.

The X-ray crystal structure of holo truncated HasAp is similar to $HasA_{SM}$ as shown in Figure 11 of Chapter 3. The heme in the structure is highly exposed to the solvent and the two axial ligands coordinating the heme-iron are located in long stretch of loops.   The strategic location of the heme pocket in HasAp could facilitate heme acquisition from hemoglobin as well as the release of heme to the cognate receptor, HasR. Moreover, as observed in Figure 46 of Chapter 3, the regions that are different in conformations between the apo and holo truncated HasAp are located in the binding pocket area. This also suggests that this part of the protein is in different conformations when heme is present or absent in the protein. The NMR structure of apo-$HasA_{SM}$ is in open conformation and the loop where His32 is located is displaced 30 Å [10] compared to the holo form and this agree with our results. This conformational difference between the apo and holo forms of HasAp could be propose as desirable conformational change so heme can be bound tightly. It can be

216

noted that in the structure of HasAp that Gly35 and Arg129 are forming hydrogen-bonds to the propionate groups of the heme which could imply that the heme is stabilized in the heme pocket by this bonding interactions aside from the axial ligands.

In addition, the calculated C_α B-factor values of the residues of the protein shown Figure 13 of Chapter 3, suggests that residues G100-G106 and 183-184 have high B-factor values. From the amino acid alignment of (Figure 3 of Chapter 1), these residues correspond to G100-P105 of HasA$_{SM}$, which were identified by Létoffé *et. al* [11] to be involved in the interaction with HasR$_{SM}$. It can be concluded that the flexibility of this loop makes it highly efficient to bind with the receptor. Moreover, the last two C-terminal residues of truncated HasAp showed also high B-factor values and this could also suggest that this part is dynamic. This is supported by the X-ray crystallography results when these residues did not show any diffraction pattern. The chemical shift index (CSI) data also supports this postulate. This part of the protein is classified as loops. Further, there was no ^{1}H-^{1}H NOE observed in the residues in the tail to the rest of the residues in the protein. Hence, the X-ray and NMR data suggest that the tail is highly unstructured and disordered part of the protein. In addition, the hydrogen-deuterium exchange experiment done on the holo truncated HasAp suggests that it is a highly dynamic protein.

2. The breaking and forming of hydrogen-bond between Tyr75 and His83 could modulate the heme uptake and release mechanism of HasAp.

The heme-iron in HasAp is a mixture of high-spin (S = 5/2) and low-spin (S = ½) species in solution as confirmed using UV-Vis spectroscopy, EPR and NMR. X-ray and NMR result suggest that there is only one heme orientation in HasAp. The heme electronic structure and coordinate state was elucidated using ^{13}C NMR coupled with the biosynthetic preparation of labeled heme. It has been reported that the chemical shift characteristics of the heme core carbons, most importantly, the carbon-meso chemical shifts can be used as a straightforward diagnostic tool to determine the coordination state of the heme-iron [12, 13]. A method to determine the coordination state of high-spin heme proteins is described in detail in Chapter 2. The ^{13}C NMR results of HasAp suggest that it is a mixture of high-spin and low-spin hexacoordinate species. At lower temperature, the carbon-mesos are moving upfield which could imply that high-spin species are populated and the hexacoordinate complex is stronger at higher temperature. Interestingly, comparison of the temperature dependence data of the carbon-mesos of HasAp in H_2O and in D_2O suggests that the low-spin carbon-mesos are the same in both solutions, whereas the high-spin carbon-mesos in H_2O are more upfield than in D_2O. Clearly, this study suggests that there is an isotopic effect responsible for the spin state and coordination state of the heme-iron. We proposed that a hydrogen-bond between Tyr75 and His83 (Scheme 1) is responsible for the high-spin and low-spin equilibrium in HasAp. The hydrogen-bond between these two residues strengthen the Tyr-iron coordination and makes Tyr a

weaker field ligand. On the other hand, the breaking of this hydrogen-bond makes Tyr a stronger field ligand. This proposed breaking and forming of H-bond between Tyr75 and His83 could modulate the heme uptake and release mechanism of HasAp. The H-bond formation could make the iron-Tyr coordination stronger so it can bind heme tightly while the breaking of this H-bond could facilitate the transfer of heme to HasR.

High Spin   **Low Spin**
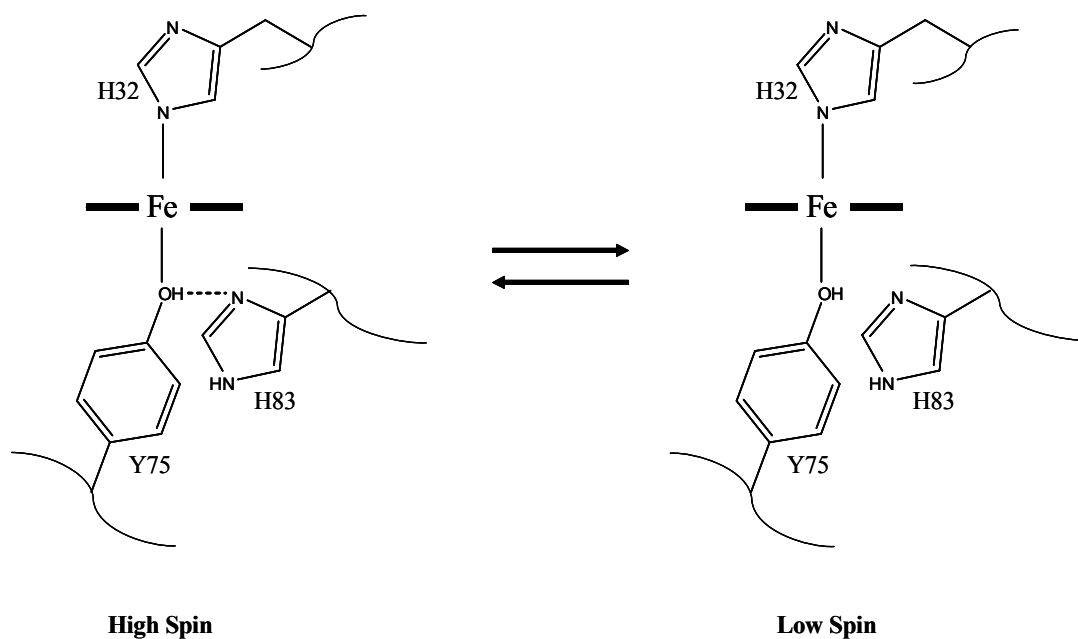
Scheme 1. The proposed breaking and forming of hydrogen-bond between Tyr75 and His83 which modulates the heme uptake and release mechanism of HasAp (hydrogen-bond is shown in dashed line).

3. HasAp can only take heme from methemoglobin and there appears to be protein-protein interaction between the two proteins before heme uptake. The heme transfer event from met-Hb to apo-HasAp is a multi-step process.

The heme transfer experiments in Chapter 3 show that apo-HasAp can only take heme from methemoglobin. Thus, it can only scavenge heme from hemoglobin if the heme-iron is in the ferric state. For this transfer to occur, the Fe-N$_{His}$ bond that anchors the heme to met-Hb must be cleaved and replaced by the Fe-N$_{His}$ and Fe-O$_{Tyr}$ bonds present in holo-HasAp. The weak-aqua ligand that coordinates the iron(III) in met-Hb is also essential to the heme transfer process since its substitution with a stronger ligand such as cyanide enhibits the heme transfer to HasAp. Considering the large number of metal ligand involved, and in analogy with the mechanism of heme heme binding to apo-Hb and apo-Mb, there is little doubt that the heme transfer event from met-Hb to apo-HasAp is a multi-step process. The heme transfer from hemoglobin to apo-HasAp is very fast and occurs in two steps. The first pseudo first order rate constant suggests that heme is taken by apo-HasAp before hemoglobin starts to dissociate in solution. Thereby, there appears to be a protein-protein interaction between the two proteins. This is supported by the NMR titration experiments between HasAp and hemoglobin. The binding sites in holo full-length and truncated HasAp are conserved but the perturbations are larger in the truncated protein than in the full-length form and this imply that the truncated form is likely to be the biologically active form of HasAp. The tail could pose as a steric hindrance for the binding interaction between HasAp and hemoglobin. The binding sites of

hemoglobin in truncated apo-HasAp are not the same as the holo forms. However, it is in the same region as the binding sites in the holo proteins.

REFERENCES

1.   Poole, K. A. M., G. A., *Iron Acquisition and Its Control in Pseudomonas aeruginosa: Many Roads Lead to Rome.* Front. Biosci., 2003. **8**: p. 661-686.

2.   Ochsner, U.A., Johnson, Z., and Vasil, M. L., *Genetics and Regulation of Two Distinct Haem-Uptake Systems, phu and has, in Pseudomonas aeruginosa.* Microbiology, 2000. **146**: p. 185-198.

3.   Ochsner, U.A., Vasil, A. I., and Vasil, M. L., *Role of the Ferric Uptake Regulator of Pseudomonas aeruginosa in the Regulation of Siderophores and Exotoxin A Expression: Purification and Activity on Iron-Regulated Promoters.* J. Bacteriol., 1995. **177**: p. 7194-7201.

4.   Nouwens, A., Beatson, S. A., Whitchurch, C. B., Nalsh, B. J., Schweizer, H. P., Mattick, J. S., and Cordwell, S. J., *Proteome Analysis of Extracellular Proteins Regulated by las and rhl Quorum Sensing System in Pseudomonas PAO1.* Microbiology, 2003. **149**: p. 1311-1322.

5.   Ratliff, M., Zhu, W., Deshmukh, R., Wilks, A., and Stojiljkovic, I., *Homologues of Neisserial Heme Oxygenase in Gram-Negative Bacteria: Degradation of Heme by the Product of the pigA Gene of Pseudomonas aeruginosa.* J. Bacteriol., 2001. **183**: p. 6394-6403.

6.   Wandersman, C., and Delepelaire, P., *Bacterial Iron Sources: From Siderophores to Hemophores.* Annu. Rev. Microbiol., 2004. **58**: p. 611-647.

7.   Arevalo-Ferro, C., Hentzer, M., Reil, G., Gorg, A., Kjelleberg, S., Givskov, M., Riedel, K., and Eberl, L., *Identification of Quorum-Sensing Regulated Proteins in the Opportunistic Pathogen Pseudomonas aeruginosa by Proteomics.* Envi. Microbiol., 2003. **5**: p. 1350-1369.

8.   Izadi-Pruneyre, N., Wolff, N., Redeker, V., Wandersman, C., Delepierre, M., and Lecroisey, A., *NMR Studies of the C-Terminal Secretion Signal of the Haem-Binding Protein, HasA.* Eur. J. Biochem., 1999. **261**: p. 562-568.

9.   Létoffé, S., Omori, K., and Wandersman, C., *Functional Characterization of the HasA$_{PF}$ Hemophore and Its Truncated and Chimeric Variants. Determination of a Region Involved in Binding to the Hemophore Receptor.* J. Bacteriol., 2000. **182**: p. 4401-4405.

10.   Wolff, N., Izadi-Pruneyre, N., Couprie, J., Habeck, M., Linge, J., Riepeng, W., Wandersman, C., Nilges, M., Delepierre, M., and Lecroisey, A., *Comparative Analysis of Structural and Dynamic Properties of the Loaded and Unloaded Hemophore HasA: Functional Implications.* J. Mol. Biol., 2008. **376**: p. 517-525.

11.   Létoffé, S., Debarbieux, L., Izadi, N., Delepelaire, P., and Wandersman, C., *Ligand Delivery by Haem Carrier Proteins: The Binding of Serratia marcescens Haemophore to Its Outer Membrane Receptor is Mediated by Two Distinct Peptide Regions.* Mol. Microbiol., 2003. **50**: p. 77-88.

12.   Rivera, M., and Caignan, G. A., *Recent Developments in the ^{13}C NMR Spectroscopic Analysis of Paramagnetic Hemes and Heme Proteins.* Anal. Bioanal. Chem., 2004. **378**: p. 1464-1483.

13.   Nakamura, M., Hoshino, A., Ikezaki, A., and Ikeue, T., *Chemical Shift of Meso-Carbon: A Powerful Probe to Determine the Coordination Structure and Electronic Configuration of Ferric Porphyrin Complexes.* Chem. Commun., 2003: p. 1862-1863.